



iJOIN

INFSO-ICT-317941



## INFSO-ICT-317941 iJOIN

### D 2.1

#### State-of-the-art of and promising candidates for PHY layer approaches on access and backhaul network

Editor:	Umer Salim, IMC
Deliverable nature:	Public
Suggested readers:	iJOIN GA
Due date:	October 31 <sup>st</sup> , 2013
Delivery date:	November 4 <sup>st</sup> , 2013
Version:	1.0
Total number of pages:	129
Reviewed by:	GA members
Keywords:	PHY State-of-the-art, RAN PHY, Backhaul PHY, RANaaS, Functional Split, iJOIN Architecture
Resources consumed	53.61 PM

#### Abstract

This report presents an overview of the activities carried out by Work Package 2 (WP2) during the first twelve months of the project. First, the state of the art of the physical layer in 3GPP LTE networks is studied. Specifically, the general architecture of LTE is discussed along with the state of the art of the radio access and backhauling technologies, which are the key enablers of the iJOIN approach at the physical layer. Following this review of the state of the art, promising candidate technologies with the potential to help meet the challenges of a small cell dense deployment are introduced. Preliminary results are presented and the integration of these candidate technologies in the iJOIN architecture is discussed. Another specificity of the iJOIN approach is to optimize the split between the processing done in the RAN-as-a-Service and the iJOIN small cells. A preliminary discussion of the impact of this functional split is provided.

## List of authors

Company	Author
<b>IMC</b>	Umer Salim ( <a href="mailto:umer.salim@intel.com">umer.salim@intel.com</a> )
<b>TUD</b>	Jens Bartelt ( <a href="mailto:jens.bartelt@ifn.et.tu-dresden.de">jens.bartelt@ifn.et.tu-dresden.de</a> )
<b>UoB</b>	Dirk Wübben ( <a href="mailto:wuebben@ant.uni-bremen.de">wuebben@ant.uni-bremen.de</a> ) Henning Paul ( <a href="mailto:paul@ant.uni-bremen.de">paul@ant.uni-bremen.de</a> ) Guang Xu ( <a href="mailto:xu@ant.uni-bremen.de">xu@ant.uni-bremen.de</a> ) Ban-Sok Shin ( <a href="mailto:shin@ant.uni-bremen.de">shin@ant.uni-bremen.de</a> )
<b>UNIS</b>	Omer Waqar ( <a href="mailto:o.waqar@surrey.ac.uk">o.waqar@surrey.ac.uk</a> ) Atta Quddus ( <a href="mailto:a.quddus@surrey.ac.uk">a.quddus@surrey.ac.uk</a> ) Muhammad Ali Imran ( <a href="mailto:m.imran@surrey.ac.uk">m.imran@surrey.ac.uk</a> )
<b>CEA</b>	Valentin Savin ( <a href="mailto:valentin.savin@cea.fr">valentin.savin@cea.fr</a> ) Matteo Gorgoglione ( <a href="mailto:matteo.gorgoglione@cea.fr">matteo.gorgoglione@cea.fr</a> )
<b>SCBB</b>	Massinissa Lalam ( <a href="mailto:massinissa.lalam@sagemcom.com">massinissa.lalam@sagemcom.com</a> )
<b>TI</b>	Boldi Mauro Renato ( <a href="mailto:mauro.boldi@telecomitalia.it">mauro.boldi@telecomitalia.it</a> ) Bruno Melis ( <a href="mailto:bruno1.melis@telecomitalia.it">bruno1.melis@telecomitalia.it</a> )

## History

Modified by	Date	Version	Comments
Umer Salim	November 4 <sup>th</sup> , 2013	1.0	Final version

## Table of Contents

List of authors.....	2
History .....	3
Table of Contents .....	4
List of Figures.....	6
List of Tables.....	8
Abbreviations .....	9
List of Symbols.....	12
1 Introduction.....	14
2 Executive Summary .....	15
3 State of the Art .....	17
3.1 3GPP LTE.....	17
3.1.1 General Architecture of LTE .....	17
3.1.2 Key PHY Layer Specifications of 3GPP LTE.....	18
3.1.3 Key Performance Indicators .....	19
3.2 PHY State of the Art for Radio Access.....	20
3.2.1 Distributed and Iterative Multi-User Detection .....	20
3.2.2 Inter-Cell Interference Coordination and Coordinated Multi-Point Transmission.....	21
3.2.3 Joint Network-Channel Coding .....	23
3.2.4 Frequency-domain Radio over Fibre (RoF).....	24
3.2.5 C-RAN.....	24
3.3 PHY State of the art for Backhauling .....	25
3.3.1 Fibre-based backhauling.....	25
3.3.2 Wireless and mmWave backhauling.....	25
3.3.3 In-band backhauling .....	28
4 PHY Candidate Technologies .....	30
4.1 CT 2.1: In-Network Processing .....	30
4.1.1 Description.....	30
4.1.2 Assumptions and Requirements.....	36
4.1.3 Preliminary Results.....	36
4.2 CT 2.2: Multi-Point Turbo Detection.....	40
4.2.1 Description.....	40
4.2.2 Assumptions and Requirements.....	48
4.2.3 Preliminary Results.....	49
4.3 CT 2.3: Joint Network-Channel Coding .....	52
4.3.1 Description.....	52
4.3.2 Assumptions and Requirements.....	56
4.3.3 Preliminary Results.....	56
4.4 CT 2.4: Sum-Rate and Energy-Efficiency metrics of DL CoMP with backhaul constraints.....	58
4.4.1 Description.....	58
4.4.2 Assumptions and Requirements.....	60
4.4.3 Preliminary Results.....	61
4.5 CT 2.5: Partially Centralized Inter-Cell Interference Coordination.....	62
4.5.1 Description.....	62
4.5.2 Assumptions and Requirements.....	66
4.5.3 Preliminary Results.....	66
4.6 CT 2.6: Data Compression over RoF.....	68
4.6.1 Description.....	68
4.6.2 Assumptions and Requirements.....	71
4.6.3 Preliminary Results.....	71
4.7 CT 2.7: Millimetre Wave Backhauling.....	76
4.7.1 Description.....	76
4.7.2 Assumptions and Requirements.....	78
4.7.3 Preliminary Results.....	78
5 PHY Logical and Functional Architecture.....	82
5.1 Input/Output and Parameters .....	82

5.2	Information Exchange within WP2 CTS .....	88
5.3	Measurement placement and measurement exchange for WP2 CTs .....	91
5.4	Interaction of Candidate Technologies .....	93
6	Functional Split .....	95
6.1	General Idea of Functional Split for WP2.....	95
6.2	Functional Split for Candidate Technologies.....	97
6.2.1	CT 2.1: In-Network Processing .....	97
6.2.2	CT 2.2: Multi-Point Turbo Detection .....	101
6.2.3	CT 2.3: Joint Network-Channel Coding .....	103
6.2.4	CT 2.4: Sum-Rate and Energy-Efficiency metrics of DL COMP with backhaul constraints..	104
6.2.5	CT 2.5: Partially Centralized Inter-Cell Interference Cancellation .....	106
6.2.6	CT 2.6: Data compression over RoF .....	107
6.2.7	CT 2.7: Millimetre Wave Backhauling.....	108
6.3	Functions Investigated in detail for Functional Split .....	110
6.3.1	Decoder.....	111
6.3.1.1	Description of Functionality .....	111
6.3.1.2	General Challenges.....	112
6.3.1.3	Options for functional split.....	112
6.3.1.4	Summary.....	114
6.3.2	Precoder .....	114
6.3.2.1	Description of Functionality .....	114
6.3.2.2	General Challenges.....	115
6.3.2.3	Options for functional split.....	115
6.3.2.4	Summary.....	118
7	Summary and Conclusions.....	120
	Acknowledgements and Disclaimer .....	121
	References .....	122

## List of Figures

Figure 3-1: Overview of the general architecture of 3GPP LTE [16] .....	17
Figure 3-2: Cumulative distribution function of the cell/user throughput.....	20
Figure 3-3: CoMP illustration .....	22
Figure 3-4: Multiple access relay channel (MARC).....	24
Figure 3-5: Basic C-RAN concept, RRH is connected to BBU using CPRI link over fibre optical cable.....	25
Figure 4-1: One UE is served by several connected iSCs .....	31
Figure 4-2: Centralized processing of a UE's uplink received data in the RANaaS .....	32
Figure 4-3: Multi-user detection via In-Network Processing among iSCs.....	35
Figure 4-4: CDF of the required iterations until convergence of the ZF-DiCE and the DC-DS algorithm for a ring topology .....	38
Figure 4-5: BER for 2 UEs transmitting $N_T^{UE} = 2$ spatial layers each and 3 receiving iSCs with $N_R^{iSC} = 4$ antennas each .....	39
Figure 4-6: BER for 2 UEs transmitting $N_T^{UE} = 4$ spatial layers each and 3 receiving iSCs with $N_R^{iSC} = 4$ antennas each .....	39
Figure 4-7: Multi-point turbo detection investigation context .....	40
Figure 4-8: UE (1Tx) baseband transmitter (PUSCH only) .....	41
Figure 4-9: Channel model for resource element (n,l) (1Tx, 2Rx).....	42
Figure 4-10: MMSE-IRC receiver chain at iSC $v$ for UE $u$ .....	43
Figure 4-11: Iterative interference cancellation principle (assuming natural ordering) .....	44
Figure 4-12: Iterative MMSE-IC receiver chain at iSC $v$ .....	44
Figure 4-13: Iterative MMSE-IC receiver chain at RANaaS .....	47
Figure 4-14: MPTD Performance Evaluation, FER vs SNR of UE <sub>1</sub> – MCS (QPSK, $R_c = 0.25$ ) .....	50
Figure 4-15: MPTD Performance Evaluation, FER vs SNR of UE <sub>1</sub> – MCS (QPSK, $R_c = 0.50$ ).....	51
Figure 4-16: MPTD Performance Evaluation, FER vs. SNR of UE <sub>1</sub> – MCS (16QAM, $R_c \approx 0.49$ ).....	51
Figure 4-17: Proposed scenario for joint network channel coding.....	52
Figure 4-18: Joint Network Channel coding for the MARC .....	53
Figure 4-19: Example of Tanner Graph of a NB-LDPC code.....	54
Figure 4-20: Separate demapping and decoding at intermediate node iSC <sub>1</sub> .....	55
Figure 4-21: Joint demapping and decoding at intermediate node iSC <sub>1</sub> .....	55
Figure 4-22: Joint network-channel factor graph .....	56
Figure 4-23: FER performance of the JNCC design for different choices of network-coding coefficients ....	58
Figure 4-24: A two-cell symmetrical network .....	58
Figure 4-25: Total energy per bit versus the location of UE from its own iSC at Cell SE = 18bps/Hz .....	61
Figure 4-26: Total energy per bit versus the location of UE from its own iSC at Cell SE = 40 bps/Hz .....	62
Figure 4-27: RANaaS with star topology .....	63
Figure 4-28: Hybrid architecture with both J1 links and J2 links.....	64
Figure 4-29: J1 links carry 5 bits and J2 links $B_{J2}$ bits for each channel element. All the nodes are equipped with a single antenna and the channel is assumed to be Rayleigh fading with the same pathloss over all the links. ....	67
Figure 4-30: Conventional downlink RoF architecture.....	68
Figure 4-31: Frequency Domain RoF architecture: downlink transmitter part .....	70
Figure 4-32: Frequency Domain RoF architecture: uplink receiver part.....	71
Figure 4-33: Downlink architecture of Frequency Domain RoF (option 2.6a).....	72
Figure 4-34: Downlink architecture of Frequency Domain RoF in case of single CW transmission (option 2.6b) .....	73
Figure 4-35: Downlink architecture of Frequency Domain RoF (option 2.6c).....	73
Figure 4-36: Uplink architecture of Frequency Domain RoF (option 2.6d).....	74
Figure 4-37: Uplink architecture of Frequency Domain RoF in case of single CW transmission (option 2.6e) .....	75
Figure 4-38: Uplink architecture of Frequency Domain RoF (option 2.6f) .....	75
Figure 4-39: mmWave backhaul deployment in cloud-based networks.....	77
Figure 4-40: Conventional decode and forward backhauling.....	77
Figure 4-41: Radio-over-radio approach .....	77
Figure 4-42: Comparison of different joint coding schemes .....	81

Figure 5-1: Exchange of user signals within veNB .....	89
Figure 5-2: Functional Architecture of PHY processing .....	93
Figure 6-1: Functional split options.....	95
Figure 6-2: Variant 2.1.a: Cooperative Joint-MUD among iSCs with one iSC performing decoding.....	97
Figure 6-3: Variant 2.1.b: Cooperative Joint-MUD among iSCs with centralized decoding in RANaaS.....	98
Figure 6-4: Variant 2.1.c: Cooperative detection and decoding within iSCs through exchange of soft estimates .....	99
Figure 6-5: Variant 2.1.d: Pre-processing per iSC and centralized detection & decoding within RANaaS by forwarding local estimates of one iSC .....	99
Figure 6-6: Variant 2.1.e: Pre-processing per iSC and centralized detection & decoding within RANaaS by forwarding local estimates of several iSCs .....	100
Figure 6-7: Variant 2.2a: SPTD with possible cooperation using the J2 interface.....	102
Figure 6-8: Variant 2.2b: MPTD performed at the RANaaS platform using the J1 interface.....	102
Figure 6-9: Variant 2.3.a: Cooperative detection & decoding within iSCs.....	103
Figure 6-10: Variant 2.3.b: Centralized detection & decoding within RANaaS .....	103
Figure 6-11: Variant 2.4.a: Centralised CoMP at RANaaS with All Computation in RANaaS.....	104
Figure 6-12: Variant 2.4.b: Centralised CoMP at RANaaS with only Precoder Computation in RANaaS ..	105
Figure 6-13: Variant 2.4.c: De-centralised CoMP at iSCs with Local Cooperation.....	105
Figure 6-14: Variant 2.6.a: Frequency domain RoF.....	107
Figure 6-15: Variant 2.6.b: Frequency domain RoF for single codeword transmission.....	108
Figure 6-16: Variant 2.7.a: Detection and decoding in iSC .....	109
Figure 6-17: Variant 2.7.b: Detection and decoding in RANaaS .....	109
Figure 6-18: Variant 2.7.c: RRH: all digital processing in RANaaS.....	110
Figure 6-19: FEC decoder is performed in iSC.....	113
Figure 6-20: FEC decoder is implemented in RANaaS.....	113
Figure 6-21: Global cooperation for Precoder by Joint usage of J1 and J2 links .....	115
Figure 6-22: Global cooperation for Precoder using J1 interface only.....	117
Figure 6-23: Local Cooperation using J2 interface only .....	118

## List of Tables

Table 3-1: Key performance indicator at PHY level.....	19
Table 3-2: Overview over wireless backhaul technologies .....	27
Table 3-3: Link Budget for 28 and 72 GHz frequencies [90].....	27
Table 3-4: Relay Types in 3GPP LTE Rel.10 .....	28
Table 4-1: List of iJOIN PHY Candidate Technologies (CTs) .....	30
Table 4-2: Mapping of PHY CTs to iJOIN Common Scenarios (CS) .....	30
Table 4-3: Categorization of non-ideal backhaul [15].....	69
Table 4-4: Layer 1 partitioning options for downlink RoF .....	74
Table 4-5: Layer 1 partitioning options for uplink RoF .....	76
Table 4-6: Link budget for mmWave link.....	79
Table 4-7: Data rates for mmWave links.....	79
Table 4-8: Overview of simulation parameters .....	80
Table 5-1: Requested Input of WP2 CTs.....	83
Table 5-2: Provided Output of WP2 CTs .....	85
Table 5-3: Explanation of Parameters .....	86
Table 5-4: Exchange signals over J1 and J2 interfaces for the different CT .....	89
Table 5-5: PHY Measurement placement and exchange.....	91
Table 5-6: Mapping of WP2 CTs to CT specific RRM CTs in WP3 .....	94
Table 6-1: Functional Split for CT 2.1 .....	101
Table 6-2: Functional Split for CT 2.2 .....	102
Table 6-3: Functional Split for CT 2.3 .....	104
Table 6-4: Functional Split for CT 2.4 .....	106
Table 6-5: Functional Split for CT 2.5 .....	107
Table 6-6: Functional Split for CT 2.6 .....	108
Table 6-7: CT2.7 parameters for exemplary BH rate calculation.....	109
Table 6-8: Functional Split for CT 2.7 .....	110
Table 6-9: Gains and challenges of the Decoder/Precoder splitting options.....	111
Table 6-10: Pros and Cons of the two options.....	114
Table 6-11: Pros and Cons of Precoder Options .....	119

## Abbreviations

3GPP	3 <sup>rd</sup> Generation Partnership Program
AF	Amplify-and-Forward
ACK	Acknowledgement
ARQ	Automatic Repeat Request
AWGN	Additive White Gaussian Noise
BBU	Base Band Unit
BER	Bit Error Rate
BD	Block Diagonalization
BH	Backhaul
bps	Bits per Second
BS	Base Station
BP	Belief Propagation
CB	Coordinated Beamforming
CDF	Cumulative Distribution Function
CoMP	Coordinated Multi-Point
CPRI	Common Public Radio Interface
C-RAN	Centralized/Cooperative/Cloud RAN
CRC	Cyclic Redundancy Check
CS	iJOIN Common Scenario Coordinated Scheduling
CSI	Channel State Information
CT	Candidate Technology
CW	Codeword
D/A	Digital to Analog
DAS	Distributed Antenna System
DCI	Downlink Control Information
DC-DS	Distributed Consensus on Demodulated Symbols
DF	Decode-and-Forward
DiCE	Distributed Consensus-Based Estimation
DMRS	Demodulation Reference Signal
DPC	Dirty Paper Coding
DSL	Digital Subscriber Line
eNB	Evolved Node B
E/O	Electrical to Optical
EPC	Evolved Packet Core
E-UTRAN	Evolved Universal Terrestrial Radio Access Network
FD	Frequency Domain
FD-RoF	Frequency Domain Radio over Fibre
FDD	Frequency Division Duplex
FEC	Forward Error Correction
FER	Frame Error Rate
FFT	Fast Fourier Transform
FSO	Free Space Optics
GF	Galois Field
GSM	Global System for Mobile Communications
HARQ	Hybrid Automatic Repeat Request
HSS	Home Subscriber Service
I	In-phase (sample)
ICI	Inter-Cell Interference
ICIC	Inter- Cell Interference Coordination
IFFT	Inverse Fast Fourier Transform
iJOIN	Interworking and JOINT Design of an Open Access and Backhaul Network Architecture for Small Cells based on Cloud Networks
IC	Interference Cancellation

INP	In-Network Processing
IRC	Interference Rejection Combining
iSC	iJOIN Small Cell
iNC	iJOIN Network Controller
iTN	iJOIN Transport Node
JNCC	Joint Network Channel Coding
JT	Joint Transmission
KPI	Key Performance Indicator
LLR	Log Likelihood Ratio
LDPC	Low Density Parity Check
LOS	Line of Sight
LS	Least Squares
LTE	Long Term Evolution
MAC	Medium Access Control
MARC	Multiple Access Relay Channel
MCS	Modulation and Coding Schemes
MIMO	Multiple-Input Multiple Output
MME	Mobility Management Entity
MMSE	Minimum Mean Square Error
MPTD	Multi-Point Turbo Detection
MUD	Multi-User Detection
NACK	Negative-acknowledge
NB	Non-Binary
NC	Network Coding
NLOS	Non Line of Sight
OBSAI	Open Base Station Architecture Initiative
O/E	Optical to Electrical OFDMOrthogonal Frequency Division Multiplexing
OFDMA	Orthogonal Frequency Division Multiple Access
ORI	Open Radio Interface
PCRF	Policy Control and Charging Function
PDCCH	Physical Downlink Control Channel
PDSCH	Physical Downlink Shared Channel
PDU	Payload Data Unit
PEG	Progressive Edge Growth
P-GW	Package Gateway
PHICH	Physical Hybrid-ARQ Indicator Channel
PHY	Physical Layer
PL	Path Loss
PMI	Precoder Matrix Index
PUSCH	Physical Uplink Shared Channel
Q	Quadrature (sample)
QAM	Quadrature Amplitude Modulation
QoS	Quality of Service
QRD	QR Decomposition
QPSK	Quadrature Phase Shift Keying
RAN	Radio Access Network
RANaaS	RAN-as-a-Service
RAP	Radio Access Point
RAT	Radio Access Technology
RB	Resource Block
RF	Radio Frequency
RE	Resource Element
RI	Rank Indicator
RIT	Radio Interface Technology
RLC	Radio Link Control
RN	Relay Node
RoF	Radio over Fibre

RoR	Radio over Radio
RRC	Radio Resource Control
RRH	Remote Radio Head
RRM	Radio Resource Management
SC	Small Cell
SC-FDMA	Single-Carrier Frequency Division Multiple Access
SDU	Service Data Unit
S-GW	Service Gateway
SINR	Signal to Interference and Noise Ratio
SNR	Signal to Noise Ratio
SotA	State-of-the-Art
SPTD	Single-Point Turbo Detection
SRS	Sounding Reference Signal
TBS	Transport Block Size
TDD	Time Division Duplex
UCI	Uplink Control Information
UE	User Equipment
UL	Uplink
W-CDMA	Wideband Code Division Multiple Access
WP	Work Package
ZF	Zero Forcing
ZFP	Zero Forcing Precoding

## List of Symbols

### System Parameter

$N_T^{UE}$	no. of transmit antennas at UE
$N_R^{UE}$	no. of receive antennas at UE
$N_T^{iSC}$	no. of transmit antennas at iSC
$N_R^{iSC}$	no. of receive antennas at iSC
$N_L^{UE,u}$	no. of spatial transmit layers by UE $u$ on UL
$N_{UE}$	no. of UEs
$N_{iSC}$	no. of iSCs
$N_{sc}$	no. of subcarriers
$N_{symp}^{DL}$	no. of symbols per time slot in downlink
$N_{symp}^{UL}$	no. of symbols per time slot in uplink
$N_{FFT}$	FFT size
$N_{quant}^{DL}$	no. of quantization bits in downlink
$N_{quant}^{UL}$	no. of quantization bits in uplink
$N_{RB}$	bandwidth configuration expressed in no. of resource blocks
$N_s$	no. of signals to be transmitted on the backhaul link
$N_{symp}$	no. of coded symbols (or symbol-nodes)
$N_{check}$	no. of check equations (or constraint-nodes)
$d_y$	symbol-node degree
$d_c$	constraint-node degree
$q$	cardinality of the Galois Field
$E_T$	total energy per bit
$z$	number of bits for each non-binary symbol
$d_{min}$	minimum (Hamming) distance
$f_s$	sampling frequency
$OF$	oversampling factor
$T_{frame}$	radio frame duration
$T_s$	symbol duration
$T_{subframe}$	subframe duration
$T_{slot}$	slot duration
$L_{BH}$	backhaul load
$Q_m$	modulation order
$T_{J1}$	iSC-RANaaS link latency (on the J1 interface)
$T_{RANaaS}$	processing time within the RANaaS platform
$BH_{lat,req}$	backhaul latency requirement
$BH_{cap,req}$	backhaul capacity requirement

### General Parameter

$C$	capacity
$D$	data rate

$R_c$	coding rate
$B$	bandwidth
$S$	spectral efficiency
$\eta$	throughput
$\mathcal{E}$	encoder, code
$P$	power
$\Pr$	probability
$p$	probability distribution function
$N_0$	noise power spectral density of the access link
$N_{0,BH}$	noise power spectral density of the backhaul link
$N_{it}$	no. of iterations

### Signals

<b>a</b>	info word
<b>c</b>	code word
<b>c'</b>	interleaved code word
<b>H</b>	channel matrix
<b>h</b>	channel vector
<b>U</b>	detector matrix
$h$	non-binary coefficient of the parity-check matrix
<b>H</b>	parity-check matrix
<b>n</b>	noise vector
<b>s</b>	modulated symbols
<b>W</b>	precoding matrix
<b>x</b>	transmitter signal vector
<b>y</b>	receiver signal vector

### General Notation of Symbols

$a$	scalar
<b>a</b>	vector
<b>a</b> <sup>T</sup>	transpose
<b>a</b> <sup>H</sup>	transpose conjugate
<b>A</b>	matrix
$\tilde{a}$	soft estimate
$\hat{a}$	hard estimate

### Indices

$u$	user
$i, j, \nu$	iSC
$n$	carrier
$l$	symbol within frame
$k$	iteration

# 1 Introduction

Recent years have seen tremendous use of mobile devices in the form of smart phones, tablets, netbooks and other handheld devices. The emergence of new applications, web surfing, video telephony, and streaming to name a few, has caused exponential growth in mobile data traffic. Furthermore, it is expected that this traffic would increase by 500 to 1000 times by 2020 [1]. In order to meet this exponential increase in throughput requirement, significant changes in today's wireless systems need to be introduced. The whole architecture needs to be thought over. Physical layer has to meet the excessive throughput requirements from upper layers. This can be achieved through dense deployment of small cells which leads to reduce significantly the pathloss and allows also achieving a higher density of simultaneous transmissions

Overlaying the existing cellular networks with small cells has three main advantages. Firstly, the distance between the small cell (SC) and user equipment (UE) decreases and thus path-loss is reduced significantly. Hence maintaining the same Quality of Service (QoS), modulation order and coding rate can be increased which results in significant gains in data rate. Secondly, small cells allow the use of aggressive frequency reuse factors compared to large cells, which means that more bandwidth becomes available in each cell. Thirdly, small cell deployment causes each user to be in the vicinity of multiple small cells. This gives a unique possibility of collaboration and cooperation between the neighbouring cells. Thus, multiple cells can transmit/receive in a cooperative way. This transmission scheme, known widely as "network MIMO", leads to huge throughput benefits. It requires however more transmitter channel state information (CSI) in the downlink and sophisticated processing techniques in the uplink. Moreover, in the absence of appropriate processing techniques to enable the cooperation of neighbouring cells, the deployment of small cells leads to a strong inter-cell interference (ICI) in both uplink and downlink, which limits the performance gains.

Within this project we introduce the iJOIN small cell (iSC) and the RAN-as-a-Service (RANaaS) concepts as practical solutions to achieve the improvements promised by the theoretical results. This approach allows for a flexible cooperative processing among iSCs and a (partly) centralized processing in the RANaaS. The communication between these entities is provided by the backhaul network. In order to maximize the overall system performance, both the radio access and the backhaul network have to be jointly optimized. In the iJOIN project, the J1 logical link is introduced to represent the backhaul links between RANaaS and iSCs while backhaul links between iSCs are realized by logical J2 links.

The main objective of WP2 in iJOIN is to investigate physical layer (PHY) approaches for a joint design of access and backhaul network with the aim of increasing the overall throughput, energy efficiency, and utilisation efficiency of very dense small networks with (partly) centralized processing. In this deliverable, the state-of-the-art (SotA) of backhaul and access network technologies from a PHY layer perspective is described. Building on this SotA, a set of innovative candidate technologies (CTs) is then presented. These CTs are selected for their potential to improve the network performance by exploiting the fact that the backhaul and the radio access are jointly designed, as well as the presence of the RANaaS environment.

## 2 Executive Summary

The objective of this work is twofold. First, this document aims at providing a clear overview of the state of the art literature for the PHY layer techniques, which are currently used or are promising for a near future. This survey provides the necessary background for the second goal of this document, which is to describe innovative methods which have the potential to reduce (or even exploit) inter-cell interference in the downlink and employ multi-user diversity in the uplink with joint processing and joint detection. The described schemes are specifically designed to use the novel possibilities offered by the joint design of the access channel and the backhaul network. In addition, the introduction of the RANaaS concept allows for novel approaches and offers the possibility of a flexible functional split between the RANaaS and the iSCs. This report is organized as follows:

Section 3 provides an overview of the state of the arte (SotA). A comprehensive description of the 3GPP LTE network is provided in Section 3.1 listing also the currently used small cell terms and definition of the key performance indicators (KPIs). Section 3.2 is about the SotA PHY techniques being applicable to small cell deployments. Techniques from the literature like distributed and iterative multi-user detection in the uplink (UL) and cooperative multi-point transmission (CoMP) in the downlink (DL) are discussed. Additionally, innovative ideas like joint network channel coding and frequency-domain radio over fibre transmission are introduced. Finally, an overview of existing centralized RAN (C-RAN) approaches is provided, where the PHY processing is executed in a centralized unit and this unit is connected by fibre links with the antennas. It is the main goal of iJOIN to allow for a more flexible function split and to overcome this strict requirement on the backhaul. Correspondingly, SotA backhaul techniques are presented in Section 3.3, where the key properties of fibre-based backhauling and wireless backhauling are discussed.

In Section 4, promising PHY candidate technologies (CT) for a dense deployment of small cells and a joint optimization of access and backhaul networks are introduced. Cooperative multi-user detection techniques for the uplink are investigated by CT2.1 “In-Network Processing” and CT2.2 “Multi-Point Turbo Detection”. The joint optimization of the forward error correction (FEC) codes for the access links and the backhaul link applying network coding is considered by CT2.3 “Joint Network-Channel Coding”. For the downlink CoMP transmission CT2.4 “Sum-Rate and Energy-Efficiency metrics of DL CoMP with backhaul constraints” and CT2.5 “Partially Centralized Inter-Cell Interference Coordination” analyse different precoder and interference coordination techniques with backhaul constraints. Techniques to reduce the backhaul throughput for radio over fibre (RoF) links are topic of CT2.6 “Data Compression over RoF”, whereas CT2.7 “Millimetre Wave Backhauling” addresses wireless backhaul links and joint access and backhaul FEC. The basic concept of each CT is introduced with detailed technical description. The considered system setting is described, the problem of interest is formulated, and the proposed solution is explained. After listing the main assumptions and requirements per CT, preliminary results for the described generic system setups are presented and directions for future works are given.

Section 5 outlines the PHY layer logical and functional architecture for the iJOIN architecture explained in D5.1 [123]. The requested input information and the provided output information of the CTs are defined and parameterized. Additionally, the entity providing the requested information and the entity processing the provided output are specified in order to develop the overall iJOIN functional architecture. This description is not only limited to the principle CTs described in Section 4, but consider already the functional split variants per CT which are introduced afterwards in Section 6. As the functional split variant will influence the backhaul traffic between the iSCs and between the iSCs and the RANaaS, the kind of CT-specific information and measurement results to be exchanged between the nodes are specified. Finally, Section 5.4 provides a schematic overview of the PHY functional architecture in order to indicate the interactions with RRM/MAC functions described in D3.1 [144] and network-layer functions defined in D4.1 [145].

Section 6 targets one of the key ideas of iJOIN, namely functional split between small cells and RANaaS. After giving the general idea of functional split from a PHY perspective, for each CT possible functional splits are considered and first evaluated by means of computational needs. Backhaul requirements are also provided. Subsequently, implementation aspects of two basic functions are detailed. For the decoder in the uplink and for the precoder in the downlink, the general challenges are specified and different options for functional placement are presented and compared.

Finally, Section 7 gives the concise summary and the conclusions of the various investigations carried out and described in this deliverable.

In this first project phase the SotA was provided, basic specifications for the iJOIN project were defined and promising candidate technologies were investigated from a principle perspective. However, the research results achieved within these first twelve month were already advanced enough to lead to publications or submissions to prestigious international conferences and journals. Subsequently, the main results of these publications are briefly described.

In [4], the general behaviour of In-Network Processing algorithms, as proposed for the distributed multi-user detection, in the presence of erroneous backhaul transmission is investigated. The applicability of such algorithms for distributed multi-user detection was demonstrated in [5] for a simple scenario. In [6], a novel approach to reduce the communication overhead induced by the distributed processing is presented. The performance of those distributed algorithms is investigated both theoretically and by simulations.

In [7], a review and survey of small cell networks is carried out from the perspective of dynamic multi-cell cooperation mechanisms as candidate solutions for interference management and capacity enhancement in small cell networks. It is proposed that cloud-processing and joint optimization of the backhaul and access network together provide a feasible remedy to overcome some key challenges and realize successful cooperation in the next generation dense small cell networks.

In [8] and [9] the cooperation of transmitters is investigated in an information theoretic framework. A fundamental and simple setting is studied in order to derive insights for the more complicated and more realistic networks. Collaborative exchanges take place over a causal and error-prone link and various collaborative transmission/reception strategies are investigated.

In [10], the use of millimetre wave transmission for the backhaul of Cloud-RAN is investigated. An approach to use mmWave similar to the popular radio over fibre technique is proposed and the properties of this transmission method are studied. In a second step, joint channel coding for the access and backhaul channel is investigated and it is demonstrated, that the reliability of the joint link can be improved by considering a joint optimization of the channel code.

Of particular interest is [11] where the backhauling aspects of the iJOIN architecture are presented. The importance of an adequate backhaul design is highlighted and the different backhaul technologies are reviewed. Finally, it is shown how exploiting the backhaul heterogeneity and a flexible centralization of the signal processing leads to a better efficiency and appears as a promising solution to meet the high performance increase required.

### 3 State of the Art

The iJOIN project builds up further on 3GPP LTE Release 10 (as a baseline radio access technology) and introduces its key innovations with respect to the joint access-backhaul design together with flexible RAN implementation. Therefore, this section briefly summarizes the general architecture of 3GPP LTE as well as the key PHY layer specifications, as these will be referred to in the forthcoming technical discussions. This will be followed by a short discussion of key performance indicators of 3GPP LTE which, as stated, in their scope are important for iJOIN project. Finally, the PHY state of the art with respect to radio access as well as backhauling will be described.

#### 3.1 3GPP LTE

##### 3.1.1 General Architecture of LTE

An overview of the general architecture of a 3GPP LTE network is depicted in Figure 3-1. It can be separated into the evolved universal terrestrial radio access network (E-UTRAN) and the evolved packet core (EPC) [26]. While the E-UTRAN is responsible for the direct radio connection to users, the EPC handles the communication with other networks as well as most of the management.

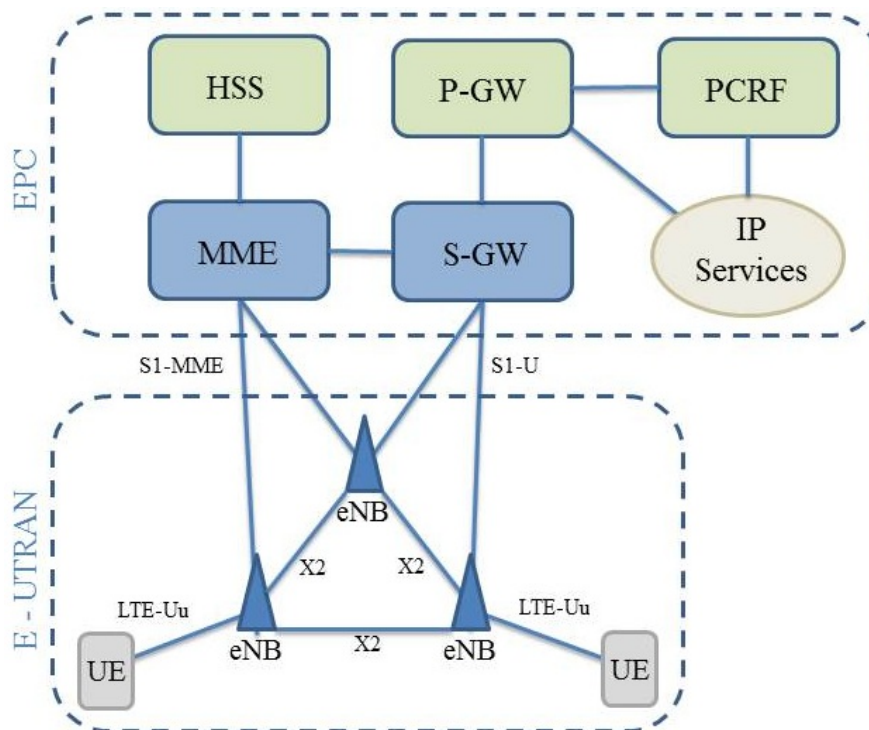


**Figure 3-1: Overview of the general architecture of 3GPP LTE [16]**

The user equipments (UEs) send their data to and receive transmissions from the base stations denoted evolved Node B (eNB), which are in turn connected to the EPC. An eNB controls multiple UEs and is responsible for radio resource management (RRM), medium access control (MAC), and the physical layer processing.

The communication with other internet protocol (IP) services is managed via the service gateway (S-GW) and the package gateway (P-GW). While the S-GW acts as a router and mobility anchor, the P-GW allocates IP addresses, enforces quality of service (QoS), and filters packets accordingly.

The mobility management entity (MME) is the central control node of the network. It manages bearers and connections as well as some security aspects. A data base of all subscribers' information is located at the Home Subscriber Service (HSS). Charging and QoS are controlled by the Policy Control and Charging Function (PCRF).

All elements are connected using different interfaces. Most important of these are the S1 and X2 interfaces, which connect an eNB to the EPC and an eNB to other eNBs, respectively, and the radio interface between the UEs and an eNB, which is called Uu.

The 3GPP EPS architecture is designed under the assumption that logical network entities correspond to physical entities, and that logical network functions are located in such physical network entities. To provide an example, the logical network entity “eNB” corresponds to a physical entity in the network, i.e. a base station. The logical function “RRM” is executed in this eNB, therefore also in a specific physical location. The separation of logical and physical network entities and functions as such is therefore not addressed specifically in the 3GPP specifications.

In the current access topology macrocell eNBs with directional antennas are used for mid-scale to large-scale coverage whereas microcell eNBs usually equipped with omnidirectional antennas typically cover distances of about 100 m [28]. The future trend to smaller cells is reflected by recent research and development of picocells and femtocells. Small cells are low power cells aimed at covering a restricted geographical area, offloading the macrocell network of users that are generally in bad conditions (indoor) or in dense environments (e.g. airport, shopping mall, and train station). Two types of cells that are usually associated to the small cell terminology can be identified:

- a) picocells usually cover small but dense areas (hot-spot) such as mall, airport, etc.,
- b) femtocells are usually located in residential or corporate environments (mainly indoor oriented)

Except some technical discrepancies obviously reflected by the type of the cell (in terms of raw computational power, simultaneously supported users, covered area, etc.) the main difference lies in the way the cells are deployed and connected to the operator’s core network. Indeed, if picocells are usually operator-deployed, thus part of the operator’s network planning, femtocells are end-user deployed and usually make use of the user’s broadband access (digital subscriber line (DSL) or cable) as a third-party backhaul. Picocells support the exact same set of functionalities and feature as macrocells in the 3GPP view. However, femtocells have some limitations due to the unplanned nature of their deployment and their possible high density resulting in mutual interference.

A further trend that can be observed in the later releases of 3GPP is the deployment of small cells that do not offer the same functionality as macro eNBs, but only work in support of them:

1. **Relays** [26]: in contrast to traditional repeaters that just amplify and re-broadcast a signal, the 3GPP relays demodulate and decode received data and then re-transmit it. They thereby enhance the signals quality. Relays can be either used to increase the network density or extend the coverage. In contrast to macro eNBs they do not require a direct backhaul link, since this is provided by the donor eNB. 3GPP has defined a few categories / types of relays, these are described in Section 0.
2. **Remote Radio Heads (RRHs)** [27]: a RRH can be seen as part of a widely distributed antenna system. It usually consists of an antenna and transceiver, but little data processing devices. Like the relay, it re-transmits the received signal to a donor eNB, e.g. via a fibre connection, but without decoding the data. It can be used to increase coverage or signal quality as well, but it also opens the possibility to combine the signals of multiple RRHs for a joint detection/transmission at the donor eNB.

### 3.1.2 Key PHY Layer Specifications of 3GPP LTE

The physical layer of 3GPP LTE is based on orthogonal frequency division multiple access (OFDMA). It is a wideband system that avoids fixed frequency planning like in GSM (global system for mobile communications) and is more flexible than W-CDMA (wideband code division multiple access) systems. While true orthogonal frequency division multiplexing (OFDM) is only used in the downlink, most of its components are reused in the uplink, which uses single-carrier FDMA (SC-FDMA).

LTE was designed to be as flexible as possible, supporting a large number of different modulation schemes, code and data rates, carriers, bandwidths, multiple-input/multiple-output (MIMO) techniques, and time division duplex (TDD) as well as frequency division duplex (FDD). Resources can be flexibly assigned to users and the transmission scheme is adapted to the momentary channel gain.

The LTE physical layer is described in the 3GPP technical specifications TS 36.211 for the physical channel [84] and TS 36.212 for the modulation and coding scheme (MCS) [91]. The PHY layer procedures are detailed in TS 36.213 [112].

### 3.1.3 Key Performance Indicators

In this section the key performance indicators (KPIs) at physical layer level for the LTE networks are analysed. The KPIs have been defined considering the minimum requirements set by ITU for IMT-Advanced systems [12] and considering also the results obtained in 3GPP during the study item on the coordinated multi-point (CoMP) transmission technique [13].

**Table 3-1: Key performance indicator at PHY level**

Name	Definition	LTE Release 8	LTE Release 10
Max. user rate	Maximum data rate that can be delivered to one user	150 Mbps (DL, MIMO 2x2, 20 MHz, UE category 4) 50 Mbps (UL, SIMO 1x2, 20 MHz, UE category 4)	1 Gbps (DL) 500 Mbit/s (UL)
U-plane Latency	Defined as the one-way transit time between a service data unit (SDU) packet being available at the IP layer in the user terminal/base station and the availability of this packet at IP layer in the base station/user terminal assuming an unloaded network.	5 – 10 ms	< 5 ms Note: depends also on used backhauling technology
Average cell spectrum efficiency	Defined as the aggregate throughput of all users (the number of correctly received bits over a certain period of time) normalized by the overall cell bandwidth and divided by the number of cells.	> 1.6 – 2.1 bit/s/Hz/cell (DL with MIMO 2x2 Spatial Multiplexing and IRC receivers) > 0.66 – 1 bit/s/Hz/cell (UL with SIMO 1x2 and IRC receivers)	> 2.6 bit/s/Hz/cell (DL Microcellular coverage) > 1.8 bit/s/Hz/cell (UL Microcellular coverage)
Cell Edge user spectrum efficiency	Defined as the 5% point of CDF of the user throughput normalized with the overall cell bandwidth.	> 0.04 – 0.06 bit/s/Hz/user (DL with 10 users per cell) > 0.02 – 0.03 bit/s/Hz/user (UL with 10 users per cell)	> 0.075 bit/s/Hz/cell (DL Microcellular coverage) > 0.05 bit/s/Hz/cell (UL Microcellular coverage)

Table 3-1 provides a list of KPIs at PHY level according to the SotA applicable to the LTE Release 8 networks currently under deployment and LTE Release 10 networks, respectively. The average cell spectrum efficiency and the cell edge user spectrum efficiency are suitable metrics for measuring the performance of a wireless dense network including the effect of the radio access technology and of the backhauling network. These two metrics are derived from the cumulative distribution function (CDF) of the cell and user throughput respectively, as shown in Figure 3-2.

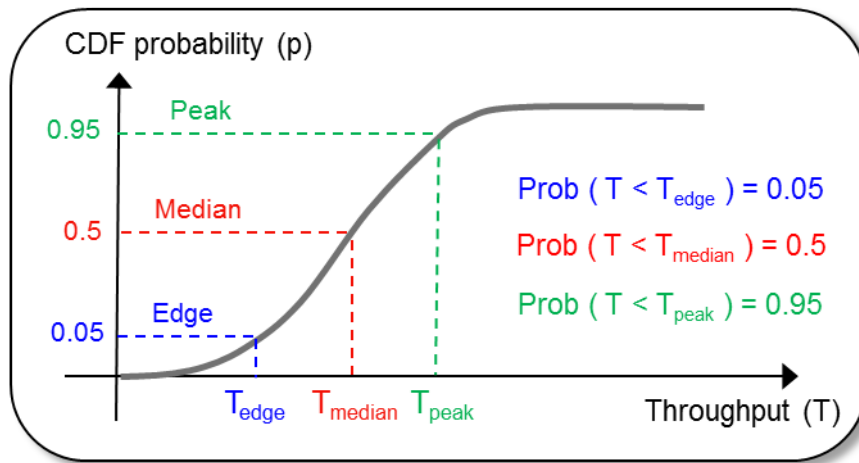


Figure 3-2: Cumulative distribution function of the cell/user throughput

Concerning the user mobility, not indicated in the table, it seems reasonable to consider the classes of stationary, pedestrian, and vehicular (with speed up to 30 km/h) as suitable for dense network scenarios. Finally, the latency objective has been set below the requirement defined for LTE in [14] but the actual value is expected to depend on the specific technology used for backhauling, as reported in the 3GPP study item on small cell enhancements [15].

## 3.2 PHY State of the Art for Radio Access

In this section, we present the state of the arte (SotA) related to radio access network especially focusing on the techniques investigated in WP2 of iJOIN project. These are primarily related to uplink distributed and iterative multi-user detection, downlink inter-cell interference coordination (ICIC), coordinated multi-point transmissions (CoMP), joint network channel coding, frequency domain radio over fibre, and the associated cloud RAN architectures that enable centralized processing by virtue of cloud computing concepts. These mechanisms will be elaborated in more detail in the following sub-sections.

### 3.2.1 Distributed and Iterative Multi-User Detection

Multi-user detection (MUD) is a common technique in digital communications that allows for the separation of signals transmitted on the same resources by multiple users. Since in a dense network superimposed uplink signals of several UEs are received by multiple base stations, the joint detection of all received signals promises diversity gains, due to the fading properties of the mobile communication channel. Although it is possible to apply conventional MUD techniques in such a scenario, this requires the collection of all received signals at a single point. Therefore, the challenge is to perform the detection of the different UEs' signals in a distributed fashion. The problem of distributed MUD has been receiving interest from the academic world for quite a long time now; e.g. in [17] a thorough survey can be found, which will be summarised in the following. In 1994, first information-theoretic investigations have been made [18], the principle of belief propagation was proposed for distributed decoding [19]-[22]. This approach requires the iterative exchange of likelihood values or extrinsic information among all involved base stations. Of course, this causes a very large traffic on the backhaul, which is particularly disadvantageous in typical star network topologies.

Alternatively, so-called distributed antenna systems (DAS) were proposed in [23]. Here the signals received at these distributed antennas are forwarded to a processing centre, where they are jointly detected and decoded. This technique can provide a signal to interference and noise ratio (SINR) gain, but also has the drawback of large resulting backhaul traffic, as it was pointed out in [24]. While it is acknowledged that a distributed MUD can provide an optimum detection, amends to practical backhaul constraints have to be made. In [17], the authors investigate the different options for information exchange among cooperating base stations: the least backhaul-intensive option is to exchange hard bits, e.g. preliminarily estimated payload data. The better option from information theoretic point of view is to exchange data with corresponding reliability information. This can be accomplished by either exchanging log likelihood ratios (LLRs) or soft-bits. According to [17], a trade-off between detection quality and amount of information exchanged on the backhaul can be achieved by varying the quantisation of the exchanged information.

Following the introduction of the turbo code [97], the turbo principle has made its way in the MUD area, where it is often referred as turbo detection or turbo equalization. Such procedure usually relies on an

iterative minimum mean square error (MMSE) linear filtering with interference cancellation (IC) [98]-[103]. In an iterative way, the users' contributions are reconstructed after their decoding and all of them except the desired user signal are subtracted from the received signal, hence the "interference cancellation" name. For this process to be possible, soft information is exchanged between these decoding and detecting stages in an iterative way. In [25] the authors propose a distributed inter-cell interference (ICI) cancellation technique that uses the turbo principle. This approach uses the exchange of soft-bits among base stations. Here, also quantisation is suggested for the reduction of resulting backhaul traffic. In [104], a similar approach is derived but using QR decomposition (QRD) based antenna selection combined with maximum likelihood process for the (non-linear) detecting stage. These works demonstrate the potential of the turbo detection approach for MUD if done either locally with information exchange or centrally.

The distributed detection of multiple users is an estimation problem which can also be addressed using techniques from the field of in-network processing (INP). INP allows for the solution of, e.g. estimation problems in a distributed, decentralized fashion within a network. The special class of consensus-based algorithms achieves this by iteratively reaching a consensus of the estimate among the processing nodes. Therefore, consensus-based linear estimation algorithms as presented in [2], [96], [113] allow for an iterative distributed MUD based on the Zero Forcing (ZF) or MMSE criterion.

### 3.2.2 Inter-Cell Interference Coordination and Coordinated Multi-Point Transmission

It is well-known that the capacity of a single-user MIMO systems increases linearly with the minimum number of transmit and receive antennas at high signal to noise ratio (SNR) [63], [64]. Using joint precoding in the downlink, the sum capacity of multi-user MIMO can be increased linearly even when each mobile user has single antenna [65], [66]. However, in a realistic cellular system the presence of inherent ICI reduces SINR of the cell-edge users. Therefore the theoretical gain in sum capacity through MIMO can be limited by the ICI factor, which can deteriorate the cell-edge users' performance. In order to combat ICI and achieve capacity gains, various techniques have been proposed in the literature [67]. Among these techniques, eNB cooperation or CoMP [146], [147] in 3GPP has gained much popularity in recent few years.

In downlink CoMP, eNBs in adjacent cells cooperate with each other before sending data to their users [68]. This transforms the interference-limited channels to noise-limited and hence the capacity of cell-edge users can be enhanced. Depending upon the level of cooperation between the eNBs, CoMP techniques have been categorized as follows by 3GPP [13], as illustrated in Figure 3-3.

#### 1. Joint Transmission (JT):

In this transmission scheme, each eNB (involved in cooperation) has data and CSI of each user [71]-[72]. Therefore, each user receives information signals from all the base stations coherently. In this way, ICI is converted into useful signal provided that perfect synchronization exists between the cooperative base stations. Moreover, JT comes with large backhaul overheads and stringent synchronization requirements.

#### 2. Coordinated Beamforming (CB):

In this case, each base station has data of its own local cell users only but also CSI of all the users present in the cooperative cells [76], although CB can also be distributed with local CSI only at each base station [77]. Hence, each base station performs its own individual precoding. Since only CSI needs to be shared among the cooperative base stations, backhaul overheads are relatively less when compared to joint-processing at the expense of reduction in sum access capacity.

#### 3. Coordinated Scheduling (CS):

This scheme is also known as "inter-cell scheduling" [68]. ICI is avoided because in one time/frequency resource, only one base station is scheduled to transmit. The attractive feature of this scheme is that the message exchange among the base stations is comparable to that of handoff which is already employed in cellular systems. The most promising advantage of CS is to achieve expanded multiuser diversity. However, due to the fact that in LTE Rel. 11, coordinated scheduling uses reference symbols (by puncturing Physical Downlink Shared Channel (PDSCH) Resource Elements (REs)) for obtaining the CSI in a low duty cycle to lower the signalling overhead, this might provide sub-optimal spectral efficiency [68].

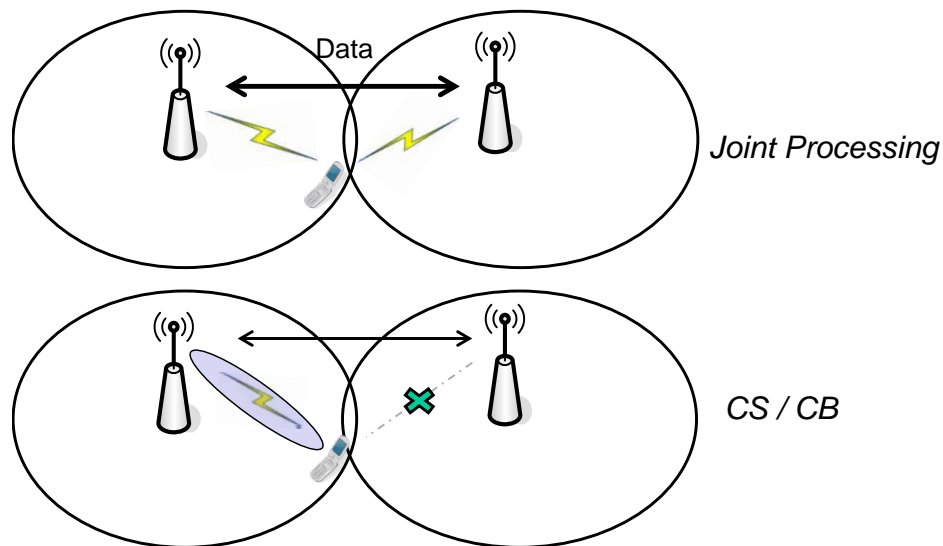


**Figure 3-3: CoMP illustration**

Dirty paper coding (DPC) with joint processing (also known as multi-cell DPC) is first proposed in [69]. Although DPC is capacity-achieving, it is not suitable for implementation in practice due to its high complexity. Motivated by this fact, several multi-cell linear precoding techniques are discussed in [70] with both total and per eNB power constraints. Even though in CoMP transmission, per eNB constraint is a more realistic assumption, it has been shown that sum capacity degrades due to this per eNB power constraint. However, besides ICI mitigation potential, CoMP provides some other additional benefits; for example power gain, channel rank/conditioning advantage, and macro diversity protection for shadowing channels [70]. The maximum achievable common rate in a coordinated network with ZF and DPC is analysed in [71] and [72]. Similarly, it is also shown in [73] that joint transmission improves the sum access capacity considerably.

The backhaul overhead and feedback requirements in FDD increase proportional to the number of cooperative base stations, number of antennas per base-station, and number of users. Therefore, for a large network, different strategies have been proposed in the literature to reduce the burden in terms of overhead. Among these strategies, one approach which has been extensively studied is clustering. In clustering, the numbers of base stations are limited to cooperate only within the cluster and inter-cluster signals are considered as interference. Multi-cell block diagonalization (BD) is used in [74] for JT within the same cluster. Moreover, in order to satisfy the per eNB power constraint, three different power allocation algorithms are proposed in [74]. In [75], adaptive switching between single-cell beamforming (also known as maximum ratio transmission) and ZF is proposed to enhance the sum rate. It is shown that less feedback is required for this adaptive scheme when compared to the static ZF. Moreover, the impact of channel quantization (for CSI feedback) is also quantified in [75].

Besides clustering, CB (as mentioned above) is also used to reduce backhaul overhead when compared to JT. In [76], an efficient algorithm is proposed to design optimal global beamformers for all the base stations without need to exchange data of other cell users. Beamformers are designed to minimize either weighted sum power or maximum per eNB power subject to SINR constraints at the users.

In practice, the backhaul capacity is limited and therefore JT is not always superior to CB. Sum capacity is analysed for different cooperative schemes under backhaul constraints in [78]-[80], and [140]. A new rate splitting scheme is proposed in [79], in which each base station splits its message into two parts: a common part and a private part. Only a common part is shared between the base stations and thus reduces the backhaul overhead. It is shown through simulations in [80] that coordinated beamforming outperforms joint processing when the backhaul capacity is low and /or the edge SNR is high. Motivated by this fact, semi-dynamic mode selection between JT and CB is proposed in [81] for different random user and orthogonal user scheduling schemes.

CS is studied in [68] and it is shown that opportunistic scheduling in multi-cell systems achieves an expanded multi-user diversity due to independent log-normal shadowing in each cell. Therefore, CS outperforms static frequency reuse (which is used in conventional cellular systems) technique while having

the same complexity. Besides this performance improvement, through inter-cell scheduling universal frequency can be adopted and hence frequency planning is not required [68].

Summarizing, the main benefits of CoMP transmission are

- **Interference Handling:** JT has the potential to turn the interference into useful signal. On the other hand, coordinated beamforming may enable the clustering entities to cooperate so as to avoid the ICI.
- **Better user experience:** joint reception from multiple base stations or sites using CoMP techniques enables the overall received power at the handset to be increased which directly translates into larger throughput and better user experience.
- **Improved Network Utilization:** by providing connections to several base stations at once, using CoMP, data can be passed through least loaded base stations for better resource utilization.
- **Better Channel Rank:** by JT, the channel rank is generally being improved as compared to single-cell scenario, and this results in higher capacity [63].
- **Macro diversity Protection:** joint processing also provides macro diversity protection for shadowing channels because shadowing is generally uncorrelated among the cooperative base stations.

### 3.2.3 Joint Network-Channel Coding

By exploiting the broadcast nature and the inherent spatial diversity of wireless communications, Sendonaris et al. introduced the concept of cooperative diversity [29], [30] over wireless relay channels and their multi-terminal extensions. Subsequently, many authors proposed cooperation protocols for the relay channel, which can be classified into two major categories, namely amplify-and-forward (AF) and decode-and-forward (DF) [31]. In AF protocols, the relay simply amplifies the received signal and forwards it to the destination. The DF protocol allows the relay to decode the received signal, re-encode it, and forward it to the destination. The forwarded message can either be identical to, or part of the initial transmission (repetition coding), or it can be obtained by using a dedicated coding scheme at the relay (distributed coding). In the first case the destination combines received signals both from source and relay, which results in an improved SNR on the received transmission. Besides, the same code is used for encoding at the source and decoding at the destination. In the second case, the destination gains knowledge of extra information, but it needs a dedicated decoding scheme able to jointly decode received signals from both source and relay. Distributed turbo and low density parity check (LDPC) codes for the relay channel have been proposed in [32]-[39].

For both AF and DF protocols, the amount of data transmitted by the relay (e.g. expressed in number of transmitted bits) is usually equal to the amount of data initially transmitted by the source. This may be particularly problematic in case of multiple access relay channels (MARC), i.e. when the same relay is simultaneously used by several users to communicate with the destination, especially if the relay-to-destination link has limited capacity. In order to overcome this limitation, network coding (NC) can be advantageously used at the relay. Instead of separately relaying data packets for each of the users accessing the channel, the NC technique [40] allows combining them together for transmission. Although it was first proposed in the context of error-free networks as a technique to achieve the maximum possible information flow, NC proved also to be particularly useful in the context of wireless networks, allowing significant improvements in network's throughput [41].

An example of MARC with 2 sources, 1 relay and 1 destination is depicted in Figure 3-4. It illustrates the case when 2 UEs use a common "relay" (RAP1 node) to communicate with a final destination (RAP2/eNB), and only concerns uplink transmissions. UEs' transmissions are encoded by two channel codes  $\mathcal{E}_1$  and  $\mathcal{E}_2$ , while a network code  $\mathcal{E}$  is used at the relay. The destination decodes the received signals using knowledge of  $\mathcal{E}_1$ ,  $\mathcal{E}_2$  and  $\mathcal{E}$ . Consequently, a joint-design of network ( $\mathcal{E}$ ) and channel ( $\mathcal{E}_1$ ,  $\mathcal{E}_2$ ) codes is desired in order to fully exploit these two coding techniques. The codewords  $\mathbf{c}_1 = \mathcal{E}_1(\mathbf{a}_1)$ , and  $\mathbf{c} = \mathcal{E}(\mathbf{a}_1, \mathbf{a}_2)$  are modulated into and transmitted over orthogonal channels. Several joint network channel coding (JNCC) schemes have been proposed in the literature [42] – [51]. While these works investigated the design of effective JNCC schemes using either Turbo or LDPC channel coding, they did not elaborate on a structure to guarantee full diversity (at maximum rate) of the proposed joint code design. The maximum achievable

coding rate that allows to achieve full diversity when NC is not used at the relay is  $R_c = 1/2$ ; the use of NC yields an increase of the maximum full diversity rate from  $R_c = 1/2$  to  $R_c = 2/3$  [44]. A rate  $2/3$  full-diversity JNCC design for the MARC, based on root-LDPC codes, has been recently proposed in [52]-[53].

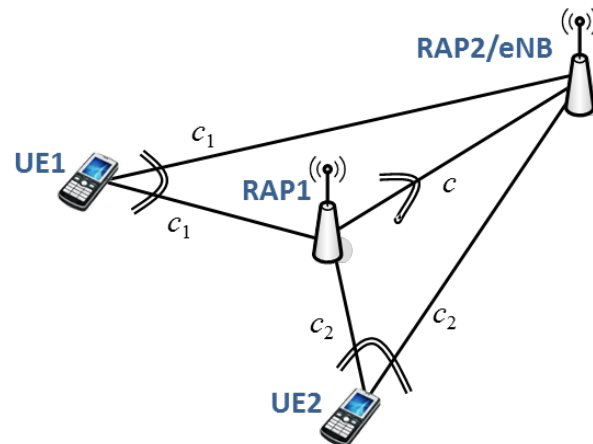


Figure 3-4: Multiple access relay channel (MARC)

### 3.2.4 Frequency-domain Radio over Fibre (RoF)

RoF is a technology to transport wireless signals in optical form by means of an optical fibre. This fibre connects a central processing unit and a certain number of remote radio units where the signals are radiated by the antennas in case of DL transmission. The remote radio units are placed in the coverage area in order to provide the wireless communication services to the end users.

The RoF solution is a widely known approach for current radio base station layouts, but it has also so-called “horizontal” applications, namely applications where it is used for implementing particular radio access architectures. These solutions are feasible provided that a good availability of fibre in terms of deployed fibre networks usually in urban environments is assumed, and they can represent a possible building element for any “cloud” oriented architectural solutions (see Section 3.2.5).

Many studies and initiatives have been put forward recently on this topic. In particular there have been some standardization works in the past, among which Common Public Radio Interface (CPRI) [82] and Open Base Station Architecture Initiative (OBSAI) [83] were the most considered. These works are carried on by an ETSI group, called ORI (Open Radio Interface) that disclosed a phase 1 specification in 2012 and is now working on a phase 2, with advanced topics in the agenda [93].

In one of the studies, among the others, performed in ORI phase 2, they treat the issue regarding the compression techniques of data to be transmitted over the fibre links (the data rate in the ORI format is usually much higher than in the backhauling). These techniques will be briefly discussed in Section 3.3.1, but frequency domain RoF (FD-RoF) is definitely to be classified as one of them, representing de facto a reduction in the data rate requested transmission. Details about frequency domain RoF will be given in Section 4.6.

### 3.2.5 C-RAN

In the recent years, an approach termed “C-RAN” was proposed by different vendors and operators and has meanwhile also been studied in NGMN’s P-CRAN project [114]. While the “C” in this abbreviation originally stood for “cloud”, it now commonly denotes any of “centralized”, “clean” or “cooperative” [118]. The main idea of C-RAN is the shift of baseband processing away from the cell to a central location where the processing is performed in a “pool” (“baseband pooling”), represented by an entity often named “base band unit” (BBU). The conversion from radio to optical or electrical is carried out by a so-called RRH. This basic concept is depicted in Figure 3-5. Regarding the hardware on which the processing is carried out, different approaches can be found. While some vendors offer dedicated hardware (e.g. Alcatel-Lucent’s Light Radio [115] and Nokia Siemens Networks’ Liquid Radio [116]), the objective of IT companies is the use of general purpose server hardware, e.g. IBM investigated the possibility of implementing a WiMax base station pool using software defined radio on a general purpose server [117]. The C-RAN field test carried out by China Mobile is supported by Intel [118], [119] and also aims for the shift of processing load into

baseband pools running on general purpose servers. Also by Alcatel Lucent's research labs, the possibility of performing processing using software defined radio on standard server hardware was investigated [120].

These centralization techniques share the requirement on a high-capacity link between the actual radio access point and the processing centre. This is commonly achieved using CPRI links operating over fibre optical connections [122]. However, it is also possible to set up CPRI links using wireless point-to-point links, as was, e.g. demonstrated by Ericsson in their Beijing LTE C-RAN test bed [121].

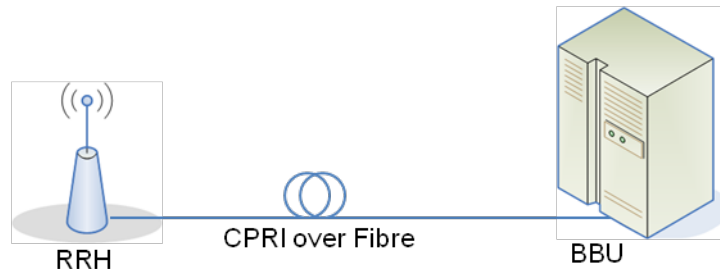


Figure 3-5: Basic C-RAN concept, RRH is connected to BBU using CPRI link over fibre optical cable

### 3.3 PHY State of the art for Backhauling

Traditionally, various technologies have been in use for backhauling operation. Backhauling has been used as the operation of information exchange between the core network and network nodes in the radio access network. Some of the technologies which have served as backhaul are free space optical communication, point-to-point microwave links, and DSL. Fibre optic based backhauling has been used for a long time, offering very large data rates. Millimetres wave (mmWave) backhauling is getting more and more attention these days because of its ability to serve as flexible backhaul. 3GPP has standardized in-band and out-of-band relaying as a possible solution for backhaul. In the following, we detail these backhaul candidate technologies. A good overview can also be found in [85].

#### 3.3.1 Fibre-based backhauling

As stated in Section 3.2.4, the transmission of radio signals over fibre is generally known as RoF. The data rate to transmit these lower OSI layer signals is much greater than “traditional” backhauling, i.e. on top of the radio access part towards the core network. These traditional backhaul links are commonly based on Gigabit Ethernet solutions or apply dedicated fibres in some deployments. In such cases, compression techniques or methods are seldom used, due to the intrinsic lower data rate with respect to the fronthauling. A global overview of the possible backhauling solutions for LTE is given in [86] and [87].

Conversely, for RoF some solutions to compress data are more and more necessary to cope with the growing capacity requested by new radio access technologies (RATs) and also by multi RAT solutions. Examples of the data rates that are requested by RoF for different RATs are reported in [86] and [87]. In particular in [86] it is also given an indication of the compression factor that is achievable through a proprietary data compression technique denoted as “Compressed CPRI”.

Other options are based on approaches similar to the FD-RoF approach that will be discussed in Section 4.6. These approaches are not based on compression of data, which usually degrades the quality of the transmission, but on alternative splitting interfaces in the transceiver chain. The FD-RoF concept is based on a specific split of the physical layer functionalities, so that the interface between RANaaS and iSC is located at the input of the inverse fast Fourier transform (IFFT) in the downlink transceiver chain. Clearly, other functional splits are possible by shifting the interface in the transceiver, achieving different trade-offs between the data rate to be transmitted over the fibre, the complexity of the iSC and of the amount of control information that must be transmitted on the interface between RANaaS and iSC

#### 3.3.2 Wireless and mmWave backhauling

For wireless backhauling a number of frequency bands have been considered so far. Apart from in-band backhaul, the available solutions can be separated into traditional microwave (6-42 GHz), sub-6-GHz microwave, unlicensed (60 GHz), and licensed (70-80 GHz) millimetre wave systems. Furthermore, free space optics (FSO) can also be considered as wireless backhaul [88].

Generally speaking, wireless backhaul has the advantage that it is easier, faster, and cheaper to deploy than wired backhaul. On the other hand, it usually offers lower data rate and lower availability. However, the different wireless systems have widely different characteristics themselves [89]:

- Free space optics offer high data rates of multiple Gbps due to the very high available bandwidth and usually do not have to be licensed, lowering cost and deployment time. However, they suffer heavily from snowfall and fog, limiting either range or availability. Due to their very narrow beamwidth, they also have to be carefully aligned and are susceptible to thermal expansion, building sway, and vibration. When they are facing east to west, they can also suffer from sunlight effects [89].
- Traditional microwave systems can only offer low data rates below 1 Gbps and use licensed spectrum, increasing costs and deployment time. The 5 GHz band is also used by many users as it is specified as a WiFi band. This increases interference, which further limits data rates and decreases availability. The 5 GHz system is also the one most vulnerable to interception, because all other systems use highly directive beams that would require an interceptor be suspiciously deployed in the connection's line of sight (LOS).
- The 60 GHz band offers up to 9 GHz of unlicensed spectrum, allowing for multi-Gbps data rates and fast deployment. However, 60 GHz faces a uniquely high attenuation through oxygen absorption and rain, limiting its range to below 2 km. In contrast, the oxygen absorption has the advantage that interference between 60 GHz links is very low, especially if combined with narrow antenna beams. This also increases the security against eavesdropping. However, the small beamwidth limits multipath effects, making spatial diversity multiplexing techniques more difficult and also requires LOS.
- The 70/80 and 90 GHz bands combine the advantages of high bandwidth, long range, and high availability. The spectrum is licensed, yet the licensing process is (at least in the US) easy and affordable. It also shares the advantages and disadvantages of narrow antenna beams with 60 GHz systems. However, since it is the highest frequency system considered, hardware design is the most challenging.

To increase reliability, different wireless backhauled can be combined, e.g. a 60 GHz system as main link and a 5 GHz link as backup in case of heavy rain. As in any communication systems, effective data rates can be lowered in favour of a more robust coding, to ensure connectivity in suboptimal situations.

An overview of the different technologies is provided in Table 3-2.

**Table 3-2: Overview over wireless backhaul technologies**

Parameter	<6GHz	6-42 GHz	60 GHz	70/80/90 GHz	FSO
Typical data rate	400 Mbps	400 Mbps	1 Gbps (commercial) 10 Gbps (demonstrator)	1 Gbps (commercial) 10 Gbps (demonstrator)	1 – 10 Gbps
Typical range	<5 km (interference limited)	5 km	0.1 – 1 km	3 km	1 km
Licensing	Licensed/ unlicensed (5.8 GHz)	Licensed	Unlicensed	“Lightly” licensed	Unlicensed
Other	Multipath for spatial diversity  High interference  Easy to intercept		Very low interference  Oxygen attenuation  NLOS might not be possible	NLOS might not be possible	High degree of alignment required  Only LOS possible  High attenuation by snow, fog

The link budget of microwave (28 GHz) and millimetre-wave (72 GHz) backhaul links for transmission powers of 35 dB and 25 dB is given in Table 3-3.

**Table 3-3: Link Budget for 28 and 72 GHz frequencies [90]**

Parameters	Case 1	Case 2	Case 3	Case 4
TX Power (dBm)	35.00	35.00	25.00	25.0
TX antenna gain (dBi)	30.00	30.00	30.00	30.00
Carrier frequency (GHz)	28.00	72.00	28.00	72.00
Distance (km)	1.00	1.00	0.50	0.50
Propagation Loss (dB)	121.34	129.55	115.32	123.53
Other losses	20.00	20.00	20.00	20.00
RX antenna gain (dBi)	15.00	15.00	15.00	15.00
Received power (dBm)	-61.34	-69.55	-65.32	-73.53
Bandwidth (GHz)	1.00	1.00	1.00	1.00
Thermal PSD(dBm)	-174.00	-174.00	-174.00	-174.00
Noise Figure (dBm)	10.00	10.00	10.00	10.00
Thermal Noise (dBm)	-74.00	-74.00	-74.00	-74.00
SNR (dB)	12.66	4.45	8.68	0.47
Implementation Loss (dB)	5.00	5.00	5.00	5.00
Data rate (Gb/s)	2.77	0.91	1.74	0.4

### 3.3.3 In-band backhauling

One important characteristic of an LTE relay node (RN) is the carrier frequency it operates on. Two operation modes can be distinguished [13]:

- **Inband:** An LTE relay node is said to be inband if the eNB-RN link shares the same carrier frequency with RN-UE links.
- **Outband:** In this case the eNB-RN link does not operate in the same carrier frequency as RN-UE links.

Depending on the relaying strategy, a relay may either be part of the donor cell or control a cell of its own. Accordingly, the following types of LTE relays can be distinguished [13]:

- **Type 1:** Such RNs control their cells with their own identity including the transmission of their own synchronisation channels and reference symbols. To ensure backwards compatibility, Type 1 RNs appear as if they are a Rel. 8 eNB to Rel. 8 UEs. The basic Type 1 LTE relay provides half duplex with inband transmissions.
- **Type 1.a:** These RNs have the same properties as the basic Type 1 RNs, except that they operate outband in full duplex mode.
- **Type 1.b:** These RNs have the same properties as the basic Type 1 RNs, except that they operate inband (with adequate antenna isolation) in full duplex mode.
- **Type 2:** These RNs do not have their own cell identity and look just like the main cell. Any UE in range is not able to distinguish a RN from the main eNB within the cell. Control information can be transmitted from the eNB and user data from the RN. The RN operates inband in full duplex mode.

The main properties of the different relaying types are summarized in Table 3-4.

**Table 3-4: Relay Types in 3GPP LTE Rel.10**

LTE Type	Relay	Cell ID	Frequency spectrum	Duplex mode
Type 1	Yes	Yes	Inband	Half duplex
Type 1.a	Yes	Yes	Outband	Full duplex
Type 1.b	Yes	Yes	Inband	Full duplex
Type 2	Yes	No	Outband	Full duplex

#### RN-eNB link for inband relay Type 1

In order to allow inband relaying, some resources in the time-frequency space are set aside for the backhaul link ( $U_n$ ) and cannot be used for the access link ( $U_u$ ). The following resource partitioning scheme is mandatory in 3GPP LTE Rel. 10.

General principle for resource partitioning at the relay:

- eNB  $\rightarrow$  RN and RN  $\rightarrow$  UE links are time division multiplexed in a single carrier frequency (only one is active at any time)
- RN  $\rightarrow$  eNB and UE  $\rightarrow$  RN links are time division multiplexed in a single carrier frequency (only one is active at any time)

Multiplexing of backhaul links in FDD:

- eNB  $\rightarrow$  RN transmissions are done in the DL frequency band
- RN  $\rightarrow$  eNB transmissions are done in the UL frequency band

Multiplexing of backhaul links in TDD:

- eNB  $\rightarrow$  RN transmissions are done in the DL subframes of the eNB and RN

- RN  $\rightarrow$  eNB transmissions are done in the UL subframes of the eNB and RN

#### **RN-eNB link for inband relay Type 1b**

If the outgoing and incoming signals at the RN are adequately isolated in the spatial domain, e.g. by appropriate arrangement of the respective antennas for the Un and Uu links, the eNB  $\rightarrow$  RN and RN  $\rightarrow$  UE (RN  $\rightarrow$  eNB and UE  $\rightarrow$  RN) links can be activated simultaneously without the need for the time division multiplexing. The operation of Type 1b relay nodes may not be supported in all deployment scenarios.

#### **RN-eNB link for outband relay**

If RN-eNB and RN-UE links are isolated enough in frequency (possibly with help of additional means such as antenna separation), then there is no interference issue in activating both links simultaneously. Therefore, it becomes possible for relay-eNB link to reuse the channels designed for UE-eNB link.

## 4 PHY Candidate Technologies

In this section we define the PHY technologies for the radio access network and the backhaul network that are promising candidates to meet the challenges of dense deployment of small cells. These CTs enable a holistic design of radio access network and backhaul network. Table 4-1 summarizes the CTs, their principle topics and the abbreviations used to indicate a CT in figures or tables. The CTs 2.1, 2.2, and 2.3 consider PHY approaches for the uplink in a dense deployment of small cells. Downlink approaches are investigated by CT2.4 and CT2.5. The focus of CT2.6 and CT2.7 is the analysis of the backhaul transmissions for UL and DL. In the subsequent sections the basic approaches of the different CTs are presented in detail. These descriptions are generic, i.e. not limited to the iJOIN architecture. However, when appropriated we use already the iJOIN terminology introduced in D5.1 [123] for RAN entities and backhaul links.

**Table 4-1: List of iJOIN PHY Candidate Technologies (CTs)**

CT	Topic	Abbreviation
2.1	In-Network-Processing	INP
2.2	Multi-Point Turbo Detection	MPTD
2.3	Joint Network-Channel Coding	JNCC
2.4	Sum-Rate and Energy-Efficiency Metrics of DL COMP with backhaul constraints	CoMP
2.5	Partially Centralized Inter-Cell Interference Coordination	ICIC
2.6	Data Compression over RoF	RoF
2.7	Millimetre wave backhauling	mmWave

The following table lists which CT will be applied to which of the iJOIN common scenarios<sup>1</sup> (CS) defined in D5.1 [123]. As the focus of a CT may change in the course of the project, this given assignment is preliminary and up to further changes. Here, “x” means that the common scenario will be considered, whereas “o” denotes that the common scenario may be considered.

**Table 4-2: Mapping of PHY CTs to iJOIN Common Scenarios (CS)**

Scenario	2.1 INP	2.2 MPTD	2.3 JNCC	2.4 CoMP	2.5 ICIC	2.6 RoF	2.7 mmWave
CS 1 Stadium		o	o	x		x	x
CS 2 Square	x	o			x	o	x
CS 3 Wide-area continuous coverage			x	o		x	x
CS 4 Indoor (Airport / Shopping Mall)	x	x		x	x	o	

### 4.1 CT 2.1: In-Network Processing

#### 4.1.1 Description

##### Scenario

For this CT we consider a very dense deployment of iSCs in which the iSCs are connected via the J2 interface. In such a deployment, distances between connected iSCs will be rather small leading to good channel conditions and the possibility to exploit rather high data rates on the J2 backhaul links. For example, mmWave transmission as investigated by CT2.7 (see Section 4.7) is an appropriate approach for connecting neighbouring iSCs with very high data rates. Furthermore, the iSCs communicate with the RANaaS via the

<sup>1</sup> Please note that the abbreviation CS was previously introduced for coordinated scheduling. However, as the meaning of the abbreviation will be always clear from the context, there is no risk of confusing both.

J1 interface. However, as the distance between the iSCs and the RANaaS may be large, lower data rates on the J1 links compared to the J2 links are likely. In addition, the communication between the iSCs and the RANaaS may be executed in a meshed multi-hop network, requiring a thorough design of the entire backhaul network.

For the basic transmission scenario, we consider a single UE located within the vicinity of several connected iSCs. Then, each iSC receives a different observation of the same user signal. In order to detect the user signal, each iSC can forward its received signal to the RANaaS which processes all received signals jointly as done by the C-RAN approach discussed in Section 3.2.5. In this so called centralized approach, forwarding the received information to the RANaaS will cause a huge traffic load and request a high data rate on the J1 interface. Thus, it would be favourable to detect the user signal in a distributed fashion among all connected iSCs and to forward only the detected signal from one iSC to the RANaaS through the J1 interface. Such an approach would benefit from the high data rate of the J2 backhaul links and reduce the traffic load on the J1 interface. This motivates the application of In-Network Processing (INP) to such a scenario. INP proposes cooperation among iSCs via an exchange of information about the received observations in order to estimate the user signal iteratively. This scheme differs from the distributed turbo detection principle mentioned in Section 3.2.1 such that INP aims to find the central solution of a generic optimization problem. In INP, each iSC calculates an estimate of the user signal by incorporating information from neighbouring iSCs. Therefore, the whole estimation procedure is placed within the network of connected iSCs. After the estimation procedure has finished, all iSCs will have the same estimate of the user signal. Then, any iSC – preferably the one with the best connection – can forward its estimate to the RANaaS over the J1 interface. This will reduce the traffic load on the J1 backhaul link significantly compared to the centralized approach. In case of MUD, each iSC will have estimates of all user signals available. Thus, a flexible transmission in which different iSCs forward estimates belonging to different users over the J1 interface is possible in order to spread the traffic. Obviously, the information which is exchanged among the iSCs needs to be quantized. These quantization effects are not considered here but will be included in future investigations.

In the following, the INP approach will be presented and investigated in detail. The centralized approach will serve as a reference in terms of performance measure for INP. Furthermore, in Section 6.2.1 mixed approaches regarding the functional split will be investigated where specific functions of the iSC like the decoding or the detection are centralized in the RANaaS. For the sake of simplicity, the detection of a single UE is considered first. A scenario with multiple UEs will be examined afterwards.

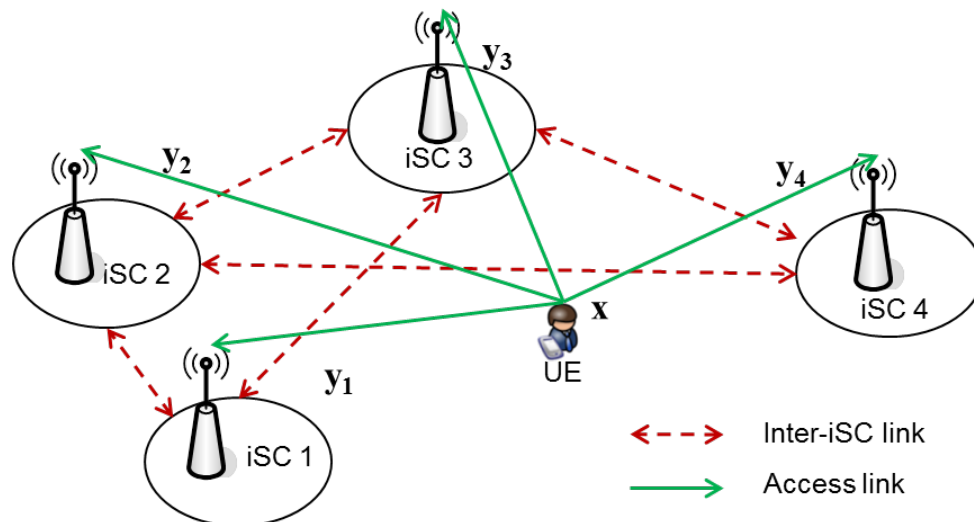


Figure 4-1: One UE is served by several connected iSCs

### System Model

Figure 4-1 depicts the described transmission scenario. The UE is equipped with  $N_T^{UE}$  antennas and uses spatial multiplexing for transmitting its message  $\mathbf{x}$  of dimension  $N_T^{UE} \times 1$ . The transmitted UE message  $\mathbf{x}$  is received by all  $N_{iSC}$  iSCs where each iSC is equipped with  $N_R^{iSC}$  receive antennas. Neighbouring iSCs are connected via the J2 backhaul link such that a certain network topology is set up. Assuming flat fading

MIMO channel matrices  $\mathbf{H}_j$  of dimension  $N_R^{iSC} \times N_T^{UE}$  and white Gaussian noise  $\mathbf{n}_j$  of power  $\sigma_n^2$ , the receive signal  $\mathbf{y}_j$  at iSC  $j$  is given by

$$\mathbf{y}_j = \mathbf{H}_j \mathbf{x} + \mathbf{n}_j. \quad (4.1)$$

By stacking the vectors  $\mathbf{y}_j$ ,  $\mathbf{n}_j$ , and the matrices  $\mathbf{H}_j$  of all  $N_{iSC}$  iSCs in the network to  $\mathbf{y}$  with dimension  $N_{iSC} N_R^{iSC} \times 1$ ,  $\mathbf{n}$  and  $\mathbf{H}$  of dimension  $N_{iSC} N_R^{iSC} \times N_T^{UE}$ , we can formulate the overall transmission of the user signal  $\mathbf{x}$  to all iSCs by

$$\mathbf{y} = \mathbf{H}\mathbf{x} + \mathbf{n}. \quad (4.2)$$

From this equation, the centralized Least-Squares (LS) problem can be formulated by

$$\tilde{\mathbf{x}}_{LS} = \arg \min_{\mathbf{x}} \|\mathbf{y} - \mathbf{H}\mathbf{x}\|^2. \quad (4.3)$$

This problem aims to find the vector  $\tilde{\mathbf{x}}_{LS}$  which minimizes the Euclidean distance between the receive signal  $\mathbf{y}$  and the estimated receive signal. Subsequently, the centralized and a distributed approach for solving that well-known problem will be presented.

### Central LS Solution

Solving (4.3) leads to the central LS solution [6], which is given by the stacked observation vector  $\mathbf{y}$  multiplied by the Moore-Penrose pseudoinverse of  $\mathbf{H}$ :

$$\tilde{\mathbf{x}}_{LS} = (\mathbf{H}^H \mathbf{H})^{-1} \mathbf{H}^H \mathbf{y}. \quad (4.4)$$

This estimate represents the well-known Zero-Forcing (ZF) solution and requires knowledge of all individual channel matrices  $\mathbf{H}_j$  and the observations  $\mathbf{y}_j$  of all iSCs at a central unit (e.g. the RANaaS entity). Thus, (4.4) can be processed in a central unit which collects the information of all iSCs. Figure 4-2 shows an illustrative example of the central approach. All iSCs are connected to the central unit, the RANaaS, and transmit their observed UE signals as well as information of the individual channels to the RANaaS via J1 backhaul links. Obviously, these transmissions cause a high traffic load on the J1 backhaul links. Furthermore, this scheme lacks robustness since an outage of the RANaaS would corrupt the whole estimation process. In case of link failures between an iSC and the RANaaS, the received information of that particular iSC will be completely lost, and thus cannot be processed by the RANaaS. Additionally, noise on the backhaul links between the iSCs and the RANaaS will further reduce the overall estimation performance. In terms of computational complexity, there is a higher demand on the RANaaS entity, since the complete processing is performed here. On the other hand, the computational demand on the iSCs is very small since these simply act as RRHs. Furthermore, the estimation process can be directly conducted without any iterative procedure.

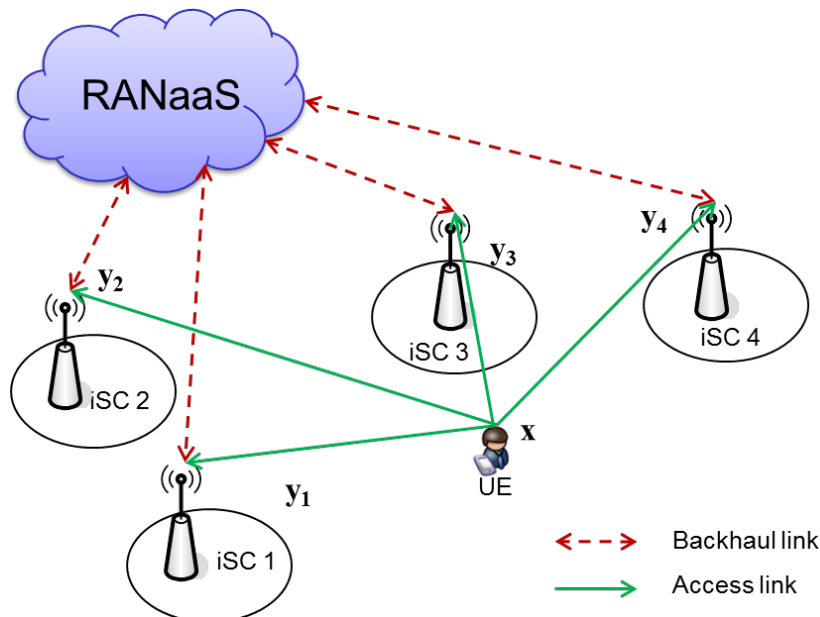


Figure 4-2: Centralized processing of a UE's uplink received data in the RANaaS

### ZF-DiCE Algorithm

In order to establish a more robust and flexible scheme compared to the centralized approach, we investigate the application of INP for the described scenario. Specifically, we present the Zero-Forcing Distributed Consensus-Based Estimation (ZF-DiCE) algorithm from [2] as a distributed approach for solving the central LS problem in (4.3).

In contrast to the central LS detection, the ZF-DiCE algorithm aims to calculate the central LS solution in a distributed way via an exchange of messages between connected iSCs. For a distributed calculation of the central solution, we introduce local estimates  $\mathbf{x}_j$  per iSC  $j$  and reformulate the LS problem in (4.3) as a set of local optimization problems:

$$\{\tilde{\mathbf{x}}_j\}_{j=1}^{N_{isc}} = \arg \min_{\mathbf{x}_j} \sum_{j=1}^{N_{isc}} \|\mathbf{y}_j - \mathbf{H}_j \mathbf{x}_j\|^2, \quad (4.5)$$

$$\text{s.t. } \mathbf{x}_j = \mathbf{x}_i, \forall j \in J, \forall i \in \mathcal{N}_j, \quad (4.6)$$

with the set  $\{\tilde{\mathbf{x}}_j\}_{j=1}^{N_{isc}}$  containing the converged estimates of all iSCs. The set  $J$  contains all considered iSCs in the network while the set  $\mathcal{N}_j$  corresponds to the neighbouring iSCs which are connected to iSC  $j$ . Equation (4.6) is a consensus constraint which states that estimates of neighbouring iSCs should be identical. This guarantees a convergence of the estimates of all iSCs to the same solution which is the central LS solution from (4.4). Due to a direct coupling of estimates of neighbouring iSCs in the consensus constraint (4.6), a parallel processing to solve (4.5) is not possible. Consequently, additional variables need to be introduced in order to reformulate the consensus constraint in an equivalent way. For the Distributed Consensus on Demodulated Symbols (DC-DS) algorithm proposed in [96], for each connection per iSC auxiliary variables are defined. E.g. in a system with  $N_{isc} = 3$  iSCs in a ring topology, 6 auxiliary variables are necessary. In contrast to that, for the ZF-DiCE approach for each iSC  $j$  one auxiliary variables  $\mathbf{z}_j$  of dimension  $N_T^{UE} \times 1$  is introduced. The distributed LS problem in (4.5) and (4.6) can then be formulated equivalently by

$$\{\tilde{\mathbf{x}}_j\}_{j=1}^{N_{isc}} = \arg \min_{\mathbf{x}_j} \sum_{j=1}^{N_{isc}} \|\mathbf{y}_j - \mathbf{H}_j \mathbf{x}_j\|^2, \quad (4.7)$$

$$\text{s.t. } \mathbf{x}_j = \mathbf{z}_i, \mathbf{x}_j = \mathbf{z}_j \quad \forall j \in J, \forall i \in \mathcal{N}_j.$$

This set of constraint optimization problems can then be solved by means of methods from optimization theory, specifically by the alternating direction method of multipliers [143]. A detailed derivation of the ZF-DiCE algorithm can be found in [2]. The derivation of the algorithm results in the following update equations:

$$\tilde{\mathbf{z}}'_j(k+1) = \frac{\mu}{|\mathcal{N}_j|+1} \sum_{i \in \mathcal{N}'_j} \left( -\lambda_{ij}(k) + \frac{\tilde{\mathbf{x}}'_i(k)}{\mu} \right), \quad (4.8)$$

$$\lambda_{ij}(k+1) = \lambda_{ij}(k) - \frac{1}{\mu} (\tilde{\mathbf{x}}'_i(k) - \tilde{\mathbf{z}}'_j(k+1)), \quad (4.9)$$

$$\tilde{\mathbf{x}}'_j(k+1) = \left( \mathbf{H}_j^H \mathbf{H}_j + \frac{|\mathcal{N}_j|+1}{\mu} \mathbf{I}_N \right)^{-1} \cdot \left[ \mathbf{H}_j^H \mathbf{y}_j + \sum_{i \in \mathcal{N}'_j} \left( \lambda_{ji}(k+1) + \frac{\tilde{\mathbf{z}}'_i(k+1)}{\mu} \right) \right]. \quad (4.10)$$

The update equations of the ZF-DiCE algorithm contain the following variables and parameters:

- $\tilde{\mathbf{z}}'_j(k+1)$ : intermediate local estimate of UE message at iSC  $j$  in iteration  $k+1$  of dimension  $N_T^{UE} \times 1$
- $\lambda_{ij}(k+1)$ : Lagrange multiplier between iSC  $i$  and iSC  $j$  stemming from the optimization method in iteration  $k+1$  of dimension  $N_T^{UE} \times 1$
- $\tilde{\mathbf{x}}'_j(k+1)$ : instantaneous local estimate of UE message at iSC  $j$  in iteration  $k+1$  of dimension  $N_T^{UE} \times 1$
- $\mathbf{y}_j$ : observation of UE message at iSC  $j$  of dimension  $N_R^{isc} \times 1$

- $\mathbf{H}_j$ : channel matrix between the UE and iSC  $j$  of dimension  $N_R^{iSC} \times N_T^{UE}$
- $\mathcal{N}_j$ : set of neighbors of iSC  $j$
- $\mathcal{N}'_j = \mathcal{N}_j \cup \{j\}$ : set of neighbours of iSC  $j$  including iSC  $j$
- $\mu$ : step-size parameter

The algorithm starts by initializing the variable  $\tilde{\mathbf{x}}'_j(0)$  according to (4.10) with  $\tilde{\mathbf{z}}'_j(0) = \boldsymbol{\lambda}_{ji}(0) = 0$  for all iSCs:

$$\tilde{\mathbf{x}}'_j(0) = \left( \mathbf{H}_j^H \mathbf{H}_j + \frac{|\mathcal{N}_j| + 1}{\mu} \mathbf{I}_N \right)^{-1} \cdot \mathbf{H}_j^H \mathbf{y}_j. \quad (4.11)$$

The initialized value  $\tilde{\mathbf{x}}'_j(0)$  represents the local instantaneous estimate at iSC  $j$  without any exchange of information among the iSCs. In the first iteration, the Lagrange multipliers  $\boldsymbol{\lambda}_{ij}(1)$  are calculated using (4.8). These calculations are done in parallel at all iSCs. After that, the Lagrange multipliers  $\boldsymbol{\lambda}_{ij}(1)$  are exchanged among neighbouring iSCs in order to calculate the intermediate estimates  $\tilde{\mathbf{z}}'_j(1)$  at each iSC according to (4.9). Then the intermediate estimates are exchanged among all neighbouring iSCs in order to update the local instantaneous estimates  $\tilde{\mathbf{x}}'_j(1)$  according to (4.10) ending the first iteration. In the second iteration these estimates are exchanged among all neighbouring iSCs and the local Lagrange multipliers  $\boldsymbol{\lambda}_{ij}$  are updated according to (4.8). This procedure is conducted iteratively until the algorithm is stopped or a certain stopping criterion is met. Consequently, in each iteration each iSC  $j$  needs to transmit its local variables  $\tilde{\mathbf{x}}'_j$ ,  $\boldsymbol{\lambda}_{ji}$ , and  $\tilde{\mathbf{z}}'_j$  to its neighbouring iSCs after they have been updated. It can be shown that all estimates  $\tilde{\mathbf{x}}'_j(k)$  converge to the central LS solution so that after convergence all iSCs will have the same estimate fulfilling the consensus constraint in (4.6) [2].

In comparison to the centralized approach (4.4), the ZF-DiCE algorithm establishes a more flexible and robust scheme since it does not solely depend on the functionality of one central node. In case of a connection loss between two iSCs, the information about the received user signal of these iSCs can still be used for the estimation since the iSCs might have stable connections to other iSCs in the network. Thus, the iSCs can forward their received user signal to other iSCs in order to preserve this information in the network. In contrast, in the centralized approach a connection loss between the RANaaS and an iSC would directly lead to an information loss. Consequently, the information of this iSC would not be included into the estimation process in the RANaaS lowering the estimation performance. However, to enhance the robustness of the centralized scheme, the J2 interface connecting iSCs could also be used in order to enable an exchange of receive signals among the iSCs. The receive signal of this iSC could be forwarded to the RANaaS via a stable connection to another iSC. However, this would require a more complicated routing protocol for the iSCs and result in a higher load on the J1 backhaul link to the RANaaS.

Due to the iterative estimation process in the ZF-DiCE algorithm, high data rates on the J2 backhaul links between iSCs and low latency for the processing at iSCs are required in order to detect a frame within a given time constraint. Furthermore, the overall transmission overhead is likely to be increased in comparison to the centralized scheme since the iSCs need to exchange information with each other. Of course, this overhead depends on the number of iterations which is required for an acceptable detection performance. However, the load on the J1 backhaul link to the RANaaS is reduced considerably since only a single iSC needs to transmit the estimated signal to the RANaaS. Additionally, the overall computational complexity is distributed over all iSCs and thus, not solely contained in the RANaaS.

### Multi-User Detection Scenario

In the following, the application of the ZF-DiCE algorithm to a multi-user scenario will be presented as investigated in [5]. Figure 4-3 depicts an exemplary multi-user uplink scenario with  $N_{UE} = 2$  UEs and  $N_{iSC} = 3$  connected iSCs. The UEs are assumed to be scheduled on the same time and frequency resources, e.g. by the RRM for INP scheme investigated in CT3.8. As can be seen, each iSC receives signals

from both UE 1 and UE 2 while the received signal quality is varying depending on the distance between UE and iSC. In order to include the distances between UEs and iSCs into the system model, individual channel gains  $\sigma_{j,u}^2$  per link between iSC  $j$  and user  $u$  are introduced. Subsequently, the system equation for the multi-user scenario is derived. With  $\mathbf{H}_{j,u}$  describing the channel matrices between user  $u$  and iSC  $j$ , the overall channel matrix  $\mathbf{H}_j$  of iSC  $j$  is given by

$$\mathbf{H}_j = [\mathbf{H}_{j,1} \quad \mathbf{H}_{j,2} \quad \cdots \quad \mathbf{H}_{j,N_{UE}}] \quad (4.12)$$

of dimension  $N_R^{iSC} \times N_{UE} N_T^{UE}$ . Furthermore, the complete signal vector  $\mathbf{x}$  contains the transmit vectors  $\mathbf{x}_u$  of all UEs mapped on the same time and frequency resources:

$$\mathbf{x} = \begin{bmatrix} \mathbf{x}_1 \\ \mathbf{x}_2 \\ \vdots \\ \mathbf{x}_{N_{UE}} \end{bmatrix}. \quad (4.13)$$

The transmission from all UEs to one iSC  $j$  can then be formulated by

$$\mathbf{y}_j = [\mathbf{H}_{j,1} \quad \mathbf{H}_{j,2} \quad \cdots \quad \mathbf{H}_{j,N_{UE}}] \cdot \begin{bmatrix} \mathbf{x}_1 \\ \mathbf{x}_2 \\ \vdots \\ \mathbf{x}_{N_{UE}} \end{bmatrix} + \mathbf{n}_j = \mathbf{H}_j \mathbf{x} + \mathbf{n}_j. \quad (4.14)$$

With this equation the overall system equation for the transmission from all UEs to all iSCs can be expressed by

$$\mathbf{y} = \begin{bmatrix} \mathbf{y}_1 \\ \vdots \\ \mathbf{y}_{N_{iSC}} \end{bmatrix} = \begin{bmatrix} \mathbf{H}_{1,1} & \cdots & \mathbf{H}_{1,N_{UE}} \\ \vdots & \ddots & \vdots \\ \mathbf{H}_{N_{iSC},1} & \cdots & \mathbf{H}_{N_{iSC},N_{UE}} \end{bmatrix} \cdot \begin{bmatrix} \mathbf{x}_1 \\ \vdots \\ \mathbf{x}_{N_{UE}} \end{bmatrix} + \begin{bmatrix} \mathbf{n}_1 \\ \vdots \\ \mathbf{n}_{N_{iSC}} \end{bmatrix} = \mathbf{H} \mathbf{x} + \mathbf{n}. \quad (4.15)$$

Similar to the single-user case, the centralized LS problem (4.3) can be formulated and solved either in a central or in a distributed fashion. For the central solution the Moore-Penrose pseudoinverse of matrix  $\mathbf{H}$  of dimension  $N_{iSC} N_R^{iSC} \times N_{UE} N_T^{UE}$  has to be calculated which is computationally complex task. In this case, each iSC  $j$  needs to transmit its observation vector  $\mathbf{y}_j$  and the channel matrix  $\mathbf{H}_j$  to the central unit. Obviously, this will cause a high traffic load on the J1 backhaul links. For the distributed calculation the ZF-DiCE executes (4.8) to (4.10) iteratively and estimates all UE messages within one vector  $\tilde{\mathbf{x}}'_j$  for each iSC  $j$  using the observation vector  $\mathbf{y}_j$ .

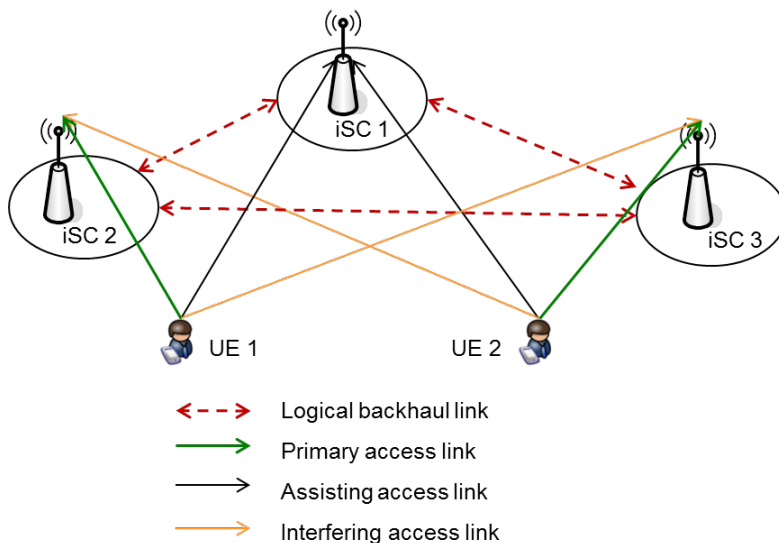


Figure 4-3: Multi-user detection via In-Network Processing among iSCs

## 4.1.2 Assumptions and Requirements

### Assumptions:

- Dense deployment of iSCs with small distance, larger distance between iSC and RANaaS
- J1 interface connecting iSCs and RANaaS for a transmission of estimated UE signals to the RANaaS
- J2 interface connecting iSCs for an exchange of information among iSCs
- UEs in close range to multiple connected iSCs
- Knowledge of local receive CSI at iSCs

### Requirements:

- High data rate on J2 interface for exchange of information among iSCs
- Low latency regarding processing time at iSCs since INP requires several iterations per UE frame
- Perfect synchronization between all iSCs

## 4.1.3 Preliminary Results

### Convergence Speed

In the following, the convergence speed of the ZF-DiCE algorithm is analysed for the case of  $N_{UE}=1$  UE with  $N_T^{UE}=2$  transmit antennas and  $N_{iSC}=3$  iSCs with  $N_R^{iSC}=2$  receive antennas each. All iSCs are connected to each other so that a ring topology is set up. The ZF-DiCE algorithm is compared to the DC-DS algorithm from [96], which is also based on a zero forcing solution with a consensus constraint.

Figure 4-4 shows the CDF  $F(k_{req})$  of the required number of iterations  $k_{req}$  until convergence over 1000 random realizations of UE messages, the channels and the noise for the ZF-DiCE and the DC-DS algorithm. The channel matrices  $\mathbf{H}_j$  of dimension  $N_R^{iSC} \times N_T^{UE}$  each contain real valued, i.i.d. and zero mean normal distributed coefficients. The same is true for the entries of the noise vectors  $\mathbf{n}_j$  and the message vector  $\mathbf{x}$ . The noise power  $\sigma_n^2$  is set accordingly to an SNR of 10dB. Both algorithms are analysed for two backhaul channel models. In the first model all backhaul links between the iSCs are ideal and stable for all considered iterations so that information exchange among iSCs is performed error-free. Thus the set of neighbours  $\mathcal{N}_j$  for each iSC  $j$  remains the same throughout the iterative estimation procedure. In the second model, backhaul links are still ideal but connections among iSCs are not stable anymore. Thus in each iteration connections can be lost with a certain probability. Here, the set of neighbours  $\mathcal{N}_j(k)$  for each iSC  $j$  can vary with the iteration  $k$ . The probability of a connection loss is set to 40% for each backhaul link. Consequently, an exchange of information among iSCs can be interrupted due to a connection loss. However, if a backhaul link is available, information is exchanged error-free for this iteration. For this backhaul channel model both the ZF-DiCE as well as the DC-DS algorithm are adapted in order to encounter possible connection losses among iSCs and to still maintain convergence to the central LS solution. For the ZF-DiCE algorithm, (4.8) and (4.10) are modified to include the current set of neighbours  $\mathcal{N}_j(k)$ :

$$\tilde{\mathbf{z}}'_j(k+1) = \frac{\mu}{|\mathcal{N}_j(k)|+1} \sum_{i \in \mathcal{N}_j(k) \cup \{j\}} \left( -\lambda_{ij}(k+1) + \frac{\tilde{\mathbf{x}}'_i(k)}{\mu} \right), \quad (4.16)$$

$$\tilde{\mathbf{x}}'_j(k+1) = \left( \mathbf{H}_j^H \mathbf{H}_j + \frac{|\mathcal{N}_j(k)|+1}{\mu} \mathbf{I}_N \right)^{-1} \cdot \left[ \mathbf{H}_j^H \mathbf{y}_j + \sum_{i \in \mathcal{N}_j(k) \cup \{j\}} \left( \lambda_{ji}(k+1) + \frac{\tilde{\mathbf{z}}'_i(k+1)}{\mu} \right) \right]. \quad (4.17)$$

Furthermore, for both algorithms the Lagrange multipliers  $\lambda_{ij}(k)$  from neighbouring iSCs are saved for one iteration at each iSC. If a connection loss to an iSC occurs in iteration  $k+1$ , the temporarily saved Lagrange multipliers from the last iteration  $k$  are used for calculating (4.16) and (4.17) following the procedures presented in [148].

Regarding the convergence criterion we examine the augmented Lagrangian cost function of the optimization problem in (4.7) for each iSC  $j$ . It contains the LS cost, the constraint terms from (4.7) as well as the squared constraint terms:

$$\mathcal{L}_j(k) = \frac{1}{2} \|\mathbf{y}_j - \mathbf{H}_j \tilde{\mathbf{x}}'_j(k)\|^2 - \sum_{i \in \mathcal{N}'_j} \lambda_{ji}^T(k) (\tilde{\mathbf{x}}'_j(k) - \tilde{\mathbf{z}}'_j(k)) + \sum_{i \in \mathcal{N}'_j} \frac{1}{2\mu} \|\tilde{\mathbf{x}}'_j(k) - \tilde{\mathbf{z}}'_j(k)\|^2 \quad (4.18)$$

We assume a consensus among all iSCs if the squared norm of the gradient of the cost function between two iterations is below a certain threshold  $\tau$  over all iSCs:

$$\sum_{j=1}^{N_{iSC}} \left\| \nabla_{\tilde{\mathbf{x}}'_j(k)} \mathcal{L}_j(k) \right\|^2 < \tau \quad (4.19)$$

In this case, it can be assumed that the minimum cost has been achieved since the cost function does not change significantly. This indicates that the central solution has been closely reached by all iSCs and the algorithm is stopped. In the implementation a threshold of  $\tau = 10^{-4}$  has been used for the squared norm of the gradient of the cost function between two iterations.

In Figure 4-4, it can be seen that for stable backhaul links the ZF-DiCE algorithm converges faster than the DC-DS algorithm. This is due to the additionally exchanged variable in the ZF-DiCE algorithm, namely the intermediate estimate  $\tilde{\mathbf{z}}'_j$  which increases the convergence speed. However, the additional variable will also result in a higher backhaul load on the J2 interface. Since each iSC needs to additionally exchange its intermediate estimate  $\tilde{\mathbf{z}}'_j$ , the number of transmissions among the iSCs is increased by  $N_{iSC}$  per iteration. For the case of unstable backhaul links among iSCs, a more robust behaviour of the adapted ZF-DiCE algorithm can be observed. While the adapted DC-DS algorithm is slowed down by connection losses, the convergence speed of the ZF-DiCE algorithm even shows a slightly faster convergence compared to the case of stable links. This behaviour of the ZF-DiCE algorithm is also due to the intermediate estimate  $\tilde{\mathbf{z}}'_i$ , by which not only information of direct neighbours at a specific iSC is included but also information of two-hop distant iSCs. Thus, a connection loss can be compensated by incorporating information via a stable two-hop connection of other neighbouring iSCs.

A faster convergence compared to stable links occurs due to a different initialization of the adapted ZF-DiCE algorithm. In the case of stable links, the initialization according to (4.11) is used. For unstable links, the update equations (4.8) and (4.10) are modified to (4.16) and (4.17) such that the instantaneous neighbourhood  $\mathcal{N}_j(k)$  is considered. Consequently, the initial estimate  $\tilde{\mathbf{x}}'_j(0)$  is changed to:

$$\tilde{\mathbf{x}}'_j(0) = \left( \mathbf{H}_j^H \mathbf{H}_j + \frac{|\mathcal{N}_j(0)| + 1}{\mu} \mathbf{I}_N \right)^{-1} \cdot \mathbf{H}_j^H \mathbf{y}_j. \quad (4.20)$$

Since the cardinality of the instantaneous neighbourhood  $|\mathcal{N}_j(k)|$  is always smaller or equal to the general neighbourhood  $|\mathcal{N}_j|$  when no connection losses occur, the initial estimate as well as the instantaneous estimates can be closer to the central solution for unstable links. This is due to the regularized pseudoinverse in (4.17) which resembles the MMSE solution and is variable for each iteration  $k$  depending on the current neighbourhood of each iSC  $j$ . Thus the algorithm can be faster in terms of convergence for the case of unstable links. On the other hand, there can be also cases where the initial estimate is further away from the central solution such that the convergence is slowed down by connection losses. According to Figure 4-4 this case occurs less often compared to the case of a faster convergence for unstable links. This behaviour needs to be investigated in the future.

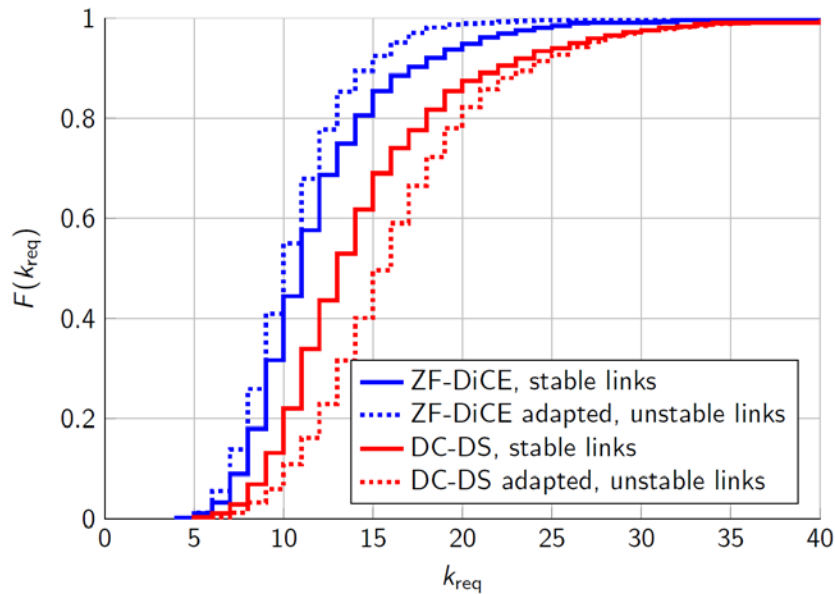


**Figure 4-4: CDF of the required iterations until convergence of the ZF-DiCE and the DC-DS algorithm for a ring topology**

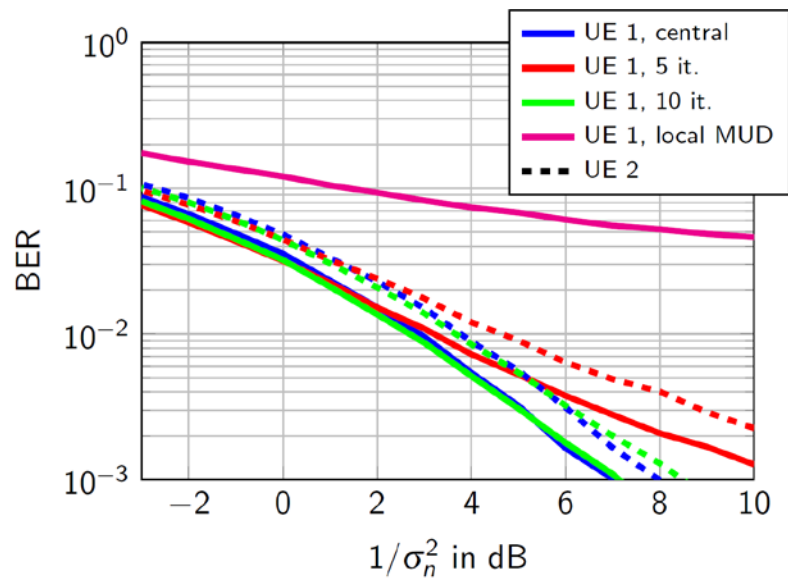
### ZF-DiCE Algorithm for MUD

For MUD via INP, we consider  $N_{iSC} = 3$  iSCs and  $N_{UE} = 2$  UEs as a generic scenario. We assume connections among all iSCs so that each iSC is able to exchange information with every other iSC. Each UE transmits unit power BPSK symbols on each of their  $N_T^{UE}$  transmit antennas. The transmission is done without any channel coding. In order to detect the transmitted bits a hard decision according to the sign of the local estimates  $\tilde{\mathbf{x}}'_j$  is used at all iSCs after the algorithm is stopped. We assume Rayleigh fading for each channel matrix  $\mathbf{H}_{j,u}$ . Furthermore, we assign the following individual channel gains between iSC  $j$  and UE  $u$ :

$$[\sigma_{j,u}^2] = \begin{bmatrix} 0.1 & 0.15 \\ 1 & 0.2 \\ 0.5 & 1 \end{bmatrix}. \quad (4.21)$$

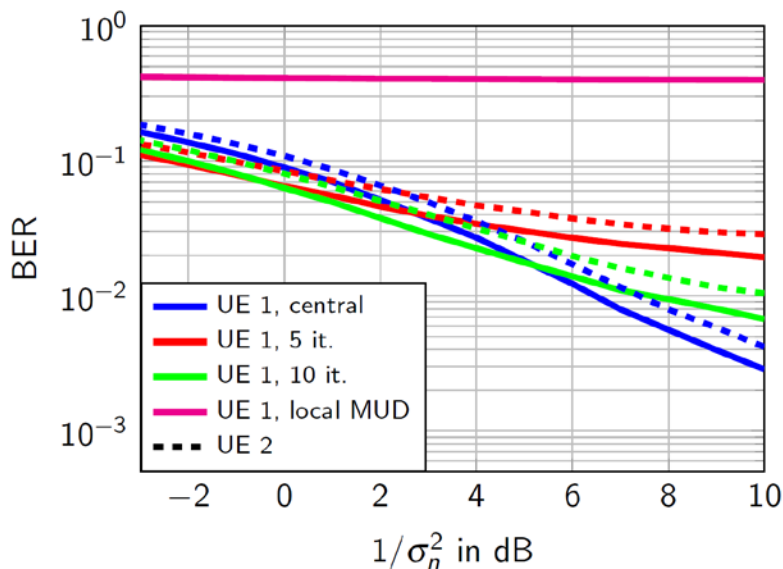
Accordingly, UE 1 has a primary access link to iSC 2 whereas UE 2 appears as an interferer. The opposite case is true at iSC 3. At iSC 1 both UEs appear with nearly equal channel gains so that both UEs have an assisting access link to iSC 1.

Figure 4-5 shows the resulting bit error rate (BER) over the noise power  $\sigma_n^2$  for  $N_T^{UE} = 2$  transmit antennas per UE and  $N_R^{iSC} = 4$  receive antennas per iSC, i.e. every iSC itself is able to separate both UEs spatially. We show the BER results for the ZF-DiCE algorithm after  $N_{it} = 5$  and 10 iterations, respectively. For reference, the BER of the central LS solution as well as the result of a non-cooperative local MUD at iSC 2 based on linear ZF equalization are depicted. As can be seen, for 10 iterations the ZF-DiCE algorithm achieves the BER performance of the central LS solution for both UEs. For 5 iterations, the BER performance degrades significantly. For both UE 1 and UE 2 an SNR loss of approximately 2dB for a BER of  $10^{-3}$  is observable indicating that more iterations are necessary to exploit the cooperation among iSCs. The local MUD without cooperation among iSCs is not able to achieve satisfying BER performances.



**Figure 4-5: BER for 2 UEs transmitting  $N_T^{UE} = 2$  spatial layers each and 3 receiving iSCs with  $N_R^{iSC} = 4$  antennas each**

Figure 4-6 depicts the BER performance for  $N_T^{UE} = 4$  transmit antennas. In this setup, each iSC itself is not able to spatially separate the user signals resulting in a constant BER for local MUD. As the initialization (4.11) of the INP approach equals a local linear equalization, the performance of the ZF-DiCE algorithm is degraded by a relatively bad initial estimate. Thus, 5 iterations are not sufficient to achieve performance close to the central solution. After 10 iterations the performance is improved significantly, however still a gap of approximately 3 dB compared to the central solution at a BER of  $7 \cdot 10^{-3}$  can be observed. Thus, more iterations are necessary for convergence of the ZF-DiCE in order to obtain the central solution. Interestingly, the ZF-DiCE algorithm outperforms the central solution for low SNR. This is due to the fact, that the update equation (4.10) of the instantaneous estimates  $\tilde{\mathbf{x}}'_j$  contains a regularization term similar to the MMSE solution.



**Figure 4-6: BER for 2 UEs transmitting  $N_T^{UE} = 4$  spatial layers each and 3 receiving iSCs with  $N_R^{iSC} = 4$  antennas each**

## Conclusion and Outlook

The preliminary results show that cooperation among iSCs for distributed MUD achieves significant performance gains compared to local processing at iSCs. Furthermore, the performance of the central LS solution can be achieved by the ZF-DiCE algorithm with a certain number of iterations depending on the

system setup. In comparison to the DC-DS algorithm from [96], the ZF-DiCE algorithm shows a faster convergence requiring less iterations. The number of required iterations is important regarding the data rate and latency demands and the load on the J2 backhaul links between connected iSCs. For the backhaul channel model including connection losses among iSCs a robust behaviour can be observed for the adapted ZF-DiCE algorithm compared to the adapted DC-DS algorithm.

For further investigations, an extension of the ZF-DiCE algorithm to the MMSE criterion will be analysed. Moreover, methods reducing the data exchange among the iSCs will be investigated. Some preliminary results have already been published in [6]. These methods can decrease the backhaul load on the J2 links between the iSCs.

## 4.2 CT 2.2: Multi-Point Turbo Detection

### 4.2.1 Description

#### Scenario

This scenario investigates the benefit of relying on the turbo detection principle to increase the (aggregated) user throughput in the uplink direction. In a dense small cell deployment, one user can more easily see other small cells in addition to its serving one (especially if he is at the edge of the cell). Under such deployment, if co-channel is used due to limited spectrum, classical approaches tend to create orthogonality in the frequency domain for OFDM-based systems, e.g. through soft or fractional frequency reuse patterns among neighbouring small cells [105]-[110]. By nature, these frequency partitioning schemes reduce the spectrum available for transmission, meaning less maximum throughput achievable in theory.

By scheduling the (edge) users on the same resources and exploiting the created interference as a source of information through the turbo detection principle in each concerned small cell, the (aggregated) throughput of the system should be improved, as “more” spectrum and diversity are made available.

The turbo detection could be performed in each small cell with or without data information exchange between the iSCs through the J2 interface: we talk about Single-Point Turbo Detection (SPTD). The turbo detection could also be performed in the RANaaS platform if the J1 interface toward it supports the data transfer (e.g. raw I/Q samples) and the latency requirements: we talk about Multi-Point Turbo Detection (MPTD).

The investigation will evaluate the performance provided by the SPTD/MPTD methods and try to identify the amount and the type of information to be exchanged to allow a scalable application of this algorithm based on the iSC/RANaaS and/or iSC/iSC links' capability. In order to do so, the deployment shown in Figure 4-7 will be investigated to perform link-level simulations. In this setup, two iSCs are connected to the RANaaS platform through the J1 interface and to each other through the J2 interface. One UE is connected to one iSC. For simplicity, UE 1 is attached to iSC 1 and UE 2 is attached to iSC 2. Both UEs are scheduled on the same resources such that they interfere with each other at their serving cell.

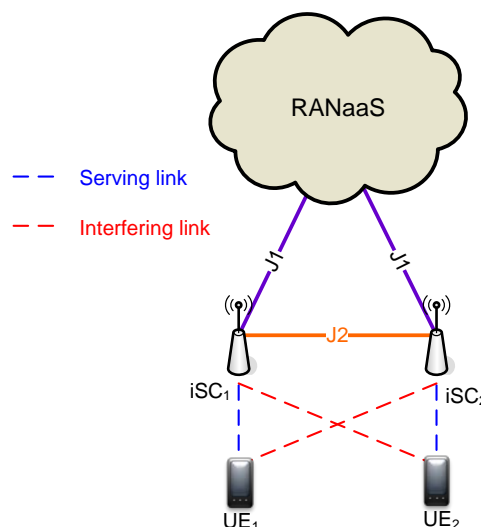
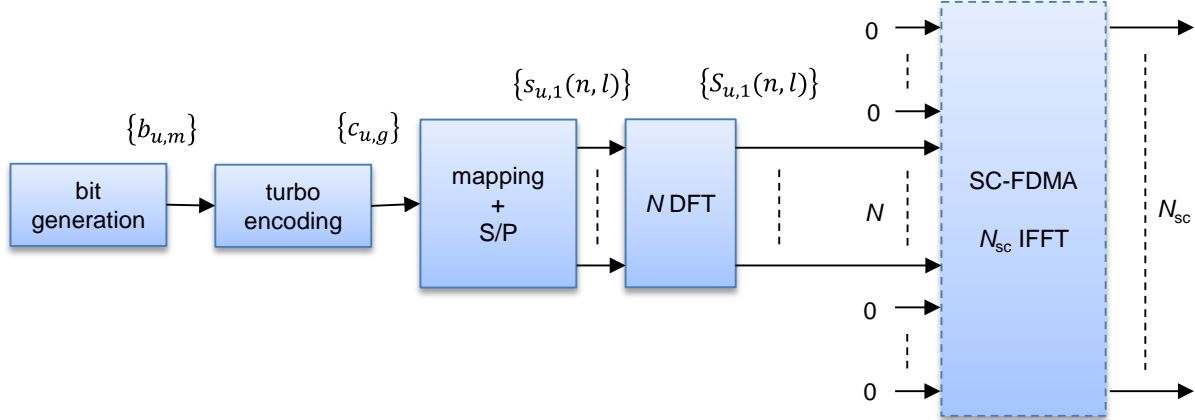


Figure 4-7: Multi-point turbo detection investigation context

### System model

We consider an LTE Release 10 system, where each UE  $u$  is equipped with  $N_T^{UE,u}$  transmit antenna and each iSC  $v$  is equipped with  $N_R^{iSC,v}$  receive antennas. In practice, UEs are often equipped with one transmit antenna while small cells have 2 receive antennas. In the following, we will assume that UEs have only one transmit antennas, i.e.  $N_T^{UE,u} = N_T^{UE} = 1$ . If only Physical Uplink Shared Channel (PUSCH) transmissions are considered, the baseband transmitter of UE  $u$  is given by Figure 4-8, where:

- $N_{sc}$  is the total number of subcarriers associated to the LTE system (e.g.  $N_{sc} = 600$  for a 10MHz bandwidth),
- $N$  is the number of allocated subcarriers for one subframe transmission (e.g.  $N = 12$  for 1 resource block (RB)),
- $L$  is the number of SC-FDMA symbols allocated for PUSCH transmission in one subframe (e.g.  $L = 12$  for a normal cyclic prefix in a subframe without sounding reference signal),
- $\{b_{u,m}\}_{1 \leq m \leq TBS_u}$  is the data bit vector of Transport Block Size (TBS) length  $TBS_u$  to be sent in one subframe,
- $\{c_{u,g}\}_{1 \leq g \leq G_u}$  is the coded bit vector after turbo encoding (compliant with the Rel.10 [91]) of length  $G_u = Q_u NL$ , where  $Q_u$  is the modulation order associated to the MCS chosen by the scheduling,
- $\{s_u(n,l)\}_{1 \leq n \leq N, 1 \leq l \leq L}$  is the time domain symbol matrix of size  $N \times L$  after mapping (compliant with the Rel.10 [84]) and serial-to-parallel (S/P) shaping (columns are filled first), each column will go through an  $N$ -DFT transform,
- $\{S_u(n,l)\}_{1 \leq n \leq N, 1 \leq l \leq L}$  is the frequency domain symbol matrix of size  $N \times L$  after  $N$ -DFT.



**Figure 4-8: UE (1Tx) baseband transmitter (PUSCH only)**

The DFT symbol transmitted on the  $n^{\text{th}}$  subcarrier for the  $l^{\text{th}}$  SC-FDMA symbol is given by:

$$S_u(n,l) = \frac{1}{\sqrt{N}} \sum_{i=0}^{N-1} s_u(i,l) e^{-j \frac{2\pi i n}{N}}. \quad (4.22)$$

Let  $P_u$  be the average power of a modulation symbol  $s_u(n,l)$ , then the DFT symbol  $S_u(n,l)$  has the same average power.

$$\mathbb{E}\left[|s_u(n,l)|^2\right] = \mathbb{E}\left[|S_u(n,l)|^2\right]. \quad (4.23)$$

If only PUSCH transmissions are considered, then  $(N_{sc} - N)$  zeros are added to each column before the  $N_{sc}$ -IFFT block which marks the ending of the SC-FDMA generation process for one symbol (with the

addition of the cyclic prefix). LTE precoding introduced in Release 10 (i.e. layer to antenna port mapping) is not mentioned here as it will only add a precoding matrix which could be integrated to the channel model.

For simplicity and without loss of accuracy, the SC-FDMA generation block (including cyclic prefix addition) is not simulated allowing a direct modelling of the channel in the frequency domain. Let us consider the  $n^{\text{th}}$  subcarrier allocated in the  $l^{\text{th}}$  SC-FDMA symbol, then the associated channel between UE  $u$  and iSC  $v$  can be modelled for this resource element in the frequency domain by a  $N_R^{\text{iSC},v} \times 1$  column vector  $\mathbf{H}^{v,u}(n,l) = \{H_r^{v,u}(n,l)\}_{1 \leq r \leq N_R^{\text{iSC},v}}$ .

Figure 4-9 shows this channel modelling with a one transmit-two receive configuration, with a focus on the signal received by iSC 1 only (similar modelling is valid for iSC 2).

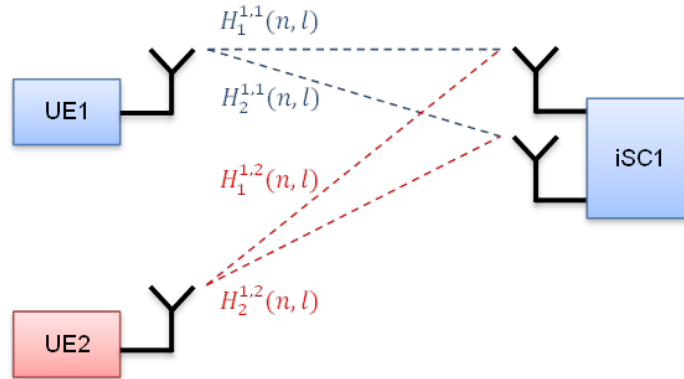


**Figure 4-9: Channel model for resource element (n,l) (1Tx, 2Rx)**

The received signal associated to the resource element  $(n,l)$  at iSC  $v$  can then be written by:

$$\mathbf{Y}^v(n,l) = \sum_u \mathbf{H}^{v,u}(n,l)S_u(n,l) + \mathbf{N}^v(n,l) \quad (4.24)$$

where  $\mathbf{N}^v(n,l) = \{N_r^v(n,l)\}_{1 \leq r \leq N_R^{\text{iSC},v}}$  is an  $N_R^{\text{iSC},v}$ -length vector capturing the thermal noise and the interference of other users scheduled on the same resource (not represented here) where each element follows a normal distribution law of variance  $\sigma^2$ .

Three receiving strategies will be investigated in order to be able to recover the transmitted symbols from the received signals (either locally or centrally).

### Baseline (advanced) receiver

The MMSE receiver with interference rejection combining (IRC) at each iSC is our baseline receiver. We assume that the iSC  $v$  has at disposal the channel state information (CSI)  $\mathbf{H}^{v,u}(n,l)$  of its served UE  $u$  (obtained thanks to the demodulation reference signal (DMRS)) and the CSI  $\mathbf{H}^{v,u'}(n,l)$  of its dominant interfering UE  $u'$ . All other interfering contributions (less dominant UEs on the same resources, thermal noise ...) are captured by the AWGN modelling of variance  $\sigma^2$ .

Errors in the CSI estimation are not considered and a minimum coordination is assumed in order for iSC  $v$  to be able to acquire the CSI of one UE which is not attached to it (e.g. J2 interface toward its serving iSC could be used to exchange such information or DMRS of this UE could be exploited by the iSC directly). The details of the coordination needed are left for further studies.

Figure 4-10 describes the MMSE-IRC receiver operated at iSC  $v$  to detect the data sent by UE  $u$ .

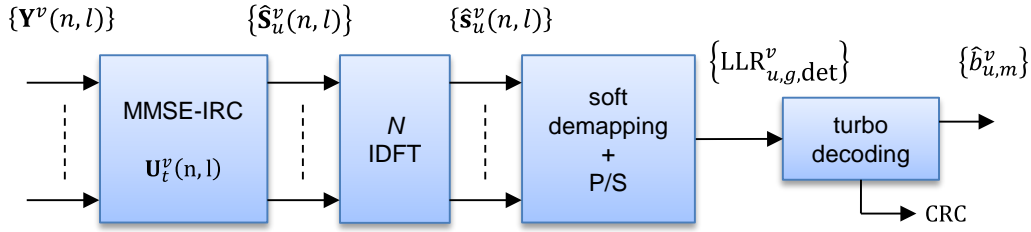


**Figure 4-10: MMSE-IRC receiver chain at iSC  $v$  for UE  $u$**

At iSC  $v$ , the unbiased MMSE-IRC linear filter  $\mathbf{U}_u^v(n,l)$  used for detecting the symbol sent by UE  $u$  on the resource element  $(n,l)$  is given by:

$$\mathbf{U}_u^v(n,l) = \frac{1}{\eta_u^v(n,l)} \mathbf{A}_u^v(n,l) \mathbf{H}^{v,u}(n,l) \quad (4.25)$$

$$\mathbf{A}_u^v(n,l) = \left[ P_u \mathbf{H}^{v,u}(n,l) \mathbf{H}^{v,u}(n,l)^H + P_{u'} \mathbf{H}^{v,u'}(n,l) \mathbf{H}^{v,u'}(n,l)^H + \sigma^2 \mathbf{I}_{N_R^{iSC,v}} \right]^{-1} \quad (4.26)$$

$$\eta_u^v(n,l) = \mathbf{H}^{v,u}(n,l)^H \mathbf{A}_u^v(n,l) \mathbf{H}^{v,u}(n,l) \quad (4.27)$$

where  $\mathbf{I}_{N_R^{iSC,v}}$  is the identity matrix of dimension  $N_R^{iSC,v}$ ,  $P_u = \mathbb{E}[|S_u(n,l)|^2]$  and  $P_{u'} = \mathbb{E}[|S_{u'}(n,l)|^2]$  are the average transmit powers of a modulation symbol from UE  $u$  and  $u'$ , respectively. Since we used an unbiased filter, we can show that the estimation of the transmitted symbol in the frequency domain can be expressed by:

$$\hat{S}_u^v(n,l) = \mathbf{U}_u^v(n,l)^H \mathbf{Y}^v(n,l) = S_u(n,l) + \Theta_u^v(n,l). \quad (4.28)$$

The residual noise from filtering has a variance which can be expressed by:

$$\mathbb{E}\left[|\Theta_u^v(n,l)|^2\right] = \frac{1}{\eta_u^v(n,l)} - P_u. \quad (4.29)$$

This variance will be used in the time domain for the soft demapping of the estimated symbol  $\hat{S}_u^v(n,l)$ , obtained after the normalized  $N$ -IDFT stage:

$$\hat{s}_u(n,l) = \frac{1}{\sqrt{N}} \sum_{i=0}^{N-1} \hat{S}_u(i,l) e^{j \frac{2\pi i n}{N}}. \quad (4.30)$$

LLRs obtained after the soft demapping  $\left\{ \text{LLR}_{u,g,\text{det}}^v \right\}_{1 \leq g \leq G_u}$  will feed the turbo decoder [97], which implements the max-log-map form of the BCJR algorithm [111]. The process within the turbo decoder is optimised to take into account the CRC added during the MCS generation process [91]. Indeed, the iterative decoding process can be stopped before reaching the maximum number of iterations allowed in case of a successful CRC at the end of one iteration. Hard outputs  $\left\{ \hat{b}_{u,m}^v \right\}_{1 \leq m \leq \text{TBS}_u}$  representing the data transmitted are provided by the turbo decoder stage to the upper layers along with the associated CRC result: OK/ Not OK.

### Single-Point Turbo Detection

If the iSC  $v$  knows in top of the previous assumptions which MCS is used by the interfering UE(s) allocated on the same resources as UE  $u$ , then it can attempt locally a (single point) turbo detection procedure which will result in the estimation of the transmission of all UEs. The principle of the turbo detection (or iterative interference cancellation) is depicted in Figure 4-11.

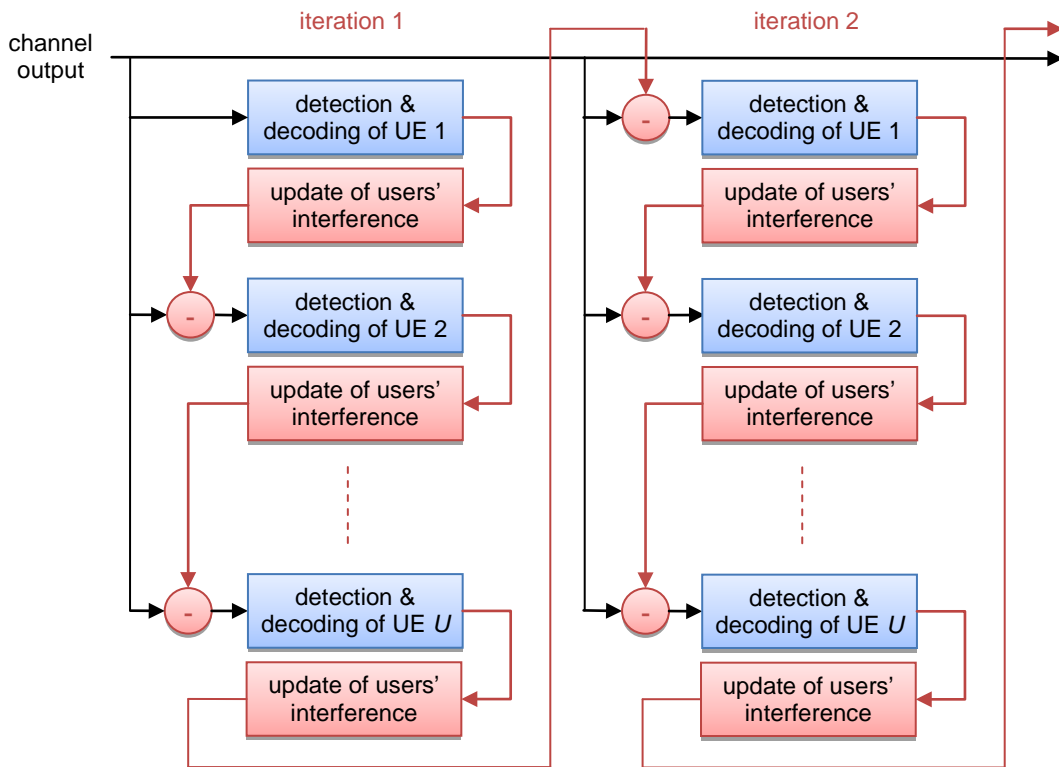


**Figure 4-11: Iterative interference cancellation principle (assuming natural ordering)**

The turbo detection principle consists of the detection of all spatial streams associated to one codeword of a given UE, the soft-input soft-output decoding of this codeword, and the reconstruction of all streams associated to this codeword in a soft manner in order for them to be subtracted from the received signal for the next UE’s codeword detection or next UE’s detection. Those operations are performed in an iterative way with information exchange of extrinsic information between the various block involved, hence the “turbo” name. In our case, one UE only sends one stream/codeword through its single antenna.

Figure 4-12 describes the iterative MMSE-IC receiver operated at iSC  $v$ .

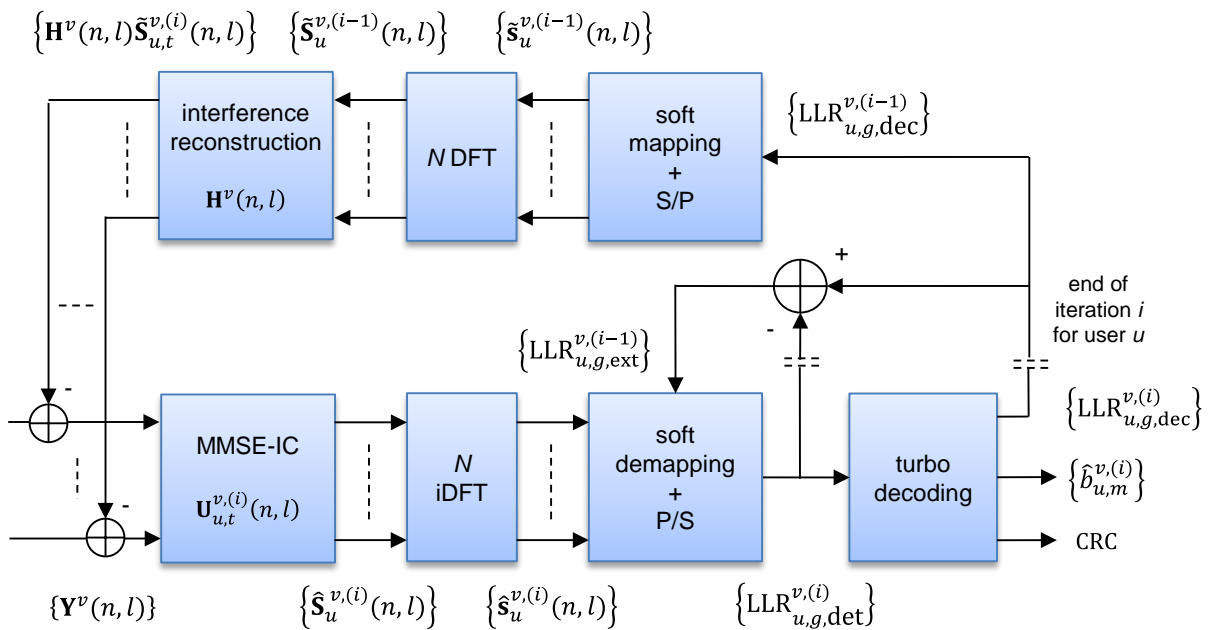


**Figure 4-12: Iterative MMSE-IC receiver chain at iSC  $v$**

Let  $N_t$  be the number of turbo detection iteration, and  $N_{UE}$  be the number of UEs to be detected by the iSC  $v$ . For the detection to be envisaged, the number of receive antennas of iSC  $v$  should be greater or equal to the sum of all transmit antennas of the considered UEs:

$$N_R^{iSC,v} \geq \sum_{u=1}^{N_{UE}} N_T^{UE,u}. \quad (4.31)$$

On subcarrier  $n$ , SC-FDMA symbol  $l$ , the equivalent channel matrix which includes all the transmitting UEs  $\mathbf{H}^v(n,l)$  of size  $N_R^{iSC,v} \times N_{UE}$  is given by:

$$\mathbf{H}^v(n,l) = \begin{bmatrix} \mathbf{H}^{v,1}(n,l) & \dots & \mathbf{H}^{v,N_{UE}}(n,l) \end{bmatrix}. \quad (4.32)$$

The received signal at iSC  $v$  can be rewritten according to the following equation:

$$\mathbf{Y}^v(n,l) = \sum_{u=1}^{N_{UE}} \mathbf{H}^{v,u}(n,l) S^u(n,l) + \mathbf{N}^v(n,l) = \mathbf{H}^v(n,l) \begin{bmatrix} S^1(n,l) \\ \vdots \\ S^U(n,l) \end{bmatrix} + \mathbf{N}^v(n,l) = \mathbf{H}^{v,u}(n,l) \mathbf{S}(n,l) + \mathbf{N}^v(n,l). \quad (4.33)$$

where  $\mathbf{S}(n,l)$  is the aggregated  $N_{UE}$ -length vector of symbols transmitted by the  $N_{UE}$  UEs (in the frequency domain).

For simplicity reason, we assume a natural order detection of the users per iteration. At iteration  $i$ , a linear unbiased MMSE-IC receiver  $\mathbf{U}_u^{v,(i)}(n,l)$  is used to detect the stream of user UE  $u$  on subcarrier  $n$ , SC-FDMA symbol  $l$ .

$$\mathbf{U}_u^{v,(i)}(n,l) = \frac{1}{\eta_u^{v,(i)}(n,l)} \mathbf{A}_u^{v,(i)}(n,l) \mathbf{H}^v(n,l) \mathbf{e}_u \quad (4.34)$$

$$\mathbf{A}_u^{v,(i)}(n,l) = \left[ \mathbf{H}^v(n,l) \Gamma_u^{v,(i)} \mathbf{H}^v(n,l)^H + \sigma^2 \mathbf{I}_{N_R^{iSC,v}} \right]^{-1} \quad (4.35)$$

$$\eta_u^{v,(i)}(n,l) = \mathbf{e}_u^H \mathbf{H}^v(n,l)^H \mathbf{A}_u^{v,(i)}(n,l) \mathbf{H}^v(n,l) \mathbf{e}_u \quad (4.36)$$

where  $\mathbf{e}_u$  is a  $N_{UE}$ -length zero vector except at position  $u$  which equals 1 and  $\Gamma_u^{v,(i)}$  is the diagonal covariance symbol matrix at iteration  $i$  defined by:

$$\Gamma_u^{v,(i)} = \text{diag} \left\{ \rho_1^{v,(i)}, \dots, \rho_{u-1}^{v,(i)}, \rho_u^{v,(i-1)}, \dots, \rho_{N_{UE}}^{v,(i-1)} \right\} \quad (4.37)$$

With generic notations,  $\rho_u^{v,(i)}$  is the symbol variance of UE  $u$  estimated by iSC  $v$  at iteration  $i$  and is given by:

$$\rho_u^{v,(i-1)} = \mathbb{E} \left[ \left| S_u(n,l) - \tilde{S}_u^{v,(i)}(n,l) \right|^2 \right] \quad (4.38)$$

where  $\tilde{S}_u^{v,(i)}(n,l)$  is the soft estimation of  $S_u(n,l)$  in iSC  $v$ , after the decoding of the associated codeword at the iteration  $i$  (soft mapping, see below for more details). Note that at the beginning of the turbo detection procedure (first iteration), soft estimation is obviously not available ( $\tilde{S}_u^{v,(0)}(n,l) = 0$ ), leading to  $\rho_u^{v,(0)} = \mathbb{E} \left[ |S_u(n,l)|^2 \right] = P_u$  (leading to the classical MMSE-IRC formula).

The estimation of the symbol transmitted of UE  $u$  is given by:

$$\hat{S}_u^{v,(i)}(n,l) = \mathbf{U}_u^{v,(i)}(n,l)^H \left[ \mathbf{R}^v(n,l) - \mathbf{H}^v(n,l) \bar{\bar{\mathbf{S}}}_u^{v,(i)}(n,l) \right]. \quad (4.39)$$

where  $\bar{\bar{\mathbf{S}}}_u^{v,(i)}(n,l)$  is the aggregated  $N_{UE}$ -length vector representing the soft estimation of the transmitted symbols of the  $N_{UE}$  users, except at the position associated to UE  $u$  which is zero. This vector is used for the interference cancellation part, hence the MMSE-IC name.

$$\bar{\mathbf{S}}_u^{v,(i)}(n,l) = \left[ \tilde{S}_1^{v,(i)}(n,l) \quad \cdots \quad \tilde{S}_{u-1}^{v,(i)}(n,l) \quad 0 \quad \tilde{S}_{u+1}^{v,(i-1)}(n,l) \quad \cdots \quad \tilde{S}_U^{v,(i-1)}(n,l) \right]^T \quad (4.40)$$

Similar to the MMSE-IRC case, the output of this unbiased MMSE-IC filter in the frequency domain can be expressed by:

$$\hat{S}_u^{v,(i)}(n,l) = S_u(n,l) + \Theta_u^{v,(i)}(n,l) \quad (4.41)$$

where  $\Theta_u^{v,(i)}(n,l)$  is the residual noise whom variance is given by:

$$\mathbb{E} \left[ \left| \Theta_u^{v,(i)}(n,l) \right|^2 \right] = \frac{1}{\eta_u^{v,(i)}(n,l)} - \rho_u^{v,(i-1)} \quad (4.42)$$

This value will be used for the soft demapping block in the estimated symbols in the time domain after the  $N$ -IDFT stage. The soft demapping will produce the LLRs  $\left\{ \text{LLR}_{u,g,\text{det}}^{v,(i)} \right\}_{1 \leq g \leq G_u}$  associated to the codeword of UE  $u$  to feed the turbo decoding block. This later block will generate in addition of an estimation of the transmitted bits  $\left\{ \hat{b}_{u,m}^{v,(i)} \right\}_{1 \leq m \leq \text{TBS}_u}$ , an update of the input LLRs after decoding  $\left\{ \text{LLR}_{u,g,\text{dec}}^{v,(i)} \right\}_{1 \leq g \leq G_u}$ . Such process includes partial turbo-encoding operation (essentially the rate matching). The soft demapping block also uses extrinsic information coming from the decoding of the codeword of UE  $u$  at iteration  $i-1$ , defined by  $\text{LLR}_{u,g,\text{ext}}^{v,(i-1)} = \text{LLR}_{u,g,\text{dec}}^{v,(i-1)} - \text{LLR}_{u,g,\text{det}}^{v,(i-1)}$ .

After the decoding process, the LLRs  $\left\{ \text{LLR}_{u,g,\text{dec}}^{v,(i)} \right\}_{1 \leq g \leq G_u}$  will be used to construct a soft estimation of the symbols transmitted  $\left\{ \tilde{s}_u^{v,(i)}(n,l) \right\}_{1 \leq n \leq N, 1 \leq l \leq L}$ , i.e. the soft mapping operation. For simplicity, let's assume that the set of  $2^Q$ -ary modulation symbols is noted  $M_Q$  and that  $\left\{ b_q^m \right\}_{1 \leq q \leq Q}$  is the  $Q$ -tuple of bits associated to the modulation symbol  $m \in M_Q$ . If we have the following  $Q$ -tuple of LLRs  $\left\{ \text{LLR}_q \right\}_{1 \leq q \leq Q}$ , then the associated soft estimation (which is an average conditionally to the LLRs) will be given by:

$$\tilde{m} = \sum_{m \in M_Q} m \Pr(m | \text{LLR}_q) = \sum_{m \in M_Q} m \prod_{q=1}^Q \Pr(b_q^m | \text{LLR}_q) = \sum_{m \in M_Q} m \frac{e^{\sum_{q=1}^Q (2b_q^m - 1) \text{LLR}_q}}{\prod_{q=1}^Q (1 + e^{\text{LLR}_q})}. \quad (4.43)$$

At the end of iteration  $i$  for user  $u$ , its soft modulation symbols are generated in the time domain and will go through the DFT process to be able to construct UE  $u$ 's (soft) contribution and subtract it from the received signal in the iSC  $v$  for the next codeword detection.

As a side note, the J2 interface has not been explicitly exploited yet, which is left for further studies during the course of the project where cooperation as shown in Figure 6-7 could be envisaged.

### Multi-Point Turbo Detection

Previously, the turbo detection process was performed in each iSC. This means that each iSC will decode independently the two UEs in our example given in Figure 4-7. In the iJOIN architecture, the iSCs are supposed to be connected to the RANaaS cloud computing platform through the J1 interface, allowing centralisation processing. Therefore, a single turbo-detection procedure could be envisaged based on the inputs of the multiple iSCs instead of multiple SPTDs attempting the detection of the same transmissions.

Of course to be able to do such centralisation, several requirements are needed on the J1 interface based on the LTE nature of the uplink signals:

- **Extremely low latency:** Due to the synchronous H-ARQ procedure in uplink, 4ms is the time separating an uplink transmission from its acknowledgement [112]. Therefore, the departing of signals, the MUD process and the acknowledge (ACK) /non-acknowledge (NACK) feedback must be done under such strict constraint if LTE-compliance is to be kept without changing the standards. If  $T_{J1}$  is the iSC-RANaaS link latency,  $T_{\text{RANaaS}}$  is the processing time within the RANaaS platform (including getting/putting data from/to the J1 interface), then the J1 latency should be such that:

$$\text{BH}_{\text{lat,req}} = 2T_{J1} + T_{\text{RANaaS}} < 4\text{ms}. \quad (4.44)$$

Such latency request points to fibre-type physical link for the J1 interface.

- **High bandwidth:** For the MPTD process to be done centrally, we only need to transmit the received signal at the iSC level after the  $N_{sc}$ -FFT, which is made of In-phase/Quadrature (I/Q) samples in the frequency domain (see CT2.6 in Section 4.6). Such transmission requires a J1 raw capacity of:

$$\text{BH}_{\text{cap,req}} = 2N_{\text{quant}}^{UL} N_R^{iSC} N \frac{1}{T_s} \quad (4.45)$$

where  $T_s = 1/15\text{kHz} \approx 66.7\mu\text{s}$  is the duration of an SC-FDMA symbol with a normal cyclic prefix and  $N_{\text{quant}}^{UL}$  is the number of quantization bits of an I or Q sample. For a 20MHz LTE system, an iSC equipped with two receive antennas ( $N_R^{iSC} = 2$ ) wanting to deport through the J1 interface the UE signal allocated over the whole bandwidth ( $N = N_{sc} = 1200$ ) and quantized over  $M = 10$  bits, will need a bandwidth of 720Mbps/s (without overhead). At least a gigabit connection is required for the J1 interface.

If we have these two constraints fulfilled for the J1 interface, then we can perform the turbo detection centrally within the RANaaS as shown in Figure 6-8. To do so, the RANaaS platform must know the MCSs and the resources allocated of the  $N_{UE}$  UEs transmitting on the same resources. Within iJOIN, centralised RRM for MPTD within the RANaaS platform will be investigated in WP3 (CT3.7), which includes the scheduling of the UEs and in particular the ones to be involved in a turbo detection process. Therefore, this assumption is easily verified. By also transmitting the SC-FDMA symbols dedicated to the DMRS, we assume that the RANaaS platform is able to estimate the channel state information for each UE  $u$ . The RANaaS should also know the noise variance experienced by each iSC  $\nu \sigma^2$ , such measure can be feedback through the J1 interface with the quantised I/Q signal or estimated from the SC-FDMA symbols dedicated to the DMRS.

The turbo detection process in the MPTD case, depicted in Figure 4-13, is very similar to the one in the SPTD case. Therefore, we will keep the same notations as in the previous section.

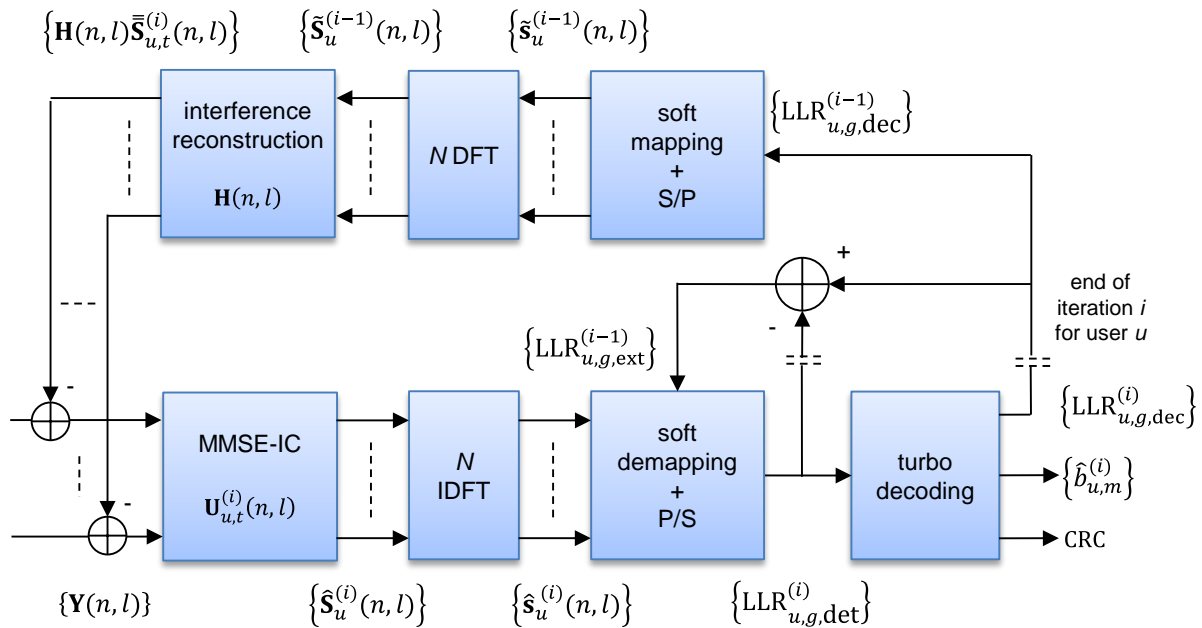


Figure 4-13: Iterative MMSE-IC receiver chain at RANaaS

Let  $N_t$  be the number of turbo detection iterations,  $N_{UE}$  be the number of UEs to be detected by the  $N_{iSC}$  iSCs. For the detection to be envisaged, the sum of all iSCs receive antennas must be greater or equal to the sum of all UE transmit antennas:

$$\sum_{v=1}^{N_{iSC}} N_R^{iSC,v} \geq \sum_{u=1}^{N_{UE}} N_T^{UE,u} \quad (4.46)$$

On subcarrier  $n$ , SC-FDMA symbol  $l$ , the equivalent channel matrix (including all the UEs)  $\mathbf{H}(n,l)$  of size  $\sum_{v=1}^{N_{iSC}} N_R^{iSC,v} \times N_{UE}$  is given by:

$$\mathbf{H}(n,l) = \begin{bmatrix} \mathbf{H}^{1,1}(n,l) & \dots & \mathbf{H}^{1,N_{UE}}(n,l) \\ \vdots & \ddots & \vdots \\ \mathbf{H}^{N_{iSC},1}(n,l) & \dots & \mathbf{H}^{N_{iSC},N_{UE}}(n,l) \end{bmatrix} \quad (4.47)$$

The received signal at the RANaaS platform can be rewritten according to the following equation:

$$\mathbf{Y}(n,l) = \begin{bmatrix} \mathbf{H}^{1,1}(n,l) & \dots & \mathbf{H}^{1,N_{UE}}(n,l) \\ \vdots & \ddots & \vdots \\ \mathbf{H}^{N_{iSC},1}(n,l) & \dots & \mathbf{H}^{N_{iSC},N_{UE}}(n,l) \end{bmatrix} \begin{bmatrix} S^1(n,l) \\ \vdots \\ S^{N_{UE}}(n,l) \end{bmatrix} + \begin{bmatrix} \mathbf{N}^1(n,l) \\ \vdots \\ \mathbf{N}^{N_{iSC}}(n,l) \end{bmatrix} = \mathbf{H}(n,l) \mathbf{S}(n,l) + \mathbf{N}(n,l) \quad (4.48)$$

where  $\mathbf{N}(n,l)$  is the aggregated  $\sum_{v=1}^{N_{iSC}} N_R^{iSC,v}$ -length vector of noise samples received by the  $N_{iSC}$  iSCs (in the frequency domain).

Similar equations governing the turbo detection principle can then be recovered from the SPTD case (from (4.35) to (4.42)), but the addition of more receive antennas in the resolution (since more iSCs are involved in the same MUD process) should improve the MPTD performance gain compared to the previous approaches.

## 4.2.2 Assumptions and Requirements

### Assumptions

- iSCs are connected to the RANaaS (through the J1 interface)
- iSCs can communicate to each other (through the J2 interface)
- Centralised scheduling already performed (at the RANaaS in CT3.7)

### Requirements

- Perfect synchronisation of the iSCs
- For MPTD:
  - The sum of involved iSC receive antennas is greater or equal to the sum of involved UE transmit antennas
  - J1 link: high capacity, low latency
  - at RANaaS: all CSIs (estimation through signal received), RB allocation (CT3.7 output, long term scheduling performed in RANaaS), all MCSs (either decided by CT3.7 or passed by iSC)
- For SPTD:
  - The number of iSC receive antennas is greater or equal to the sum of involved UE transmit antennas
  - J2 link: low to high capacity, low latency
  - At iSC: all CSIs (estimation through signal received), RB allocation (CT3.7 output, long term scheduling performed in RANaaS), all MCS (for its scheduled UE obvious, for interfering UE(s) either decided by CT3.7 or passed by other iSC)

### 4.2.3 Preliminary Results

#### System setup

To evaluate the three previous approaches, we assume the simple setup described in Figure 4-7, where two couples of (iSC-UE) are communicating on the same resources. The iSCs are assumed to be deployed close enough from each other (small cell deployment). We assume that the received power from the serving UE and the interfering UE are equivalent at each iSC (typically when both UEs are at the cell edge and not attached to the same small cell). As we consider a small cell deployment, we also assume that the noise contribution is the same at both iSCs. We define the signal-to-noise ratio at the iSC level by:

$$\text{SNR} = \frac{P_u}{\sigma^2}. \quad (4.49)$$

We assume a realistic LTE configuration where one UE is equipped with one transmit antenna  $N_T^{UE,1} = N_T^{UE,2} = 1$  and one iSC is equipped with two receive antennas  $N_R^{iSC,1} = N_R^{iSC,2} = 2$ . Both UEs are transmitting:

- on the same resource block:  $N = 12$ ,  $L = 12$ , i.e. 144 modulation symbols available for PUSCH per subframe,
- with the same LTE-compliant MCS:
  - QPSK with a TBS equal to 72 bits (codeword length  $G = 288$ ,  $R_c = 0.25$ )
  - QPSK with a TBS equal to 144 bits (codeword length  $G = 288$ ,  $R_c = 0.50$ )
  - 16QAM with a TBS equal to 280 bits (codeword length  $G = 576$ ,  $R_c \approx 0.49$ )

We consider that the channel time and frequency coherences are far greater than the equivalent RB dimensions (due to low mobility). Therefore, we model each channel realisation over one RB by a single unitary Rayleigh coefficient per Tx-Rx link.

A Monte-Carlo methodology is used to assess the performance of the three receivers on the same received signal. For the MMSE-IRC receiver, a maximum of 8 iterations is authorised (less in case of successful CRC) for the turbo decoding algorithm. For the SPTD and the MPTD receiver, two cases are evaluated:

- **case 1:**  $N_{it} = 4$  iterations for the turbo detection loop and a maximum of 8 iterations for the turbo detection of one UE.
- **case 2:**  $N_{it} = 2$  iterations for the turbo detection loop and a maximum of 2 iterations for the turbo detection of one UE. If all the turbo decoding iterations are performed, then MMSE-IRC and SPTD/MPTD case 2 will have the same number of turbo decoder iterations (which is the more complicated block).

For SPTD, the iSC will start the detection with the interfering UE (UE 2 for iSC 1 and UE 1 for iSC 2), while for MPTD the natural ordering is assumed for simplicity. More investigations may be done for optimising the order.

#### Results for QPSK, $R_c = 0.25$

The three previous receiving approaches are compared when UEs are using an MCS with a QPSK and a turbo code coding rate of 0.25 (spectral efficiency of 0.5bit/s/Hz). Figure 4-14 represents the frame error rate (FER) of UE 1 versus the SNR (and not the SINR). “Similar” results are obtained for UE2 due to the symmetric nature of the setup, except for MPTD as UE2 performance is a bit better for the low number of turbo detection iterations, since this UE is the last one to be detected.

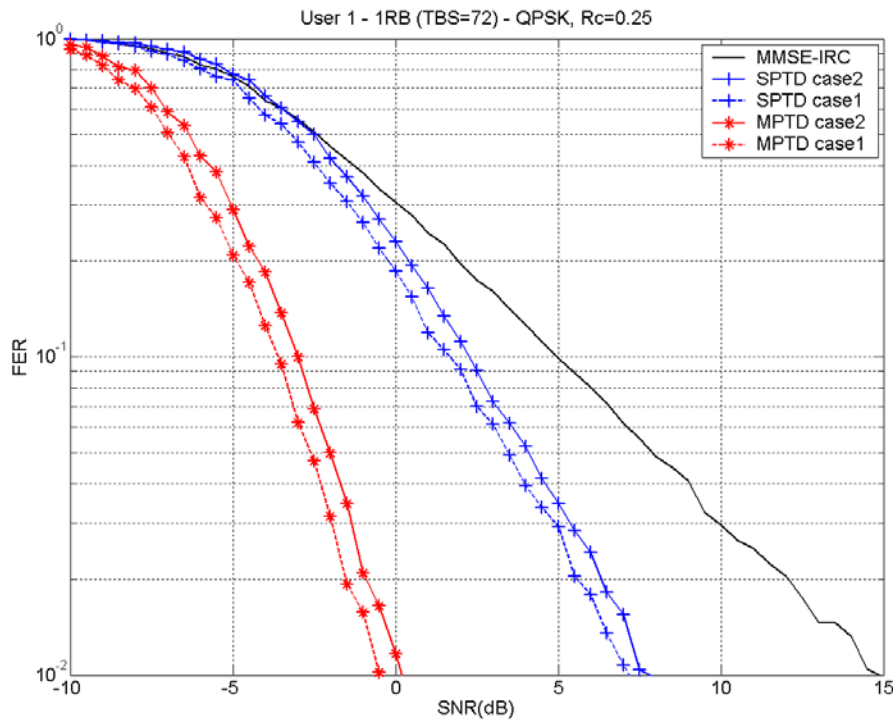


**Figure 4-14: MPTD Performance Evaluation, FER vs SNR of UE<sub>1</sub> – MCS (QPSK,  $R_c = 0.25$ )**

As expected the SPTD receiver outperforms the advanced MMSE-IRC receiver. In the  $10^{-1}$  FER region, this gain is around 3.5dB for the SPTD case 1. This area is usually the one chosen when defining an MCS reporting (at least in the downlink), the hybrid ARQ process allowing transmission improvement through incremental redundancy repetition. By targeting a lower FER, e.g.  $10^{-2}$ , the SPTD case 1 performs roughly 8dB better than MMSE-IRC. By using the turbo detection, one can target either higher spectral efficiency or rely less on the HARQ for the same MCS.

The MPTD case 1 significantly outperforms the previous receivers at a FER of  $10^{-1}$ , with a gain of around 5dB and 8.5dB compared to the SPTD and the MMSE-IRC, respectively. Those gains jump to 7.5dB and 15.5dB at a FER of  $10^{-2}$ , respectively. The system seen by the RANaaS is equivalent to a 2x4 antenna configuration which greatly explains the gap in performance brought by the MPTD algorithm. Indeed, even by reducing the number of iterations of the turbo detection and the maximum number of iterations of the turbo decoder, i.e. case 2, the penalty is roughly equal to 0.5dB compared to the case 1.

### Results for QPSK, $R_c = 0.50$

The same simulations have been carried out with UEs using an MCS with a QPSK modulation and a turbo code coding rate of 0.5 (spectral efficiency of 1bit/s/Hz). FER of UE1 against the SNR is given in Figure 4-15 where the same trends as previously can be observed. The MPTD brings significant gain over the SPTD and completely outperforms the MMSE-IRC receiver.

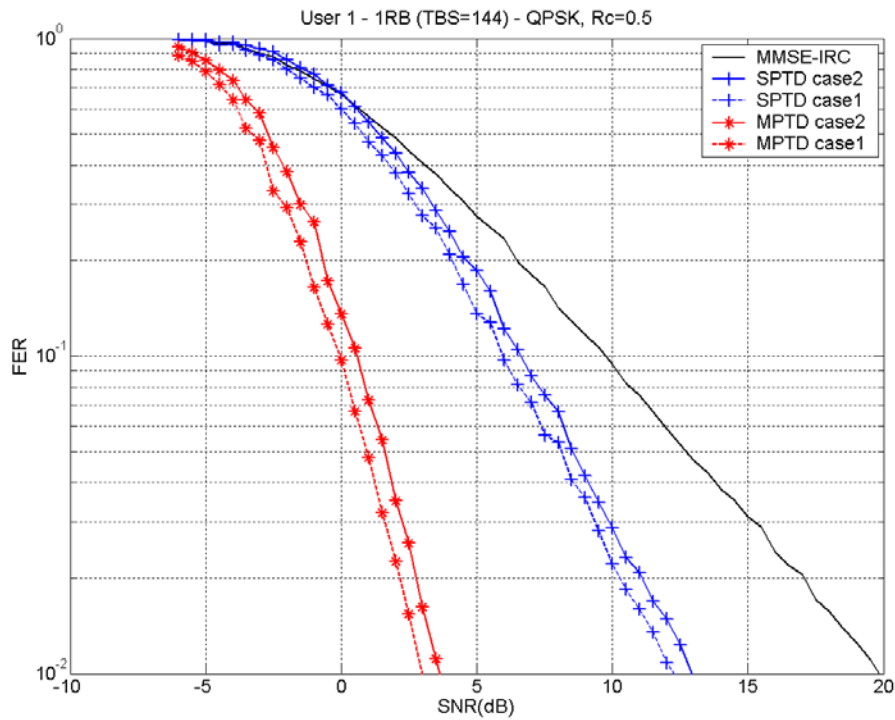


Figure 4-15: MPTD Performance Evaluation, FER vs SNR of UE<sub>1</sub> – MCS (QPSK,  $R_c = 0.50$ )

**Results for 16QAM,  $R_c \approx 0.49$**

The spectral efficiency has been pushed to 1.95bits/s/Hz with a 16QAM and a turbo code coding rate of almost 0.49 (280/576) in this case. FER of UE1 against the SNR is given in Figure 4-16. The same general trends can be observed. However, the reduction of the number of iterations in case 2 degrades more significantly the performance when a high order modulation is used (almost 1dB of loss compared to the 0.5dB observed previously for the MPTD). In any case, the MPTD and SPTD solutions outperform the MMSE-IRC solution, with a strong advantage to the MPTD solution (almost 10dB of gain for a FER of  $10^{-1}$ ).

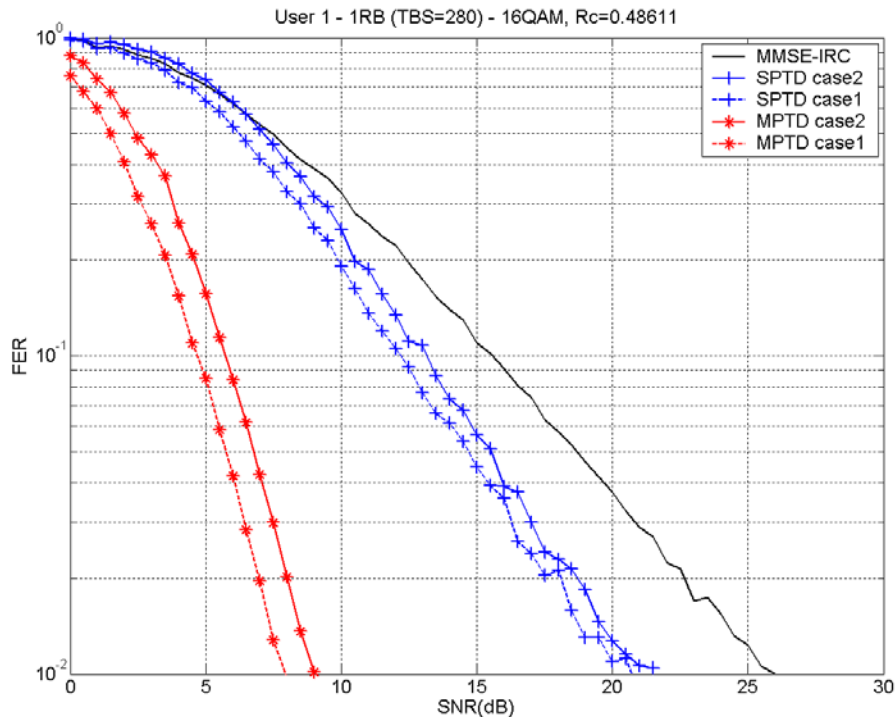


Figure 4-16: MPTD Performance Evaluation, FER vs. SNR of UE<sub>1</sub> – MCS (16QAM,  $R_c \approx 0.49$ )

## Conclusions and Perspectives

While the turbo detection receiver performed locally (SPTD) outperforms a classical MMSE-IRC receiver in our case (even with the same maximum number of turbo decoding iterations as in case 2), the centralisation of this process into the RANaaS platform (MPTD) exhibits consequent gains.

Of course such centralisation is only possible if the requirements on the capacity/latency of the interface J1 and on the processing time of the RANaaS platform are satisfied for an LTE-compliant solution. Under such assumptions, the MPTD can significantly increase the reliability of a transmission which could be used to reduce the number of repetitions or use more powerful MCS leading in both cases to a user and system throughput increase in the uplink.

For the future, we may have a look at the J2 interface, which connects two iSCs and could be used to exchange information (whom content will have to be defined, e.g. LLRs). Such cooperation should increase the performance of the SPTD solution, while the MPTD solution should remain the best option.

## 4.3 CT 2.3: Joint Network-Channel Coding

### 4.3.1 Description

#### Scenario

The proposed scenario concerns uplink transmissions and is depicted in Figure 4-17. As shown in this figure, two or more UEs use a common intermediate iSC<sub>1</sub>, which acts as a relay, to communicate with a final destination (iSC<sub>2</sub> or macro-cell eNB). The association of the UEs to the iSCs can be done through the mechanisms described by the CT3.2 in which the system capacity is optimized taking into account the characteristics of the backhaul and of the radio access. UEs' transmissions are encoded by two channel codes  $\mathcal{C}_1$  and  $\mathcal{C}_2$ , while a network code  $\mathcal{C}$  is used at the relay. The destination decodes the received signals using knowledge of  $\mathcal{C}_1$ ,  $\mathcal{C}_2$ , and  $\mathcal{C}$ .

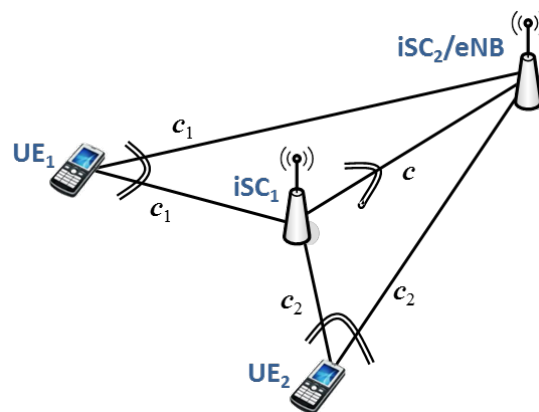


**Figure 4-17: Proposed scenario for joint network channel coding**

The use of the joint network channel coding (JNCC) is aimed at increasing the users' throughput in the uplink direction, and it is particularly suitable when the intermediate iSC<sub>1</sub> has limited resources to supply the users it serves with the services they demand. If iSC<sub>2</sub> has available backhaul resources (e.g. iSC<sub>2</sub> serves a smaller number of users than iSC<sub>1</sub>), it can take over responsibility of the backhaul access for users UE<sub>1</sub> and UE<sub>2</sub>. The drawback is that the users are penalized by the increasing distance to iSC<sub>2</sub> node, which generally results in a degraded capacity of the wireless links. However, iSC<sub>1</sub> can help increasing the users' throughput, by providing iSC<sub>2</sub> with additional data pertaining to the user transmissions. Since the additional data is actually provided by the network code used at iSC<sub>1</sub>, the whole coding scheme can be optimized such as to minimize the amount of data to be transmitted on the iSC<sub>1</sub> to iSC<sub>2</sub> link, subject to a target throughput for users UE<sub>1</sub> and UE<sub>2</sub>.

**System Model**

The goal of the investigation is to propose a joint-design of network  $\mathcal{E}$  and channel  $(\mathcal{E}_1, \mathcal{E}_2)$  codes to fully exploit the spatial diversity of the MARC, while reducing the traffic-load on the relay-to-destination (iSC<sub>1</sub>-iSC<sub>2</sub>) link. The overall idea of the joint-design is illustrated in Figure 4-18 where  $\mathbf{c}_u = \mathcal{E}_u(\mathbf{a}_u)$ , and  $\mathbf{c} = \mathcal{E}(\mathbf{a}_1, \mathbf{a}_2)$  are the codewords generated by the channel and the network encoders, respectively.

The channel codes<sup>2</sup>  $\mathbf{c}_1, \mathbf{c}_2$  are mapped into a binary or non-binary constellation and  $\mathbf{x}_u$  (with  $u = 1, 2$ ) indicates the vector of the mapped symbols transmitted over orthogonal channels. The relay iSC<sub>1</sub> receives and demodulates the two signals  $\mathbf{y}_{1D}$  and  $\mathbf{y}_{2D}$  and encodes the estimated information messages by the network encoder. The network code  $\mathbf{c}$  is successively modulated and  $\mathbf{x}$  represents the vector of mapped symbols transmitted on the channel between iSC<sub>1</sub>-iSC<sub>2</sub>. iSC<sub>2</sub> receives the three streams  $\mathbf{y}_{1D}$  and  $\mathbf{y}$  that are successively demodulated and jointly decoded as described in the following. The modulator and the demodulator blocks are omitted in the figure for the sake of simplicity.

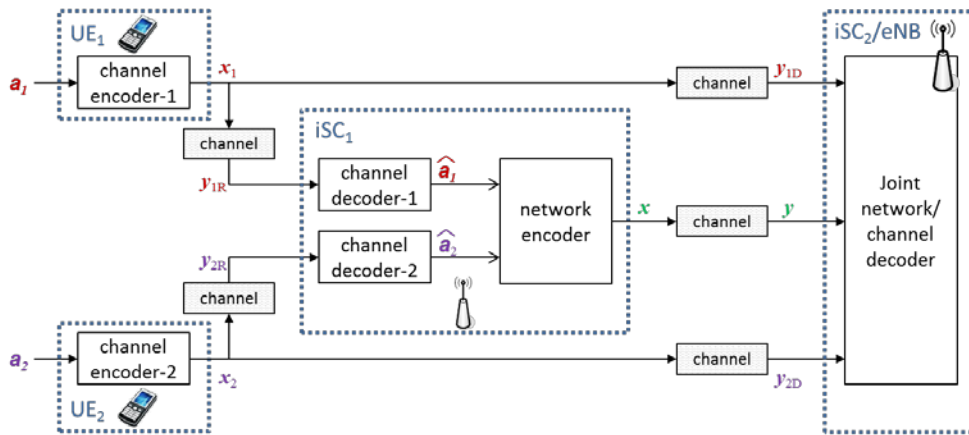


**Figure 4-18: Joint Network Channel coding for the MARC**

Our approach is based on the use of non-binary (NB) network coding, also referred to as vector network coding [54]. Non-binary network coding offers a natural generalization of binary network coding, allowing further optimization of the design and significant performance improvement.

**Non-binary LDPC codes**

The use of NB network coding at the intermediate node iSC<sub>1</sub> can accommodate the use of both binary and non-binary channel codes at UE<sub>1</sub> and UE<sub>2</sub>. We consider the use of Low-Density Parity-Check (LDPC) codes [55], known for their near-capacity performance on a large class of transmission channels [56], and for their low-complexity message-passing decoding algorithms [57].

An LDPC code could be characterized through the parity-check matrix<sup>3</sup>  $\mathbf{H}$ . A codeword  $\mathbf{c}$  is a solution of the linear system  $\mathbf{H} \cdot \mathbf{c}^T = 0$ . Let  $\text{GF}(q)$  denote the Galois Field of  $q$  elements, where  $q$  is a power of 2. A non-binary LDPC code is said to be defined over  $\text{GF}(q)$  if each entry of  $\mathbf{H}$  is to an element of  $\text{GF}(q)$ .

We can associate to the parity-check matrix a Tanner graph [58], which is constituted by  $N_{\text{symp}}$  symbol-nodes, corresponding to the  $N_{\text{symp}}$  columns of  $\mathbf{H}$  and represented by circles and  $N_{\text{check}}$  constraint-nodes, corresponding to the  $N_{\text{check}}$  rows of  $\mathbf{H}$  and represented by squares. A symbol-node and a constraint-node connected by an edge corresponds to a non-zero entry of  $\mathbf{H}$ .

Figure 4-19 is an example of a Tanner graph for a non-binary LDPC code with 6 check-nodes and 3 symbol-nodes. The non-zero coefficients of the parity-check matrix

<sup>2</sup> With an abuse of language, “codeword” can be replaced by “code” if the context allows it.

<sup>3</sup> We use bold italic  $\mathbf{H}$  in order to differentiate the parity-check matrix from the MIMO channel matrix  $\mathbf{H}$ .

$$\mathbf{H} = \begin{bmatrix} 6 & 2 & 0 & 5 & 0 & 0 \\ 0 & 1 & 4 & 0 & 7 & 0 \\ 3 & 0 & 5 & 0 & 0 & 5 \end{bmatrix} \quad (4.50)$$

are elements of Galois Field  $\text{GF}(8) = \{0, 1, 2, 3, 4, 5, 6, 7\}$  represented in the labelled edges of the graph. The represented code is systematic because the information part is embedded in the codeword. This code has coding rate equal to  $R_c = 1/2$ .

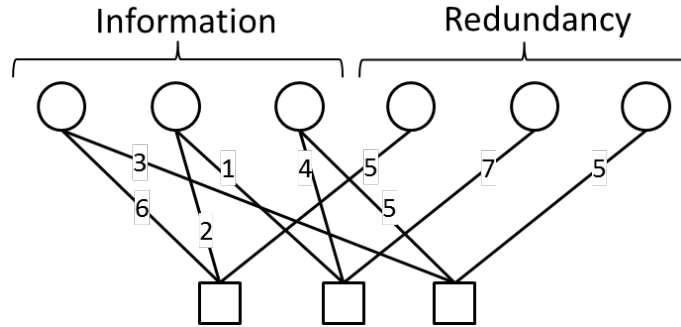


Figure 4-19: Example of Tanner Graph of a NB-LDPC code

### JNCC strategies

The use of NB LDPC [59] codes allows deploying two different strategies at the intermediate node  $i\text{SC}_1$  (illustrated in Figure 4-20 and Figure 4-21). We consider the case when both  $\text{UE}_1$  and  $\text{UE}_2$  use the same non-binary LDPC code defined over  $\text{GF}(q)$  to encode information words  $\mathbf{a}_u \in \text{GF}(q)^K$  into non-binary codewords  $\mathbf{c}_u \in \text{GF}(q)^{N_{\text{syml}}}$ , where  $u = 1, 2$ . We further assume that non-binary codewords  $\mathbf{c}_u \in \text{GF}(q)^{N_{\text{syml}}}$  are mapped into a  $q$ -QAM complex constellation, by using a bijective mapping between coded and modulated symbols. Let  $\mathbf{x}_u$  ( $u=1, 2$ ) denote the vector of complex symbols that is transmitted by UE  $u$  to both  $i\text{SC}_1$  and  $i\text{SC}_2$ .

The objective of the intermediate node  $i\text{SC}_1$  is to compute the (non-binary) network-encoded vector  $\mathbf{c} = h_1 \hat{\mathbf{c}}_1 \oplus h_2 \hat{\mathbf{c}}_2$ , where  $h_1, h_2 \in \text{GF}(q)$  and  $\hat{\mathbf{c}}_1, \hat{\mathbf{c}}_2$  are the estimated codewords. This vector is then mapped into a sequence of  $q$ -QAM symbols, denoted by  $\mathbf{x}$ , and transmitted to  $i\text{SC}_2$ . In order to compute  $\mathbf{c}$ , two different strategies can be deployed at the intermediate node  $i\text{SC}_1$  which are considered in the following.

#### Strategy 1: Separate demapping and decoding at $i\text{SC}_1$

Received sequences are assumed to be orthogonal in either time or frequency. The sequences of noisy symbols received from  $\text{UE}_1$  and  $\text{UE}_2$  are demapped separately. Each demapper outputs a sequence  $\mathbf{Pr}_u = (\mathbf{Pr}_{u,1}, \dots, \mathbf{Pr}_{u,N})$ , where  $\mathbf{Pr}_{i,n} = (\Pr_{i,n}(t))_{t \in \text{GF}(q)}$  is the probability distribution of  $c_{i,n}$ , where  $c_{i,n}$  is the  $n$ -th symbol within the codeword  $\mathbf{c}_i$ , conditional on the channel output, that is:

$$\mathbf{Pr}_{i,n}(t) = p(c_{i,n} = t \mid y_{iR,n}) \quad (4.51)$$

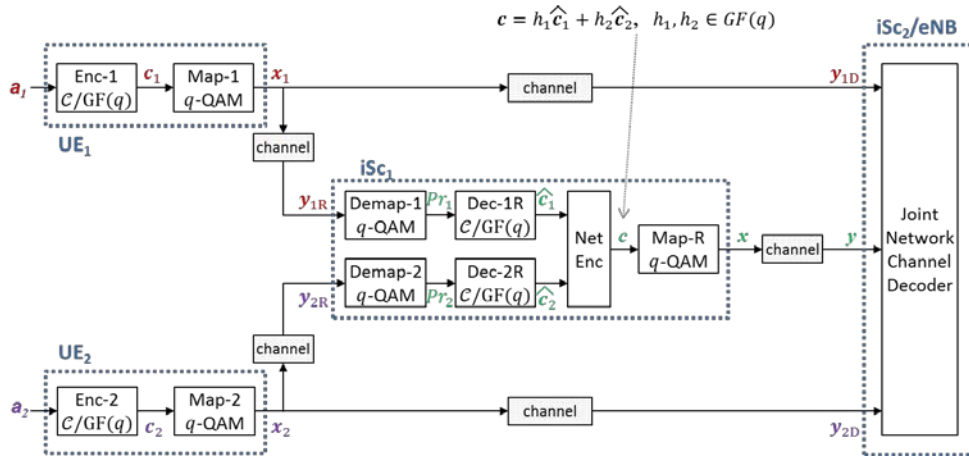


Figure 4-20: Separate demapping and decoding at intermediate node  $iSC_1$

As shown in Figure 4-20, codewords  $\mathbf{c}_i$  are then decoded separately and, assuming that both codewords are successfully decoded, the network encoder module computes  $\mathbf{c} = h_1 \hat{\mathbf{c}}_1 \oplus h_2 \hat{\mathbf{c}}_2$ . If  $iSC_1$  fails to decode both messages, then it either forwards the correctly decoded message (if any), or remains silent.

### Strategy 2: Joint demapping and decoding at $iSC_1$

This strategy exploits the fact that the network-encoded vector  $\mathbf{c} = h_1 \hat{\mathbf{c}}_1 \oplus h_2 \hat{\mathbf{c}}_2$  is also a codeword of the non-binary LDPC code used at  $UE_1$  and  $UE_2$  (this follows from the linearity property of the LDPC code). Therefore, the sequences of noisy symbols received from  $UE_1$  and  $UE_2$  are fed to a joint demapper that outputs a sequence  $\mathbf{Pr} = \{\Pr_n(t)\}_{n=1,\dots,N}$ , with  $t \in GF(q)$ , being the probability distribution of  $c_n$ , conditional on both channel outputs, that is:

$$\Pr_n(t) = p(c_n = t | y_{1R,n}, y_{2R,n}) = \sum_{\substack{t_1, t_2 \in GF(q) \\ h_1 t_1 + h_2 t_2 = t}} \Pr_{1,n}(t_1) \Pr_{2,n}(t_2) \quad (4.52)$$

The sequence  $\mathbf{Pr}$  is then fed to a decoder module to estimate  $\mathbf{c}$  directly (without decoding  $\mathbf{c}_1$  and  $\mathbf{c}_2$  first). This strategy allows reducing the computational complexity at the intermediate  $iSC_1$  node by almost 50%. However, the drawback is that the joint demapping strategy amplifies the noise effect on the received signals, which degrades the error-rate performance of the joint decoder.

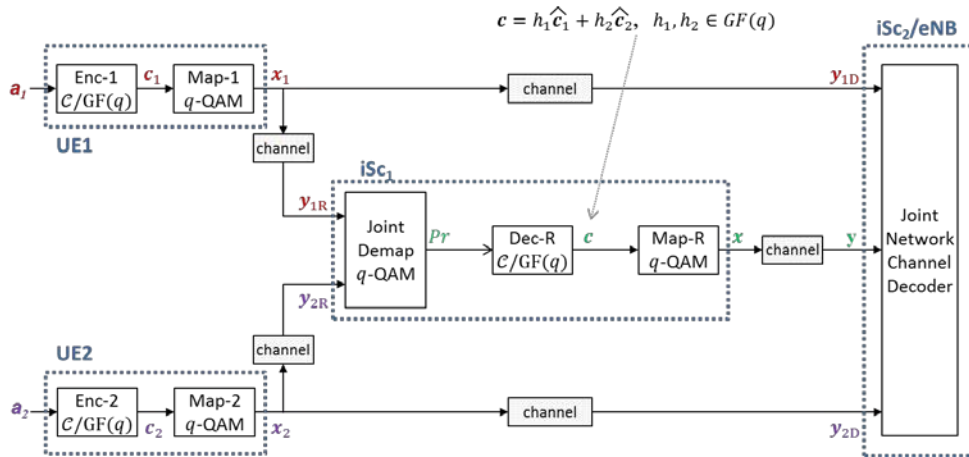


Figure 4-21: Joint demapping and decoding at intermediate node  $iSC_1$

Concerning the destination node  $iSC_2$ , we remark that the same joint network channel decoding strategy is used, irrespective of the strategy used at the intermediate  $iSC_2$  node.

### Strategy at destination: Joint network channel decoding at $iSC_2$

As shown in Figure 4-22, the factor graph of the joint network-channel code consists of three sub-graphs. The top and bottom sub-graphs correspond to the factor graphs of the channel codes used at  $UE_1$  and  $UE_2$ ,

respectively. These sub-graphs are connected through a third one, in the middle, corresponding to the network coding operation performed at the intermediate node iSC<sub>1</sub>. Each check-node of the network-coding graph corresponds to an operation  $c_n = h_1 c_{1n} + h_2 c_{2n}$ .

At the destination node iSC<sub>2</sub>, the joint network-channel decoder is fed with the probability distributions of the symbol nodes in the joint factor graph, which are computed according to the noisy symbols received from UE<sub>1</sub>, UE<sub>2</sub>, and iSC<sub>1</sub>, respectively. Decoding is then performed by an iterative message-passing algorithm that operates on the joint factor graph.

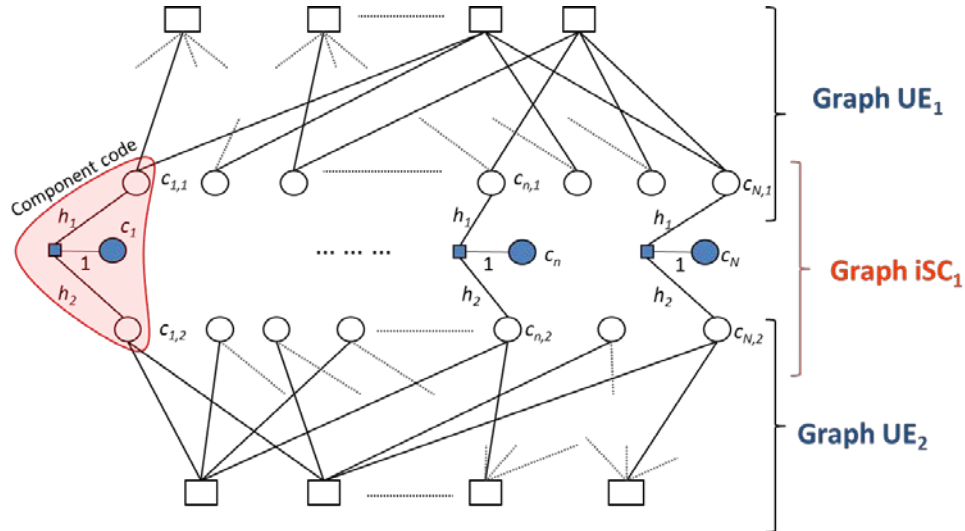


Figure 4-22: Joint network-channel factor graph

### 4.3.2 Assumptions and Requirements

The preliminary set of assumptions for CT2.3 is:

- Wireless inter-node links between iSCs and between iSCs and RANaaS (60GHz)
- Knowledge of receiving (Rx) CSI for the links UE-iSCs, iSC-iSC, and iSC-RANaaS
- Adaptive Coding and Modulation

The preliminary set of requirements for CT2.3 is:

- Limited capacity for J1 and J2 links according to the distributed or centralized processes
- Perfect synchronization among iSCs
- Slowly varying channels

### 4.3.3 Preliminary Results

This section presents preliminary results concerning the optimization of the JNCC design for the Gaussian MARC, i.e., the transmissions between the nodes are affected by AWGN noise but now channel fading or interference of channels has been considered. The goal is to demonstrate the gain brought by the use of non-binary network coding at the intermediate node iSC<sub>1</sub>.

For LDPC codes defined over  $GF(q)$ , it has been shown in [60] that selecting carefully the non-binary entries of the parity-check matrix  $\mathbf{H}$  can improve the overall performance of the code. The approach proposed in [60] consists in choosing the non-zero entries of  $\mathbf{H}$  such that the binary image of each non-binary check-node has the maximum minimum Hamming distance  $d_{\min}$ , together with the minimum multiplicity of codewords with Hamming weight  $d_{\min}$ .

We applied the same approach in order to optimize the non-binary coefficients  $(h_1, h_2)$  of the network coding graph. As shown in Figure 4-22, each check-node of the network-coding graph corresponds to a non-binary parity-check equation  $\mathbf{H}_c \cdot \mathbf{c}_c^T = 0$ , or, making it explicit,  $[1, h_1, h_2] \cdot (c_{R,n}, c_{1,n}, c_{2,n})^T = 0$ . Each entry

of  $\mathbf{H}_c$  can be seen as a  $z \times z$  binary matrix, with  $z = \log_2(q)$  such that the multiplication of a symbol  $c$  by  $h$  corresponds to the multiplication of a binary image of  $c$  by the matrix associated with  $h$ . The binary parity-check matrix is obtained by replacing each entry  $h$  by the associated binary  $p \times p$  matrix. Hence, the binary image of the check-node is then obtained by taking the binary image  $f[1, h_1, h_2] \in \text{GF}(q)^3$ . This results into a binary parity-check matrix of size  $z \times 3z$ , of the form  $[\mathbf{I}_z, \mathbf{H}_1, \mathbf{H}_2]$ , where  $\mathbf{I}_z$  is the identity matrix of 1, while  $\mathbf{H}_1$  and  $\mathbf{H}_2$  are the binary images of coefficients  $h_1$  and  $h_2$ , respectively. Therefore, coefficients  $(h_1, h_2)$  are chosen to maximize the minimum Hamming distance  $d_{\min}$  of  $[\mathbf{I}_z, \mathbf{H}_1, \mathbf{H}_2]$ , together with the minimum multiplicity of codewords with Hamming weight  $d_{\min}$ .

To illustrate the above optimization procedure, we consider the case of non-binary network coding defined over  $\text{GF}(16)$ . According to our optimization procedure, the best coefficients are  $h_1 = 3$  and  $h_2 = 5$ , in which case  $d_{\min} = 3$  with exactly 16 codewords of weight 3.

We further consider a non-binary LDPC code defined over  $\text{GF}(16)$ , which is used at both  $\text{UE}_1$  and  $\text{UE}_2$ . The code is regular, with symbol-nodes of degree  $d_v = 2$  and check-node of degree  $d_c = 4$ . The code rate is  $R_c = 1/2$  and the code length is  $N_{\text{symp}} = 300$   $\text{GF}(16)$ -symbols (or equivalently 1200 bits). The graph of the LDPC code is constructed by using the progressive edge growth (PEG) algorithm [61] and has a girth  $g = 6$ . Since our goal is to assess the gain brought by the optimization of the non-binary network-coding coefficients, the non-zero entries of the parity-check matrix are chosen randomly from  $\text{GF}(16)$ .

Finally, we assume that the 16-QAM constellation is used to modulate the signals transmitted over all the links of the MARC, and that the intermediate  $\text{iSC}_1$  node successfully decodes the received signals (using one of the strategies presented in Section 4.3.1), and then transmits the network-encoded vector  $\mathbf{c} = h_1 \mathbf{c}_1 \oplus h_2 \mathbf{c}_2$  to the destination node  $\text{iSC}_2$ .

The Frame Error Rate (FER) performance of the proposed JNCC design is shown in Figure 4-23. We simulate the transmission over a symmetric scenario in which the quality of the links are the same, thus the SNR value shown on the abscissae is considered to be the same for the three links  $\text{UE}_1 - \text{iSC}_2$ ,  $\text{UE}_2 - \text{iSC}_2$ , and  $\text{iSC}_1 - \text{iSC}_2$ .

We assume that the signals transmitted by  $\text{UE}_1$ ,  $\text{UE}_2$ , and  $\text{iSC}_1$  are orthogonal in either frequency or time. At the destination  $\text{iSC}_2$  node, Belief-Propagation (BP) decoding [62] is performed on the joint factor graph as explained in Section 4.3.1. The three curves shown in Figure 4-23 correspond to three different choices of network-coding coefficients. The blue curve shows the performance of the JNCC design with optimized coefficients  $(h_1 = 3, h_2 = 5)$ , while the red curve shows the performance of the JNCC design with binary network-coding, corresponding to coefficients  $(h_1 = 1, h_2 = 1)$ . For comparison purposes, we also included the performance of the JNCC design with “random” coefficients  $(h_1 = 13, h_2 = 15)$  – for these coefficients, the binary image of the network-coding check-node has minimum Hamming distance  $d_{\min} = 2$ . It can be seen that the non-binary network coding with optimized coefficients has a coding gain of about 0.5 dB.

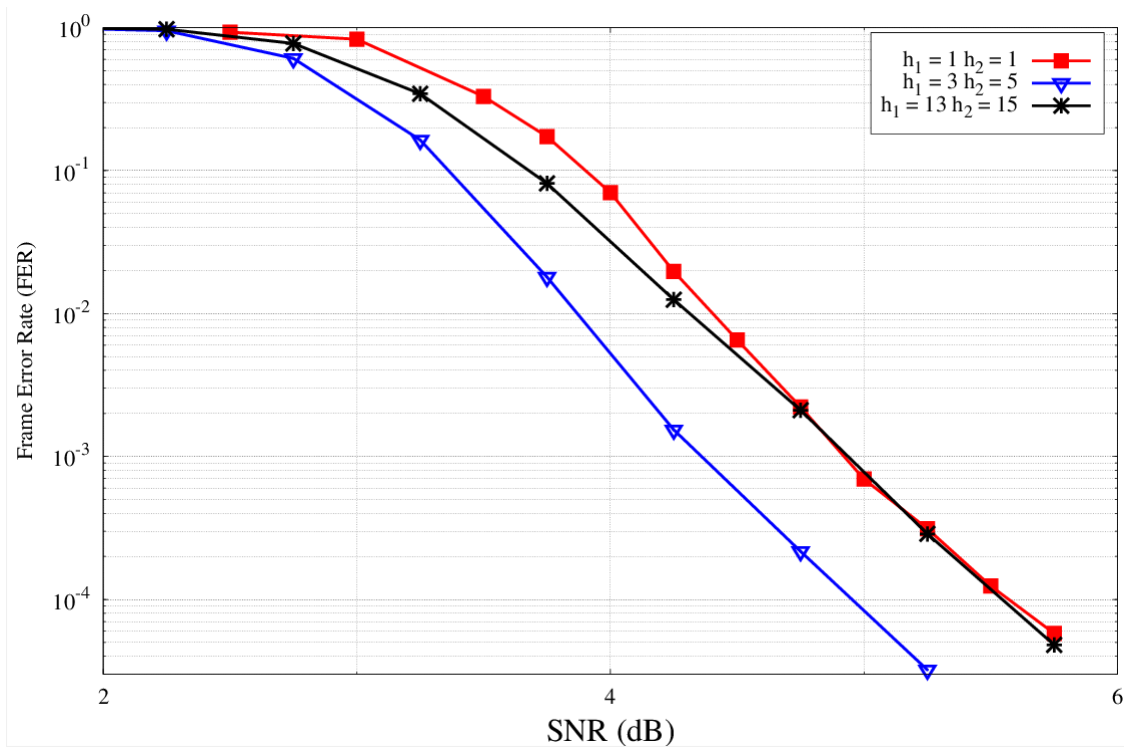


Figure 4-23: FER performance of the JNCC design for different choices of network-coding coefficients

#### 4.4 CT 2.4: Sum-Rate and Energy-Efficiency metrics of DL CoMP with backhaul constraints

##### 4.4.1 Description

###### Scenario

In this CT, we consider a downlink cellular system in which  $N_{iSC}$  iSCs are involved (see Figure 4-24 for an example scenario with only two iSCs) either in joint transmission (JT) or coordinated beamforming (CB) mode. In JT mode, the precoding is done at a central location considering the full channel matrix and all individual user messages to be jointly transmitted from the iSCs. Our objective is to analytically find the conditions under which JT is more energy efficient than CB. To this end, new analytical results have been derived for the total energy consumption per bit for both JT and CB schemes considering power consumption for backhauling. Using these results, we derive the conditions under which JT is more energy efficient than CB and vice versa.

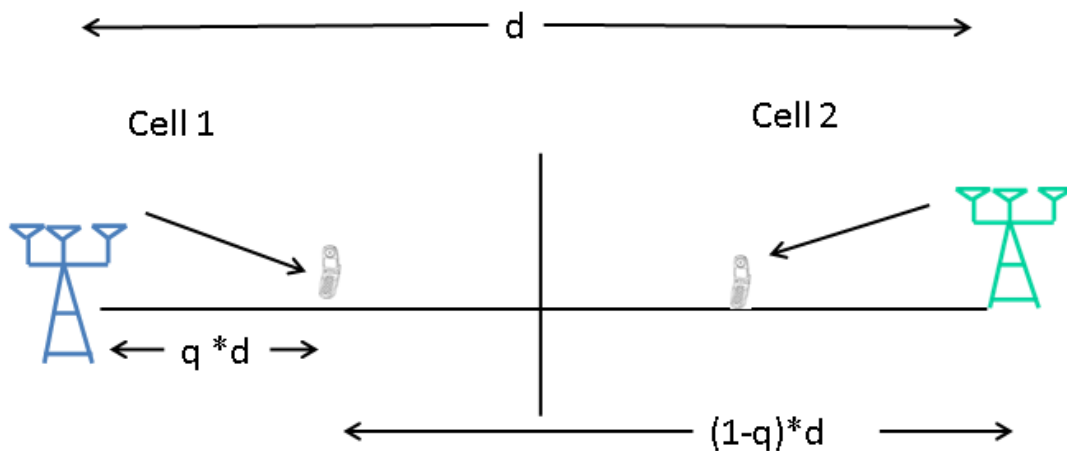


Figure 4-24: A two-cell symmetrical network

### System Model

Let us assume orthogonal scheduling of users, i.e. only one user is served by each iSC at a given time, and we also assume that each UE has a single antenna. The small scale flat-fading channel vector between the  $i$  th iSC and the user in the  $j$  th cell is denoted as  $\mathbf{g}_j^i$  which is a complex vector of dimension  $1 \times N_T^{iSC}$  where  $N_T^{iSC}$  represents the number of antennas at each iSC and  $i, j = 1, \dots, N_{iSC}$ . All channel vectors are assumed to be mutually independent and identically distributed (i.i.d.) complex Gaussian random vector with zero mean and  $E[\|\mathbf{g}_j^i\|^2] = N_T^{iSC}$ . Now let  $\alpha_j^i$  denotes the large scale path-loss between the  $i$  th iSC and the user in the  $j$  th cell and  $\mathbf{h}_j^i = \alpha_j^i \mathbf{g}_j^i$  is the composite channel vector between the  $i$  th iSC and the user in the  $j$  th cell. The global channel vector for the user in the  $j$  th cell is represented as  $\mathbf{h}_j = [\mathbf{h}_j^1, \mathbf{h}_j^2, \dots, \mathbf{h}_j^{N_{iSC}}]$  having dimensions  $1 \times N_{iSC} N_T^{iSC}$ . It is assumed that the global channel vectors for each user are known at the RANaaS for zero-force precoding (ZFP). In order to perform ZFP for CB, the condition that is required is that  $N_T^{iSC} \geq N_{iSC}$ , i.e. the number of transmit antennas should be greater than or equal to the number of iSCs, whereas this condition is not required to be satisfied for JT. Wireless backhaul is considered between RANaaS and each iSC, and it is assumed that the backhaul link operates in the millimetre-wave band and has noise/interference modelled as Gaussian random variable.

### Information Theoretic Analysis

With the above described system model, we can write from information theory:

$$C_{BH} = B_{BH} \log_2 \left( 1 + \frac{P_{BH} \alpha_{BH}^2}{N_{0,BH} B_{BH}} \right) \quad (4.53)$$

where  $B_{BH}$  is the bandwidth of the backhaul link and is taken as 1GHz,  $P_{BH}$  denotes the power consumption of each backhaul link,  $\alpha_{BH}^2$  is the backhaul path-loss, and  $N_{0,BH} B_{BH}$  denotes the noise-power of the backhaul link, and  $N_{0,BH}$  is the noise power spectral density of the backhaul link which is assumed to be Gaussian distributed.

Now, from the above equation (4.53), we have

$$P_{BH} = \frac{\left( 2^{\frac{C_{BH}}{B_{BH}}} - 1 \right) N_{0,BH} B_{BH}}{\alpha_{BH}^2}. \quad (4.54)$$

For the case of JT, making use of Jensen's inequality [130] and the assumption that  $N_T^{iSC}$  is a large number, we can write an equation for sum-capacity for joint-transmission as

$$C_{Sum}^{JT} = B \sum_{j=1}^{N_{iSC}} \log_2 \left( 1 + \frac{P_{Sum}}{N_{iSC} N_0 B} N_T^{iSC} \alpha_{N_{iSC}}^2 \right) \quad (4.55)$$

where  $P_{sum}$  is the total RF power for all iSCs,  $\alpha_{N_{iSC}}^2 \equiv \alpha^2 + \sum_{i=1, i \neq j}^{N_{iSC}} \alpha_i^2$ , where  $\alpha^2$  is the path-loss from own-cell

while the summation terms sums the path-losses from neighbouring cells, and  $B$  is the bandwidth of the access link, and  $N_0$  is the noise power spectral density of the access link which is again assumed to be Gaussian distributed.

In case of symmetric network (uniformly distributed users and deterministic positioning of the iSCs uniformly distributed on the coverage area), we can write the above equation as

$$C_{Sum}^{JT} = N_{iSC} B \log_2 \left( 1 + \frac{P_{Sum}}{N_{iSC} N_0 B} N_T^{iSC} \alpha_{N_{iSC}}^2 \right). \quad (4.56)$$

Now the effective end-to-end capacity,  $C_{e2e}$ , is given as

$$C_{e2e} = \min(C_{BH}, C_{Sum}^{JT}). \quad (4.57)$$

Assuming that the system is capacity limited at radio access end and not at the backhaul end  $C_{BH} \geq C_{Sum}^{JT}$ , we can write

$$C_{e2e} = C_{Sum}^{JT}. \quad (4.58)$$

Using the equations for end to end capacity, (equation (4.58), and equation (4.56) and for total power including the backhaul power, equation (4.54)), we can find the relation of power and capacity that gives us Joule per Bit total energy consumption. After some manipulations, the total energy per bit (in J/bit) for the JT scheme denoted as  $E_T^{JT}$  is given as

$$E_T^{JT} = \frac{(2^{S_{cell}^{JT}} - 1)N_0}{N_T^{iSC} \alpha_{N_{iSC}}^2 S_{cell}^{JT}} + N_{iSC} \frac{\left(2^{\frac{C_{BH}}{B_{BH}}} - 1\right) N_{0,BH} B_{BH}}{\alpha_{BH}^2} \quad (4.59)$$

where  $S_{cell}^{JT}$  denotes the spectral efficiency per cell for JT scheme and defined as  $S_{cell}^{JT} = \frac{C_{cell}^{JT}}{B}$ .

In contrast to JT, coordinated beamforming only needs partial information about the user channels and can compute a precoding vector that will result in better interference management. Following the same derivation steps, the total energy per bit (in J/bit) for the CB scheme is given as

$$E_T^{CB} = \frac{(2^{S_{cell}^{CB}} - 1)N_0}{N_T^{iSC} \alpha^2 S_{cell}^{CB}} + \frac{\left(2^{\frac{C_{BH}}{B_{BH}}} - 1\right) N_{0,BH} B_{BH}}{\alpha_{BH}^2}. \quad (4.60)$$

Now, comparing the above two equations, we get the necessary condition under which JT is more energy efficient than CB scheme and this is given as follows

$$\frac{1}{\alpha^2} - \frac{1}{\alpha_{N_{iSC}}^2} \geq \frac{(N_{iSC} E_{BH}^{JT} - E_{BH}^{CB}) N_T^{iSC} S_{cell}}{(2^{S_{cell}} - 1) N_0}. \quad (4.61)$$

Please note that these analytical results represent lower bound on the energy efficiency of CoMP schemes. Numerical results based on these equations will be shown in Section 4.4.3.

#### 4.4.2 Assumptions and Requirements

- Orthogonal scheduling is assumed between the active users served by the same iSC. The scheduling information might be provided by CT3.5 on the access link and for backhaul scheduling by CT3.1.
- Rayleigh fading is assumed to model the small-scale fading between the transmit and receive antennas.
- Each iSC is equipped with a large number of antennas i.e.  $N_T^{iSC}$  is a large number.
- Zero-forcing precoding is assumed in order to cancel the inter-cell interference. Therefore,  $N_t \geq N_{iSC}$  should be satisfied for CB.
- J1 links are modelled as millimetre-wave wireless links and thus are highly directional i.e. no interference between the J1 links.
- Centralized architecture for the CoMP implementation and J2 links do not exist.
- For analytical derivations the transmit signals on the access and the backhaul links are assumed to be Gaussian distributed.

### 4.4.3 Preliminary Results

Consider a symmetrical two-cell network as shown in the Figure 4-24 where  $q \in (0,0.5)$  where the aim is to investigate energy efficiency of JT- and CB-CoMP schemes as a function of distance of users from their respective iSCs. Using the analysis derived in section 4.4.1, the total energy per bit is plotted in the Figure 4-25 and Figure 4-26 versus the location of UEs from its own iSC for  $S_{cell}=18$  bps/Hz and 40 bps/Hz, respectively. For these results, it has been assumed that  $B_{BH}=1$  GHz at a carrier frequency of 72 GHz,  $\alpha_{BH}^2 = 1.10917e^{-11}$ ,  $\alpha^2 = 10^{-3} d^{-3}$ ,  $d = 750$  m,  $N_T^{iSC} = 10$ , and  $N_0 = -174$  dBm/Hz.

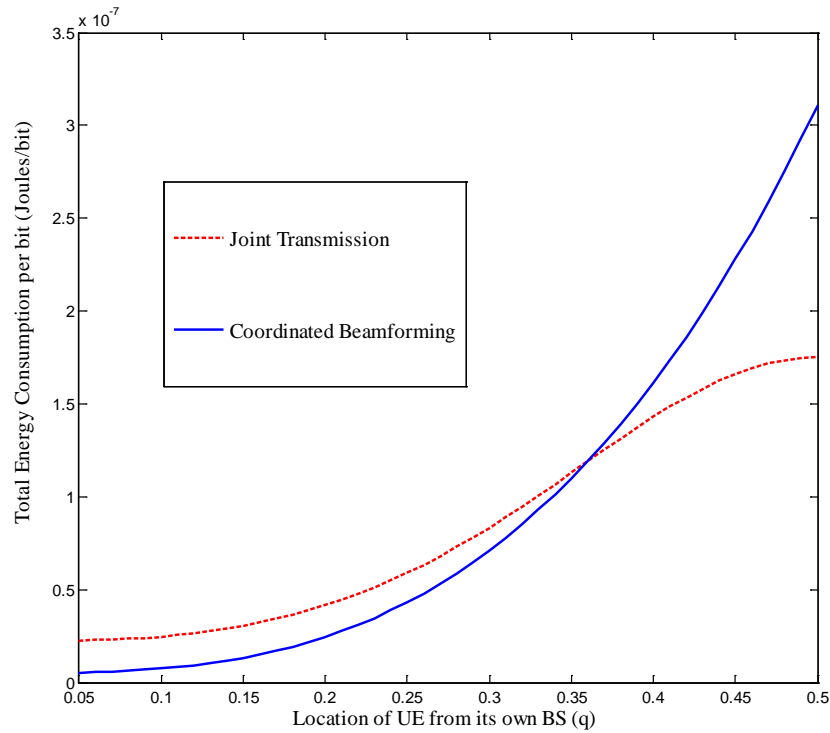
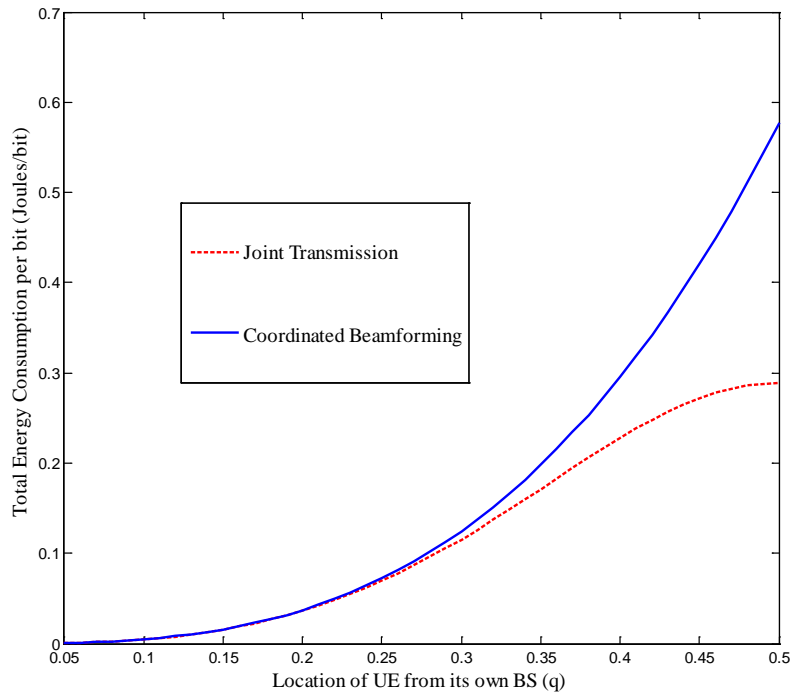


Figure 4-25: Total energy per bit versus the location of UE from its own iSC at Cell SE = 18bps/Hz



**Figure 4-26: Total energy per bit versus the location of UE from its own iSC at Cell SE = 40 bps/Hz**

It is shown in the Figure 4-25 that there exists a cut-off point after which JT is more energy efficient than CB. This is because when each UE is closer to its desired iSC (in this case interference is low), backhaul energy is more dominant as compared to the transmission energy (as the diversity iSC is farther away) and thus CB is more energy efficient. On the other hand, when the interference is high (e.g. when the UE is at the cell-edge), JT is more energy efficient because transmission energy is dominant in this scenario.

The total energy per bit is plotted in the Figure 4-26 for a high value of spectral efficiency i.e.,  $S_{cell} = 40\text{bps/Hz}$ . As the spectral efficiency is high, the transmission energy is more dominant as compared to the backhaul energy and there is as such no cross over point between JT and CB. Near the iSC, both schemes perform almost same from energy efficiency perspective as almost no diversity is obtained by using JT; however, the diversity effect is more significant when the UE is close to the cell-edge and therefore JT is more energy efficient in that region. It is observed in the Figure 4-26 that up-to 50% energy per bit can be saved using JT as compared to CB when the UE is at the cell-edge, which is quite significant.

## 4.5 CT 2.5: Partially Centralized Inter-Cell Interference Coordination

### 4.5.1 Description

The interference generated from a total reuse of the spectral resources across neighbouring iSCs can be in principle handled through centralized processing in the RANaaS. In this scenario the objective is to mimic the gain of so-called network MIMO (Joint Processing CoMP) while using the RANaaS as a computing resource with which each iSC can communicate over the J1 links. The typical network architecture which has been so far considered in the literature uses a star topology, where the  $i$ -th iSC is linked to the RANaaS via a link of capacity  $C_{iR}$  in one direction and a link of capacity  $C_{Ri}$  in the other [125], [126], [127]. The RANaaS is equipped with the necessary computing power in order to complete precoding operation (downlink) or decoding operation (uplink). The traditional star topology is illustrated in the figure below for 3 cooperating iSCs.

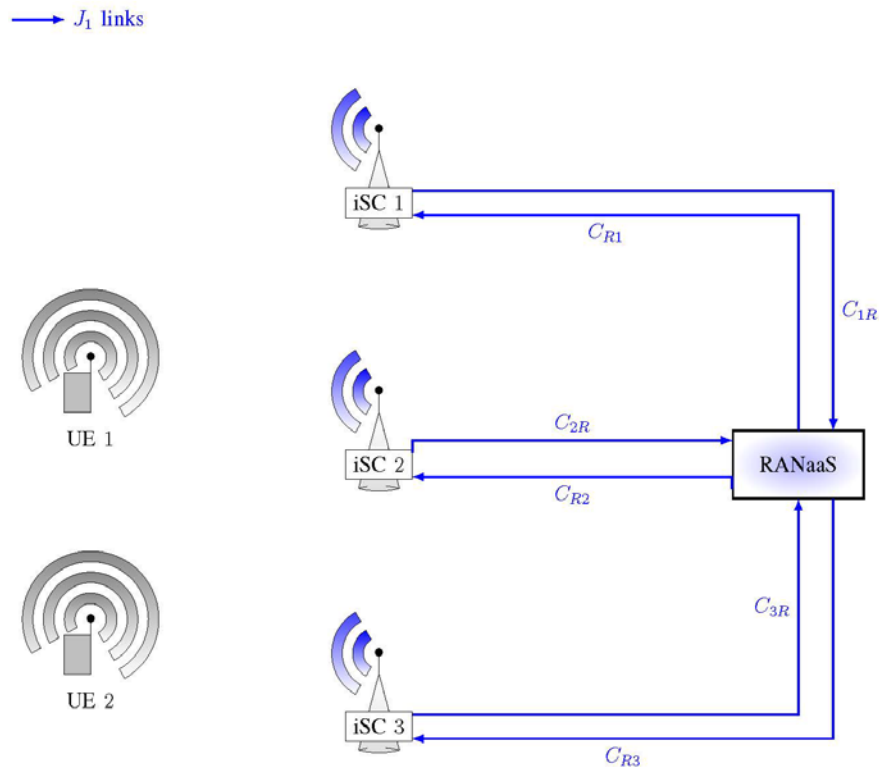


**Figure 4-27: RANaaS with star topology**

Let us consider the downlink transmission in the physical layer where all the RRM has already occurred and is known at the RANaaS and at the adequate iSCs. In fact, the RRM can also be optimized to exploit in the most efficient manner the network architecture. This question is investigated in WP3 and in particular in D3.1 by CT3.9.

Considering FDD, the downlink CSI is first estimated at the UE as a result of a training phase. The downlink CSI is then feedback from the UEs to one iSC. This downlink CSI is then shared via the  $J_1$  links to the RANaaS. In the RANaaS, the modulated user's data symbols to transmit are then precoded. The signal to be transmitted by iSC  $i$  is then sent to iSC  $i$  via the  $J_1$ -link. Each iSC then decompresses the received signal and simply forwards it over-the-air to the UEs.

In the existing star-topology, the integrality of the signal processing is assumed to be done exclusively in the RANaaS while the iSCs are simple RRH which forward the signal that they have received. Although this strategy is interesting and even optimal if the  $J_1$  links become perfect (in both directions), it does neither exploit the possibility for the iSCs to do some local processing nor to communicate amongst them via the  $J_2$  links.

### Hybrid Architecture

However, the star topology described above does not make use of the  $J_2$  links. This fully centralized architecture has also bad scaling properties and becomes quickly unpractical as the number of iSCs increases. For a better exploitation of existing backhaul architectures, an interesting question is therefore how one can make use of the  $J_2$  links between iSCs and of the processing in the RANaaS simultaneously, for any backhaul scenario. For instance, certain deployments will feature high capacity  $J_1$  links but poor  $J_2$  links. In fact, the  $J_2/J_1$  links can also have heterogeneous qualities. Answers to such a question will allow us to understand how precoding/decoding can be partitioned in an effective manner to reflect the notion of partially centralized processing.

### System Setting

The hybrid backhaul architecture is characterized by a set of  $J_2$  links between the  $i$ -th iSC to the  $j$ -th iSC with rate  $C_{ij}$ . In addition, iSC  $i$  is linked to the RANaaS via a  $J_1$  link of rate  $C_{iR}$ , while in the other direction the RANaaS is linked to iSC  $i$  with a link of rate  $C_{Ri}$ . The rates  $C_{ij}$  can be chosen arbitrarily such that the hybrid architecture encompasses both the distributed processing offered by classical distributed precoding and the centralized processing done in the RANaaS. Note that for infinite  $C_{ij}$ , it is possible to realize ideal multicell processing at the iSCs themselves without the need for the cloud other than for the purpose of forwarding the UE messages. We are interested in operations on the backhaul performing a combination of linear filtering (for simplification) with the aim of interference cancelling, together with quantization to make full use of the finite rate links.

We further assume here that the data symbols are available at all iSCs. This sharing of the data symbols consumes some of the backhaul resources. However, the sharing of the user's data symbols does not have tight delay constraint, which is one of the critical issue for the transmitter cooperation. We consider in this first analysis that the backhaul links are of finite capacity but do not introduce any delay. The goal of our work is to study how the precoder design can be split between the iSCs and the RANaaS and to find new and innovative precoding schemes which make more efficient use of this architecture than conventional solutions.

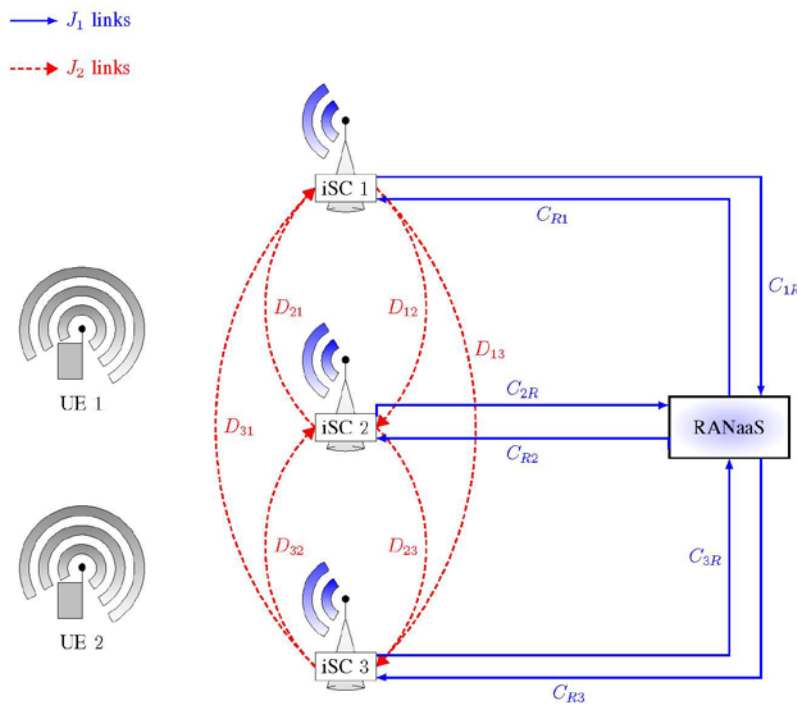


**Figure 4-28: Hybrid architecture with both J1 links and J2 links**

In the first scenario that we study, we consider a setting with  $N_{iSC}$  iSCs and  $N_{UE}$  UEs such that  $N_{UE} = N_{iSC}$ . The multi-user channel matrix from all the iSCs to all the UEs is then denoted by  $\mathbf{H}$  of size  $N_{iSC} \times N_{UE}$  with  $\mathbf{H}$  equal to

$$\mathbf{H} = [\mathbf{h}_1 \quad \dots \quad \mathbf{h}_{N_{UE}}]. \quad (4.62)$$

with the channel from all the iSCs to UE  $u$  equal to  $\mathbf{h}_u^H$  of size  $1 \times N_{iSC}$ . The received signals at the UEs is then written as

$$\mathbf{y} = \mathbf{H}^H \mathbf{x} + \mathbf{n}. \quad (4.63)$$

where  $\mathbf{x}$  (of size  $N_{iSC} \times 1$ ) is the signal vector transmitted jointly by all the iSCs,  $\mathbf{y}$  (of size  $N_{UE} \times 1$ ) is the vector made of the stacked received signals at all the UEs, and  $\mathbf{n}$  (of size  $N_{UE} \times 1$ ) a vector containing the additive white Gaussian noise of unit variance at all the UEs.

In this first analysis, we assume that the J2 links are used to exchange quantized versions of the downlink CSI between the iSCs. The quality of the quantized version which is exchanged depends on the quality of the J2 links. This CSI sharing step leads to a setting where iSC  $j$  has the knowledge of a quantized version of the full multi-user matrix. We denote this estimate at iSC  $j$  by  $\mathbf{H}^{(j)}$ . This corresponds to a so-called distributed CSIT scenario [128]. We then denote the variance of the estimation done over  $\mathbf{h}_i$  at iSC  $j$  by  $(\sigma_i^{(j)})^2$

In addition, the CSI is shared to the RANaaS with a high bandwidth J1 link such that we assume that the RANaaS has perfect knowledge of the full CSI, i.e. of the multi-use channel matrix  $\mathbf{H}$ . Based on the CSI and the user's data symbols to transmit, the RANaaS designs the signals that are then sent back to the iSCs, this time via the J1 links in the downlink direction. We assume that the bandwidth of the J1 link in that direction is much more restricted. This represents one particular configuration of heterogeneous backhaul architecture. The other possible configurations will be investigated in the future, with the ultimate goal to have a unified framework for any heterogeneous backhaul configuration.

Finally, the RANaaS is aware of the MCS used in the J2-links which means that all the  $\mathbf{H}^{(j)}$  are known in the RANaaS. We consider here that ZF precoding is used but other precoding schemes will be investigated in subsequent works.

Building upon the results of rate distortion theory, we approximate the distortion introduced by the finite capacity links by considering that the quantization of a random Gaussian variable of variance  $\sigma^2$  using  $N_{Quant}$  bits leads to a Gaussian quantization noise of variance  $\sigma^2 2^{-N_{Quant}}$  [130].

Our precoding scheme is as follows.

- In the  $j$ th iSC, the precoder is designed based on  $\mathbf{H}^{(j)}$ . The beamforming vector obtained to transmit to UE  $i$  is then denote by  $\mathbf{w}_i^{(j)}$  and is equal to

$$\mathbf{w}_i^{(j)} = (\mathbf{I} - \mathbf{H}_i^{(j)} (\mathbf{H}_i^{(j)\text{H}} \mathbf{H}_i^{(j)})^{-1} \mathbf{H}_i^{(j)\text{H}}) \mathbf{h}_i^{(j)} \sqrt{P} \quad (4.64)$$

where we have defined the nullspace formed by the other users by

$$\mathbf{H}_i^{(j)} = \begin{bmatrix} \mathbf{h}_1^{(j)} & \dots & \mathbf{h}_{i-1}^{(j)} & \mathbf{h}_{i+1}^{(j)} & \dots & \mathbf{h}_{N_{UE}}^{(j)} \end{bmatrix} \quad (4.65)$$

Note that the  $j$ th iSC computes the complete precoder  $\mathbf{W}^{(j)} = [\mathbf{w}_1^{(j)} \dots \mathbf{w}_{N_{UE}}^{(j)}]$  but only the  $j$ th row of this matrix is actually used in the transmission due to the precoding being distributed across all the iSCs. Indeed, the  $j$ th iSC only transmits

$$x_j = \mathbf{e}_j^{\text{H}} \mathbf{W}^{(j)} \mathbf{s}. \quad (4.66)$$

Where the vector  $\mathbf{s}$  is the vector containing all the user's data symbols to transmit.

- In the RANaaS, the CSI is assumed to be perfectly known thanks to the J1 having a large bandwidth in the direction iSC-RANaaS. Note that our scheme can in fact be applied as long as the CSI is known more accurately in the RANaaS, even if it is imperfectly. This assumption will not be verified in every scenario but it corresponds to a first configuration where we can obtain results. We will focus in later works on the other backhaul configurations where this assumption is not verified.
- Based on this perfect CSI, the precoding vector  $\mathbf{w}_i$  is computed as

$$\mathbf{w}_i = (\mathbf{I} - \mathbf{H}_i (\mathbf{H}_i^{\text{H}} \mathbf{H}_i)^{-1} \mathbf{H}_i^{\text{H}}) \mathbf{h}_i \sqrt{P}. \quad (4.67)$$

where we have similarly defined

$$\mathbf{H}_i = \begin{bmatrix} \mathbf{h}_1 & \dots & \mathbf{h}_{i-1} & \mathbf{h}_{i+1} & \dots & \mathbf{h}_{N_{UE}} \end{bmatrix}. \quad (4.68)$$

Furthermore, the RANaaS uses its knowledge of the CSI and of the J2-links parameters to reproduce the processing done at every iSC and hence computes all the  $\mathbf{w}_i^{(j)}$ , for all the UEs  $i$  and all the iSCs  $j$ .

#### 4.5.2 Assumptions and Requirements

- Radio access parameters are known in the RANaaS and at every iSC
- Backhaul parameters are known in the RANaaS
- J1 and J2 links of finite capacity
- Users data symbols are available at the iSCs
- The RRM has already been or is done based on the information provided as output by this CT as discussed by WP3 in D3.1. Similarly to the precoder studied here, the scheduler design can be split between the RANaaS and the iSCs. This question is investigated by WP3 and in particular in CT 3.9 of D3.1.

#### 4.5.3 Preliminary Results

Our first approach consists in exploiting only the local processing done at the iSCs to let the RANaaS share to the iSCs only the refinement information, i.e. to share  $\mathbf{w}_i - \mathbf{w}_i^{(j)}$  to the iSCs. Note in fact that due to the assumption of distributed precoding, it is only necessary to share the  $j$ th row of the precoding matrix to the  $j$ th iSC to analyse the amount of information represented by  $\mathbf{w}_i - \mathbf{w}_i^{(j)}$ , we use a Taylor approximation in the estimation error  $\mathbf{H} - \mathbf{H}^{(j)}$ . Indeed, we can show that

$$E[|\mathbf{e}_k^H(\mathbf{w}_i - \mathbf{w}_i^{(j)})|^2] \approx 2 \sum_{m=1, m \neq i}^{N_{UE}} (\sigma_m^{(j)})^2 + (\sigma_i^{(j)})^2. \quad (4.69)$$

From this equation, the variance of the signal that has to be transmitted to the  $j$ th iSC is known and can be seen to decrease as the accuracy of the CSI at the  $j$ th iSC increases. The information shared by the RANaaS to the iSC has then a smaller variance and can be more precisely quantized with the same number of bits. Hence, it is possible to evaluate analytically the improvement brought by our partially centralized precoding scheme.

To highlight the potential gains, we have simulated a simple network consisting of 5 iSCs and 5 UEs where every J1 links can be used to share 5 bits/ backhaul use to the iSCs and all the J2 links have the same capacity. We further consider a homogeneous scenario where the pathloss of all the wireless links is the same.

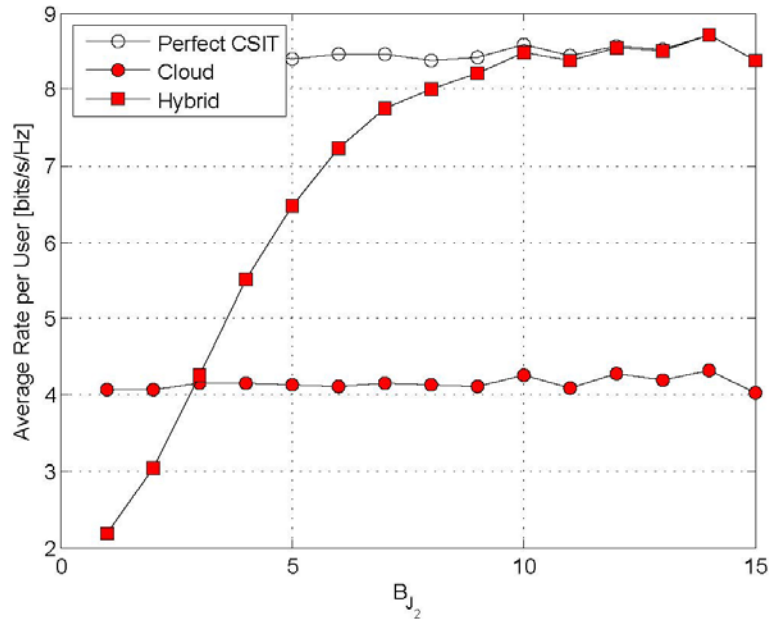


**Figure 4-29: J1 links carry 5 bits and J2 links  $B_{j_2}$  bits for each channel element. All the nodes are equipped with a single antenna and the channel is assumed to be Rayleigh fading with the same pathloss over all the links.**

As expected, the proposed scheme converges to the transmission with perfect CSI when the capacity of the J2 links increases. Our scheme is only outperformed by the conventional centralized one when the J2 links are too weak. This follows from the assumption that the channel estimates obtained at the iSCs are relatively precise. This is not the case when the number of bits used for the quantization is too low. Note that the number of bits for the J2 links has to be relatively large because all these bits are divided among the NiSC channel coefficients of the channel vector  $h_i$ .

Our preliminary results confirm the strong potential of exploiting the hybrid architecture. Yet, the proposed precoding scheme remains relatively naive and we have also introduced some assumptions that need to be discussed to make the proposed contribution more applicable to realistic networks. For example, we need to investigate what is the impact of delay in the backhaul links. Also we have modeled the distortion introduced by the backhaul and we will carry out simulations with practical quantization schemes. Finally, we will also investigate more advanced precoding algorithm to exploit more efficiently any possible backhaul architecture. Indeed, we have restricted the type of information which is exchanged via the J1 and the J2 links as well as the precoding scheme used. This means that the proposed scheme is interesting only for some ranges of bandwidth of the J1/J2 backhaul links, while our goal is to use optimally any backhaul configuration.

Our future work will consist in investigating the literature relative to Game Theory, Team Decision Theory [131], and Coordination Theory [132] to obtain tools and methods to conceive new precoding and cooperation schemes adapted to this scenario.

As already mentioned, the user scheduling, and more generally the RRM, can also be designed in order to exploit the hybrid architecture in the most efficient way possible. The design of the scheduler with the same architecture as in this CT is investigated in CT3.9 by WP3 as described in D3.1. The fundamental aspects of these two problems have a lot in common since they both mostly come down to the coordination problem mentioned above. Furthermore, studying these two problems jointly could lead to synergistic gains. It is therefore planned to investigate in the coming months the design of cross-layer algorithms and to exploit the insights obtained in both cases.

## 4.6 CT 2.6: Data Compression over RoF

### 4.6.1 Description

The deployment of dense networks based on a large number of small cells brings two main problems: the interference among the iSCs that limits the spectrum efficiency and the availability of high capacity backhauling connections.

The problem of the interference can be mitigated through the adoption of coordinated transmission techniques like CoMP, where several iSCs coordinate their transmission/reception towards/from a given UE. The capacity of the backhauling can be instead increased by leveraging on the structure of the OFDMA and SC-FDMA signals that are transmitted on the downlink and uplink of the LTE system, respectively.

In the following, we consider a network architecture based on Radio over Fibre (RoF), which is composed by a central unit RANaaS where the baseband processing is concentrated. The RANaaS is connected by means of fibre links to a large number of iSCs distributed over the coverage area. The access points are in the form of iSCs that are small and easy to install on the existing urban infrastructure of the operator like cabinets, phone boots, lampposts, etc.

In a conventional RoF architecture, the central unit performs the signal processing operations of traditional base station equipment including the higher layer protocols: Radio Resource Control (RRC), Radio Link Control (RLC), Medium Access Control (MAC), and the physical layer (L1) signal processing operations up to the generation of the composite digital baseband signal, as shown in Figure 4-30. The composite digital baseband signal is converted from electrical to optical (E/O) and transmitted over the fibre.

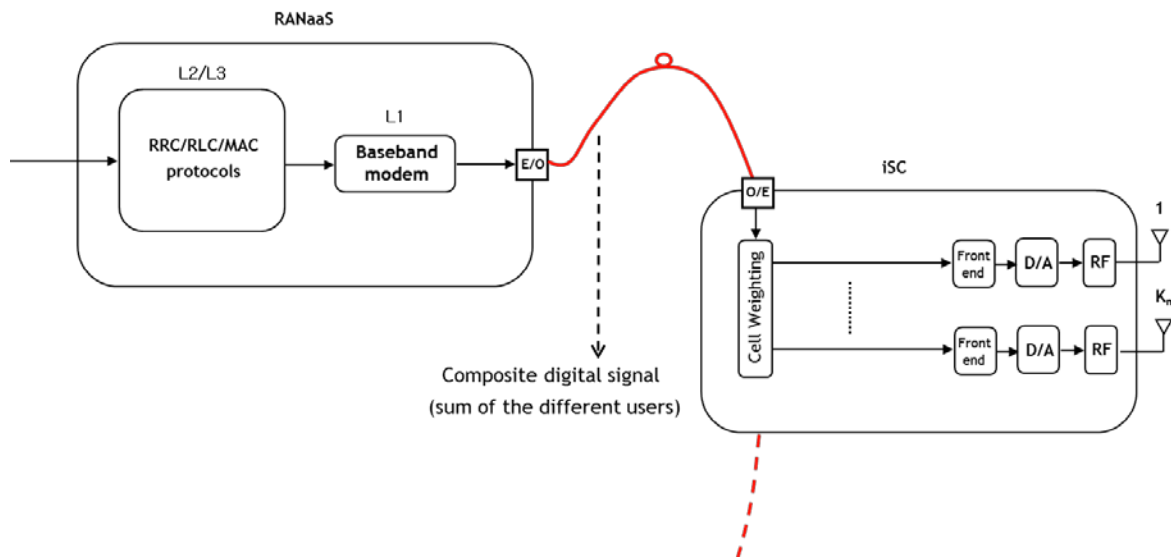


**Figure 4-30: Conventional downlink RoF architecture**

The iSC receives the composite baseband signal that is first converted from optical to electrical (O/E). The signal is then subject to a weighting operation that operates on cell basis (i.e. for all the users camped or served by the iSC). The weighting operation is optional (i.e. in conventional iSC implementations may not be present) and its purpose is to shape the radiation diagram of the iSC antennas in order to optimize the coverage. For example some antenna parameters, like vertical tilt or 3dB azimuth beamwidth, can be adapted in a semi-static way under the control of the RANaaS.

After the cell weighting operation, the signal is then filtered by a front-end, converted from digital to analogue form (D/A), up-converted from baseband to radio frequency (RF), amplified by a power amplifier, and radiated by the antennas. The previous signal processing steps refer to the downlink. In the uplink the inverse operations are performed both in the iSC and the RANaaS, and the signal transmitted over the optical fibre is still a composite signal formed by the sum of the different user signals. In the case of a radio access technology like LTE, the time domain signal at the output of the IFFT module at the transmitter is sent over the optical fibre link. Accordingly, the composite baseband signal, which is made by the sum of the various user signals, can be transmitted over the optical fibre link by using standard transmission formats defined by international consortia such as CPRI (Common Public Radio Interface) [82] or OBSAI (Open Base Station Architecture Initiative) [83].

An estimate of the backhauling capacity required for the transmission of one LTE carrier over the fibre link is easily obtained considering the characteristics of the OFDM signal. The signal at the IFFT output is sampled with a frequency of  $f_s = 30.72$  MHz in case of a  $B_{RAN} = 20$  MHz carrier [84]. The signal is typically oversampled by a factor  $OF=2$ , so that the sampling frequency of the signal transmitted on the fibre is 61.44 Mbit/s. Besides, two signals must be transmitted when considering a MIMO with  $N_T^{iSC} = 2$  antennas at the iSCs. Finally, assuming that the quantization of the In-phase (I) and Quadrature (Q) components of the OFDM signal is done using  $N_{quant}^{DL} = 10$  bits, it is possible to estimate the throughput  $D$  on the fibre with the following formula

$$D = (N_T^{iSC}) \cdot (OF) \cdot (f_s) \cdot 2 \cdot (N_{quant}^{DL}) \quad (4.70)$$

and substituting the parameter values it provides

$$D = \underbrace{2}_{\text{number of iSC antennas}} \cdot \underbrace{61.44}_{\text{sampling frequency}} \cdot \underbrace{2}_{\text{I/Q components}} \cdot \underbrace{10}_{\text{signal quantization}} = 2.46 \text{ Gbit/s} \quad (4.71)$$

The value calculated above shows that the backhauling may become a potential bottleneck when considering a scenario with a large number of small cells, or a MIMO configuration with a large number of antennas or also a multi-RAT scenario. The obtained value must be compared with the throughput that can be provided by the different technologies used for backhauling. The Table 4-3 derived from [15] provides a categorization of the different backhauling technologies (i.e. typical backhaul widely used in the market). A further categorization of the backhauling technologies can be also found in [86]. The analysis of the throughput that can be carried by the current backhauling technologies shows that only a limited number of LTE carriers can be transmitted over a fibre link or alternatively only a limited number of iSCs can be connected over a unique fibre link. It then follows that the data compression techniques for increasing the transmission efficiency over the backhauling are of paramount importance for the dense network scenarios. It must be pointed out that the new RoF architecture described in the following, denoted as Frequency Domain RoF (FD-RoF), it is not based on “compression of data” (usually degrading quality) but on an alternative split of the physical layer functionalities between RANaaS and iSC.

**Table 4-3: Categorization of non-ideal backhaul [15]**

Backhaul categories	Latency (one way)	Throughput
Fibre Access 1	10 – 30 ms	10 M – 10 Gbps
Fibre Access 2	5 – 10 ms	100 – 1000 Mbps
DSL Access	15 – 60 ms	10 – 100 Mbps
Cable	25 – 35 ms	10 – 100 Mbps
Wireless Backhaul	5 – 35 ms	10Mbps – 100 Mbps typical, maybe up to Gbps range

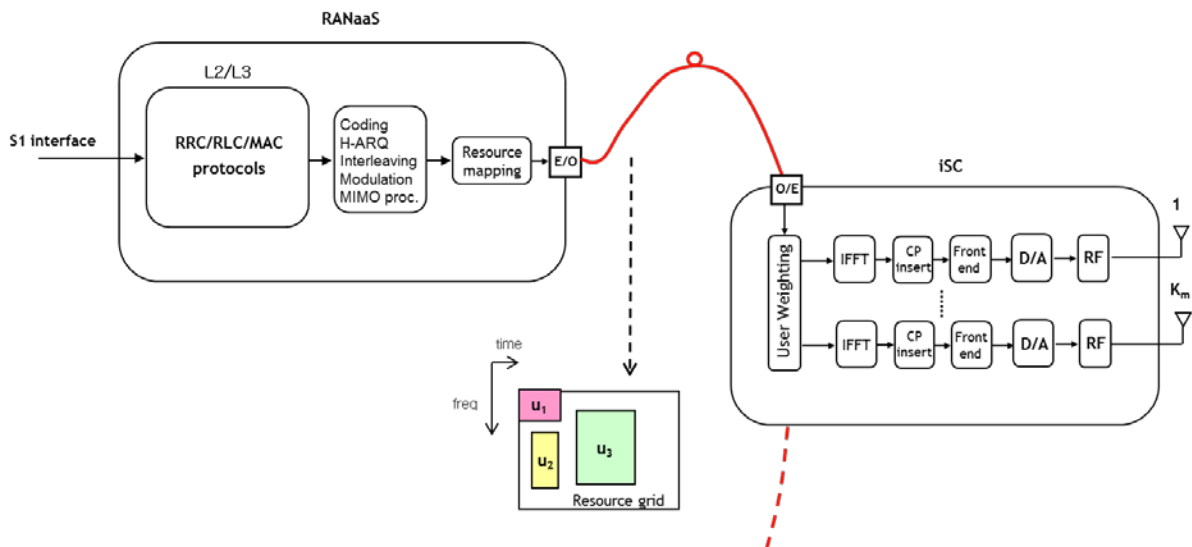
Besides, the conventional RoF architecture shown in

Figure 4-30 is highly non-efficient when it is necessary to perform signal processing operations on a per-user basis, like for example adaptive beamforming or coordinated transmissions between multiple iSCs. In this context, the weight factors are different for each user, and they have to be continuously updated in order to track the movement of the user within the cell and to track the channel variations [141]. The signal processing algorithms operating on user basis consist in separately multiplying each user signal at the different antenna branches for complex weight factors, which are applied to the signals before they are radiated in downlink, or before that the received signals from the different antennas are combined in uplink. The application of these algorithms in the small cells, especially in case of dense scenarios limited by the interference, can provide significant gains in terms of throughput and quality of service perceived by the users.

The application of these algorithms in a conventional RoF architecture requires performing all the signal processing operations in the RANaaS prior to the IFFT operation, where the signals of the different users are still separately available. As already mentioned, this architecture lacks of flexibility because it is necessary to transmit one composite signal for each antenna element of each iSC. It follows that, as the number of iSCs connected via one link increases, the available transmission capacity on the fibre becomes rapidly a bottleneck.

To cope with the problems listed above it is possible to define a new RoF architecture, denoted as Frequency Domain RoF (FD-RoF) that enables the signal processing on a per-user basis in the iSCs, by providing the necessary level of flexibility and scalability. Besides, this architecture should also provide advantages in terms of throughput reduction of the signals transmitted over the backhauling link with respect to state of the art solutions. The throughput reduction is particularly important considering that broadband wireless communication systems (e.g. LTE and WiMAX) are capable of providing aggregate per-cell throughput in the order of hundreds of Mbps. Furthermore, a more efficient use of transmission resources between the RANaaS and the iSCs permits also to increase the maximum number of iSCs that can be connected to a given fibre ring.

Such new architecture should enable the signal processing on a per-user basis either within the iSCs or in a cooperative form involving multiple iSCs thanks to a particular partitioning of the baseband (L1) modem functionalities between the RANaaS and the iSCs. In particular, coding, Hybrid Automatic Repeat request (HARQ), interleaving, modulation, MIMO processing, and resource mapping are still performed in the RANaaS, while IFFT, cyclic prefix insertion, filtering and RF conversion are performed in the iSC, as shown in Figure 4-31 for the downlink transmitter part and Figure 4-32 for the uplink receiver part. So, the signal transmitted over the optical fibre is the signal at the output/input of the resource mapping, where the user signals are separated in the frequency domain and the overall throughput with respect to the traditional RoF architecture is significantly reduced. The reduction comes from the fact that some ancillary information that just represents overhead (e.g. the cyclic prefix, the null subcarrier at the band edge) does not need to be transmitted over the fibre.



**Figure 4-31: Frequency Domain RoF architecture: downlink transmitter part**

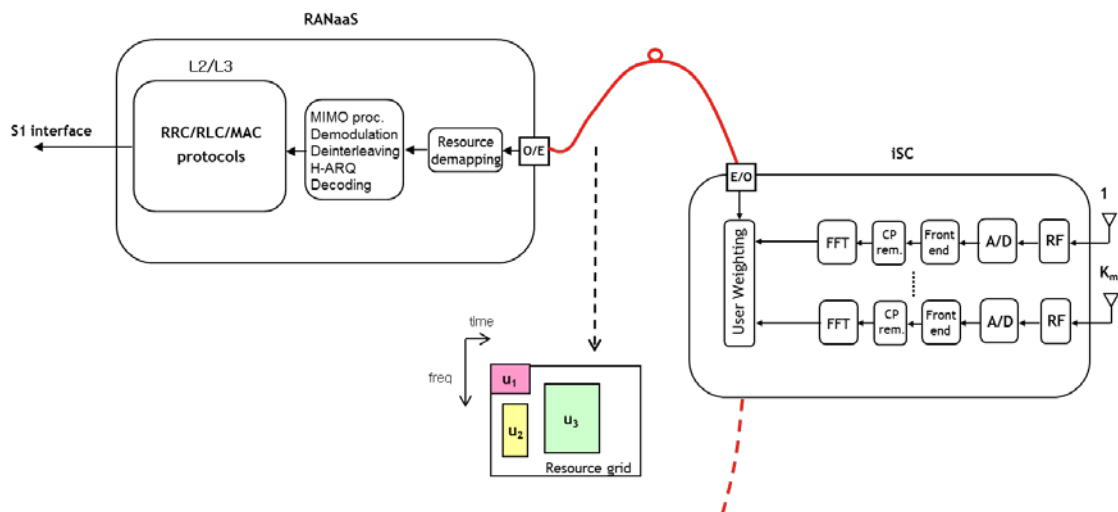


**Figure 4-32: Frequency Domain RoF architecture: uplink receiver part**

As it can be easily seen, this novel architecture allows user-based signal processing operations such as adaptive beamforming or coordinated multi-point transmission to be performed in the iSC for each user separately while the calculation of the adaptive weighting coefficients can be performed either in the iSC or in the RANaaS if network coordination algorithms are required.

#### 4.6.2 Assumptions and Requirements

##### Assumptions:

- Large number of iSCs in the coverage area
- Wired connection (fibre based) between iSCs and between iSCs and RANaaS
- Optional availability of an iNC for joint RAN/BH optimization

##### Requirements:

- Limited capacity for J1 and preferably fibre based
- Access to the transceiver to implement FD approach

#### 4.6.3 Preliminary Results

The physical layer functionalities can be partitioned between RANaaS and iSC in different ways. In general, more layer 1 functions that are remotely executed at the iSC correspond to a reduction of the data throughput load on the backhaul link between RANaaS and iSC. On the other hand, more layer 1 functions at the iSC corresponds to an increase of the C-Plane signalling load, as more control information is required at the iSC side to perform functions like modulation, spatial precoding, resource element (RE) mapping, power scaling of the different users/channels, etc.. This makes more complex the RANaaS/iSC interface and clearly increases the complexity of the iSC.

##### Layer 1 partitioning options for the downlink

A first possible layer 1 partitioning for the downlink is depicted in Figure 4-33, where the IFFT operation is moved from the RANaaS to the iSC. The RANaaS transmits over the backhaul link the I/Q OFDM user signal in the frequency domain after the operations of channel encoding, scrambling, modulation, spatial precoding, and RE mapping. In particular the iSC executes the following layer 1 signal processing operations for each transmit antenna: IFFT, cyclic prefix insertion, oversampling, filtering, D/A conversion, and RF processing.

The execution of the spatial precoding at the RANaaS maps the regular symbol constellation (e.g. QPSK, 16-QAM and 64-QAM) used by the different physical channels into a more complex and, in some way less predictable, signal pattern on the I/Q complex plane. It follows that the direct quantization of the I/Q signal components at the IFFT input is the most practical way for the transmission of the signal over the backhaul link.

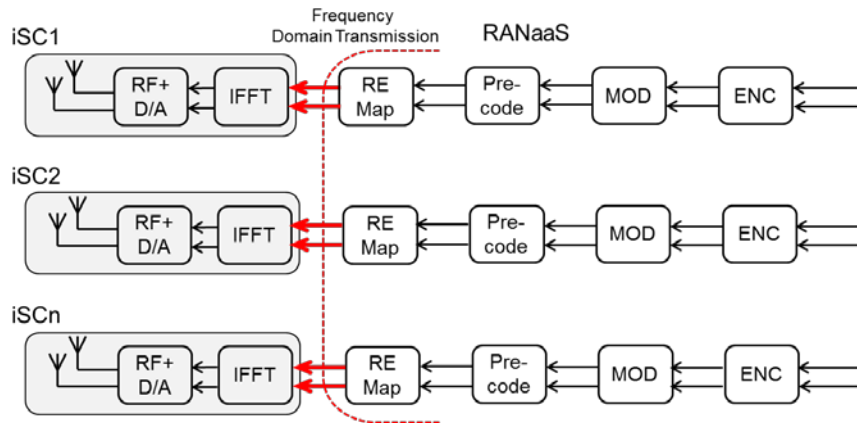


**Figure 4-33: Downlink architecture of Frequency Domain RoF (option 2.6a)**

In the following it is considered the case of MIMO transmission with  $N_T^{iSC} = 2$  transmit antennas at the iSC side. Assuming the case of spatial multiplexing transmission, the maximum number of signals  $N_s$  to be transmitted on the backhaul link is equal to  $N_T^{iSC}$ . Considering the case of a LTE carrier with bandwidth  $B_{RAN} = 20 \text{ MHz}$ , the throughput  $D$  on one backhaul link can be expressed by the following formula:

$$D = 2 \cdot (N_{sc}) \cdot (N_s) \cdot (N_{quant}^{DL}) \cdot (1/T_s) \tag{4.72}$$

where  $N_{sc}$  is the number of active (i.e. modulated) subcarriers,  $N_{quant}^{DL}$  is the number of bits used for the quantization of the I/Q components and  $T_s = 66.6 \mu\text{s}$  is the OFDM symbols duration for the LTE system. The multiplication factor 2 in the equation above and in some other equations in the following takes into account that each baseband complex signal is composed by two components (i.e. I/Q). In case of  $N_s = 2$  signals to be transmitted on the BH, assuming  $N_{quant}^{DL} = 10$  bits and  $N_{sc} = 1200$  the required throughput on the backhaul link is equal to:

$$D = 2 \cdot 1200 \cdot 2 \cdot 10 \cdot (1/66.6 \cdot 10^{-6}) = 720 \text{ Mbit/s}$$

that corresponds to a reduction factor of more than 3 times compared to the time domain transmission of the OFDM signal. Notice that the equation above does not consider the line coding that can be used to protect the transmitted information. A typical line code is the 8b/10b [142] that corresponds to a rate increase of a factor  $10/8=1.25$  over the backhauling.

A further reduction by a factor 2 can be obtained in case of single codeword (CW) transmission by moving the precoding operation locally at the iSC side. In such a case in fact a unique signal ( $N_s = 1$ ) must be transmitted on the backhauling link. The spatial precoding can be for example an adaptive beamforming on a per user basis. This mode of operation corresponds to the transmission mode 7 (Single layer beamforming) introduced in the Release 8 of the LTE standard [112]. The system block diagram for this specific mode of operation is depicted in Figure 4-34.

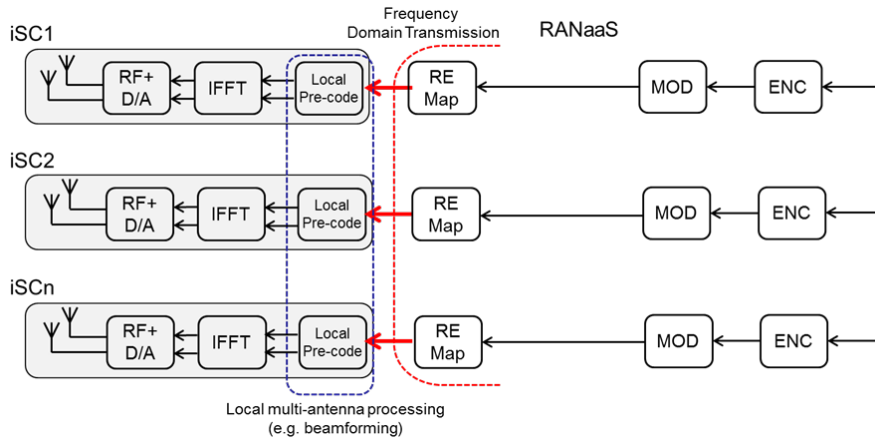


**Figure 4-34: Downlink architecture of Frequency Domain RoF in case of single CW transmission (option 2.6b)**

By applying the equation given above, the data throughput over one backhaul link in case of single codeword transmission is equal to

$$D = 2 \cdot (N_{sc}) \cdot (N_s) \cdot (N_{quant}^{DL}) \cdot (1/T_S) \tag{4.73}$$

and substituting the parameter values (i.e.  $N_s=1$ ) it provides

$$D = 2 \cdot 1200 \cdot 1 \cdot 10 \cdot (1/66.6 \cdot 10^{-6}) = 360 \text{ Mbit/s}$$

that corresponds to a reduction of about 6 times over the conventional time domain transmission.

A different layer 1 partitioning can be also analysed by moving the RANaaS/iSC interface so that more physical layer functions are locally executed at the iSC. The Figure 4-35 shows this option where the interface is located at the output of the channel encoder so that the encoded data bits are transmitted on the RANaaS-iSC backhaul link.

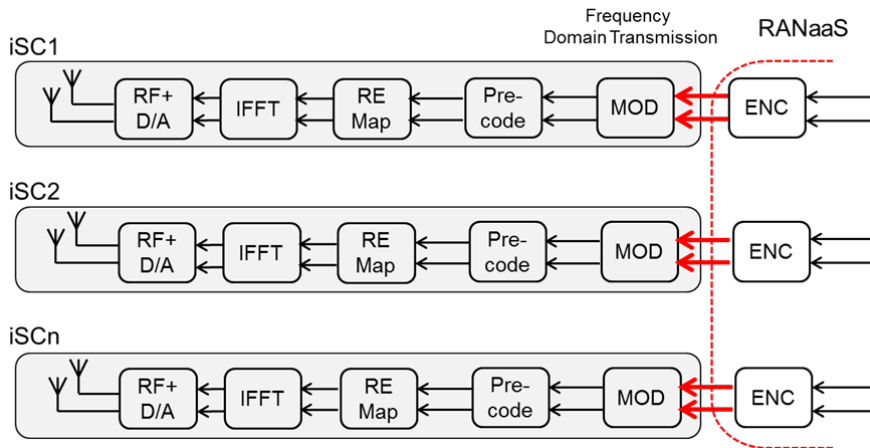


**Figure 4-35: Downlink architecture of Frequency Domain RoF (option 2.6c)**

In this case the iSC executes the modulation, spatial precoding, RE mapping, IFFT, CP insertion, upsampling, filtering, DA conversion, and RF processing. The data throughput on the backhaul link can be expressed with the following formula

$$D = N_{sc} \cdot Q_m \cdot N_s \cdot (1/T_S) \tag{4.74}$$

where  $N_{sc}$  is the number of active (i.e. modulated) subcarriers,  $Q_m$  is the number of bits carried by each subcarriers,  $N_s$  is the number of transmitted signals and  $T_S = 66.6 \mu s$  is the OFDM symbols duration. Considering the case of a 20 MHz LTE carrier ( $N_{sc} = 1200$ ), MIMO transmission with  $N_s = 2$  signals and the worst case of 64-QAM modulation ( $Q_m = 6$ ) the data rate on the backhaul is equal to

$$D = 1200 \cdot 6 \cdot 2 \cdot (1/66.6 \cdot 10^{-6}) = 216 \text{ Mbit/s}$$

that corresponds to a reduction factor of about ten times compared with the conventional time domain RoF transmission. The problem with this solution is that much larger Layer 1/2 control information is required at the iSC in order to execute the modulation, spatial precoding, and RE mapping operations, which requires the definition of a more complex interface between RANaaS and iSC. Besides, as this control information must be refreshed every subframe (1 ms) according to the scheduling decisions, the actual backhaul load could be higher than the value calculated above.

Notice also that in the option 2.6a the spatial precoding operation is performed in the RANaaS while, on the contrary, it is executed at the iSC for the options 2.6b and 2.6c. In the former case (i.e. option 2.6a) the downlink CSI is available at the RANaaS by means of the feedback information reported by the UE over the uplink in the form for example of RI (Rank Indicator), PMI (Precoding Matrix Indicator), and CQI (Channel Quality Indicator). In particular the downlink CSI after being estimated at the UEs from downlink training sequences, it is fed back from the UEs to one iSC and then subsequently shared via the J1 links to the RANaaS. In the latter case (i.e. options 2.6b and 2.6c) the downlink CSI can be directly exploited at the iSC by extracting from the uplink signal the CSI feedback information reported by the UE or, alternatively, by estimating the downlink CSI from the uplink signal if the uplink/downlink channel reciprocity is applicable.

The different layer 1 partitioning options for the downlink are summarized in Table 4-4.

**Table 4-4: Layer 1 partitioning options for downlink RoF**

DL Technique	Functions executed at iSC	L1/L2 control info necessary at iSC
TD-RoF	D/A conversion, RF processing	None
FD-RoF (option 2.6a)	IFFT, CP insertion, oversampling, Filtering, D/A conversion, RF processing	None
FD-RoF (option 2.6b)	Same of option 2.6a + local precoding	Partial mapping information (RB allocation)
FD-RoF (option 2.6c)	Modulation, precoding, RE mapping, IFFT, CP insertion, oversampling, Filtering, D/A conversion, RF processing	Full mapping information for each user on subframe basis (RB allocation, modulation scheme, power scaling, precoding scheme, etc.)

**Layer 1 partitioning options for the uplink**

The equivalent of the option 2.6a for the uplink is depicted in Figure 4-36, where the signal at the FFT output after proper quantization is transmitted on the backhaul link. With this kind of uplink layer 1 partitioning the signals received from different iSCs can be both separately or jointly processed at the RANaaS. In the second case, schemes that perform the cooperative detection and/or decoding of the iSCs signals can be envisaged depending on the baseband processing capability available at the RANaaS.

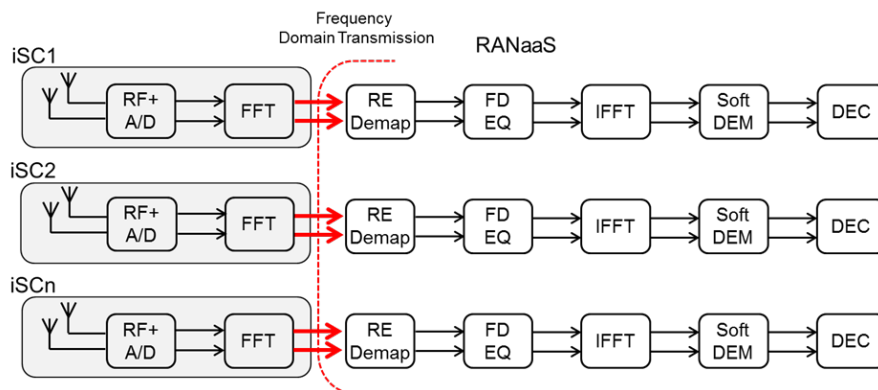


**Figure 4-36: Uplink architecture of Frequency Domain RoF (option 2.6d)**

Similarly to the downlink the data throughput on the backhaul link can be expressed with the following formula

$$D = 2 \cdot (N_{sc}) \cdot (N_s) \cdot (N_{quant}^{UL}) \cdot (1/T_s) \tag{4.75}$$

Considering the case of a 20 MHz LTE carrier and Release 10 MIMO transmission (i.e. double codeword transmission, with  $N_s = 2$ ) we then have

$$D = 2 \cdot 1200 \cdot 2 \cdot 10 \cdot (1/66.6 \cdot 10^{-6}) = 720 \text{ Mbit/s}$$

still assuming a 10-bit quantization of the I/Q signal at the FFT output. In the uplink case, the Release 8 of the LTE specifications provides support only for single codeword transmission [112]. It follows that the option 2.6b described for the downlink is directly applicable to the Release 8 LTE uplink, as shown in Figure 4-37.

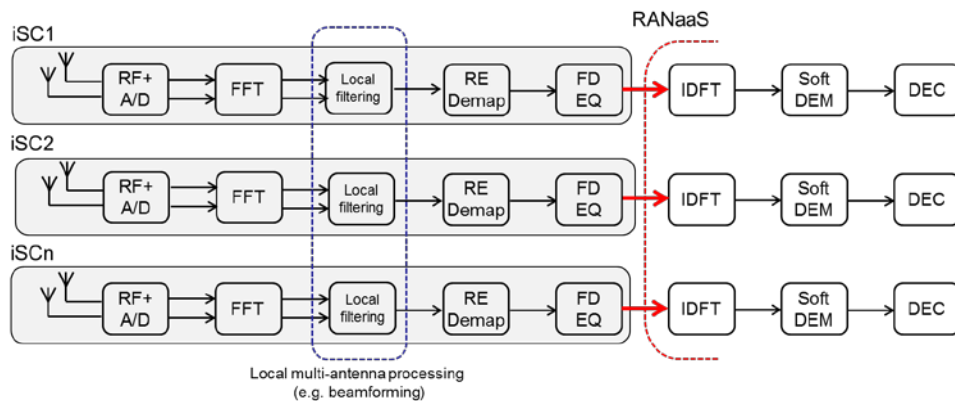


**Figure 4-37: Uplink architecture of Frequency Domain RoF in case of single CW transmission (option 2.6e)**

Also in this case, the combining or spatial filtering function can be locally executed at the iSC side. The filtering can be a simple MRC (Maximum Ratio Combining) scheme or possibly more complex adaptive beamforming algorithms can be conceived for the implementation at the iSC (for example interference rejection combining techniques). It must be pointed out that, differently from the option 2.6d, the option 2.6e requires the execution of the uplink channel estimation function at the iSC side. The advantage of this solution is that a single signal ( $N_s = 1$ ) needs to be transmitted on the backhaul, reducing the load of a factor two on the iSC-RANaaS link

$$D = 2 \cdot 1200 \cdot 1 \cdot 10 \cdot (1/66 \cdot 10^{-6}) = 360 \text{ Mbit/s}$$

Finally, also the equivalent of the option 2.6c can be considered for the uplink. In this case the soft bits at the soft demodulator output are transmitted over the backhaul link. This option can be denoted as “LLR over fibre” (LLR, Log Likelihood Ratios) [95]. It must be noticed that this option, depicted in Figure 4-38, it is not a frequency domain transmission because the LLRs are taken after the IDFT inverse precoding at the receiver.

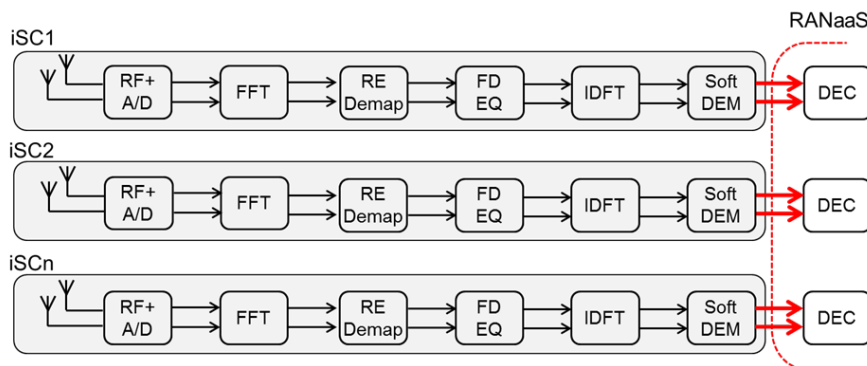


**Figure 4-38: Uplink architecture of Frequency Domain RoF (option 2.6f)**

The data throughput on the backhaul link can be calculated with the following formula

$$D = (N_{sc}) \cdot Q_m \cdot N_s \cdot (N_{quant}^{UL}) \cdot (1/T_S) \quad (4.76)$$

where  $N_{quant}^{UL}$  is here equal to the number of bits used for the LLR quantization (a typical value is in the order of 4-5 bits). Considering the case of a 20 MHz LTE carrier, MIMO Release 10 double codeword transmission ( $N_s = 2$ ),  $N_{quant}^{UL} = 4$  and the worst case of 64-QAM modulation ( $Q_m = 6$ ) we then obtain

$$D = 1200 \cdot 6 \cdot 2 \cdot 4 \cdot (1/66.6 \cdot 10^{-6}) = 865 \text{ Mbit/s}$$

which corresponds to a reduction factor of about 3 times compared to the conventional time domain RoF. It can be observed that the reduction factor of the option 2.6f is practically equivalent to that of option 2.6d but at the price of a higher complexity of the iSC as the functions like channel estimation, RE demapping, frequency domain equalization, and soft demodulation need to be moved at the iSC side. Clearly, the higher complexity of the iSC may reflect on the size of the equipment and in turn to a more difficult on field deployments.

Besides by bringing more processing to the iSC, shifting some processing at each iSC may provide lower performance compared to centralized cooperative detection and/or decoding schemes that are instead applicable together with the option 2.6d.

The different layer 1 partitioning options for the uplink are summarized in Table 4-5.

**Table 4-5: Layer 1 partitioning options for uplink RoF**

Uplink Technique	Functions executed at iSC	L1/L2 control info necessary at iSC
TD-RoF	RF processing, A/D conversion	None
FD-RoF (option 2.6d)	RF processing, A/D conversion, filtering, CP removal, FFT	None
FD-RoF (option 2.6e)	Same of option 2.6d + Channel Estimation, local precoding, Freq. Dom. Equalization	Partial mapping information (RB allocation)
RoF – LLR over fibre (option 2.6f)	RF processing, A/D conversion, filtering, CP removal, FFT, RE demapping, Channel Estimation, Freq. Dom. Equalization, IDFT inverse precoding, soft demodulation	Full mapping information for each user on subframe basis (RB allocation, modulation scheme, power scaling, precoding scheme, etc.)

## 4.7 CT 2.7: Millimetre Wave Backhauling

### 4.7.1 Description

#### Millimetre Wave as a Transport Technology

A dense deployment of small cells is a key enabler in the iJOIN architecture and therefore an equally dense backhaul network is required. Also, due to some of the centralized processing envisioned, the small cells require backhaul links with very high capacity, which usually are only achieved by fibre. However, in locations where fibre is either too expensive or complex to deploy, wireless mmWave technology has become a viable replacement, which is investigated by this CT. Section 4.7.3 describes some of the features that makes mmWave technology a promising alternative to fibre.

Figure 4-39 shows a part of the physical architecture envisioned in iJOIN, highlighting the utilization of mmWave links. They can be deployed to directly connect iSCs with the RANaaS, as depicted in the bottom part of the figure. Alternatively, mmWave are used as components of a multi-hop backhaul in order to transmit over larger distances. In such a multi-hop backhaul iJOIN transport nodes (iTN) [123]) are applied to connect several backhaul links and allows also to switch from one transmission technique to another, e.g. switch from mmWave to fibre as depicted in the top part of the figure. Furthermore, mmWave links can interconnect iSCs among each other to exchange information via the J2 interface, or they can form a multi-hop backhaul chain to extend the mmWave range as depicted in the top left part of the figure.

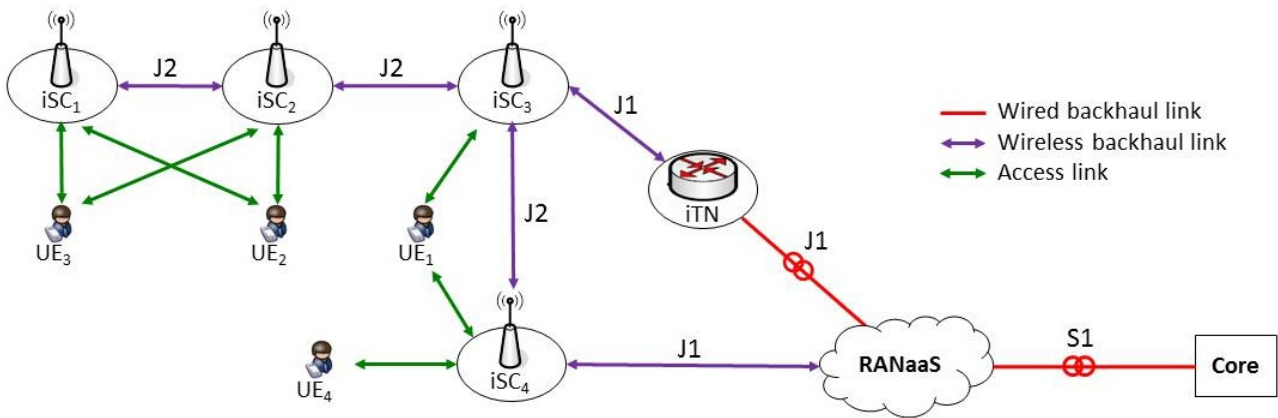


**Figure 4-39: mmWave backhaul deployment in cloud-based networks**

Deployed in these ways, mmWave links serve as an enabling technology for other CTs, as any data can be carried by them.

Apart from using mmWave links as a pure transport technology, a functional split that physically separates a part of the PHY layer processing from the receiving node opens new opportunities for optimizing the joint access and backhaul link. The conventional approach for uplink wireless backhaul which is used in current commercial products is depicted in Figure 4-40.

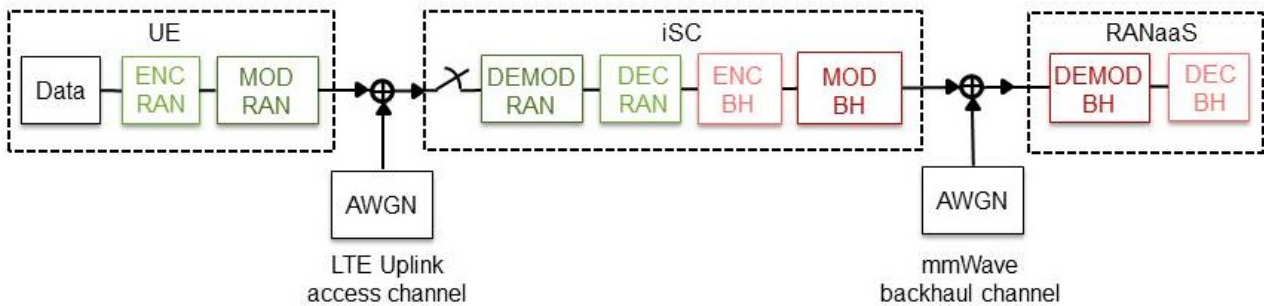


**Figure 4-40: Conventional decode and forward backhauling**

It corresponds to a decode-and-forward scheme: the user data transmitted from the UE to the iSC is decoded, then encoded for the BH link and transmitted to the RANaaS. However, this design does not enable some of the cooperative techniques envisioned by iJOIN. Some of these techniques, e.g. CT2.2, require not only the decoded user data, but the received signals in the RANaaS. This means that decoding cannot take place at the iSC, but instead a baseband I/Q- stream of symbols has to be transmitted. This kind of architecture is already used in the RoF approach (CT2.6 described in Section 4.6). CT2.7 now proposes a similar approach, but instead of fibre, mmWave backhaul is used. Similar to RoF, we call this approach Radio-over-Radio (RoR). The baseband model is depicted in Figure 4-41.

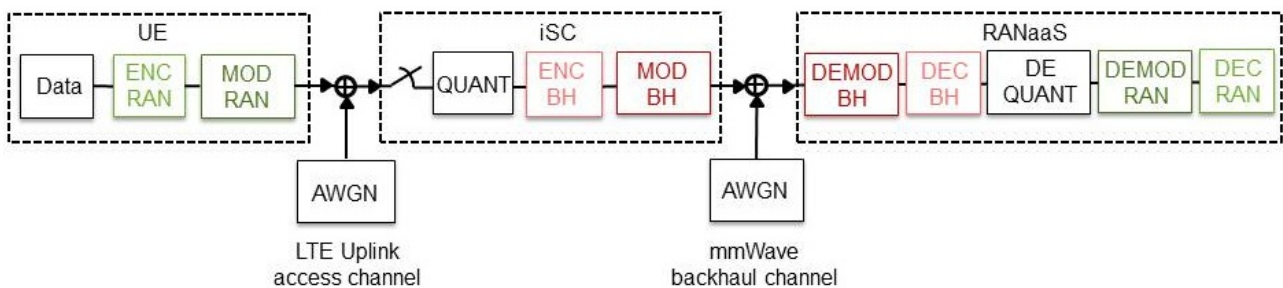


**Figure 4-41: Radio-over-radio approach**

It corresponds to a functional split where the decoding is centralized in the RANaaS, while RF-processing and analog to digital conversion is done at the iSCs. Intermediate steps like equalization, FFT/IFFT or precoding can be done either at the iSC or in the RANaaS, with benefits similar to the ones investigated by CT2.6. For details on possible functional splits, see Section 6.2.7.

### Joint Coding for Access and Backhaul

The wireless mmWave channel is a much more attenuated than a fibre channel, resulting in a lower average SNR. This usually requires a better channel coding on the BH link to ensure reliable communications. As the access channel already employs a channel code, this leads to the question whether two separate codes are needed for both channels. If we consider the uplink and decoding of the access code in the RANaaS, the sampled data on the BH link is still protected by the access links code. Therefore, it might be beneficial to not re-encode the digitalized data, but just reuse the RANs code, possibly adapting its code rate to the channel quality of both the access and BH channel.

The increased high data rate demands on the backhaul due to I/Q backhauling might become a constraint on the iJOIN architecture and functional split, with the BH link being the bottleneck. As channel codes introduce additional overhead, the code rates on the access and BH channel are a key parameter to this data rate demand. Therefore, the coding schemes of RAN and BH channel under a constraint BH should be jointly optimized. The data rate required on the backhaul channel can be calculated as:

$$D_{BH} = \frac{D_{UE} \cdot N_{quant}^{UL} \cdot 2}{R_c^{RAN} \cdot Q_m^{RAN} \cdot R_c^{BH}} \quad (4.77)$$

By constraining the BH data rate to  $D_{BH} = const$  and keeping the quantization  $N_{quant}^{UL}$ , modulation schemes  $Q_m$  and user data rate  $D_{UE}$  constant as well, the constraint reduces to a joint code rate  $R_c^{RAN} \cdot R_c^{BH} = const$ . Conventionally, each code rate is set independently depending on each channels quality. However, in this case, the product code rate is constrained. This code rate can now only be “shifted” between the access and BH channel, resulting in either a more strongly encoded BH and weak access channel or vice versa. Some results on the effect of this code shifting are given in Section 4.7.3.

#### 4.7.2 Assumptions and Requirements

- Direct wireless connection between iSC and RANaaS (LOS, no iTN)
- Single UE connected to a single iSC
- Limited capacity on BH link
- Perfect CSI at iSC
- Perfect synchronisation between UE/iSC/RANaaS

#### 4.7.3 Preliminary Results

##### General Characteristics of mmWave Technology

Because mmWave technology can be used as a general transport technology, general investigations were undertaken to summarize some of its characteristics for the benefits of other CTs.

By mmWave technology, we refer to the bands in the range of 60 to 90 GHz, also sometimes called the E-band. It is well known that these bands offer a very large bandwidth and simple licensing [89]. However, based on Friis formula, it is apparent that mmWaves are much more strongly attenuated than the waves used in access technology. Also, they face additional atmospheric attenuation of up to 15 dB/km [89]. A link budget, based on internal calculations is summarized in Table 4-6.

**Table 4-6: Link budget for mmWave link**

Parameter	Unit	value
Max. effective isotropic radiated power (EIRP)	dBm	40
thermal noise (BW 4 GHz)	dBm	-78
rx noise figure	dB	8
receiver noise	dBm	-70
analog losses	dB	6
digital losses	dB	3
req SINR (4QAM)	dB	11.4
receiver sensitivity	dBm	-49.6
rx antenna gain	dBi	35
rain margin	dB	3
oxygen attenuation (300m)	dB	4.5
max pathloss	dB	117.1
<b>max range</b>	<b>m</b>	<b>285</b>

As can be seen, the range is fairly limited to a few hundred meters. It should be kept in mind that this range can scale, if antennas with even higher gains are used (up to 51 dBi in commercial products) or other carrier frequencies are used (60 GHz faces severe attenuation by oxygen). In fact, the gain of an antenna of a fixed aperture size scales quadratically with higher frequencies, which can more than mitigate the higher pathloss. Currently, ranges of up to 10 km can be achieved. The high antennas gain results in a very directional, point-to-point link that requires LOS. This has the advantage that multi-path effects are very limited while at the same time the receivers and transmitters are immobile. Therefore, the channel is very static requiring little equalization and can be seen as an AWGN channel with free space propagation (pathloss exponent  $\epsilon=2$ ).

The data rate that mmWave links can provide is currently between 1 Gbps (commercial products) and 5 Gbps (iJOIN 60 GHz demonstrator) as described in IR6.1 [124]. In future these data rate might increase, a cautious forecast can be found in Table 4-7. It is based on the iJOIN 60 GHz demonstrator's capabilities and extrapolates it using technologies that are viable in principle, yet are not implemented in the demonstrator due to practical limitations of the hardware and architecture. By doubling the bandwidth (four ECMA-387 channels instead of two), doubling the spectral efficiency by using, e.g. 16-QAM instead of 4-QAM and using 4-fold spatial diversity (2x2 MIMO and vertical/horizontal polarization), the data rate could be increased 16 fold to 80 Gbps in the future.

**Table 4-7: Data rates for mmWave links**

Parameter	Unit	60 GHz demonstrator	Exemplary forecast
Bandwidth	GHz	4.32	8.64
Symbol rate	GHz	3.456	6.912
Code rate		3/4	3/4
Spectral efficiency of modulation scheme	Bits/cu	2	4
Overhead	%	4	4
Spatial diversity		1	4
Data rate	Gbps	5	80

Further investigations will be carried out to also determine the delay and energy consumption of mmWave links.

### Joint Coding for Access and Backhaul

Simulations were undertaken to evaluate the effect of a constrained product code rate as described in Section 4.7.1. For this, the end-to-end (UE to RANaaS) BER was evaluated for various access and BH channel qualities with four of gradually shifted coding schemes of product code rate 1/3. An overview of the simulation parameters can be found in Table 4-8. The results are depicted in Figure 4-42. The gradient bars in the legend illustrate the gradual “shift” of the code rates.

**Table 4-8: Overview of simulation parameters**

Parameter	Value
$N_{UE}$	1
$N_{iSC}$	1
$N_T^{UE}$	1
$N_R^{iSC}$	1
$N_{quant}^{UL}$	4
$Q_m$	2
$\Gamma$	turbo code
$R_c^{RAN}$	{1, 2/3, 1/2, 1/3}
$R_c^{BH}$	{1, 2/3, 1/2, 1/3}
Channel	AWGN
SNR RAN	0-20 dB
SNR BH	{0 dB, 5 dB, 10 dB, 15 dB}

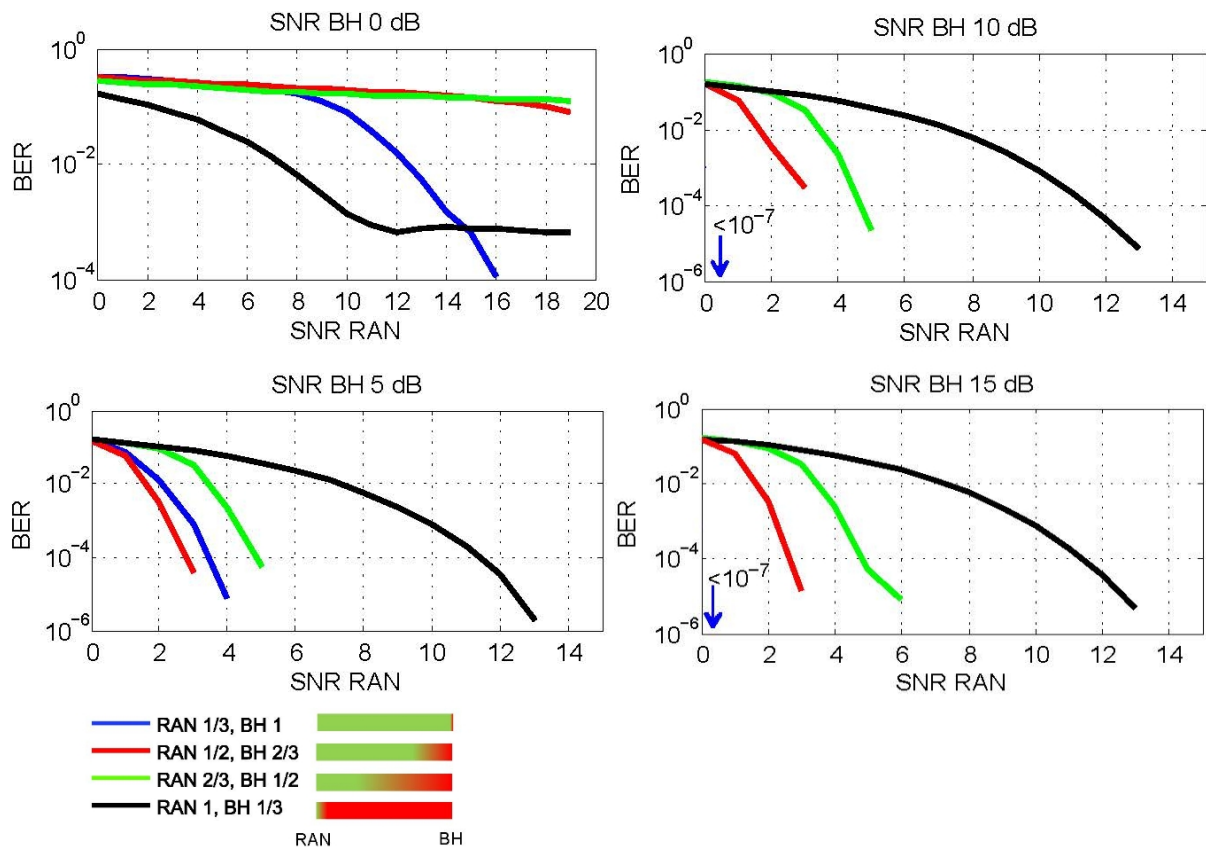


**Figure 4-42: Comparison of different joint coding schemes**

As can be seen from the top left plot (SNR BH = 0dB), the best coding scheme for this very low SNR on both the BH and access channel is to only encode the BH link. However, this scheme meets an error floor for high SNR access channels that corresponds to the BER that can be achieved on the BH channel with the used total code rate of 1/3. The coding scheme where only the access channel is coded does not meet this error floor and therefore achieves better results. For higher BH channel qualities, the coding scheme that only encodes the access channel shows the best performance over the whole SNR range.

These results indicate that a strong code on the access channel can protect the BH channel as well and achieve an even better performance in terms of BER. The reason for this is that the encoded information transmitted by the UE is sampled at the iSC at a higher resolution than the actual information rate (8 bit per symbol quantization for 4-QAM modulation, which carries two bit per symbol of information). This effectively lowers the code rate on the BH channel and is therefore superior to a scheme where a weaker code is used on the access channel in favour of a separate BH channel code.

However, as can be seen from the bottom left plot, an intermediate scheme with two separate codes might show the best performance under certain channel conditions. This shows that the coding scheme on both backhaul and access channel should be chosen jointly, taking both channels' quality into account. In current architectures each code is chosen separately only on its respective channel's quality. The same might be true for the modulation scheme, as it also influences the achievable BER. An outcome of the investigations of this CT could be modulation and coding schemes similar to the ones specified in LTE, but taking both access and BH channel into account.

## 5 PHY Logical and Functional Architecture

The two key pillars of the iJOIN project are the RANaaS concept and the joint RAN/backhaul optimization with a dense deployment of iSCs. The physical layer approaches for realizing both concepts are developed in WP2.

### PHY processing on RAN in veNB

A RANaaS platform together with the one or several connected iSCs builds a virtual evolved Node B (veNB) which represents the evolution of the LTE eNB in the iJOIN architecture [123]. However, the veNB allows for a flexible distribution of RAN functionalities between the RANaaS and the iSCs. The actual shift of functionality is controlled by the iJOIN virtual eNB Controller (iveC) located in the RANaaS. Neighbouring iSCs can exchange information with each other directly by the logical J2 interface and are connected to the RANaaS platform by the logical J1 interface.

Within WP2 the PHY processing of the signals transmitted and received by the iSCs is performed. As a consequence of the dense deployment, a geographical area can be covered by several iSCs. Thus, joint transmission and detection schemes enabled either by distributed processing among the iSCs or by centralized processing within the RANaaS can be exploited. This allows for new and evolved PHY approaches, where some functionalities will be executed in the particular iSCs and other parts may be implemented in the RANaaS platform.

### PHY processing for joint RAN/BH design

In the envisaged iJOIN architecture, the exchange of information bearing signals among the distributed RAN entities has to be realized over the different kind of backhaul links. In order to derive an overall optimized distributed RAN architecture, the transmission properties of the backhaul links have to be considered as well. The iJOIN architecture introduces a controller element, the iJOIN Network Controller (iNC), in charge of gathering RAN and backhaul status enabling joint optimization. A promising approach is joint design of RAN and BH links, e.g. by exploiting the RAN channel code also for neglecting transmission errors on the backhaul links. For such a joint processing the RAN and the BH transmission have to be controlled together by the iNC and the iveC.

### Interactions

In order to define the interfaces between the WP2 CTs with basic PHY functions and other iJOIN CTs the requested input information and the provided output information per CT is defined in Section 5.1. The kind of information to be exchanged within one CT between the RAN entities over the J1 and J2 interface will vary among the functional split options per CT. In addition, also the localisation of channel measurements for the RAN links and the location where this information is needed may change with the functional split option. Thus, Section 5.2 defines the kind of CT-specific exchange information and Section 5.3 the exchange of measurement information. Based on these definitions, the functional architecture describing the interactions of WP2 CTs will be presented in Section 5.4.

## 5.1 Input/Output and Parameters

Table 5-1 lists the information required by each CT, specifies the source of information by means of other CTs or system functions as well as by logical network entity in the iJOIN architecture. Thus, connections to the MAC functionality described D3.1 [144] and mobile network functions discussed in D4.1 [145] are identified. Finally, the principle interface is defined by means of a parameter list. Similarly, Table 5-2 lists the provided output information per CT with sink of information and interface definition. Furthermore, Table 5-3 describes the used acronyms and indicates whether the related parameter is already defined by 3GPP LTE or has to be introduced by iJOIN.

**Table 5-1: Requested Input of WP2 CTs**

In	CT	Requested Input	Source of Information		Parameter
			CT or system function	Logical network entity	
<b>Network Information</b>					
I2.1	2.1 2.2 2.4 2.5 2.6 2.7	System Parameter		NMS, EMS	<RAN_BW, N_PRB, CP_length, N_sub, N_iSC, {N_Tx_iSC}, {N_Rx_UE}>
I2.2	2.4 2.7	Estimated distance or SNR for wireless BH link	BH Measurement	iNC	<BH_ID, BH_SNR, BH_PathLoss>
I2.3	2.1 2.2 2.3 2.4 2.5 2.6 2.7	RAN connection table of iSCs and UEs	RRM/RRC - 2.1: RRM for INP (CT3.8) may override	veNB	<Conn_UE_iSC{UE_ID, iSC_ID}>
I2.4	2.1 2.3 2.4 2.5 2.7	BH connection table for iSC-iSC links and iSCs-RANaaS links	Network layer	iNC	<Conn_iSC_iSC {iSC_ID1, iSC_ID2}, Conn_iSC_RANaaS {iSC_ID}>
<b>Functional Control</b>					
I2.5	2.1 2.2 2.3 2.4 2.5 2.6 2.7	Functional control for shifting/splitting functions	iveC per CT	veNB	<FuncCtrl>
<b>RRM Information</b>					
I2.6	2.1 2.2 2.3 2.4 2.5 2.6 2.7	RRM information per UE	RRM (MAC Layer) - 2.1: RRM for INP (CT3.8) - 2.2: RRM for MPTD (CT3.7) - 2.3: RRM for JNCC (CT3.2) - 2.5: RRM for ICIC (CT3.4, CT3.9)	veNB	<UE_ID, N_Tx_UE, {RI, PMI}, I_MCS, RV, HARQ_ID, NDI, TBS, RB allocation type (RBstart, L_CRB) >
I2.7	2.5 2.7	MCS for backhaul link	BH RRM	iSC or RANaaS	<BH_ID, I_MCS_BH>

<b>PHY Information (Access Link)</b>					
I2.8	2.1 2.2 2.3 2.6 2.7	Instantaneous RxCSI and SNR and/or noise variance of each UE-iSC link	UL Channel Estimation (PHY functionality)	iSC or RANaaS	<UE_ID, RxCSI, RxSNR, RxNVar>
I2.9	2.1 2.2 2.3 2.6 2.7	Received signal at iSC in frequency domain	UL Baseband Processing	iSC	<yRx>
I2.10	2.4 2.5 2.6	TxCSI, noise variance, and path-loss of each iSC-UE link	DL Channel Estimation (TDD UL CE, FDD Feedback) (PHY functionality)	veNB	<UE_ID, TxCSI, iSC_UE_PathLoss, TxNVar>
I2.11	2.4 2.5 2.6	User data to be transmitted in DL	MAC layer	veNB	<UE_ID, data_UE>
<b>PHY Information (Backhaul Link)</b>					
I2.12	2.1 2.2 2.3 2.6 2.7	Instantaneous RxCSI, SNR and/or noise variance of iSC-RANaaS link	BH Channel Estimation for iSC-RANaaS link	RANaaS	<iSC_ID, RxCSI_iSC_R, RxSNR_iSC_R, RxNVar_iSC_R>
I2.13	2.1 2.2 2.3 2.6 2.7	Parameter of iSC-RANaaS link	MM	iNC	<BH_ID, N_quant_iSC_R, BH_BW, BH_lat>
I2.14	2.4 2.5 2.6	Instantaneous RxCSI, SNR and/or noise variance of RANaaS-iSC link	BH Channel Estimation for iSC-RANaaS link	iSC	<RxCSI_R_iSC, RxSNR_R_iSC, RxNVar_R_iSC >
I2.15	2.4 2.6	Parameter of RANaaS-iSC link	MM	iNC	<BH_ID, N_quant_R_iSC, BH_BW, BH_TxPow>
I2.16	2.3 2.5	Instantaneous RxCSI, SNR and/or noise variance of iSC-iSC link	Channel Estimation for iSC-iSC link (PHY functionality)	iSC	<iSC_ID, RxCSI_iSC_iSC, RxSNR_iSC_iSC, RxNVar_iSC_iSC>
I2.17	2.1 2.2 2.3 2.4 2.5	Parameter of iSC-iSC link	MM	veNB	<BH_ID, N_quant_iSC_iSC, BH_BW, BH_TxPow>

**Table 5-2: Provided Output of WP2 CTs**

Out	CT	Provided Output	Sink of Information		Parameter
			CT or system function	Logical network entity	
<b>Functional Control</b>					
O2.1	2.4 2.5	Estimated backhaul load (including overhead) for CoMP schemes	- 2.4: Coop. RRM for ICIC in RANaaS (CT3.5) - 2.5: SD Scheduler (CT3.4) and HL Scheduler (CT3.9)	veNB	<BH_cap, BH_energ>
O2.2	2.6	Estimated BH parameter (latency, capacity/load, energy, BER)	MM	iNC	<BH_lat, BH_cap, BH_load, BH_energ, BH_BER>
<b>RRM Information</b>					
O2.3	2.1	Effective SINR per UE	RRM for INP (CT3.8)	veNB	<UE_ID, effRxSINR_INP>
O2.4	2.1	Effective SINR per UE-iSC link	RRM for INP (CT3.8)	veNB	<UE_ID, iSC_ID, effRxSINR_iSC>
O2.5	2.1 2.2 2.3	Estimated PER	- 2.1: RRM for INP (CT3.8) - 2.2: RRM for MPTD (CT3.7) - 2.3: RRM for JNCC (CT3.2)	veNB	<UE_ID, PER>
O2.6	2.4 2.5	Effective SNR/SINR of each UE (with precoding)	RRM (MAC layer)	veNB	<UE_ID, effTxSINR>
<b>PHY Information (Access Link)</b>					
O2.7	2.1 2.2 2.3	ACK/NACK (based on CRC), HARQ process	HARQ (MAC layer)	veNB	<HARQ_ID, ACK/NACK>
O2.8	2.1 2.2 2.3 2.6 2.7	If ACK, user data (decoded Layer 2 PUSCH) to upper layers	MAC layer (MAC PDU)	veNB	<UE_ID, HARQ_ID, data_UE_est>
O2.9	2.4 2.5 2.6	Transmit signal at iSC in frequency domain on RAN	DL Baseband Processing	iSC	<xTx>
O2.10	2.4	Access link capacity and energy efficiency	Cooperative RRM for ICIC in RANaaS (CT3.5)	veNB	<Access_Cap, Access_Energy>

In the following table the parameters exchanged on the interfaces are described. Either definitions from 3GPP LTE are used or specific definitions will be introduced by the CTs. In particular, the parameter FuncCtrl is

specified to define the different functional split options per CT. A detailed description of these functional split variants is provided in Section 6.2.

**Table 5-3: Explanation of Parameters**

Parameter	Full Name (including explanation if necessary)	LTE or CT specific
<b>Identifier</b>		
BH_ID	Backhaul link identifier (for logical network) <ul style="list-style-type: none"> <li>iSC_ID_tx – iSC_ID_rx</li> <li>iSC_ID_tx – RANaaS_rx</li> <li>RANaaS_tx – iSC_ID_rx</li> </ul>	iJOIN
veNB_ID	ID of virtual eNodeB (for logical network)	iJOIN
CELL_ID	ID of macro cell (specifies location of pilots)	LTE
iSC_ID	ID of iSC (for logical network) <ul style="list-style-type: none"> <li>iSC_ID_tx: ID of transmitting iSC</li> <li>iSC_ID_rx: ID of receiving iSC</li> <li>iSC_ID_i: ith- iSC to differentiate iSCs</li> </ul>	iJOIN
UE_ID	UE ID	LTE
Conn_iSC_iSC	Table listing available links between iSCs	iJOIN
Conn_iSC_RANaaS	Table listing available links between iSCs and RANaaS	iJOIN
Conn_UE_iSC	Table listing available links between UEs and iSCs	iJOIN
<b>RAN transmission parameter</b>		
N_PRB	Number of available RBs within the system bandwidth	LTE
N_Tx_iSC	Number of transmit antennas per iSC	LTE
N_Rx_iSC	Number of receive antennas per iSC	LTE
N_sub	Number of active (i.e. modulated) subcarriers	LTE
N_Tx_UE	Number of transmit antennas of UE	LTE
N_Rx_UE	Number of receive antennas of UE	LTE
RAN_BW	System bandwidth [MHz] (e.g. BW=20 MHz for a 20 MHz LTE carrier)	LTE
CP_length	Cyclic prefix length [ $\mu$ s]	LTE
N_iSC	Number of iSCs serving a defined group of UEs	LTE
N_UE_per_iSC	Number of users per iSC	LTE
<b>BH parameter</b>		
BH_SNR	Signal to Noise Ratio in backhaul	BH Measurement
BH_load	Estimated BH load [%]	CT specific
BH_cap	Estimated max. BH capacity [Mbps]	BH Measurement
BH_lat	Estimated BH latency [ $\mu$ s]	BH Measurement
BH_energ	Estimated BH energy consumption [mW]	BH Measurement or CT2.4
BH_BER	Estimated BH BER [float]	BH Measurement
BH_PathLoss	Path loss of BH link	CT2.4
BH_BW	Bandwidth of BH link	CT2.4
BH_TxPow	Tx Power of BH link	CT2.4
<b>PHY parameter</b>		
PMI	Pre-Coding Matrix Index	LTE
RI	Rank Indicator	LTE
CDI	Channel Direction Information	LTE
I_MCS	Modulation and Coding Scheme (0... 31)	LTE
I_MCS_BH	Modulation and Coding Scheme for BH	CT2.7
HARQ_ID	ID of HARQ process	LTE
NDI	New Data Indicator	
TBS	Transport Block Size (0 ... 24)	LTE
RB allocation type	DL { <b>0</b> ,1,2} UL { <b>0</b> ,1} (bold = default)	LTE
RBstart	UL: First allocated RB	LTE

L_CRB	UL: Number of continuous RBs allocated (starting from RBstart)	LTE
RV	Redundancy Version (0 ... 3)	LTE
ACK/NACK	ACK/NACK per packet	LTE
PER	Estimated packet error rate	LTE
RE	Resource Elements	LTE
RI	Rank Indicator	LTE
RRM	Radio Resources Management	LTE
RRC	Radio Resources Control	LTE
NMS	Network Management Subsystem	LTE
EMS	Element Management System	LTE
<b>Access link: Signals and transmission variables (CSI, Noise Variance, SINR, etc.)</b>		
RxCsi	Receive side Channel State Information for UE-iSC link	LTE
RxSNR	Signal to Noise Ratio on UL for UE-iSC link	LTE
RxNVar	Noise variance on UL for UE-iSC link	LTE
TxCsi	Transmit side Channel State Information for iSC-UE link	LTE
TxNVar	Noise variance on DL for iSC-UE link	LTE
xTX	Transmit signal on DL for iSC-UE link in frequency domain	LTE
yRx	Receive signal on UL for at iSC in frequency domain	LTE
data_UE	Transmit data of user delivered by upper layer	LTE
data_UE_est	Estimated data of User to pass to the upper layer	LTE
effRxSINR_INP	Effective SINR per UE after INP processing	CT2.1
effRxSINR_iSC	Effective SINR per UE-iSC link after INP processing	CT2.1
effTxSINR	Effective SNR/SINR of UE after precoding	CT2.4, CT2.5
Access_Cap	Access link achievable Capacity	CT2.4
Access_Energy	Access link achievable Spent Energy (or efficiency)	CT2.4
iSC_UE_Pathloss	Pathloss from iSC to UE	CT2.4
<b>BH links: Signals and transmission variables (CSI, Noise Variance, SINR, etc.)</b>		
RxCsi_iSC_R	Receive side Channel State Information for iSC-RANaaS link	LTE
RxCsi_R_iSC	Receive side Channel State Information for RANaaS-iSC link	LTE
RxCsi_iSC_iSC	Receive side Channel State Information for iSC-iSC link	LTE
RxSNR_iSC_R	Signal to Noise Ratio on iSC-RANaaS link	LTE
RxSNR_R_iSC	Signal to Noise Ratio on RANaaS-iSC link	LTE
RxSNR_iSC_iSC	Signal to Noise Ratio on iSC-iSC link	LTE
RxNVar_iSC_R	Noise variance on iSC-RANaaS link	LTE
RxNVar_R_iSC	Noise variance on RANaaS-iSC link	LTE
RxNVar_iSC_iSC	Noise variance on iSC-iSC link	LTE
N_quant_iSC_R	Number of quantization levels on iSC-RANaaS link	iJOIN
N_quant_R_iSC	Number of quantization levels on RaNaaS-iSC link	iJOIN
N_quant_iSC_iSC	Number of quantization levels on iSC-iSC link	iJOIN
<b>Functional Split Control</b>		
FuncCtrl	Functional control for shifting / splitting functions (CT specific) <ul style="list-style-type: none"> <li>- CT2.1: INP (Indicator where to execute functions) <ul style="list-style-type: none"> <li>o 0: only local processing</li> <li>o 1: cooperation among iSCs by exchange of local estimates (INP) <ul style="list-style-type: none"> <li>▪ 2.1.a: Cooperative Joint-MUD among iSCs with decoding at one iSC</li> <li>▪ 2.1.b: Cooperative Joint-MUD among iSCs with centralized decoding in RANaaS</li> <li>▪ 2.1.c: Cooperative detection and decoding within iSCs</li> <li>▪ 2.1.d: Pre-processing per iSC and centralized detection &amp; decoding within RANaaS by forwarding local estimates of one iSC</li> <li>▪ 2.1.e: Pre-processing per iSC and centralized detection &amp; decoding within RANaaS by forwarding local estimates of several iSCs</li> </ul> </li> </ul> </li> </ul>	

- N\_Iterations: Set number of iterations for data exchange among iSCs according to functional split variant
- CT2.2: MPTD (Local turbo processing indicator)
  - 0: centralise processing
    - 2.2.b: deport processing to the RANaaS platform
  - 1: (cooperative) processing
    - 2.2.a: perform processing locally
- CT2.3: JNCC
  - 0: cooperating processing
    - 2.3.a: perform joint network-channel decoding within iSC
  - 1: centralize processing
    - 2.3.b: deport joint network-channel decoding to the RANaaS platform
- CT2.4: CoMP (Precoding is shifted)
  - 2.4.a: to the RANaaS platform (for centralized architecture) and time domain signal is sent over J1 interface
  - 2.4.b: to the RANaaS platform (for semi-centralized architecture) and only PMI and RI along with information bits are sent over J1 interface
  - 2.4.c: processed locally within iSC (for decentralized architecture) and exchanged over J2 interface
- CT2.5: ICIC
  - 2.5.a: Centralized processing at RANaaS node.
  - 2.5.b: Centralized processing at a master iSC.
  - 2.5.c: Hybrid processing split between RANaaS node and iSCs
  - 2.5.d: Fully distributed implementation at the iSCs
- CT2.6: RoF
  - 0: link based on CPRI-like architecture
  - 1: Frequency Domain architecture
    - 2.6.a: only IFFT in iSCs for DL
    - 2.6.b/2.6.c: IFFT and local processing in iSC for DL
    - 2.6.d: only FFT in iSC for UL
    - 2.6.e/2.6.f FFT and local processing in iSC for UL
- CT2.7: mmWave
  - 0: 2.7.a - Detection and decoding in iSC
  - 1: 2.7.b - Detection and decoding in RANaaS
  - 2: 2.7.c - RRH: all digital processing in RANaaS

## 5.2 Information Exchange within WP2 CTS

The iJOIN RAN architecture consists of several iSCs and the corresponding RANaaS which together form a veNB. Due to this structure, cooperative transmission and reception approaches can be implemented. For the different flavours of cooperation, signals have to be exchanged between the different RAN entities. Figure 5-1 visualizes, for the case of three iSCs within a veNB, the signals to be exchanged on the J1 links from the iSCs to the RANaaS (e.g.  $x\text{Exch}_{1R} \rightarrow y\text{Exch}_{1R}$  for iSC<sub>1</sub>) or from the RANaaS to the iSCs (e.g.  $x\text{Exch}_{R1} \rightarrow y\text{Exch}_{R1}$  for iSC<sub>1</sub>) and between iSCs on the J2 links (e.g.  $x\text{Exch}_{12} \rightarrow y\text{Exch}_{12}$  for iSC<sub>1</sub> towards iSC<sub>2</sub>). Furthermore, the signals to be transmitted over the radio access channel to the UEs (e.g.  $x\text{Tx}_1$  for iSC<sub>1</sub>) and the signals received at the iSCs from the UEs (e.g.  $y\text{Rx}_1$  for iSC<sub>1</sub>) are shown. Finally, the RANaaS has at input the information to be transmitted to the UEs in the DL and delivers the estimated information for the UL.

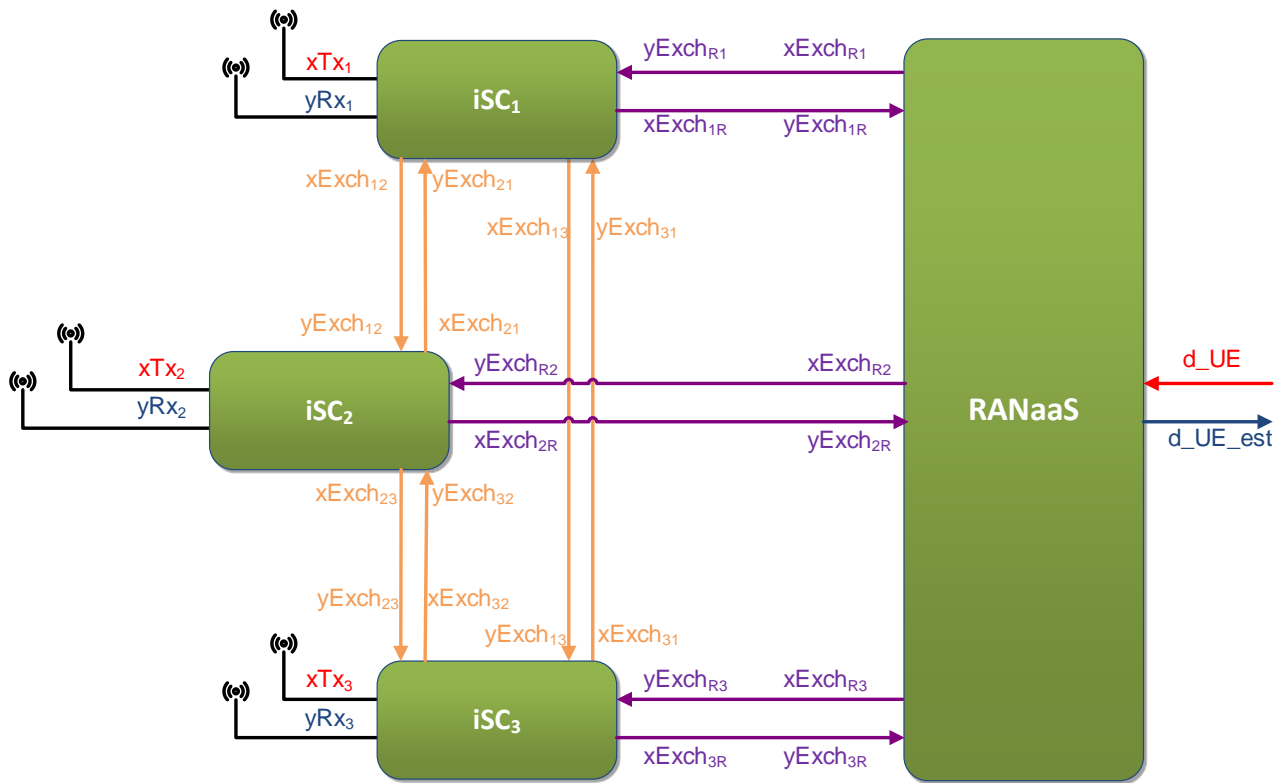


Figure 5-1: Exchange of user signals within vNB

The actual kind of signals to be exchanged between the RAN entities iSCs and RANaaS depends on the PHY approach considered by the particular CTs and can also vary among the functional split options per CT. Table 5-4 describes the exchanged signals over the J1 and the J2 links within one CT for each of the functional split variant. For the future investigations this table lays down the foundation for determining the necessary data rate on the different links.

Table 5-4: Exchange signals over J1 and J2 interfaces for the different CT

Functional Split Approach	iSC → iSC	iSC → RANaaS	RANaaS → iSC
<b>CT2.1 INP</b>			
2.1.a) Cooperative Joint-MUD among iSCs with decoding at one iSC	Local estimates of UE signal, auxiliary variables	One iSC transmits consensus based estimated UE signal (bits)	ACK/NACK (per UE/HARQ process)
2.1.b) Cooperative Joint-MUD among iSCs with centralized decoding in RANaaS	Local estimates of UE signal, auxiliary variables	One iSC transmits LLRs for UE code bits	ACK/NACK (per UE/HARQ process)
2.1.c) Cooperative detection and decoding within iSCs	Local quantized LLRs	One iSC transmits decoded UE bits	ACK/NACK (per UE/HARQ process)
2.1.d) Pre-processing per iSC and centralized detection & decoding within RANaaS by forwarding local estimates of one iSC	Local estimates of UE signal, auxiliary variables	One iSC transmits finely quantized estimates of UE signal	ACK/NACK (per UE/HARQ process)
2.1.e) Pre-processing per iSC and centralized detection & decoding within RANaaS by forwarding local estimates of several iSCs	Local estimates of UE signal, auxiliary variables	All iSCs transmit finely quantized estimates of UE signal	ACK/NACK (per UE/HARQ process)

<b>CT2.2 MPTD</b>				
2.2.a) Local turbo processing	Locale estimates (e.g. LLRs)	—	—	—
2.2.b) Centralized turbo processing	—	(UL) I/Q SC-FDMA MIMO receive signal of UE signal	—	ACK/NACK (per UE/HARQ process)
<b>CT2.3 JCNC</b>				
2.3.a) Perform joint network-channel decoding within iSC	Estimated user data (bits)	Estimated user data (bits), PER	—	ACK/NACK (per UE/HARQ process)
2.3.b) Deport joint network-channel decoding to the RANaaS platform	—	From iSC 1 to RANaaS: network encoded data (bits), PER from iSC 2 to RANaaS: quantized soft bits (LLR values), PER	—	ACK/NACK (per UE/HARQ process)
<b>CT2.4 CoMP</b>				
2.4.a) Centralised architecture in which all PHY processing takes place in RANaaS and only time domain I/Q samples are sent over J1 interface	—	—	—	Precoded transmit signals in the Time domain
2.4.b) Semi-Centralised architecture in which only PMI and RI are computed at RANaaS and sent over J1 interface along with Info bits.	—	—	—	PMI, RI, Info. bits
2.4.c) De-centralised architecture in which only local exchange of PMI, RI, and local channel matrix take place over J2 interface	PMI and RI	—	—	Info bits
<b>CT2.5 ICIC</b>				
2.5.a) Centralized precoding in the RANaaS node	—	Downlink CSI	—	Quantized precoded signal
2.5.b) Centralized precoding in the master iSC	Quantized downlink CSI	—	—	Users data symbols
2.5.c) Hybrid precoding split between RANaaS and iSCs	Quantized downlink CSI	—	—	Users data symbols, refinement information relative to the precoded signal
2.5.d) Precoding distributed across all iSCs without master-slave organization	Quantized downlink CSI	Downlink CSI	—	All users data symbols, Quantized refinement information
<b>CT2.6 RoF (DL)</b>				
2.6.a) Only IFFT in iSCs	—	—	—	I/Q OFDMA transmit signal in the frequency domain before IFFT
2.6.b) IFFT in iSCs but with local remote processing in iSCs	—	—	—	I/Q OFDMA transmit signal in the frequency domain before IFFT with local remote processing in iSCs
2.6.c) IFFT in iSCs but with local remote processing in iSCs	—	—	—	Bit streams at the channel encoder output

<b>CT2.6 RoF (UL)</b>			
2.6.d) Only FFT in iSCs	—	I/Q SC-FDMA receive signal in the frequency domain after FFT	—
2.6.e) FFT in iSCs but with local remote processing in iSCs	—	I/Q SC-FDMA receive signal after FD equalization and antenna combining at iSC	—
2.6.f) FFT in iSCs but with local remote processing in iSCs	—	Soft bits at the soft demodulator output	—
<b>CT2.7 mmWave</b>			
2.7.a) Detection and decoding in iSC	—	Estimated UE data (bits)	—
2.7.b) Detection and decoding in RANaaS	—	Received SC-FDMA signal after IFFT (I/Q digital signal)	—
2.7.c) RRH: all digital processing in RANaaS	—	Received SC-FDMA signal before FFT (I/Q digital signal)	—

### 5.3 Measurement placement and measurement exchange for WP2 CTs

Depending on the functional split, the different CTs may require basic measurement information like channel state information (CSI) for the UL or the DL, signal-to-noise-ratios per UE, etc. at different entities of the RAN architecture. If measurement location and entity where this information is required differs, such measurement information has to be exchanged over the J1 and / or J2 interfaces.

In order to specify where a measurement is executed and where is it required, Table 5-5 lists for each functional split option of each CT, the kind of measurement signals, the place where it is measured and, if necessary, to which other entity it has to be delivered by means of J1 or J2 link.

**Table 5-5: PHY Measurement placement and exchange**

Functional Split Approach	Measurement	Measurement Location	Exchange link
<b>CT2.1 INP</b>			
2.1.a) Cooperative Joint-MUD among iSCs with decoding at one iSC	RxCSI, RxSNR per UE	each iSC	—
2.1.b) Cooperative Joint-MUD among iSCs with centralized decoding in RANaaS	RxCSI, RxSNR per UE	each iSC	—
2.1.c) Cooperative detection and decoding within iSCs	RxCSI, RxSNR per UE	each iSC	—
2.1.d) Pre-processing per iSC and centralized detection & decoding within RANaaS by forwarding local estimates of one iSC	RxCSI, RxSNR per UE	each iSC	J1 interface, towards RANaaS
2.1.e) Pre-processing per iSC and centralized detection & decoding within RANaaS by forwarding local estimates of several iSCs	RxCSI, RxSNR per UE	each iSC	J1 interface, towards RANaaS
<b>CT2.2 MPTD</b>			
2.2.a) Local turbo processing	RxCSI, RxSNR per UE	each iSC	—
2.2.b) Centralized turbo processing	RxCSI, RxSNR per UE	RANaaS	—

<b>CT2.3 JCNC</b>			
2.3.a) Perform joint network-channel decoding within iSC	RxCSI, SNR per UE	Each iSC	—
	RxCSI, SNR of iSC-RANaaS link	RANaaS	J1 interface, towards iSC
	RxCSI, SNR of iSC-iSC link	iSC2	J2 interface, towards iSC1
	RxCSI, SNR of RANaaS-iSC link	iSC2	J1 interface, towards RANaaS
2.3.b) Deport joint network-channel decoding to the RANaaS platform	RxCSI, SNR per UE	RANaaS	J1 interface, towards iSC
	RxCSI, SNR of iSC-RANaaS link	RANaaS	J1 interface, towards iSC
<b>CT2.4 CoMP</b>			
2.4.a) Centralised architecture in which all PHY processing takes place in RANaaS and only time domain I/Q samples are sent over J1 interface	Tx CSI, Rx SINR	iSC	J1 interface, towards RANaaS
2.4.b) Semi-Centralised architecture in which only PMI and RI are computed at RANaaS and sent over J1 interface along with Info bits.	Tx CSI, Instantaneous Rx CSI, Rx SINR	iSC	J1 interface, towards RANaaS
2.4.c) De-centralised architecture in which only local exchange of PMI, RI, and local channel matrix take place over J2 interface	Tx CSI, Local channel matrix H, Rx CSI, Rx SINR	iSC	J2 interface, towards other iSCs
<b>CT2.5 ICIC</b>			
2.5.a) Centralized precoding in the RANaaS node	Tx CSI, Noise variance, Pathloss	Obtained at one iSC	J1 interface, towards RANaaS
2.5.b) Centralized precoding in the master iSC	Tx CSI	Obtained at one iSC	J2 interface, towards master iSC
2.5.c) Hybrid precoding split between RANaaS and iSCs	Tx CSI	Obtained at one iSC	J1 interface, to RANaaS. J2 interface, to all iSCs
2.5.d) Distributed precoding at the iSCs	Tx CSI	Obtained at one iSC	J2 interface, to all iSCs
<b>CT2.6 RoF (DL)</b>			
2.6.a) Only IFFT in iSCs	Tx CSI	RANaaS	—
2.6.b/2.6.c) IFFT in iSCs but with local remote processing in iSC	Tx CSI	Obtained at one iSC	—
<b>CT2.6 RoF (UL)</b>			
2.6.d) only FFT in iSCs	Rx CSI	RANaaS	—
2.6.e/2.6.f) only FFT in iSCs but with local remote processing in iSCs	Rx CSI	Obtained at one iSC	—

CT2.7 mmWave			
2.7.a) Detection and decoding in iSC	RxCSI, RxSNR per UE, SNR of iSC-RANaaS link	iSC RANaaS	—
2.7.b) Detection and decoding in RANaaS	RxCSI, RxSNR per UE, SNR of iSC-RANaaS link	iSC RANaaS	—
2.7.c) RRH: all digital processing in RANaaS	RxCSI, RxSNR per UE, SNR of iSC-RANaaS link	RANaaS	—

### 5.4 Interaction of Candidate Technologies

This section summarizes the interactions of PHY candidate technologies basic PHY functions as well as interaction of WP2 with WP3 and WP4.

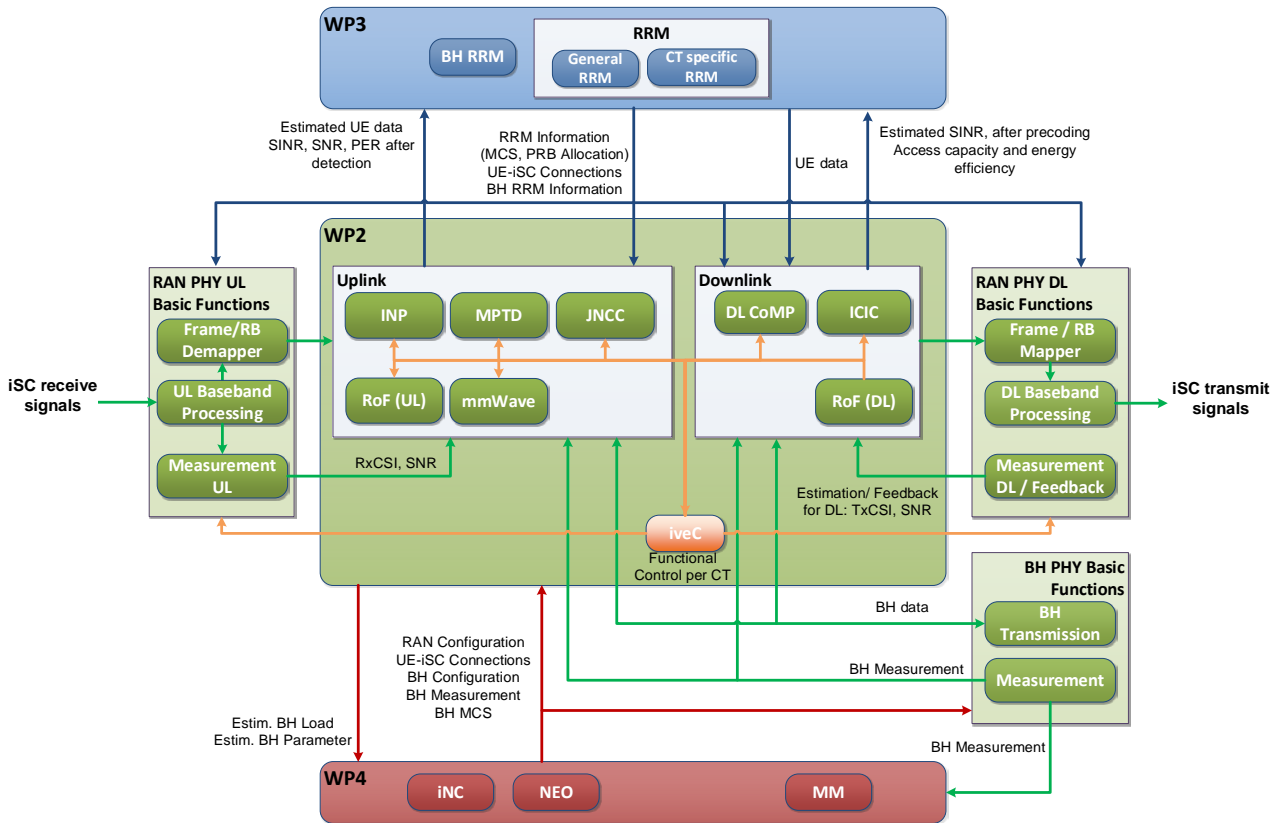


Figure 5-2: Functional Architecture of PHY processing

Figure 5-2 depicts the overall functional architecture of PHY processing approaches by means of interactions with PHY basic functions on the RAN and the BH, WP3, and WP4. A grouping of WP2 CTs with respect to UL or DL transmission has been introduced to indicate the main objective of each CT.

On the UL the different iSCs have received the UE signals over different channels. The antenna signals are processed in the “UL Baseband Processing” block yielding the I/Q receive signals in frequency domain. After an optional resource block demapping based on the UL RRM information provided by WP3, the I/Q signals are forwarded to the CTs for further processing as described in Section 4, and their functional split options discussed in Section 6.2. Additionally, the block “Measurement UL” estimates the receive CSI and the receive SNR. It provides this information to CTs as well. Note that the actual location of the measurement block and the execution of functions in the RAN architecture depend on the chosen functional split option, which is controlled by the iveC. The required exchange of signals over the backhaul links is organized by the iNC in cooperation with the iveC. This cooperative control also requires BH information provided by the “BH Measurement” block. Based on the available UL signals, the CTs perform an estimation of the transmitted information signals and provide the estimate to WP3. For the RRM either common LTE functions or CT specific functions according to Table 5-6 are used.

**Table 5-6: Mapping of WP2 CTs to CT specific RRM CTs in WP3**

WP2			WP3		
CT	Topic	Abb	CT	Topic	Abb
2.1	In-Network-Processing	INP	3.8	Radio Resource Management for In-Network-Processing	INP RRM
2.2	Multi-Point Turbo Detection	MPTD	3.7	Radio resource management for scalable multi-point turbo detection/In-network Processing	MPTD RRM
2.3	Joint Network-Channel Coding	JNCC	3.2	Partly decentralized mechanisms for joint RAN and backhaul optimization in dense small cell deployments	Coordinated Cell Selection
2.4	Sum-Rate and Energy-Efficiency Metrics of DL COMP with backhaul constraints	CoMP	3.5	Cooperative RRM for Inter-Cell Interference Coordination in RANaaS	Coop. RRM
2.5	Partially Centralized Inter-Cell Interference Coordination	ICIC	3.4	Computational Complexity and Semi-Deterministic Scheduling	SD Scheduler
			3.9	Rate adaptive strategies for optimized uplink transmissions	HL Scheduler

The processing on the DL is executed accordingly. For TDD transmission mode, the DL CSI can be estimated from the corresponding UL channel. In case of FDD, feedback based schemes are used. Based on this measurement and the RRM information from WP3, the user data is processed. After mapping to resource blocks, the DL baseband processed signal is transmitted over the iSCs. Again, either general LTE RRM functions or CT-specific RRM functions according to Table 5-6 are used.

## 6 Functional Split

### 6.1 General Idea of Functional Split for WP2

The iJOIN concept in WP2 relies on the idea of implementing a so-called “functional split” in the transceiver chain, as well as on a joint access and backhauling design approach. From a very general standpoint for “functional split” it is intended as a physical separation of functionalities between the iSCs and the RANaaS. The execution of specific physical layer functions in the iSCs opens also the possibility of local cooperative processing among the iSCs by exploiting the J2 interface. In Figure 6-1 a schematic representation of the possible “splits” that can be realized in the transceiver chain for UL and DL transmission are given, where the vertical dotted lines indicate the different options.

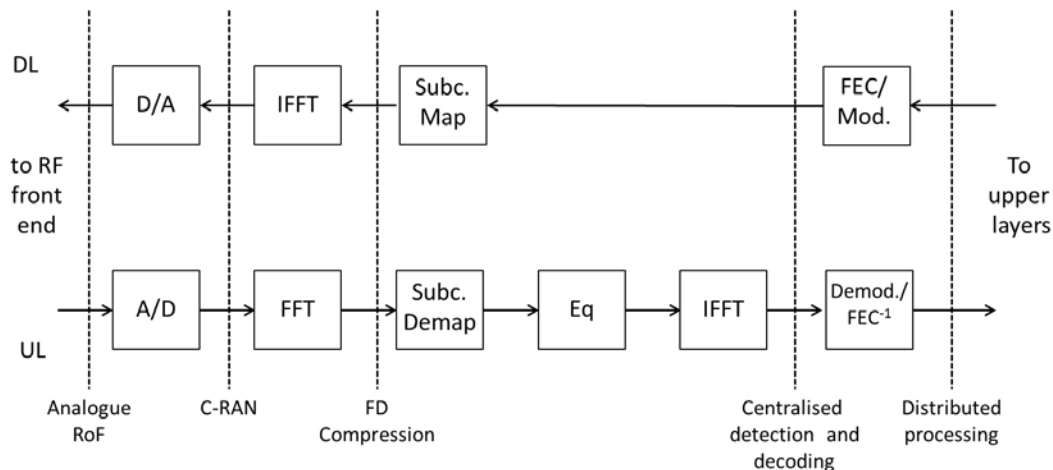


**Figure 6-1: Functional split options**

The line is intended so as that whatever is on its left is executed in the iSCs, while functions on the right are executed in the RANaaS. If the split is made on the extreme left the so called “Analogue RoF” is achieved; if it is after the FFT/IFFT then the split implements a somewhat traditional “C-RAN”-like approach, and so on.

Depending on the selected functional split option, the processing functionalities in the transceiver changes from fully centralized (all the processing or most of it is done in the RANaaS), to fully localized (all the processing or most of it is done remotely in the iSCs). Moreover, a cooperative/collaborative processing is still possible in both cases, exploiting not only the J1 interface of the iJOIN architecture, but also the J2 interface among the iSCs. As it is clear from Figure 6-1, the split could happen both in downlink and in uplink. More insight will be given in the per-CT analysis that follows. In principle the functional split in downlink is closely related to the coordination of the transmission from different scattered nodes, while in uplink it is mainly related to the detection of UE signals exploiting the receive signals at different iSCs cooperatively.

In terms of functional split, performance advantages and disadvantages of the different options are to be assessed. In particular the most relevant issues are:

- **Computational needs** in the iSCs and in the RANaaS for a specific functional split (e.g. if the decoding is implemented in the iSC rather than in the RANaaS)
- **Bandwidth** to be allocated for the J1 and J2 interfaces for a specific functional split (e.g. CT2.6 studies a method to limit the required bandwidth by means of a specific split in the transceiver chain)
- **Link reliability** being necessary to implement a specific functional split (e.g. a CoMP scheme applied with a specific split could require a given reliability that has to be ensured anyway)
- **Latency** in the overall transceiver chain for a particular functional split (to ensure that the overall system requirement is still met)

It is also of relevant importance to estimate for each solution the overall cost and complexity that its introduction could imply in terms of deployment and in terms of standardization actions needed to adopt the solution. Moreover, in any functional split alternative, the compliance with standards should be checked, in particular with reference to 3GPP (consider in particular [84], [91], [112]) and with reference especially to

latency, throughput, and maximum reachable physical distance. For 3GPP standard compliancy, the latency should be of particular interest as the transmission procedure is based on strict timing, especially in the uplink. The following recalls this timing relation between scheduling, transmission and acknowledgment for the FDD case [112].

- **Downlink**

When an eNB schedules one UE in subframe  $n$  for its H-ARQ process  $p$ , Downlink Control Information (DCI) format greater than 0 and lower than 4 is transmitted on the PDCCH, together with the associated PDSCH data in the same subframe. On the uplink side the eNB expects an acknowledgement (ACK/NACK) for this specific H-ARQ process from the UE either on PUCCH or PUSCH uplink channels in subframe  $n+4$  (carried by the Uplink Control Information (UCI)). The eNB is then able to schedule a (re)transmission using this H-ARQ process  $p$  from subframe  $n+8$ . This H-ARQ retransmission cannot be performed before subframe  $n+8$  but after is perfectly possible, due to the “asynchronous” notion of the H-ARQ procedure in DL.

This means that there is no “strong” latency constraint due to the acknowledgement procedure. The processing in the UE is meant to acknowledge in 4 ms and to not erase its H-ARQ process  $p$  until it is commanded to.

In case of functional split (or cooperation) of the PHY layer:

- J1 (J2) latency will “only” affect the validity of the UE’s reporting (low mobility helps mitigating this effect).
- J1 (J2) bandwidth should be sufficient for quantized transmission (it can have error with retransmission, but this should be considered).

- **Uplink**

When an eNB schedules one UE in subframe  $n$  by transmitting a DCI with format equal to 0 or 4 in PDCCH, the eNB commands the UE to send its data on PUSCH in subframe  $n+4$ . The UE then expects an acknowledgement (ACK/NACK) from the eNB in subframe  $n+8$  (normally on the PHICH (Physical Hybrid-ARQ Indicator Channel) control channel, but DCI can also be transmitted on the PDSCH to overwrite the MCS previously used).

- If an ACK is detected, the UE can use again the same H-ARQ process in subframe  $n+12$  (based on DCI if present or exploiting persistent scheduling).
- If a NACK is detected, then the UE will retransmit in subframe  $n+12$  on the same H-ARQ process either on the same resources previously allocated at subframe  $n+4$  or on the resources indicated in the DCI of subframe  $n+8$  if present. In the former case there is no need to signal again the resource allocated, while the latter case is used for adaptive H-ARQ scheduling purpose.

Due to this fixed 8 ms period in the use of an H-ARQ process, there is no need to signal the H-ARQ process number to be used. Basically the TTI modulo 8 is always assigned to the same H-ARQ process, due to the “synchronous” notion of the H-ARQ procedure in UL.

This means that there is a “strong” latency constraint due to the acknowledgement procedure. The processing in the (v)eNB is meant to acknowledge in 4 ms, otherwise the UE will assume a NACK.

In case of functional split (or cooperation) of the PHY layer:

- J1 (J2) latency should respect the 4 ms ACK/NACK timing of the UE’s H-ARQ transmission procedure.
- J1 (J2) bandwidth should be sufficient for quantized transmission (it can have error with retransmission, but this should be considered).

The remaining of the chapter presents the functional split for each of the candidate technologies in the physical layer of iJOIN and afterwards an insight into the decoder (for the uplink) and precoder (for the downlink) in terms of analysis of the possible options for the functional splits.

## 6.2 Functional Split for Candidate Technologies

### 6.2.1 CT 2.1: In-Network Processing

In order to perform the detection of UE signals based on the receive signals at several iSCs, different approaches with varying degrees of cooperation and centralization using the philosophy of INP as presented in Section 4.1 are possible.

#### Variant 2.1.a: Cooperative Joint-MUD among iSCs with one iSC performing decoding

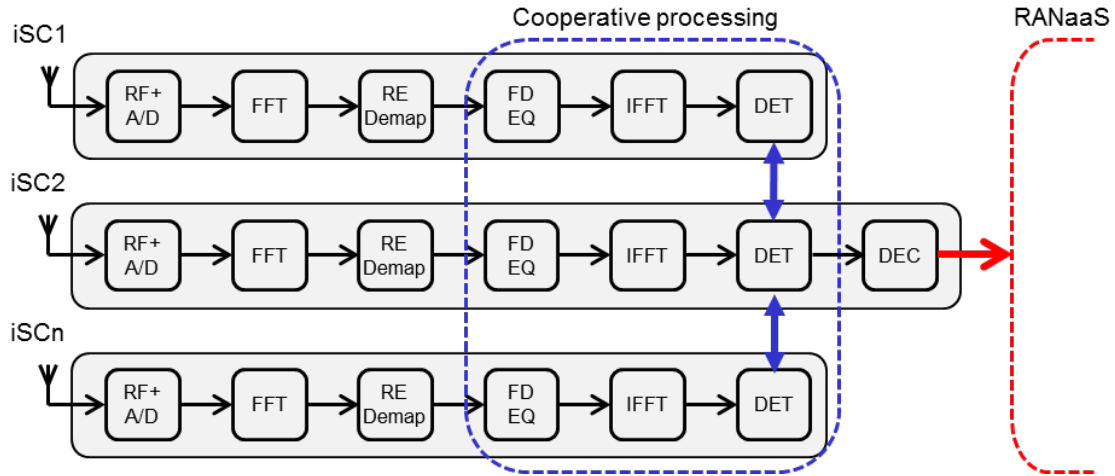


**Figure 6-2: Variant 2.1.a: Cooperative Joint-MUD among iSCs with one iSC performing decoding**

The INP implementation is done entirely at the iSCs as shown in Figure 6-2. iSCs cooperatively solve the optimization problem to estimate UE signals in the UL by exchanging local signal estimates and variables, achieving consensus after several iterations. Afterwards, the iSC with the best J1 link is selected to perform the decoding and forwards the decoded bits to the RANaaS, where the MAC processing takes place. There is also the possibility to apply decoding at each iSC to evaluate the CRC and stop the iterative processing if one iSC decodes correctly. Then, this iSC will forward the decoded bits over its J1 link to the RANaaS. It is possible to flexibly shift the decoding to another iSC if the properties of the current J1 link change, and this iSC now offers the best J1 link.

In this variant, all symbol estimation is performed in the iSCs, more computation effort is required at the iSC where the channel decoding is carried out. The computational needs for the iSCs generally depend on the estimation functionality as well as the number of UEs, the number spatial layers transmitted by UEs, the bandwidth of transmitted data, and the number of iterations. There is no need for additional computation power in the RANaaS and since no centralization is performed, there is no corresponding gain or cost. Very low latency is required for the iSC-iSC interface, because the update of estimates needs to be performed among all iSCs within each iteration, and there is no strict requirement for the link reliability, since sporadic loss of messages can be tolerated [4]. For the iSC-RANaaS interface, moderate latency is required but strong link reliability is needed, since only one J1 link exists and sporadic loss or error of messages cannot be recovered or corrected in RANaaS.

The required data rate on the iSC-iSC interface depends on the number of users  $N_{UE}$  that are connected to the iSC, the number of transmitting spatial layers  $N_L^{UE,u}$ , and the bandwidth configuration  $N_{RB}^{UE,u}$  (each resource block contains 12 subcarriers [91]) for user  $u$ , as well as the number of quantized bits  $N_{quant,J2}^x$ ,  $N_{quant,J2}^z$  and  $N_{quant,J2}^\lambda$  for the inter-exchanged symbols  $\tilde{\mathbf{x}}$ ,  $\tilde{\mathbf{z}}$  and  $\tilde{\boldsymbol{\lambda}}$  according to (4.8),(4.9),(4.10), and the number of iterations  $N_{it}$  performed for detection of one symbol within duration  $T_s$ :

$$D_{iSC-iSC} = N_{It} \cdot (N_{quant,J2}^x + N_{quant,J2}^z + N_{quant,J2}^{\lambda}) \cdot 12 \cdot \sum_u^{N_{UE}} (N_{RB}^{UE,u} \cdot N_L^{UE,u}) \cdot T_s^{-1}. \quad (6.1)$$

The required data rate of the iSC-RANaaS link is determined by the total bits delivered via the J1 link, which mainly depends on the number of users  $N_{UE}$  and the user data rate  $D_{UE}^u$  for each user  $u$ , which is determined by the MCS and TBS in [112] as

$$D_{iSC-RANaaS} = \sum_u^{N_{UE}} D_{UE}^u. \quad (6.2)$$

### **Variant 2.1.b: Cooperative Joint-MUD among iSCs with centralized decoding in RANaaS**

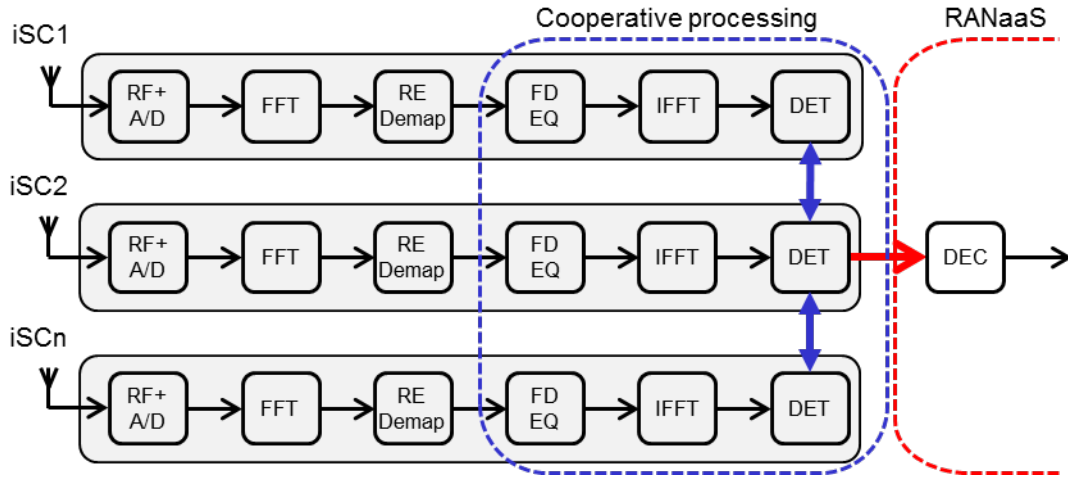


**Figure 6-3: Variant 2.1.b: Cooperative Joint-MUD among iSCs with centralized decoding in RANaaS**

Similar to the variant 2.1.a, a cooperative detection of the UE signals reaching a consensus on the estimates is performed at the iSCs as shown in Figure 6-3; but in contrast to the former, one iSC forwards the consensus estimates (the equalized symbols) to the decoder which is implemented in the RANaaS. The only difference between variants 2.1.a and 2.1.b is the functional shift of the decoder. Like above, forwarding can be switched by the iNC from iSC to another if it offers a better J1 link, without any change of processing load at the iSC.

In this variation, all the iSCs perform cooperative symbol-wised estimation, so the computational efforts for each iSC are the same. Regarding the required reliability on the iSC-RANaaS link, in contrast to variant 2.1.a, higher error tolerance can be achieved because of the exploitation of FEC in RANaaS. The bandwidth requirement on the J2 interface is the same as in variant 2.1.a, which is given in (6.1), but significantly more traffic load is brought to the iSC-RANaaS interface, since it has to carry quantized symbols instead of decoded bits. The required data rate of the iSC-RANaaS link then depends on the number of quantization bits  $N_{quant,J1}^x$  for the soft symbol that carries the information for the centralized decoding:

$$D_{iSC-RANaaS} = N_{quant,J1}^x \cdot 12 \cdot \sum_u^{N_{UE}} (N_{RB}^{UE,u} \cdot N_L^{UE,u}) \cdot T_s^{-1}. \quad (6.3)$$

**Variant 2.1.c: Cooperative detection and decoding within iSCs**

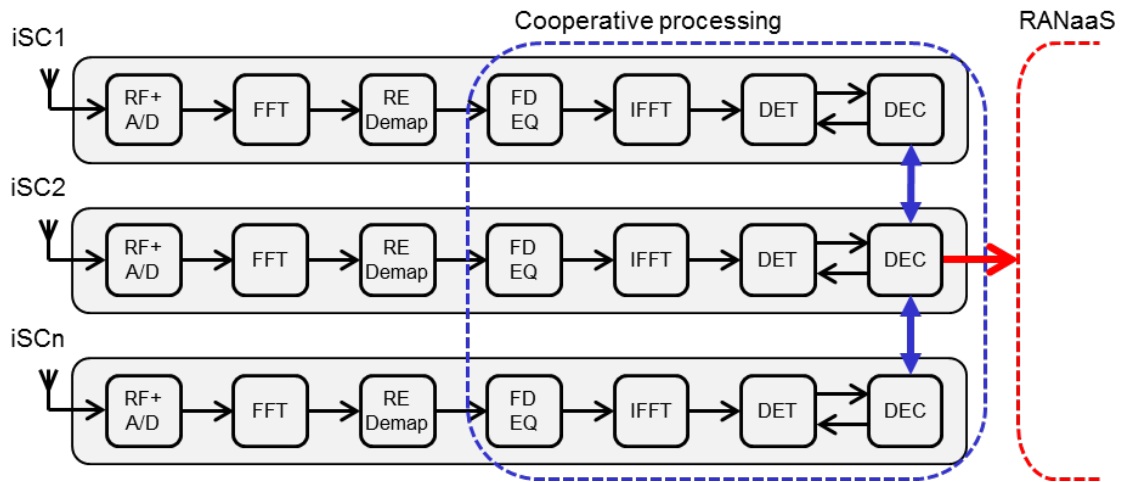


**Figure 6-4: Variant 2.1.c: Cooperative detection and decoding within iSCs through exchange of soft estimates**

As shown in Figure 6-4 the split is located between decoder and MAC processing, which is similar to variant 2.1.a. However, in this variant, soft estimates, e.g. LLRs, instead of estimated symbols, are exchanged among iSCs to perform a distributed joint detection and decoding, which is different from variants 2.1.a and 2.1.b. Those cooperating iSCs exchange the soft estimates of their local decoders to achieve a consensus on the information bits after several iterations, and then one iSC forwards the decoded bits to the RANaaS. This is a more general approach for MUD similar to CT2.2, and is not limited to INP.

The iSC-RANaaS interface needs stronger link reliability than the iSC-iSC interface, because only one iSC forwards bits to the RANaaS, but as for previous variants, another iSC may take over the iSC-RANaaS link at any time, if initiated by the iNC. Significant computation effort is needed among all the iSCs compared to the other variants, since each iSC needs to perform decoding. However, the required number of joint detection and decoding iterations may be reduced compared to variants 2.1.a and 2.1.b. Additionally the amount of data exchanged on the iSC-iSC interface per iteration is lower, because only quantized LLRs (with number of bits  $N_{quant,J2}^{LLR}$ ) are exchanged instead of several quantized symbols and variables:

$$D_{iSC-iSC} = N_{It} \cdot N_{quant,J2}^{LLR} \cdot 12 \cdot \sum_u^{N_{UE}} (N_{RB}^{UE,u} \cdot N_L^{UE,u}) \cdot T_s^{-1} \cdot \tag{6.4}$$

As in variant 2.1.a, the iSC-RANaaS interface only carries decoded bits, so (6.2) describes the data rate on this link.

**Variant 2.1.d: Pre-processing per iSC and centralized detection & decoding within RANaaS by forwarding local estimates of one iSC**

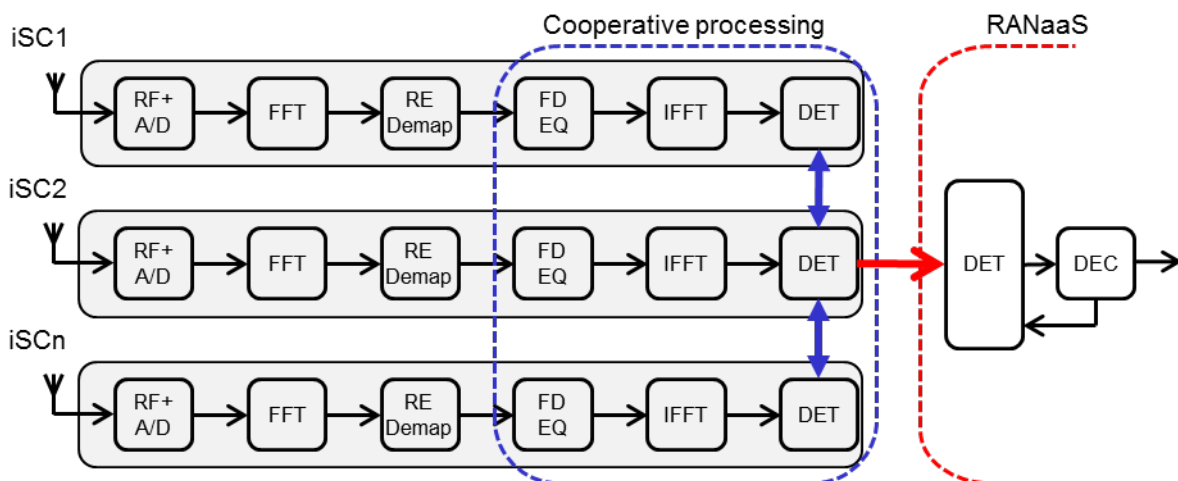


**Figure 6-5: Variant 2.1.d: Pre-processing per iSC and centralized detection & decoding within RANaaS by forwarding local estimates of one iSC**

Different from the other variants above, this variation shown in Figure 6-5 performs a cooperative pre-detection within iSCs by exchanging the local signal estimates for a fixed number of iterations, not reaching a consensus yet. Afterwards, only one iSC forwards its pre-equalized symbols to the RANaaS, where the final detection and decoding, presumably through iterative processing, is implemented.

In this variant, the requirements on the J1 interface are the same to variant 2.1.b. Similarly, for the J2 interface also low link reliability is sufficient (cf. CT2.1.a), but since erroneous information exchange leads to a higher required number of iterations among iSCs to achieve consensus in INP [4], the estimation quality is reduced if the number of iterations is fixed. In this case, more iterations are required in the turbo decoder in the RANaaS. The choice of the number of iterations at the iSCs allows an influence on the processing load. In the RANaaS, the computation effort is higher than in the previous variants, since an iterative detection and decoding is performed there. The amount of data exchanged on the iSC-iSC interface per iteration is identical to variants 2.1.a and 2.1.b, see (6.1), but the number of iterations performed will be significantly less. Like for variant 2.1.b, the iSC-RANaaS interface needs to carry finely quantized symbols, since the further detection is carried out in the RANaaS. Therefore, the data rate is given by (6.3). Regarding the reliability of the iSC-RANaaS link, in principle the same holds as for variant 2.1.b, but with the restriction that since the consensus algorithm is not converged completely, the pre-detected symbols at the different iSCs will not be identical. Therefore, if the J1 link to the RANaaS is taken over by another iSC, the effective performance or the required number of iterations of the joint detector in the RANaaS might change.

**Variant 2.1.e: Pre-processing per iSC and centralized detection & decoding within RANaaS by forwarding local estimates of several iSCs**

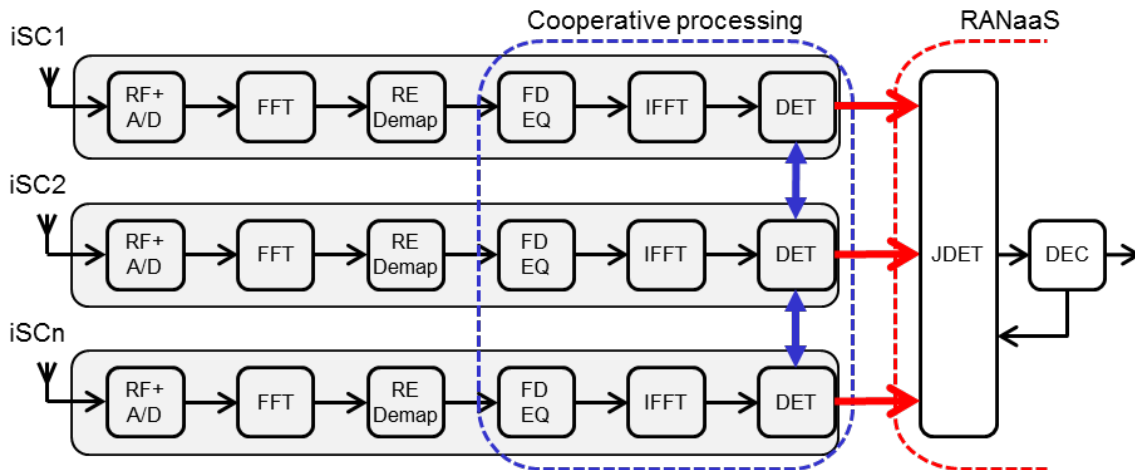


**Figure 6-6: Variant 2.1.e: Pre-processing per iSC and centralized detection & decoding within RANaaS by forwarding local estimates of several iSCs**

Similar to variant 2.1.d, the functionalities of detector and decoder are shifted from iSC to RANaaS as can be seen in Figure 6-6, and iSCs also cooperatively perform the pre-detection by exchanging local signal estimates for certain iterations. But in this variant, several iSCs will forward the pre-equalized symbols to the RANaaS where the iterative centralized processing is performed. This ensures that all available information is used in the subsequent joint detection and decoding process.

In this variant, the reliability of the iSC-RANaaS link can be reduced compared to variant 2.1.d, since the data is forwarded by several iSCs instead of one, and they are jointly detected in the RANaaS. Thus more computation effort is needed for the centralized processing. The bandwidth requirement on the iSC-iSC interface is equal to that in variant 2.1.a, 2.1.b and 2.1.d given in (6.1), but the bandwidth requirement on the iSC-RANaaS interface is larger, since more than one iSCs (total number  $N_{iSC}$ ) deliver finely pre-equalized symbols to the RANaaS, resulting in a data rate

$$D_{iSC-RANaaS} = N_{iSC} \cdot N_{quant,J1}^x \cdot 12 \cdot \sum_u^{N_{UE}} (N_{RB}^{UE,u} \cdot N_L^{UE,u}) \cdot T_s^{-1}. \quad (6.5)$$

The Table 6-1 illustrates the requirements regarding the computational needs as well as the link bandwidth, reliability and latency of these five possible functional splits that have been discussed above.

**Table 6-1: Functional Split for CT 2.1**

Functionality	2.1.a	2.1.b	2.1.c	2.1.d	2.1.e
<b>Computational Needs for iSC</b>	Moderate, higher at decoding iSC	Moderate	Higher, but reduction of no. of iterations possible	Lower	Lower
<b>Computational Needs for RANaaS</b>	None	Moderate	None	Moderate	High
<b>Bandwidth req. on iSC-iSC interface</b>	High	High	High, but reduction of no. of iterations possible	Moderate (due to reduced no. of iterations)	Moderate (due to reduced no. of iterations)
<b>Bandwidth req. on iSC-RANaaS interface</b>	Low	High	Low	High	Very high
<b>Link reliability req on iSC-iSC interface</b>	Low	Low	Low	Low	Low
<b>Link reliability req on iSC-RANaaS interface</b>	Moderate (any iSC might take over decoding and link to RANaaS)	Moderate (any iSC might take over link to RANaaS)	Moderate (any iSC might take over link to RANaaS)	Moderate (any iSC might take over link to RANaaS)	Moderate (link failures might however deteriorate performance)
<b>Latency req. on interface on iSC-iSC interface</b>	Very low	Very low	Very low	Very low	Very low
<b>Latency req. on interface on iSC-RANaaS interface</b>	Moderate	Moderate	Moderate	Moderate	Moderate

## 6.2.2 CT 2.2: Multi-Point Turbo Detection

The functional split in the physical layer for the multi-point turbo detection concerns the detection part, right after the FFT block in the uplink for the SC-FDMA process.

### Variant 2.2.a: SPTD with possible cooperation using the J2 interface

In its first variation, no functional split is performed in the physical layer as shown in Figure 6-7. However, cooperation could be envisaged through the J2 interface linking iSCs. Without information exchange related to the turbo detection loop, we have the SPTD solution evaluated in section 4.2.3, which brings some interesting gains over the classical receiver in the worst case where served and interfering users are received with the same power level at an iSC. The use of cooperation, if the J2 interface supports it, could bring some additional improvements and is left for further studies.

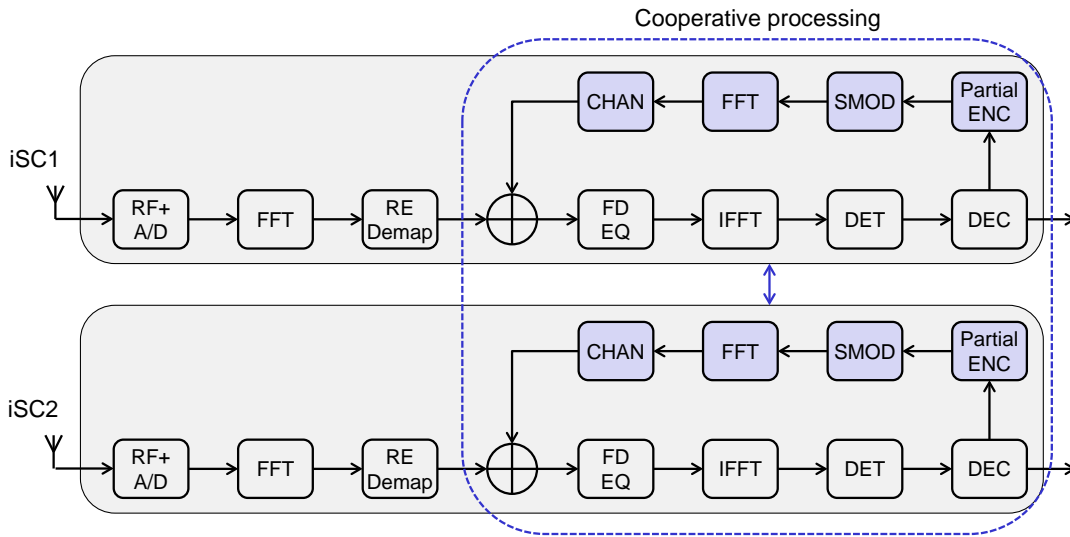


Figure 6-7: Variant 2.2a: SPTD with possible cooperation using the J2 interface

**Variant 2.2.b: MPTD performed at the RANaaS platform using the J1 interface**

In its second variation, the functional split is performed in the physical layer just after the FFT block as shown in Figure 6-8. This variation represents the MPTD solution done at the RANaaS platform when the J1 interface can support it. Its evaluation in section 4.2.3 has demonstrated that significant gains could be obtained even in the worst case scenario (same power received from both users).

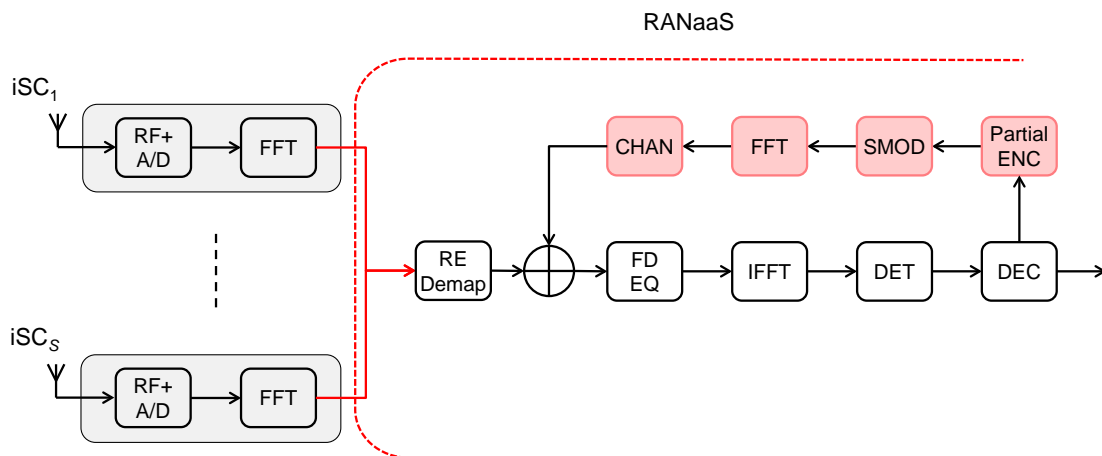


Figure 6-8: Variant 2.2b: MPTD performed at the the RANaaS platform using the J1 interface

Table 6-2: Functional Split for CT 2.2

Functionality	2.2.a	2.2.b
Computational Needs for iSC	High	Low
Computational Needs for RANaaS	Low (none at PHY level)	High
Bandwidth req. on iSC-iSC interface	Low (High if information exchange between iSCs is envisaged)	Low
Bandwidth req. on iSC-RANaaS interface	Low (none at PHY level)	High (Gbps order)
Link reliability req on iSC-iSC interface	Low	N/A
Link reliability req on iSC-RANaaS interface	Low	High
Latency req. on interface on iSC-iSC interface	Very Low Latency (<1ms)	N/A
Latency req. on interface on iSC-RANaaS interface	Moderate (<40ms)	Very Low latency (<1ms)

### 6.2.3 CT 2.3: Joint Network-Channel Coding

The functional split for CT2.3 JNCC (Section 4.3) concerns the deployment of the demapping and of the decoding modules whether centralised in the cloud or distributed within the two small cells. Two functional splits are proposed:

#### Variant 2.3.a: Distributed JNCC within iSC<sub>1</sub> and iSC<sub>2</sub>.

The first functional split, illustrated in Figure 6-9, implements cooperative detection and decoding within iSCs. Cooperation processing is represented by the blue arrow between the two iSCs, indicating that network encoded data is transmitted from iSC 1 to iSC 2 by the J2 link. The destination node iSC 2 jointly decodes the received signals from UEs and iSC 1, using knowledge of the joint factor graph, as explained in Section 4.3.1. Decoded data is then transmitted to the RANaaS.

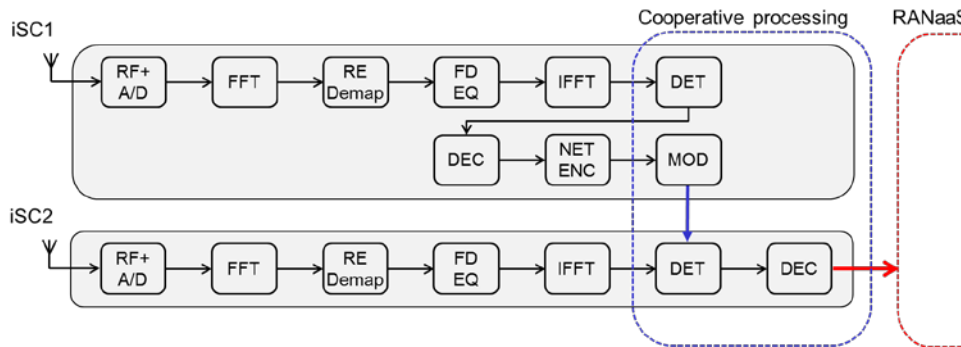


Figure 6-9: Variant 2.3.a: Cooperative detection & decoding within iSCs

#### Variant 2.3.b: Centralized JNCC within RANaaS.

The second functional split, illustrated in Figure 6-10, implements centralized detection and decoding within RANaaS. As shown in this figure, the intermediate node iSC<sub>1</sub> transmits the network encoded data directly to the RANaaS. Also, the destination node iSC<sub>2</sub> forwards pre-processing soft-information to RANaaS. This allows joint detection and decoding to be centralized on RANaaS.

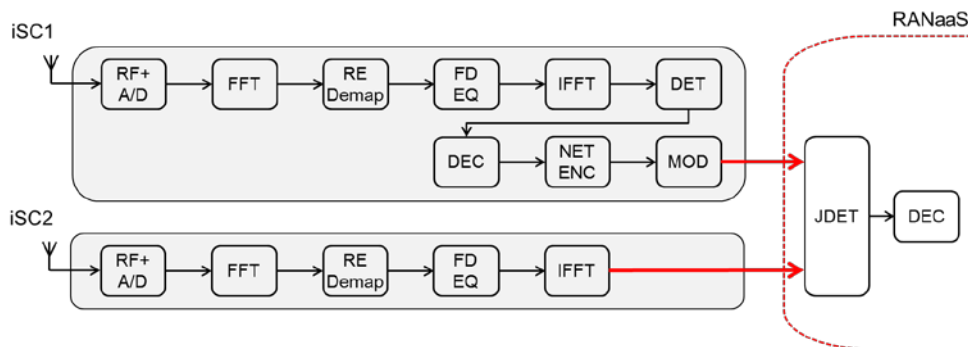


Figure 6-10: Variant 2.3.b: Centralized detection & decoding within RANaaS

The goal of the CT2.3b functional split is to offload the iSC<sub>2</sub> node of part of the baseband processing load. However this option comes at the cost of an increased data load on the backhaul link iSC<sub>2</sub>-RANaaS, since it requires soft information to be forwarded from iSC<sub>2</sub> to RANaaS.

Concerning the intermediate node iSC<sub>1</sub>, we remark that both functional splits induce the same data load on its backhaul. Indeed, for the first functional split the network encoded data is transmitted from iSC<sub>1</sub> to iSC<sub>2</sub>, while for the second one, the same data is transmitted from iSC<sub>1</sub> to RANaaS.

The requirements of the two possible functional splits that have been discussed above are described in the Table 6-3.

**Table 6-3: Functional Split for CT 2.3**

Functionality	2.3.a	2.3.b
Computational Needs for iSC	High	Moderate
Computational Needs for RANaaS	Very low	High
Bandwidth req. on iSC-iSC interface	Moderate	None
Bandwidth req. on iSC-RANaaS interface	Moderate	High
Link reliability req on iSC-iSC interface	High	None
Link reliability req on iSC-RANaaS interface	Moderate	High
Latency req. on interface on iSC-iSC interface	Low	None
Latency req. on interface on iSC-RANaaS interface	Moderate	Low

**6.2.4 CT 2.4: Sum-Rate and Energy-Efficiency metrics of DL CoMP with backhaul constraints**

Different functional splits for CT2.4 DL CoMP with backhaul constraints (Section 4.4) can be envisaged depending upon whether the precoder implementation is centralised in the cloud or not, and for centralised cloud implementation whether the entire transmit chain is implemented or only a few functionalities (pertaining to CoMP) are computed and then passed onto each iSC individually. This impact very much depends upon the backhaul and its characteristics in terms of capacity, delay, availability, etc. In the following, we elaborate in detail the major possible functional splits.

**Variant 2.4.a: Centralised CoMP at RANaaS with precoded time-domain transmit signal sent over J1 interface**

This function split is illustrated in Figure 6-11 and, as shown, the entire transmit chain is in the RANaaS and only the time domain I/Q samples of the precoded signal are sent over J1 interface. This architecture is suitable for joint transmission (JT) CoMP with the assumption that global CSI is available, and it also relies heavily on the availability of high speed, high capacity J1 interface between RANaaS and each individual iSC.

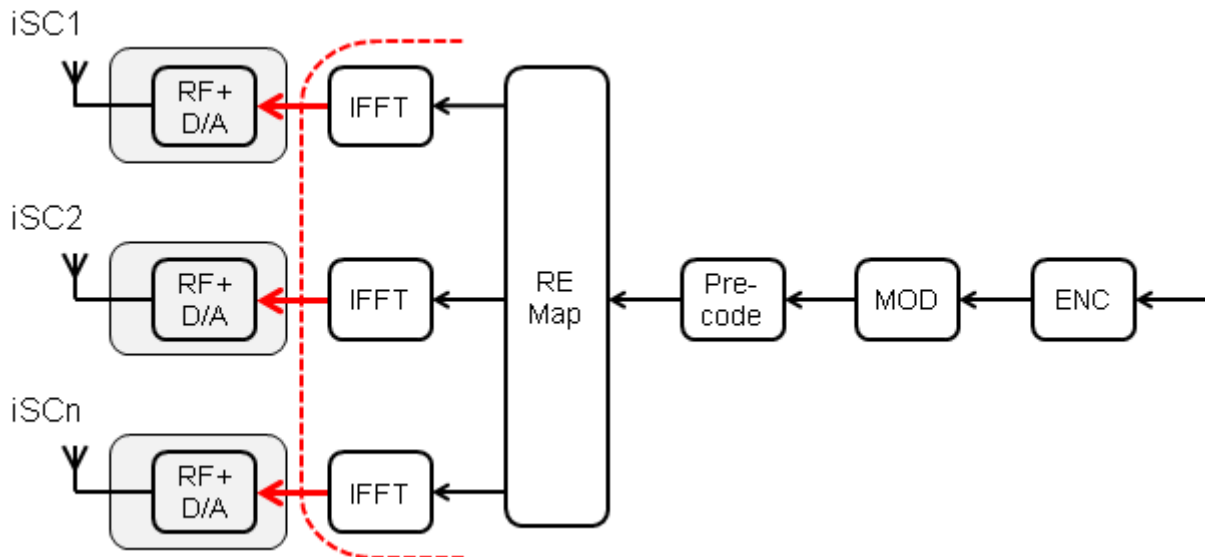


**Figure 6-11: Variant 2.4.a: Centralised CoMP at RANaaS with All Computation in RANaaS**

**Variant 2.4.b: Centralised CoMP at RANaaS with only PMI, RI, and Information bits sent over J1 interface**

The second variant of centralised CoMP at RANaaS that is illustrated in Figure 6-12 computes only the PMI and RI information in the cloud and send these together with information bits to each iSC individually. This is suitable when the J1 interface is capacity constrained and cannot carry the high bandwidth associated with time domain I/Q samples of the precoded signal. This variant still relies on availability of global CSI for computation of PMI for each iSC.

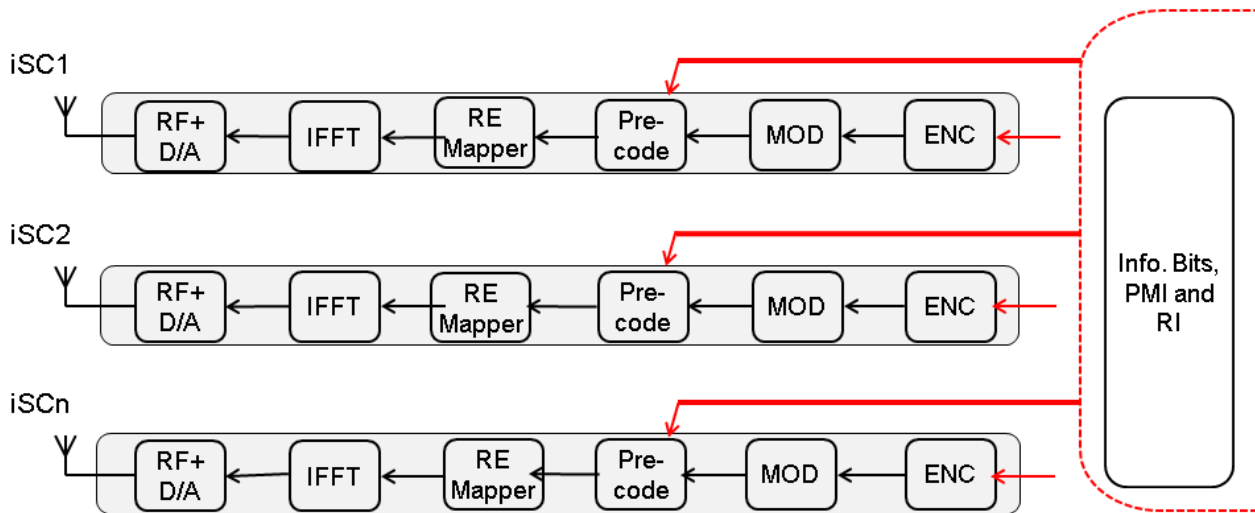


Figure 6-12: Variant 2.4.b: Centralised CoMP at RANaaS with only Precoder Computation in RANaaS

**Variant 2.4.c: De-centralised CoMP by cooperation between iSCs using J2 interface**

This functional split (as shown in Figure 6-13) does not make use of centralised processing at RANaaS, and instead relies only on local cooperation between the iSCs. This architecture is suitable when for example the latency on J1 interface is quite high and J2 interface is reliably available and incurs much less delay than the one on J1 interface. This architecture is also suitable when only partial CSI is available due to limited capacity of J2 interface, hence only coordinated beamforming / scheduling CoMP is possible.

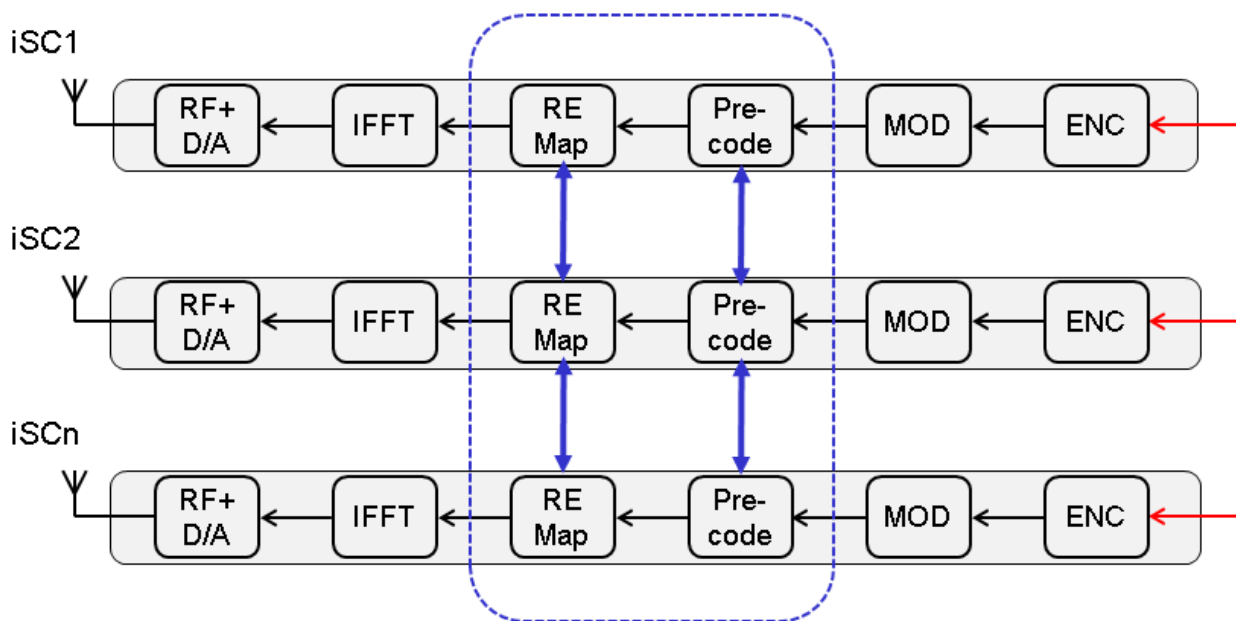


Figure 6-13: Variant 2.4.c: De-centralised CoMP at iSCs with Local Cooperation

The Table 6-4 illustrates the requirements and gains of the three possible functional splits that have been discussed above.

**Table 6-4: Functional Split for CT 2.4**

Functionality	2.4.a	2.4.b	2.4.c
Computational Needs for iSC	Very low	Moderate	High
Computational Needs for RANaaS	High	Moderate	None
Bandwidth req. on iSC-iSC interface	None	None	High
Bandwidth req. on iSC-RANaaS interface	High	Moderate	Low
Link reliability req on iSC-iSC interface	None	None	High
Link reliability req on iSC-RANaaS interface	High	High	Low
Latency req. on iSC-iSC interface	None	None	Very low latency
Latency req. on interface on iSC-RANaaS interface	Very low	Very low	Moderate

### 6.2.5 CT 2.5: Partially Centralized Inter-Cell Interference Cancellation

A precoding scheme exploiting both the J1 and the J2 backhaul links is provided Section 4.5. For this CT, several functional splits have been envisioned and are presented in the following. Note that the functional splits are in fact not really dependent on this particular CT, but rather generally linked to the constraints of precoder design. Hence, the functional splits of this CT are essentially the same as in the previous CT2.4 and we will refer to the figures presented in Section 6.2.4 for the sake of brevity.

The proposed precoding scheme aims at bridging the gap between the two extreme scenarios where the precoder is designed either centrally in the RANaaS or in a distributed manner at the iSCs. We have considered the 4 most relevant functional splits for this CT which can be described as follows

#### **Variant 2.5.a: Centralised CoMP at RANaaS with precoded time-domain transmit signal sent over J1 interface**

This functional split corresponds to the “star topology”, i.e., the centralized case with all the processing done in the RANaaS and the iSCs being solely RRHs. This functional split can be associated to the block diagram in Figure 6-11.

#### **Variant 2.5.b: Centralised CoMP in a master iSC by cooperation between iSCs using J2 interface**

In this configuration, a master-slave organization is chosen with all the processing being done in the master done. The precoding remains centralized but is carried out in a master iSC instead of being done in the RANaaS. This is similar to the block diagram in Figure 6-11 with the processing done in a master iSC.

#### **Variant 2.5.c: Partially centralised CoMP by cooperation between iSCs and the RANaaS using both the J1 and the J2 interfaces**

This functional split corresponds to the new hybrid precoding scheme proposed where the precoder is partly computed in the RANaaS and partly in the iSCs. The functional split is the same as in the block diagram Figure 6-12. Indeed, the precoder is computed in the RANaaS and shared to the iSC. The difference being that an additional step of processing is done at the iSC to refine the precoder received.

#### **Variant 2.5.d: Distributed CoMP in a master iSC by cooperation between iSCs using J2 interface**

In this scenario, the J1 links to the RANaaS are used only to transmit the higher layer information and the physical layer is completely implemented in a distributed manner in the iSCs. This scenario is described in Figure 6-13.

The requirements on the architecture for these 4 different functional splits are described in Table 6-5.

**Table 6-5: Functional Split for CT 2.5**

Functionality	2.5.a	2.5.b	2.5.c	2.5.d
Computational Needs for iSC	Low	High	Medium	Medium
Computational Needs for RANaaS	High	Low	High	Low
Bandwidth req. on iSC-iSC interface	None	High	Medium	High
Bandwidth req. on iSC-RANaaS interface	High	Low	Medium	Low
Link reliability req on iSC-iSC interface	—	High reliability	Low reliability	Low reliability
Link reliability req on iSC-RANaaS interface	High reliability	High reliability	Medium reliability	Low reliability
Latency req. on interface on iSC-iSC interface	—	Low Latency	Low Latency	Low Latency
Latency req. on interface on iSC-RANaaS interface	Low Latency	High Latency	—	High Latency

**6.2.6 CT 2.6: Data compression over RoF**

The functional split concerns the deployment of the FFT/IFFT and the spatial precoding modules. Two functional splits based on the frequency domain transmission of the signals are proposed in Section 4.6 for both the downlink and uplink. In the following the downlink splitting is taken as reference but the same split is symmetrically applicable for the uplink.

**FFT/IFFT operations in the iSC**

The first functional split, illustrated in Figure 6-14 for the downlink, foresees the execution of the IFFT operation at the iSC, so that the OFDM signal in the frequency domain is transmitted on the backhaul link. The RANaaS transmits over the backhaul link the quantized I/Q OFDM signal in the frequency domain for each iSC transmit antenna, after the operations of channel encoding, scrambling, modulation, spatial precoding, and RE mapping. The iSC performs the following Layer 1 signal processing operations for each transmit antenna: IFFT, cyclic prefix insertion, oversampling, filtering, D/A conversion, and RF processing.

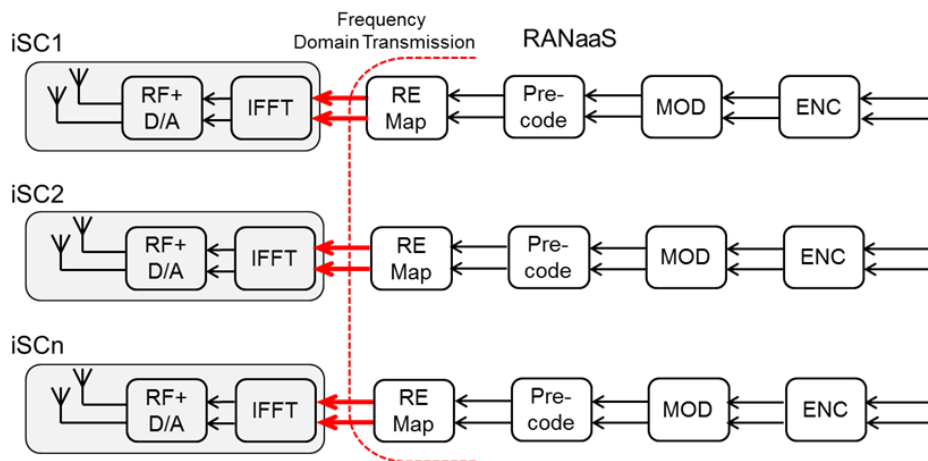


**Figure 6-14: Variant 2.6.a: Frequency domain RoF**

**FFT/IFFT operations and local processing in the iSC**

The second functional split, illustrated in Figure 6-15 still for the downlink, is specific for the case of single codeword transmission. This mode of operation is applicable for example to the transmission mode 7 (Single layer beamforming) introduced in the Release 8 of the LTE standard [112]. In this case the spatial precoding operation is moved at the iSC side so that a unique signal must be transmitted on the backhauling link. Various form of spatial precoding can be conceived, like for example adaptive beamforming on a per user basis.

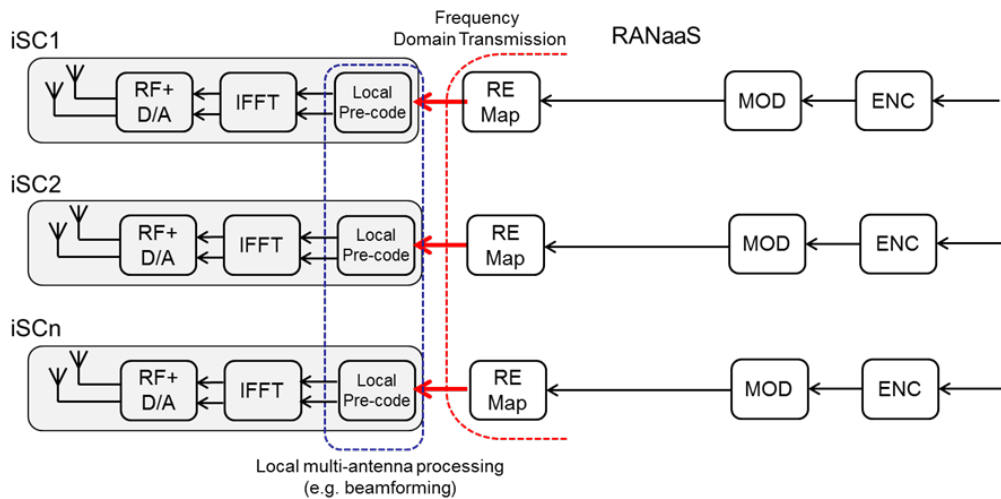


Figure 6-15: Variant 2.6.b: Frequency domain RoF for single codeword transmission

The goal of CT2.6 functional split is to reduce the throughput load on the backhaul link by avoiding the transmission of elements that just represent overhead like cyclic prefix and the null subcarriers at the edge of the spectrum. The transmission in the frequency domain over the backhaul link enables also the execution at the iSC side of signal processing operations separately for each user. The functional splits illustrated in the Figures above are identically applicable to the uplink by shifting the FFT and local precoding operations at the iSC side. The requirements of the two possible functional splits that have been discussed above are described in the Table 6-6.

Table 6-6: Functional Split for CT 2.6

Functionality	Conventional TD-RoF	FD-RoF (option 2.6.a)	FD-RoF (option 2.6.b)
Computational Needs for iSC	Low	Moderate	High
Computational Needs for RANaaS	High	Moderate	Low
Bandwidth req. on iSC-iSC interface	N.A.	N.A.	N.A.
Bandwidth req. on iSC-RANaaS interface	Very High	Moderate	Low
Link reliability req on iSC-iSC interface	N.A.	N.A.	N.A.
Link reliability req on iSC-RANaaS interface	High	High	High
Latency req. on interface on iSC-iSC interface	N.A.	N.A.	N.A.
Latency req. on interface on iSC-RANaaS interface	Moderate	Moderate	Moderate

### 6.2.7 CT 2.7: Millimetre Wave Backhauling

As described in Section 4.7, mmWave backhaul is a basic transport technology that can be used to enable various different functional splits, as any type of data can be transported. The functional split then requires certain parameters like data rate and delay to be fulfilled to enable each split. Apart from that, this CT investigates joint access and BH channel coding, which requires a shift of detection and decoding of the access link into the RANaaS. This is also required by certain other CTs as CT2.5. Therefore, three possible functional split variants are discussed in the following and compared in terms of BH data rate requirements. The parameters used for the data rate calculation can be found in Table 6-7.

**Table 6-7: CT2.7 parameters for exemplary BH rate calculation**

Parameter	Symbol	Value
Bandwidth	$B$	20 MHz
Sampling frequency	$f_s$	30.72 MHz
Oversampling factor	$OF$	2
Number of subcarriers	$N_{sc}$	1200
Time slot duration	$T_{slot}$	1 ms
Symbols per time slot	$N_{symp}^{UL}$	14
FFT size	$N_{FFT}$	2048
Number of antennas	$N_R^{iSC}$	2
Quantization resolution	$N_{quant}^{UL}$	10 bit
User data rate	$D_{UE}$	134.4 Mbps
Modulation scheme access	$M_{RAN}$	6 bit/symbol

**Variant 2.7.a: Detection and decoding in iSC**

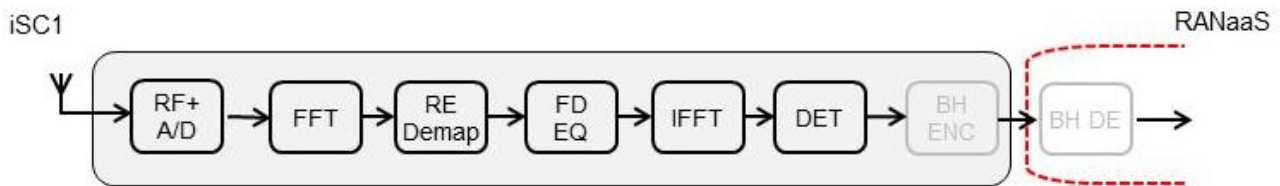


**Figure 6-16: Variant 2.7.a: Detection and decoding in iSC**

This variant corresponds to the conventional decode and forward scheme, which means that decoded user data is backhauled. It is used for comparison to the other two variants, as joint access and channel coding as well as other CTs as CT2.5 cannot be used in this variant. The required data rate on the BH can be calculated as:

$$D_{BH} = D_{UE} = 134.4 \text{ Mbit/s} . \tag{6.7}$$

**Variant 2.7.b: Detection and decoding in RANaaS**

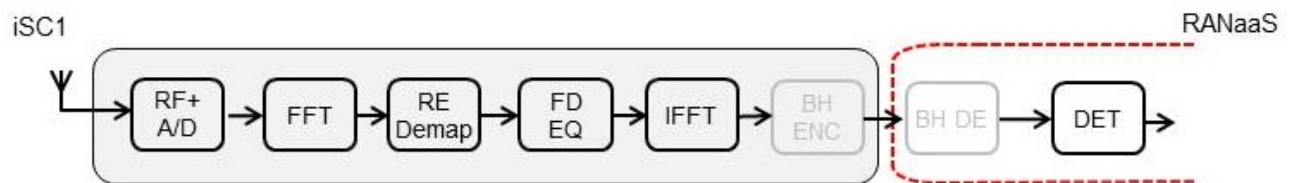


**Figure 6-17: Variant 2.7.b: Detection and decoding in RANaaS**

In this variant, detection and decoding are shifted to the RANaaS, which means that an I/Q-data stream of received signals is being backhauled and joint access and channel coding can be used. However, the received signals are already pre-processed in terms of RE demapping and channel equalization. The required data rate on the BH can be calculated as:

$$D_{BH} = N_{sc} N_{sym}^{UL} T_{slot}^{-1} 2 N_{quant}^{UL} N_R^{iSC} = 672 \text{ Mbit/s.} \tag{6.8}$$

**Variant 2.7.c: RRH: all digital processing in RANaaS**

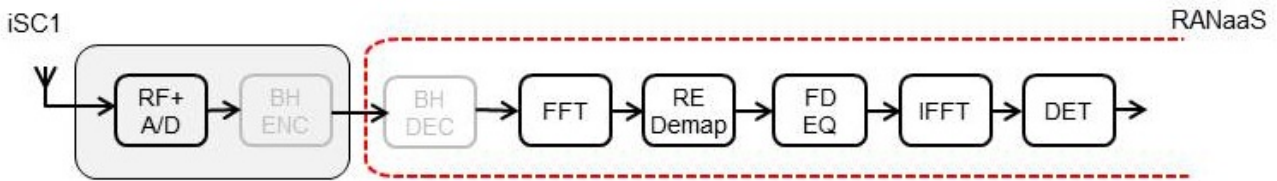


**Figure 6-18: Variant 2.7.c: RRH: all digital processing in RANaaS**

In this variant, only analog and A/D conversion is performed at the iSC, meaning that unprocessed I/Q- data is backhauled. The required data rate on the BH can be calculated as:

$$D_{BH} = f_s \cdot OF \cdot N_R^{iSC} \cdot 2 \cdot N_{quant}^{UL} = 2457.6 \text{ Mbit/s.} \tag{6.9}$$

As can be seen from the calculations in Equations (6.7), (6.8) and (6.9), the RoR architecture increases the required data rate/load on the BH link tremendously, yet this shift of decoding into the RANaaS is, as mentioned, required by other CTs as CT2.5. Variant 2.7a can only be used if no PHY layer processing is shifted to the RANaaS.

The main gains within this CT are achieved by optimizing the joint access and backhaul channel by means of joint coding. These gains include:

- Lower BER/higher data rate on UE-RANaaS link due to optimized coding on access and BH link
- Reduced hardware in iSCs in the case of no separate BH channel code

Ideally, these gains will multiply with the gains achieved by the other CTs using the same split.

The basic trade-off is that the coding scheme has an influence on the required data rate/load on the BH and access link. Removing the separate BH channel code might require a lower code rate on the access channel, which increases its load. Further impacts on the architecture for these three different functional splits are described in Table 6-8.

**Table 6-8: Functional Split for CT 2.7**

Functionality	2.7.a	2.7.b	2.7.c
Computational Needs for iSC	High	Medium	low
Computational Needs for RANaaS	Low	Medium	high
Bandwidth req. on iSC-iSC interface	none	none	none
Bandwidth req. on iSC-RANaaS interface	Low	High	Very high
Link reliability req on iSC-iSC interface	none	none	none
Link reliability req on iSC-RANaaS interface	High	Very high	Very high
Latency req. on interface on iSC-iSC interface	none	none	none
Latency req. on interface on iSC-RANaaS interface	Medium	Very low	Very low

**6.3 Functions Investigated in detail for Functional Split**

The FEC decoder and the precoder are two fundamental components of the physical layer for the uplink and the downlink respectively. In the following sections, the functional split options of these two functions with the related gains and challenges are analysed in detail.

The FEC decoder is the last functional component of the physical layer (at the receiver side) and basically two functional split strategies are possible, depending on whether the FEC decoder is implemented in the iSC or in the RANaaS. In the former case with the decoder implemented in the iSC, there are not specific impacts or requirements on the RAN implementation. However, the J1 interface connecting the iSC and the RANaaS needs to be reliable, in order to ensure that decoded data is correctly received at the RANaaS.

For the second option, with the uplink FEC decoder implemented in the RANaaS, the soft LLR values must be transmitted from the iSC to the RANaaS. The J1 interface connecting the iSC to the RANaaS needs to be high capacity to accommodate the increased data rate but does not need to be completely reliable, as the FEC code may be designed such as to correct errors occurring on both RAN and backhaul links. The cloud implementation of FEC decoders in the RANaaS poses a significant demand of computational resources, even though the advent of multi-core processors and the inherent decoding parallelism of modern FEC techniques open new perspectives for massively parallel implementations.

The precoder is a key building block for the implementation of Coordinated Multi-point Transmission (CoMP) techniques in downlink. Several options for the placement of the precoder are applicable depending on the deployment configuration and availability of J1 and J2 backhaul links. The implementation of the precoder in the RANaaS makes possible to address interference that comes not only from immediate neighbours but also from farther cells (i.e. global cooperation). In this case both J1 and J2 interfaces can be synergistically exploited or, if the J2 interface is not available, a fully centralized architecture with star topology and high quality J1 interface can be conceived. As a second option, the precoder is implemented in the iSCs with a decentralised configuration in which iSCs use only J2 interface for local cooperation while J1 interface is used for carrying only information bits. In this case, only local cooperation among neighbouring iSCs is practically feasible.

Table 6-9 summarizes the main gain/challenges related to the splitting options for the decoder and precoder functions.

**Table 6-9: Gains and challenges of the Decoder/Precoder splitting options**

Function	Splitting option	Gains	Challenges
Decoder	Performed at RANaaS	J1 interface does not need to be completely reliable  FEC code may be designed to correct errors occurring on both radio and backhaul links	High J1 capacity  Low J1 latency  High decoding parallelism (i.e. cloud implementation of FEC decoder)
	Performed at iSC	No specific impact on RAN implementation	High J1 reliability
Precoder	Performed at RANaaS	Global cooperation	Optimal and synergic use of J1 and J2 interfaces when both available (especially for heterogeneous backhaul links that may be also varying in time)  High J1 capacity and reliability (if J2 interface is not available)
	Performed at iSC	Reduced J1 latency requirements	High J2 capacity and reliability  Low J2 latency

### 6.3.1 Decoder

#### 6.3.1.1 Description of Functionality

Forward Error Correction (FEC) or channel coding is a fundamental technique used in virtually any communication system that needs to reliably transmit data over noisy channels. It consists of adding redundant information to the transmitted data, which can be advantageously exploited at the receiver side to correct transmission errors. The channel encoder is responsible of computing the redundant information to be transmitted along with the useful data over the noisy channel, while the channel decoder is responsible of the

error correction at the receiver side. Modern FEC codes use soft decision decoders that are able to exploit the multi-level quantization at the channel output, hence increasing the error correction capability. Among these codes, Turbo [97] and Low-Density Parity-Check (LDPC) [55] codes can provide error-correction performance very close to the theoretical limit (channel capacity), by using iterative soft-decoding algorithms with constant computational complexity per decoded bit (i.e. linear complexity in the code length) [56]. Moreover, Turbo and LDPC decoders have an inherent (and sometimes flexible) degree of parallelism, which can be exploited in practical implementations in order to further increase the decoding throughput.

In the context of a cloud-based flexible RAN architecture, different options (or functional splits) exist for the placement of the physical layer's functional components, including the FEC decoder. Moreover, due to the fact that the FEC decoder is the last functional component of the physical layer (at the receiver side), its cloud implementation acts as an enabler for different functional split strategies in the uplink direction. Hence, this section discusses the possible options for the uplink FEC decoder implementation, along with their pros and cons and impact on the iJOIN architecture.

### 6.3.1.2 General Challenges

The cloud implementation of FEC decoders poses a significant challenge to the design of a cloud-based flexible RAN architecture. Indeed, due to their heavy demand of computational resources, FEC decoders are usually implemented on specialized hardware. However, the advent of many-core architectures provides outstanding computing power and opens new perspectives for massively parallel implementations. Advanced many-core CPUs already have more than 100 processing cores, and more processing cores are expected to become available as the computer architecture progresses.

In order to meet stringent requirements on data rate, cloud-based FEC decoders will need to fully exploit the high level of parallelism available in the computing architecture. While both Turbo and LDPC decoders mentioned above allow some level of parallelization, LDPC decoders are known for accommodating a wide range of parallelization levels, from serial to completely parallel implementations. This flexibility makes them a good candidate for cloud-based implementations [133], [134], [135], [136], [137], [138], [139].

### 6.3.1.3 Options for functional split

Two functional split strategies are possible, depending on whether the FEC decoder is implemented in the iSC or in the RANaaS. These strategies are discussed below. For the sake of simplicity, only the case of single user detection/decoding per iSC will be illustrated. However, both strategies also apply in case of more general detection schemes, even those requiring an exchange of information between several iSCs, as for instance cooperative/distributed multiuser detection. Moreover, some detection schemes may require a feedback loop between decoding and detection.

#### 6.3.1.3.1 Option A: Decoding in iSC

The first option corresponds to the classical RAN implementation, in which the FEC decoder is implemented in the iSC (Figure 6-19). In this case, there are not specific impacts or requirements on the RAN implementation. However, the J1 interface connecting the iSC and the RANaaS needs to be reliable, in order to ensure that decoded data is correctly received at the RANaaS.

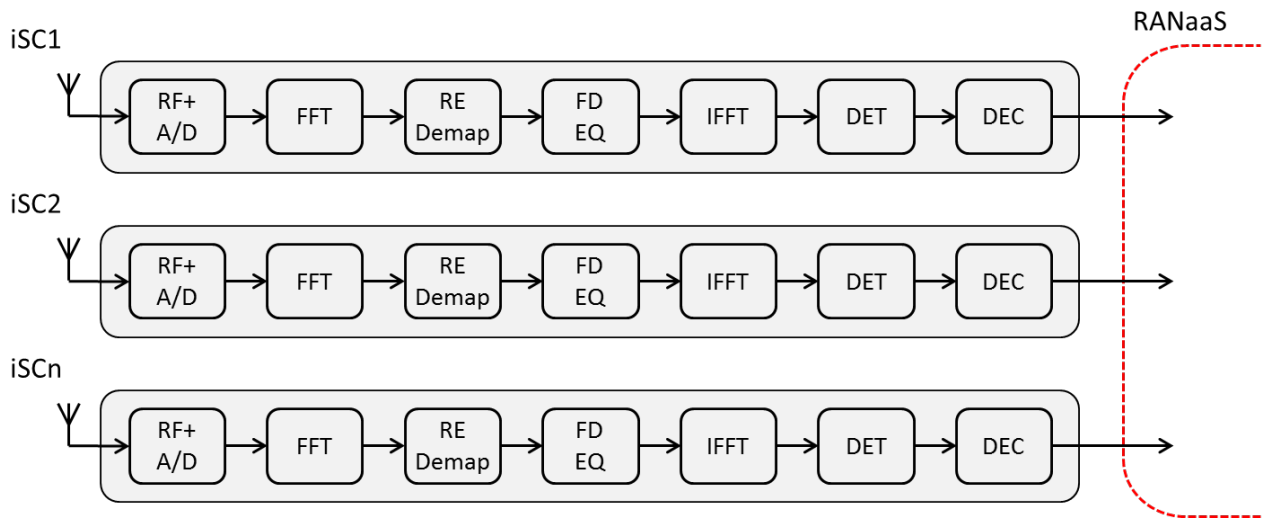


Figure 6-19: FEC decoder is performed in iSC

**Overview**

- Decoder for UL is performed in iSC
- Decoded data is transmitted from iSC to RANaaS

**Impacts/requirements on implementation**

- Similar to classical RAN implementation

**iJOIN Interface requirements**

- J1 interface needs to be reliable

**6.3.1.3.2 Option B: Decoding in RANaaS**

For the second option, the uplink FEC decoder is implemented in the RANaaS (Figure 6-20). In order to do so, the soft LLR values that constitute the decoder input must be transmitted from the iSC to the RANaaS. The J1 interface connecting the iSC to the RANaaS needs to be high capacity, such as to accommodate the increased data rate due to the transmission of the LLR values. However, the J1 interface needs not be completely reliable, as the FEC code may be designed such as to correct errors occurring on both RAN and backhaul links. In this context, it is worth mentioning that several candidate technologies, e.g. CT2.3 and CT2.7, investigate the design and/or use of joint coding for the RAN and backhaul links.

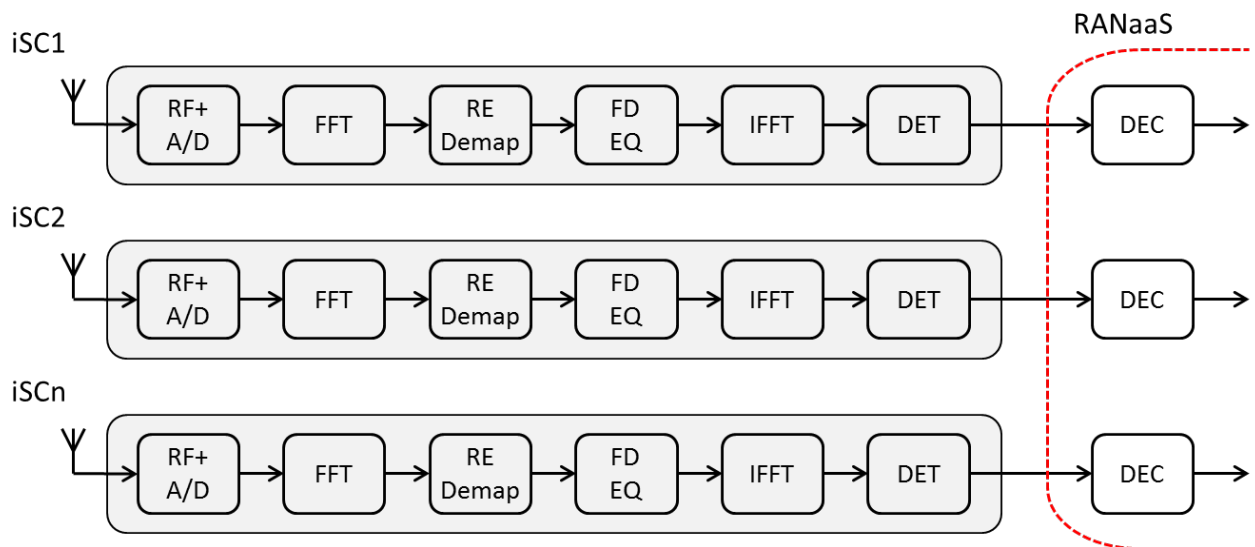


Figure 6-20: FEC decoder is implemented in RANaaS

## Overview

- Soft LLR values are transmitted from iSC to RANaaS
- UL decoder is performed in RANaaS

## Impacts/requirements on implementation

- Requires a cloud implementation of the FEC decoder in the RANaaS

## iJOIN Interface requirements

- Each iSC needs to be connected to its serving cloud via J1 interface
- J1 interface needs to be high capacity
- J1 interface does not need to be completely reliable, but might be prone to errors

### 6.3.1.4 Summary

The Pros and Cons of the two options are summarized in Table 6-10.

**Table 6-10: Pros and Cons of the two options**

	<b>Option A: Decoder@iSC</b>	<b>Option B: Decoder@RANaaS</b>
<b>PROS</b>	Lower demand in terms of capacity of the J1 interface	Can be used even if the J1 interface is not completely reliable (prone to errors)
	Standard implementation and possible reuse of common decoder hardware	Acts as an enabler for different functional split strategies at the PHY layer in the uplink direction
	Less stringent latency requirements on J1 interface	Allows joint-FEC code design, such as to protect both the RAN uplink and the backhaul link
		Allows higher flexibility in terms of FEC codes/decoders
<b>CONS</b>	Requires highly reliable J1 interface, in order to ensure that decoded data is correctly received at the RANaaS	Requires high capacity J1 interface, such as to accommodate the increased data rate due to the transmission of the LLR values
	Any functional split requiring a different PHY layer functional component being implemented in the RANaaS, would necessitate to retransmit data back from RANaaS to iSC to perform the FEC decoding.	Requires very low latency J1 interface
	Only a limited number of FEC codes/decoders can be implemented	

## 6.3.2 Precoder

### 6.3.2.1 Description of Functionality

CoMP is a promising means of enhancing the spectral efficiency of small cells and handling ICI that naturally increases as the cells become smaller and smaller. In essence, CoMP is achieved by the precoder design that takes into account the channel and interference conditions for all the small cells (or iSCs) in the cluster or CoMP set that co-operate on a mutual benefit basis. Thus, considering the iJOIN architecture of a flexible split of functionality between the RANaaS platform and the access network taking into account the joint design of access and the backhaul links; several options exist for the placement and the design of the precoder, these are captured below along with their pros and cons.

### 6.3.2.2 General Challenges

A precoder plays a central role in the CoMP processing, its design is quite important for enhancing the performance of macrocells particularly at the cell-edges; however in the context of small cells where ICI is more strong, an efficient design of the precoder becomes even more important. In particular, in the context of iJOIN project where a flexible cloud based implementation is investigated, the following general challenges need to be considered for the placement of the precoder and its design:

- Local cooperation among neighbouring iSCs or global cooperation via a cloud based implementation to address interference that comes not only from immediate neighbours but also from farther cells in the 2nd / 3rd tier of cells.
- Efficient precoder design with finite set with accurate PMI selection at the receiver, and a reasonable feedback overhead.
- Exchange of information such as CSI and / or data between cooperating iSCs or between iSCs and RANaaS over constrained J2 and J1 interfaces, respectively.

### 6.3.2.3 Options for functional split

The following major options exist for precoder functional split depending upon deployment configuration and availability of J1 and J2 backhaul links:

- Option A: Precoder split between RANaaS and iSC: Global cooperation using jointly J1 and J2 interfaces
- Option B: Precoder in RANaaS: Global Cooperation using J1 interface only
- Option C: Precoder in iSC: Local Cooperation using J2 interface only

Option A is most generic of all enabling global cooperation by making best use of both J1 and J2 interfaces, while both Option B and Option C are special cases of Option A. This is because in Option B, J2 interface is not available or even if it is available, it may not be worthwhile to use in the presence of J1 interface if the J1 interface is of low latency and high bandwidth enabling rapid global cooperation. On the other hand Option C relies only on J2 interface for CoMP purposes even though J1 interface is available and carries only the information bits; this is possible for example when the latency on J1 interface is quite high as compared to J2 interface. Each one of these precoder options are elaborated below in more details.

#### 6.3.2.3.1 Option A: Precoder split between RANaaS and iSC: Global Cooperation using jointly the J1 and J2 interfaces

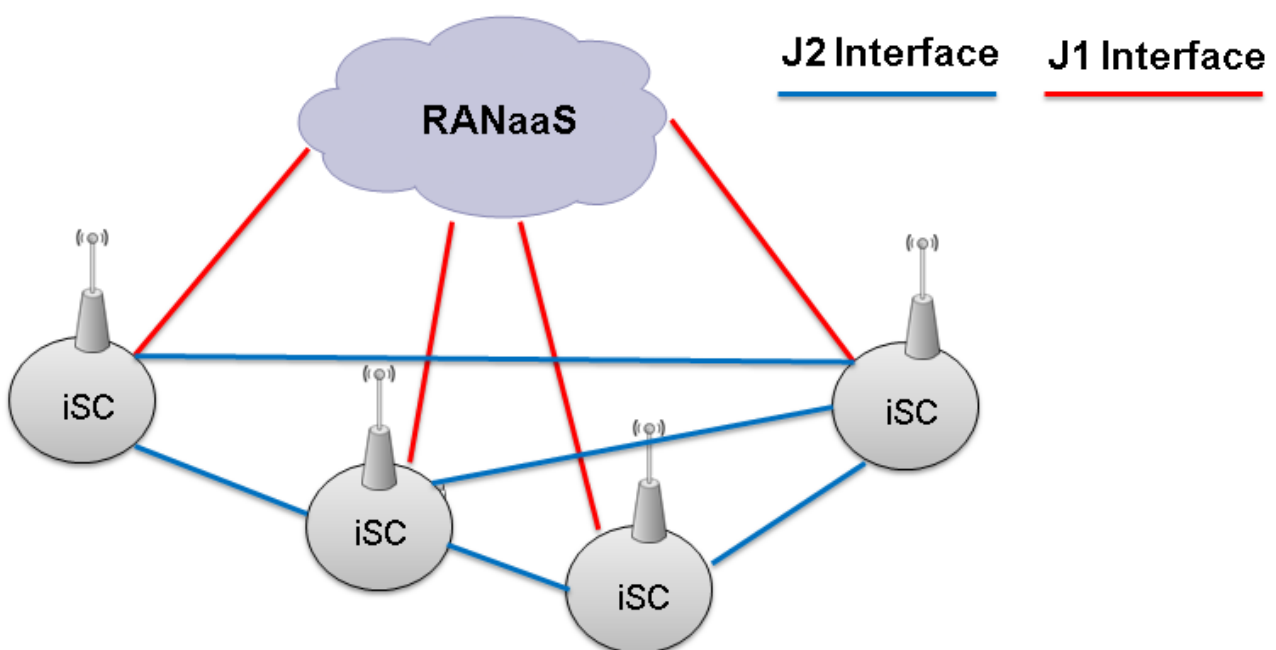


Figure 6-21: Global cooperation for Precoder by Joint usage of J1 and J2 links

**Overview**

- Both J1 and J2 links are present but the quality of the links may vary for each link, from perfect to unreliable. This scenario represents in fact the most general case and includes all the others. It is also the most complex one as the J1 and J2 links can be exploited in many ways.
- The generality of this scenario has for consequence that the optimal design of the precoder remains an open problem. For certain backhaul configurations (e.g. J1 links with large bandwidth, J2 links with large bandwidth, etc...), the optimal precoder design is known, but in general, the optimal approach depends on the backhaul architecture and it is not yet known how to always exploit optimally every backhaul link available. The optimal precoder design in this general setting will be further investigated during the rest of the iJOIN project.

**Impacts/requirements on implementation**

- A hybrid architecture where the J2 links can be used to replace/reduce the J1 links.
- The precoder design could potentially be split between several nodes which makes more complex the standardization of the interfaces.

**iJOIN Interface requirements**

- Both J1 and J2 links need to be low delay and of comparable bandwidth to really obtain synergistic benefits from this scenario.
- Knowledge of the general architecture and of the properties of all the J2 and J1 links allows to better optimizing the use of the hybrid architecture.
- The backhaul links may be heterogeneous and even varying in time.
- The joint use of J1 and J2 links could be used to exploit even unreliable links, with a proper detection of the failure events and an adequate signal processing. What kind of signal processing and how to divide it between the iSCs and the RANaaS in order to gain from the joint use of the J1 and the J2 interfaces remains however an open problem which will be investigated in the framework of the iJOIN project.

**C-Plane/U-Plane considerations**

- Not all C-plane data needs to be communicated to RANaaS as some C-plane functionalities could be executed locally in the iSCs
- Sharing the U-plane to the iSCs could be interesting in some cases so as to allow the iSCs to do more local processing and hence to better exploit the hybrid backhaul architecture.

### 6.3.2.3.2 Option B: Precoder in RANaaS: Global Cooperation using J1 interface only

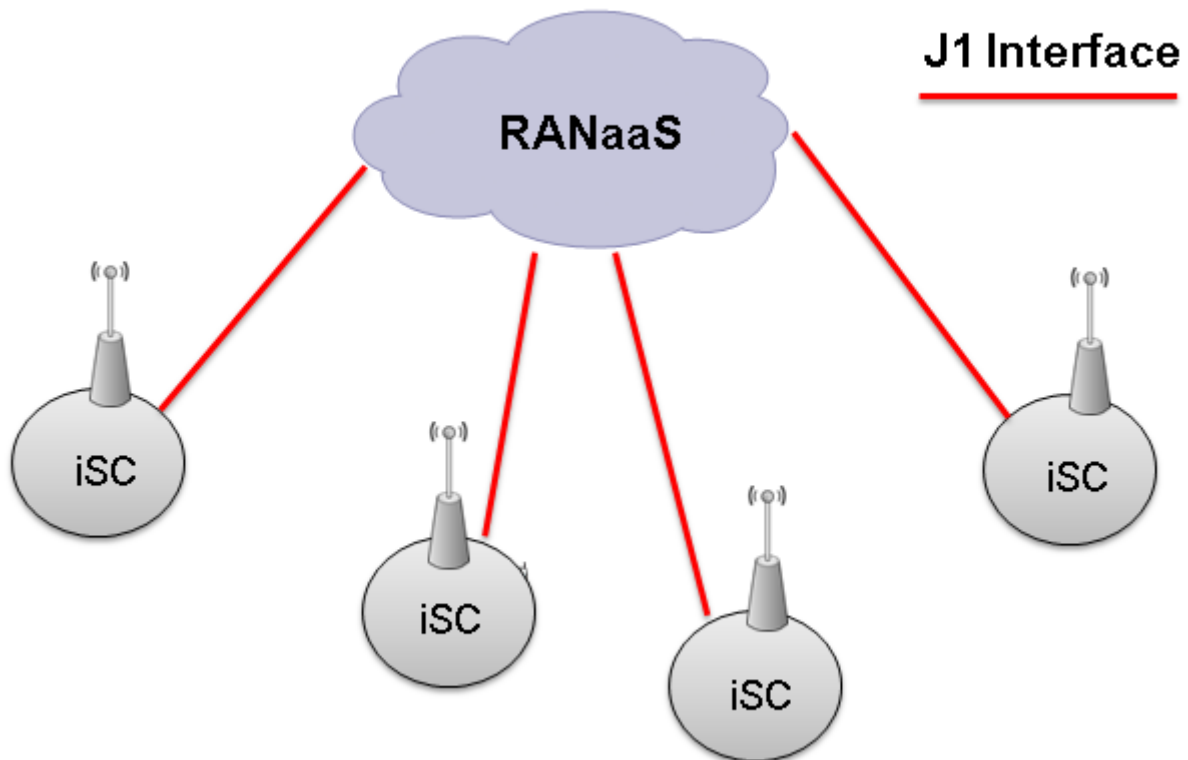


Figure 6-22: Global cooperation for Precoder using J1 interface only

#### Overview

- This is a fully centralised architecture with global cooperation and star deployment configuration of iSCs in relation to the RANaaS.
- All intelligence is in the RANaaS including the precoder.
- iSCs have only the RF functionality.
- iSCs communicate via J1 interface to the RANaaS platform while J2 interface is not required since all intelligence and processing happens in RANaaS.
- Precoders are computed and applied in RANaaS for the signal of each iSC respectively and I/Q samples of the transmit signals have to be sent over the J1 interface.

#### Impacts/requirements on implementation

- A centralised implementation very similar to the C-RAN architecture [114].

#### iJOIN Interface requirements

- Each iSC needs to be connected to RANaaS via J1 interface.
- J1 interface needs to be high speed and highly reliable with low latency, preferably fibre based but could also be wireless.
- J2 interface is not required.

#### C-Plane/U-Plane considerations

- Both C-/U-plane data originate from RANaaS for all iSCs.

### 6.3.2.3.3 Option C: Precoder in RANaaS: Local Cooperation using J2 interface only

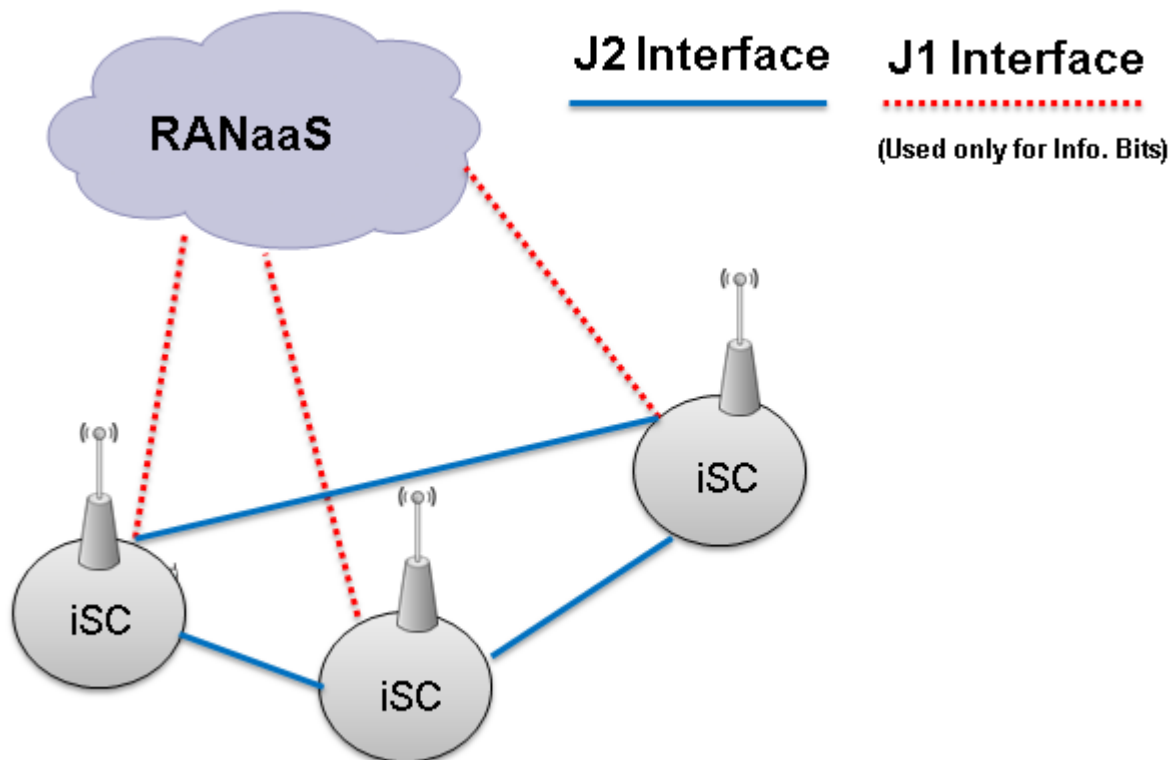


Figure 6-23: Local Cooperation using J2 interface only

#### Overview

- This is a decentralised deployment configuration in which iSCs use only J2 interface for local cooperation while J1 interface is used for carrying only information bits. This may happen when the iSCs have J1 connectivity with RANaaS, however due to large latency on J1 interface (that may happen for example with DSL backhauling), it is not suitable to be used for CoMP purposes.

#### Impacts/requirements on implementation

- A decentralised architecture from CoMP perspective with local cooperation only.

#### iJOIN Interface requirements

- High bandwidth, high reliability and low latency requirement for J2 interface from CoMP perspective.

#### C-Plane/U-Plane considerations

- Both C- and U-plane could be exchanged over J2 interface for CoMP.

### 6.3.2.4 Summary

In this section, various possibilities by which precoders can be implemented in the cloud (or RANaaS) have been highlighted with pros and cons of each. Option A is most generic of all in which best trade-off between performance and complexity is possible taking into account the constraints on J1 and J2 interfaces; Option B is one extreme case in which all global information is available in the RANaaS by using very good J1 links and there is no need to use J-2 links; while Option C is the other extreme in which J1 interface cannot be used due to for example latency constraints, and CoMP has to rely on local cooperation between iSCs using J2 interface. A summary table is also presented in Table 6-11 illustrating the pros and cons of each approach.

**Table 6-11: Pros and Cons of Precoder Options**

	<b>Option A: Precoding in RANaaS: Global cooperation using both J1 and J2 interfaces</b>	<b>Option B: Precoding in RANaaS: Global cooperation using J1 interface only</b>	<b>Option C: Precoding in iSCs: Local cooperation using J2 interface only</b>
<b>PROS</b>	The backhaul links may heterogeneous and may be varying in time.	This presents a compromise to Option A where similar performance can be obtained by using J1 only links provided they are reliable and of high capacity with low latency, at relatively low complexity.	This option still provides decent CoMP performance if J1 interface has a high latency and cannot be used for CoMP purposes.
	Even un-reliable links can be handled as typically large combinations of J1 and J2 interface are possible which also provides for redundancy.		
	The system is more robust to failure of a J1 or J2 link due presence of redundant links.		
	Global cooperation implies that ICI coming even from 2 <sup>nd</sup> / 3 <sup>rd</sup> tier of cells, which could be significant in some conditions, can be efficiently handled.	Global cooperation implies ICI coming even from 2 <sup>nd</sup> / 3 <sup>rd</sup> tier of cells which could be significant in some conditions, can be efficiently handled.	
<b>CONS</b>		Requires high capacity and low latency J1 interface so that for example Joint-Processing CoMP can take place.	Requires high capacity and low latency J2 interface so that for example Joint-Processing CoMP can take place.
	Since, a lot of combinations exist of joint usage of J1 and J2 links, the complexity and / or signaling associated with this scheme is higher than in the other two options.	This option is less robust to unreliable backhaul links and cannot recover in the case of a backhaul link failure.	This option is less robust to unreliable backhaul links and cannot recover in the case of a backhaul link failure.
	Optimal approach is not known.		Lack of global cooperation implies that ICI coming even from 2 <sup>nd</sup> / 3 <sup>rd</sup> tier of cells, which could be significant in some conditions, cannot be efficiently handled.

## 7 Summary and Conclusions

This report provides a first discussion at the physical layer of the joint optimization of the radio access and the backhaul in the system design. At the same time, the functional split between the signal processing done in the RAN-as-a-Service (RANaaS) and at the iJOIN small cells (iSCs) is optimized to reduce further the requirements over the backhaul architecture. It is shown how these additional degrees of freedom in the system design allow a more efficient exploitation of the available architecture and enable a higher degree of cooperation between the iSCs.

This work starts by describing the state-of-the-art (SotA) for the backhauling and the access channel technologies. A good knowledge of the SotA is necessary in order to analyse the potential and the feasibility of the proposed improvements. Promising candidate technologies (CTs) have been selected for their ability to realize the performance improvements targeted by the iJOIN approach. For each CT, a general description of the CT principle is provided. Preliminary results showing the potential of the approach are given.

The requirements of each CT and how it integrates in the iJOIN architecture has been studied in details. The information required as inputs by the CTs have been precisely described as well as the signals provided as output by the CTs. In particular, the tables containing the input and output parameters of each of the novel scheme designed have been the basis to identify the functional interactions with the other work packages and basic functions. This allows for a cross layer analysis of the network which leads to a joint design of the PHY layer and of the other layers. The iJOIN architecture is studied in detail by WP5 taking into account the requirements and assumptions relative to the other WPs. A global discussion of the iJOIN architecture can be found in the deliverable D5.1.

For each of the new schemes developed, a particular care has been given to discuss the different functional split possibilities per CT. Additionally, the implementations of the precoder and of the decoder have been carefully investigated as they represent the core elements of the downlink and the uplink transmission, respectively. It is shown how the optimization of the functional split allows for a better use of the architecture available and a better cross layer design.

The preliminary results show the potential of the iJOIN architecture and give research directions for the future works. Indeed, although some gains could already been achieved by comparison with the legacy systems, many open problems have been encountered throughout the investigations of the iJOIN architecture. The investigation of these problems will lead to more advanced schemes and a better understanding of the iJOIN architecture which will surely gain to further performance improvements.

## **Acknowledgements and Disclaimer**

This work was partially funded by the European Commission within the 7th Framework Program in the context of the ICT project iJOIN (Grant Agreement No. 317941).

## References

- [1] Cisco Visual Networking Index: Global Mobile Data Traffic Forecast Update, 2012-2017, [www.cisco.com](http://www.cisco.com), 2013.
- [2] D. Gesbert, S. Hanly, H. Huang, S. (Shitz) Shamai, O. Simeone, and W. Yu, "Multi-cell MIMO cooperative networks: a new look at interference," *IEEE Trans. on Inf. Theory*, vol. 28, no. 9, pp. 1380–1408, 2010.
- [3] H. Paul, J. Fliege, and A. Dekorsy, "In-network-processing: Distributed consensus-based linear estimation," *IEEE Commun. Lett.*, vol. 17, no.1, pp. 59-62, Jan.2013.
- [4] H. Paul, B.-S. Shin, and A. Dekorsy, "Distributed Consensus-Based Linear Estimation with Erroneous Links," in *Proc. VDE/ITG International Workshop in Smart Antennas (WSA)*, 2013.
- [5] H. Paul, B.-S. Shin, D. Wübben, and A. Dekorsy, "In-Network-Processing for Small Cell Cooperation in Dense Networks," in *Proc. IEEE Vehicular Technology Conference (VTC) workshops, First International Workshop on Cloud Technologies and Energy Efficient in Mobile Communications Networks (CLEEN)*, 2013.
- [6] B.-S. Shin, H. Paul, D. Wübben, and A. Dekorsy, "Reduced Overhead Distributed Consensus-Based Estimation Algorithm," to appear in *Proc. IEEE Global Communications Conference (GLOBECOM) workshops, The first International Workshop on Cloud-Processing in Heterogeneous Mobile Communication Networks (IWCPM)*, 2013.
- [7] E. Katranas, E. Pateromichelakis, and M. A. Imran, "Enhancing Performance in Dense Small Cell Networks: Towards Cooperation in the Cloud," submitted to *IEEE Communication Surveys and Tutorials*, 2013.
- [8] M. Cardone, D. Tuninetti, R. Knopp, and U. Salim, "On the interference channel with causal cognition", in *Proc. IEEE International Conference on Communication (ICC)*, 2013.
- [9] M. Cardone, D. Tuninetti, R. Knopp, and U. Salim, "Gaussian Half-Duplex Relay Channels: Generalized Degrees of Freedom and Constant Gap Results," in *Proc. IEEE International Conference on Communication (ICC)*, 2013.
- [10] J. Bartelt and G. Fettweis, "Radio-over-radio: I/Q-stream backhauling for cloud-based networks via millimetre wave links," to appear in *Proc. IEEE Global Communications Conference (GLOBECOM) workshops, The first International Workshop on Cloud-Processing in Heterogeneous Mobile Communication Networks (IWCPM)*, 2013.
- [11] J. Bartelt, G. Fettweis, D. Wübben, M. Boldi, and B. Mellis, "Heterogeneous Backhaul for Cloud-Based Mobile Networks," in *Proc. IEEE Vehicular Technology Conference (VTC) workshops, First International Workshop on Cloud Technologies and Energy Efficient in Mobile Communications Networks (CLEEN)*, 2013.
- [12] REPORT ITU-R M.2134, "Requirements related to technical performance for IMT-Advanced radio interface(s)".
- [13] 3GPP TR 36.814, "Further Advancements for E-UTRA Physical Layer Aspects (Release 9)". V9.0.0 (2010-03).
- [14] 3GPP TR 25.913, "Requirements for Evolved UTRA (E-UTRA) and Evolved UTRAN (E-UTRAN) (Release 8)". V8.0.0 (2008-12).
- [15] 3GPP TR 36.932, "Scenarios and Requirements for Small Cell Enhancements for E-UTRA and E-UTRAN (Release 12)". V12.0.0 (2012-12).
- [16] R. Fahimeh, "A Comprehensive Analysis of the LTE Physical Layer," PhD Thesis, University of Nebraska - Lincoln, USA, Feb 2010.
- [17] S. Khattak, W. Rave, and G. Fettweis, "Distributed Iterative Multiuser Detection through Base Station Cooperation", *EURASIP Journal on Wireless Communications and Networking*, 2008.
- [18] A. D. Wyner, "Shannon-theoretic approach to a Gaussian cellular multiple-access channel", *IEEE Transactions on Information Theory*, vol. 40, no. 6, p. 1713–1727, 1994.

- [19] A. Grant, S. Hanly, J. Evans, and R. Müller, “Distributed decoding for Wyner cellular systems,” in Proc. The 5th Australian Communications Theory Workshop (AusCTW '04), Newcastle, Australia, 2004.
- [20] E. Aktas, J. Evans, and S. Hanly, “Distributed decoding in a cellular multiple-access channel,” in Proc. IEEE International Symposium on Information Theory (ISIT '04), Chicago, USA, 2004.
- [21] E. Aktas, J. Evans, and S. Hanly, “Distributed base station processing in the uplink of cellular networks,” in Proc. IEEE International Conference on Communications (ICC '06), Istanbul, Turkey, 2006.
- [22] O. Shental, A. J. Weiss, N. Shental, and Y. Weiss, “Generalized belief propagation receiver for near-optimal detection of two-dimensional channels with memory,” in Proc. IEEE Information Theory Workshop (ITW '04), San Antonio, USA, 2004.
- [23] A. Sklavos and T. Weber, “Interference suppression in multiuser OFDM systems by antenna diversity and joint detection,” in Proc. of the COST 273 Management Committee Meeting (MCM '01), Bologna, Italy, 2001.
- [24] S. Khattak, W. Rave, and G. Fettweis, “SIC based multiuser turbo detection in a distributed antenna system for non gray mapping,” in Proc. 9th International Symposium on Wireless Personal Multimedia Communications (WPMC '06), San Diego, USA, 2006.
- [25] T. Mayer, H. Jenkac, and J. Hagenauer, “Turbo Base-Station Cooperation for Intercell Interference Cancellation,” in Proc. IEEE International Conference on Communications (ICC '06), Istanbul, Turkey, 2006.
- [26] 3GPP, TS 36.300, “Evolved Universal Terrestrial Radio Access (E-UTRA) and Evolved Universal Terrestrial Radio Access Network (E-UTRAN); Overall description; Stage 2 (Release 11),” Nov. 2012
- [27] C. Lanzani, G. Kardaras, and Deepak Boppana, “Remote Radio Heads and the Evolution Towards 4G Networks,” Altera Corporation White Paper, Feb. 2009, [online: [www.altera.com/literature/wp/wp-01096-rrh-4g.pdf](http://www.altera.com/literature/wp/wp-01096-rrh-4g.pdf), accessed Feb. 2013]
- [28] S. Sesia, I. Toufik, and M. Baker, LTE - The UMTS Long Term Evolution: From Theory to Practice, John Wiley & Sons, 2009.
- [29] A. Sendonaris, E. Erkip, and B. Aazhang, “User cooperation diversity. Part I. System description,” IEEE Transactions on Communications, vol. 51, no. 11, pp. 1927–1938, 2003.
- [30] A. Sendonaris, E. Erkip, and B. Aazhang, “User cooperation diversity. Part II. Implementation aspects and performance analysis,” IEEE Transactions on Communications, vol. 51, no. 11, pp. 1939–1948, 2003.
- [31] J.N. Laneman, D.N. Tse, and G.W. Wornell, “Cooperative diversity in wireless networks: efficient protocols and outage behaviour,” IEEE Trans. on Information Theory, vol. 50, no. 12, pp. 3062–3080, 2004.
- [32] M. C. Valenti and B. Zhao, “Distributed turbo codes: towards the capacity of the relay channel,” in Proc. IEEE Vehicular Technology Conference (VTC), 2003, pp. 322–326.
- [33] P. Razaghi and W. Yu, “Bilayer low-density parity-check codes for decode-and-forward in relay channels,” IEEE Trans. on Information Theory, vol. 53, no. 10, pp. 3723–3739, 2007.
- [34] A. Chakrabarti, A. De Baynast, A. Sabharwal, and B. Aazhang, “Low density parity-check codes for the relay channels,” IEEE Journal on Selected Areas in Communications, vol. 25, no. 2, pp. 280–291, 2007.
- [35] J. Hu and T. M. Duman, “Low density parity check codes over wireless relay channels,” IEEE Trans. on Wireless Communications, vol. 6, no. 9, pp. 3384–3394, 2007.
- [36] C. Li, G. Yue, M. A. Khojastepour, X. Wang, and M. Madhian, “LDPC coded cooperative relay systems: performance analysis and code design,” IEEE Trans. on Communications, vol. 56, no. 3, pp. 485–496, 2008.

- [37] J. Cances and V. Meghdadi, "Optimized low density parity check codes designs for half duplex relay channels," *IEEE Trans. on Wireless Communications*, vol. 8, no. 7, pp. 3390–3395, 2009.
- [38] D. Duyck, J. J. Boutros, and M. Moeneclaey, "Low-density parity check coding for block fading relay channels," in *Proc. IEEE Inform. Theory Workshop (ITW)*, 2009, pp. 248–252.
- [39] V. Savin, "Split-Extended LDPC codes for coded cooperation," in *Proc. IEEE International Symposium on Information Theory and Applications (ISITA)*, Taichung, Taiwan, October 2010.
- [40] R. Ahlswede, N. Cai, S.-Y. R. Li, and R. W. Yeung, "Network information flow," *IEEE Trans. Inform. Theory*, vol. 46, no. 4, pp. 1204–1216, Jul. 2000.
- [41] M. Di Renzo, L. Iwaza, M. Kieffer, P. Duhamel, and K. Al-Agha, "Robust wireless network coding—an overview," *Lecture Notes of the Institute for Computer Sciences, Social Informatics and Telecommunications Engineering*, 2010.
- [42] S. Zhang, Y. Zhu, S. C. Liew, and K. B. Letaief, "Joint design of network coding and channel decoding for wireless networks," in *IEEE Wireless Communications and Networking Conference (WCNC)*, 2007, pp. 779–784.
- [43] D. H. Woldegebreal and H. Karl, "Multiple-access relay channel with network coding and non-ideal source-relay channels," in *Proc. IEEE International Symposium on Wireless Communication Systems (ISWCS)*, 2007, pp. 732–736.
- [44] C. Hausl, "Joint network-channel coding for wireless relay networks," Ph.D. thesis, Technische Universität München, Germany, 2008.
- [45] T. Tran, T. Nguyen, and B. Bose, "A joint network-channel coding technique for single-hop wireless networks," in *Proc. IEEE Workshop on Network Coding, Theory and Applications (NetCod)*, 2008, pp. 1–6.
- [46] C. Hausl, "Joint network-channel coding for the multiple-access relay channel based on turbo codes," *European Transactions on Telecommunications*, vol. 20, no. 2, pp. 175–181, 2009.
- [47] X. Xu, M.F. Flanagan, N. Goertz, and J. Thompson, "Joint channel and network coding for cooperative diversity in a shared-relay environment," *IEEE Transactions on Wireless Communications*, vol. 9, no. 8, pp. 2420–2423, 2010.
- [48] A. Hatefi, R. Visoz, and A. O. Berthet, "Joint channel-network coding for the semi-orthogonal multiple access relay channel," in *Proc. IEEE Vehicular Technology Conference Fall (VTC-Fall)*, 2010.
- [49] P. H. Tan, C. K. Ho, and S. Sun, "Joint network-channel code design for block fading cooperative multiple access channel," in *Proc. IEEE Information Theory Workshop (ITW)*, 2010.
- [50] J. Li, J. Yuan, R. Malaney, M. H Azmi, and M. Xiao, "Network coded LDPC code design for a multi-source relaying system," *IEEE Transactions on Wireless Communications*, vol. 10, no. 5, pp. 1538–1551, 2011.
- [51] Z. Guo, J. Huang, B. Wang, S. Zhou, J.-H. Cui, and P. Willett, "A practical joint network-channel coding scheme for reliable communication in wireless networks," *IEEE Transactions on Wireless Communications*, vol. 11, no. 6, pp. 2084–2094, 2012.
- [52] D. Duyck, D. Capirone, M. Moeneclaey, and J. J. Boutros, "A full-diversity joint network-channel code construction for cooperative communications," in *Proc. IEEE Int. Symp. on Personal, Indoor and Mobile Radio Communications (PIMRC)*, 2009, pp. 1282–1286.
- [53] D. Duyck, D. Capirone, J. J. Boutros, and M. Moeneclaey, "Analysis and construction of full-diversity joint network-LDPC codes for cooperative communications," *EURASIP Journal on Wireless Communications and Networking*, vol. 2010, pp. 9, 2010.
- [54] J. Ebrahimi and C. Fragouli, "Vector network coding," EPFL Technical Report, 2010.
- [55] R. Gallager, "Low density parity check codes," *IEEE Trans. Inform. Theory*, it-8, pp. 21–28, 1962.
- [56] T. J. Richardson, M. A. Shokrollahi, and R. L. Urbanke, "Design of capacity approaching irregular low density parity check codes," *IEEE Trans. Inform. Theory*, vol. 47, no. 2, pp. 619–637, 2001.

- [57] N. Wiberg, "Codes and decoding on general graphs," PhD Thesis, Linköping University, Sweden, Oct 1996.
- [58] R. M. Tanner, "A recursive approach to low complexity codes," *IEEE Transactions on Information Theory*, vol.27, no.5, pp.533-547, Sep 1981.
- [59] M. C. Davey and D. J. C. MacKay, "Low density parity check codes over GF(q)," *IEEE Commun. Lett.*, vol. 2, no. 6, pp. 165-167, 1998.
- [60] C. Poulliat, M. Fossorier, and D. Declercq, "Design of regular (2, dc)-LDPC codes over GF(q) using their binary images," *IEEE Transactions on Communications*, vol. 56, no. 10, pp. 1626-1635, 2008.
- [61] X. Y. Hu, E. Eleftheriou, and D. M. Arnold, "Regular and irregular progressive edge-growth tanner graphs," *IEEE Transactions on Information Theory*, vol. 51, no 1, p. 386-398, 2005.
- [62] D. Declercq and M. Fossorier, "Decoding Algorithms for Non-binary LDPC Codes Over GF(q)," *IEEE Transactions on Communications*, vol. 55, no 4, p. 633-643, 2007.
- [63] G. J. Foschini and M. J. Gans, "On limits of wireless communications in a fading environment when using multiple antennas," *Wireless Personal Communications*, vol. 6, pp. 311-335, 1998
- [64] E. T. Ar and I. E. Telatar, "Capacity of multi-antenna Gaussian channels," *European Transactions on Telecommunications*, vol. 10, pp. 585-595, 1999.
- [65] J. Lee and N. Jindal, "High SNR Analysis for MIMO Broadcast Channels: Dirty Paper Coding Versus Linear Precoding," *IEEE Trans. Inform. Theory*, vol. 53, no.12, pp. 4787 - 4792, Dec. 2007.
- [66] D. Gesbert, M. Kountouris, R. W. Heath, C-B. Chae and T. Salzer, "Shifting the MIMO Paradigm," *IEEE Sig. Process. Mag.*, vol. 24, no. 5, pp. 36 - 46, Sept. 2007.
- [67] E. Pateromichelakis, M. Shariat, A. Quddus and R. Tafazolli, "On the evolution of multi-cell scheduling in 3GPP LTE/LTE-A," *IEEE Comm. Surveys & Tutorials*, vo. 15, no. 2, pp. 701-717, May 2013.
- [68] W. Choi, J. G. Andrews, "The capacity gain from intercell scheduling in multi-antenna systems," *IEEE Trans. Wireless Comm.*, vol. 7, no. 2, pp. 714-725, Feb. 2008.
- [69] S. Shamai (Shitz) and B. M. Zaidel, "Enhancing the cellular downlink capacity via co-processing at the transmitting end," in *Proc. IEEE Veh. Technol. Conf.*, Rhodes, Greece, May 2001, pp. 1745-1749.
- [70] H. Zhang and H. Dai, "Cochannel interference mitigation and cooperative processing in downlink multicell multiuser MIMO networks," *European J. Wireless Commun. and Networking*, no. 2, pp. 222-235, 4th Quarter 2004.
- [71] K. Karakayali, G. J. Foschini, R. A. Valenzuela, and R. Yates, "On the maximum common rate achievable in a coordinated network," in *Proc. IEEE Int. Conf. Commun.*, Istanbul, Turkey, June 2006, pp. 4333-4338.
- [72] G. J. Foschini, H. Huang, K. Karakayali, R. A. Valenzuela, and S. Venkatesan, "The value of coherent base station coordination," in *Proc. Conference on Information Sciences and Systems (CISS)*, Johns Hopkins University, Mar. 2005.
- [73] O. Somekh, O. Simeone, Y. Bar-Ness, and A. M. Haimovich, "Distributed multi-cell zero-forcing beamforming in cellular downlink channels," in *Proc. IEEE Global Communications Conference (GLOBECOM)*, San Francisco, Nov. 2006.
- [74] J. Zhang, R. Chen, J. G. Andrews, A. Ghosh and R.W. Heath, "Networked MIMO with clustered linear precoding," *IEEE Trans. Wireless Comm.*, vol. 8, no. 4, April 2009.
- [75] J. Zhang and J. G. Andrews, "Adaptive spatial intercell interference cancellation in multicell wireless networks," in *IEEE Jour. Sel. Areas Comm.*, vol. 28, no. 9, Dec. 2010.
- [76] H. Dahrouj and W. Yu, "Coordinated beamforming for the multicell multi-antenna wireless system," in *IEEE Trans. Wireless Comm.*, vol. 9, no. 5, May 2010.
- [77] R. Zakhour and D. Gesbert, "Distributed multi-cell MISO precoding using the layered virtual SINR framework", in *Proc. IEEE Global Communications Conference (GLOBECOM)*, 2011.

- [78] P. Marsch and G. Fettweis, "On downlink network MIMO under a constrained backhaul and imperfect channel knowledge," in Proc. IEEE Global Communications Conference (GLOBECOM), 2009.
- [79] R. Zakhour and D. Gesbert, "Optimized data sharing in multicell MIMO with finite backhaul capacity," IEEE Trans. Sig. Process., vol. 59, no.12, pp. 6102-6111, Dec. 2011.
- [80] N. Seifi, M. Viberg, R. W. Heath, J. Zhang, and M. Coldrey, "Coordinated single-cell vs multi-cell transmission with limited-capacity backhaul," in Proc. IEEE ACSSC, 2010.
- [81] Q. Zhang, C. Yang and A. F. Molisch, "Cooperative downlink transmission mode selection under limited-capacity backhaul," in Proc. Wireless Communications and Networking Conference (WCNC), Apr. 2012, pp. 1082 – 1087.
- [82] Common Public Radio Interface, [online: <http://www.cpri.info/>]
- [83] Open Base Station Architecture Initiative, [online: <http://www.obsai.com/>]
- [84] 3GPP TS 36.211, "Radio Access Network; Evolved Universal Terrestrial Radio Access; (E-UTRA); Physical channels and modulation," Release 10, (2012 - 12).
- [85] Small Cell Forum, "Backhaul Technologies for Small Cells," Technical Report, Feb. 2013
- [86] J. Segel, M. Weldon, Light Radio Portfolio: Technical Overview, Alcatel Lucent Technology White Paper, 2011, [online: <http://www.alcatel-lucent.com/>].
- [87] NGMN White Paper on LTE Backhauling deployment scenarios, [online: [http://www.ngmn.org/uploads/media/NGMN\\_Whitepaper\\_LTE\\_Backhauling\\_Deployment\\_Scenarios\\_01.pdf](http://www.ngmn.org/uploads/media/NGMN_Whitepaper_LTE_Backhauling_Deployment_Scenarios_01.pdf), accessed Oct. 2013].
- [88] Ceragon, "Wireless Backhaul Solutions for Small Cells", Solution Brief, [online: [http://www.ceragon.com/files/library/Ceragon\\_Small\\_Cell-Solution\\_Brief.pdf](http://www.ceragon.com/files/library/Ceragon_Small_Cell-Solution_Brief.pdf), accessed Feb. 2013].
- [89] J. Wells, "Faster than fibre: The future of multi-G/s wireless," IEEE Microwave Magazine, vol.10, no.3, pp.104-112, May 2009.
- [90] Z. Pi and f. Khan, "An introduction to millimetre-wave mobile broadband systems", IEEE Comm. Mag., pp. 101-107, June 2011.
- [91] 3GPP TS 36.212, "Radio Access Network; Evolved Universal Terrestrial Radio Access; (E-UTRA); Multiplexing and channel coding," Release 10, (2012 - 12).
- [92] Rohde & Schwarz, "UMTS Long Term Evolution (LTE) Technology Introduction," Application Note 1MA111, 2008.
- [93] ETSI, "Open Radio Equipment Interface (ORI); Requirements for Open Radio equipment interface (ORI)", Release 2, ETSI GS ORI 001 V2.1.1 (2013 - 05), [online: [http://www.etsi.org/deliver/etsi\\_gs/ORI/001\\_099/001/02.01.01\\_60/gs\\_ori001v020101p.pdf](http://www.etsi.org/deliver/etsi_gs/ORI/001_099/001/02.01.01_60/gs_ori001v020101p.pdf), accessed October 2013].
- [94] ETSI TR 101 112: "Selection procedures for the choice of radio transmission technologies of the UMTS," UMTS 30.03 version 3.1.0.
- [95] F. Tosato and P. Bisaglia, "Simplified Soft-Output Demapper for binary interleaved COFDM with application to HIPERLAN/2," HP Laboratories Bristol, 2001.
- [96] H. Zhu, A. Cano, and G. Giannakis, "Distributed consensus-based demodulation: algorithms and error analysis," IEEE Trans. Wireless Commun., vol. 9, no. 6, pp. 2044-2054, Jun. 2010
- [97] C. Berrou, A. Glavieux, and P. Thitimajshima, "Near Shannon limit error-correcting coding and decoding," in Proc. IEEE ICC'93, Geneva, Switzerland, pp. 1064–1070, May 1993.
- [98] J. Hagenauer, "The turbo principle: Tutorial introduction and state of the art," in Proc. 1st International Symposium on Turbo Codes, Brest, France, pp. 1–12, Sept. 1997.
- [99] X. Wang and H.V. Poor, "Iterative (turbo) soft interference cancellation and decoding for coded CDMA," IEEE Trans. Commun., vol. COM-47, no. 7, pp. 1046–1061, July 1999.
- [100] H. El Gamal and E. Geraniotis, "Iterative multiuser detection for coded CDMA signals in AWGN and fading channels," IEEE J. sel. Areas Commun., vol. 18, no. 1, pp. 30–41, Jan. 2000.

- [101] G. Caire and R. Müller, “The optimal received power distribution of IC-based iterative multiuser joint decoders”, in Proc. 39th Annual Allerton Conf. on Communications, Control and Computing, Monticello, IL, USA, Oct. 2001.
- [102] M. Tüchler, R. Koetter, and A. Singer, “Turbo equalization: Principles and new results,” IEEE Trans. Commun., vol. COM-50, no. 5, pp. 754–767, May 2002.
- [103] R. Visoz, A.O. Berthet, and M. Lalam, “Semi-Analytical Performance Prediction Methods for Iterative MMSE-IC Multiuser MIMO Joint Decoding,” IEEE Trans. Commun., vol COM-58, no. 9, pp. 2576–2589, Sept. 2010.
- [104] Y.L. Wong, W.R. Wu, and Y.P Hsu, “Turbo equalization for MIMO-OFDM systems with inter-site CoMP,” in Proc. IEEE Int. Conf. Commun. in China: Wireless Communication Systems (WCS), pp. 642-646, Aug. 2012
- [105] H.-C. Lee, D.-C. Oh, and Y.-H. Lee, “Mitigation of inter-femtocell interference with adaptive fractional frequency reuse,” in Proc. of IEEE ICC, May 2010.
- [106] G. Boudreau, J. Panicker, N. Guo, R. Chang, N. Wang, and S. Vrzic, “Interference coordination and cancellation for 4G networks,” in IEEE Communications Magazine, Apr. 2009.
- [107] S. H. Ali and V. C. M. Leung, “Dynamic frequency allocation in fractional frequency reused OFDMA networks,” IEEE Trans. on Wireless Communications, Aug. 2009.
- [108] A. Simonsson, “Frequency reuse and intercell interference co-ordination in E-UTRA,” in Proc. of IEEE VTC Spring, Apr. 2007.
- [109] M.-S. Kim, M. R. Jeong, F. Watanabe, and F. Tobagi, “Band-distributed channel-aware fractional frequency reuse in OFDMA systems,” in Proc. of IEEE VTC Fall, Sept. 2009.
- [110] M. Rahman and H. Yanikomeroglu, “Enhancing cell-edge performance: a downlink dynamic interference avoidance scheme with inter-cell coordination,” IEEE Trans. on Wireless Communications, Apr. 2010.
- [111] L. Bahl, J. Cocke, F. Jelinek, and J. Raviv, “Optimal decoding of linear codes for minimizing symbol error rate,” IEEE Trans. Inform. Theory, vol. IT-20, no. 2, pp. 284–287, Mar. 1974.
- [112] 3GPP TS 36.213, “Evolved Universal Terrestrial Radio Access (E-UTRA); Physical layer procedures (Release 10),” Release 10, (2012 - 12)
- [113] F. S. Cattivelli and A. H. Sayed, “Diffusion LMS Strategies for Distributed Estimation,” IEEE Transactions on Signal Processing, Vol. 58, No. 3, March 2010.
- [114] Next Generation Mobile Networks (NGMN), “Suggestions On Potential Solutions To C-RAN” [Online: [http://www.ngmn.org/uploads/media/NGMN\\_CRAN\\_Suggestions\\_on\\_Potential\\_Solutions\\_to\\_CRAN.pdf](http://www.ngmn.org/uploads/media/NGMN_CRAN_Suggestions_on_Potential_Solutions_to_CRAN.pdf)].
- [115] S. Kemp and T. Gruba, „lightRadio™ Technology Overview,“ Alcatel-Lucent TechZine, 2011.
- [116] Nokia Siemens Networks Corporation “Liquid Radio - Let traffic waves flow most efficiently,” White Paper, Espoo, Finland, 2011.
- [117] Z. Zhu, Q. Wang, Y. Lin, P. Gupta, S. Sarangi, S. Kalyanaraman, and H. Franke, “Virtual Base Station Pool: Towards A Wireless Network Cloud for Radio Access Networks,” Computing Frontiers, p. 34, 2011.
- [118] China Mobile Research Institute, “C-RAN - The Road Towards Green RAN,” White Paper, October 2011.
- [119] G. Li, “IA based large-scale baseband pool research,” 2012 International Mobile Internet Conference, August 2012.
- [120] S. Bhaumik, S. P. Chandrabose, M. K. Jataprolu, G. Kumar, A. Muralidhar, P. Polakos, V. Srinivasan und T. Woo, “CloudIQ: A Framework for Processing Base Stations in a Data Center,” in Proc. MobiCom '12, Istanbul, Turkey, 2012.
- [121] L. Lu, “C-RAN the new transmission architecture of multi-level heterogeneous networks,” in Proc. International Mobile Internet Conference, August 2012.

- [122] “Common Public Radio Interface (CPRI), Common Public Radio Interface (CPRI): Interface Specification,” 2011, [Online: [http://www.cpri.info/downloads/CPRI\\_v\\_5\\_0\\_2011-09-21.pdf](http://www.cpri.info/downloads/CPRI_v_5_0_2011-09-21.pdf)].
- [123] iJOIN Project, “D5.1- Revised definition of requirements and preliminary definition of the iJOIN architecture,” October 2013.
- [124] iJOIN Project, “IR6.1- Proof-of-concept requirements, evaluation criteria, and performance measures,” July 2013.
- [125] A. Sanderovich, O. Somekh, H. V. Poor, and S. Shamai, “Uplink macro diversity of limited backhaul cellular network,” *IEEE Trans. Inf. Theo.*, vol. 55, no. 8, pp 3457-3478, Aug. 2009.
- [126] Seok-Hwan Park, Osvaldo Simeone, Onur Sahin, and S. Shamai, “Joint Precoding and Multivariate Backhaul Compression for the Downlink of Cloud Radio Access Networks,” submitted to *IEEE Trans. on Signal Process.*, 2013.[Online: <http://arxiv.org/pdf/1304.3179v1.pdf>].
- [127] Lei Zhou, and Wei Yu, “Uplink Multicell Processing with Limited Backhaul via Per-Base-Station Successive Interference Cancellation,” *IEEE J. sel. Areas Commun.*, Special issue on Virtual MIMO, vol. 31, no. 10, pp. 1981–1993, Oct. 2013.
- [128] P. de Kerret and D. Gesbert, “Degrees of Freedom of Network MIMO with Distributed CSI,” *IEEE Trans. Inf. Theo.*, vol. 58, no. 11, pp. 6806-6824, Nov. 2012.
- [129] P. de Kerret and D. Gesbert, “CSI Sharing Strategies for Transmitter Cooperation in Wireless Networks,” *IEEE Wireless Comm. Mag.*, Feb. 2013.
- [130] T. Cover and A. Thomas, “Elements of Information Theory,” Wiley-Interscience, 2006.
- [131] J. Marschak and R. Radner, “Economic Theory of Teams,” Yale University Press, 1972.
- [132] P. Cuff, H. Permuter, and T. Cover, “Coordination Capacity,” *IEEE Trans. Inf. Theo.*, vol. 56, no. 9, pp. 4181-4206, Sept. 2010.
- [133] A. Diavastos, P. Petrides, G. Falcao, P. Trancoso, “LDPC Decoding on the Intel SCC,” in *Proc. Euromicro International Conference on Parallel, Distributed and Network-Based Processing (PDP)*, 2012.
- [134] G. Falcao, V. Silva, L. Sousa, and J. Marinho, “High coded data rate and multicodeword WiMAX LDPC decoding on Cell/BE,” *Electronics Letters*, 2008.
- [135] G. Falcao, L. Sousa, and V. Silva, “Massively LDPC decoding on multicore architectures,” *IEEE Transactions on Parallel and Distributed Systems*, 2011.
- [136] H. Ji, J. Cho, and W. Sung, “Massively parallel implementation of cyclic LDPC codes on a general purpose graphics processing unit,” in *Proc. IEEE workshop on Signal Processing Systems (SiPS)*, 2009.
- [137] S. Seo, T. Mudge, Y. Zhu, and C. Chakrabarti, “Design and analysis of LDPC decoders for software defined radio,” in *Proc. IEEE Workshop on Signal Processing Systems*, 2007.
- [138] J. Zhao, M. Zhao, H. Yang, J. Chen, X. Chen, and J. Wang, “High Performance LDPC Decoder on CELL BE for WiMAX System,” in *Proc. Third International Conference on Communications and Mobile Computing (CMC)*, 2011.
- [139] Y. Zhu and C. Chakrabarti, “Architecture-aware LDPC code design for multiprocessor software defined radio systems,” *IEEE Transactions on Signal Processing*, 2009.
- [140] T. Biermann, L. Scalia, C. Choi, H. Karl and W. Kellerer, “CoMP clustering and backhaul limitations in cooperative cellular mobile access networks,” *Pervasive and Mobile Computing*, vol. 8, no. 5, pp. 662-681, Oct.2012.
- [141] M.K. Karakayali, G. J. Foschini, and R. A. Valenzuela, “Network Coordination for spectrally efficient communications in cellular systems,” *IEEE Wireless communications*, Volume 13, Issue 4, August 2006.
- [142] N. K. Babu and P. S. S. Babu, “Design of Physical Coding sublayer using 8B/10B algorithm,” *International Journal of Recent Technolgy and Engineering (IJRTE)*, ISSN: 2277-3878, Volume 2, Issue 2, May 2013

- [143] S. Boyd, N. Parikh, E. Chu, B. Peleato, and J. Eckstein, "Distributed optimization and statistical learning via the alternating direction method of multipliers," *Foundations and Trends in Machine Learning*, vol. 3, no. 1, pp. 1–122, 2010.
- [144] iJOIN Project, "D3.1- Final report on MAC/RRM state-of-the-art, Requirements, scenarios and interfaces in the iJOIN architecture," October 2013.
- [145] iJOIN Project. "D4.1- Report on SotA and requirements for network-layer algorithms and network operation and management," October 2013.
- [146] G. J. Foschini, K. Karakayali, and R. A. Valenzuela, "Coordinating multiple antenna cellular networks to achieve enormous spectral efficiency," *IEE Proc. Commun.*, vol. 153, no. 4, Aug. 2006, pp. 548–555.
- [147] D. Lee, H. Seo, B. Clerckx, E. Hardouin, D. Mazzaresse, S. Nagata, and K. Sayana, "Coordinated multipoint transmission and reception in LTE-advanced: deployment scenarios and operational challenges," *IEEE Communications Magazine*, vol.50, no.2, pp.148-155, February 2012.
- [148] H. Zhu, A. Cano, and G. B. Giannakis, "Distributed in-network channel decoding," *IEEE Trans. Signal Process.*, vol. 57, no. 10, Oct. 2009.